Uranium incorporation in andraditic garnet

C. Ackermann[1,2], H.R. Marschall[1,2], M. Kutzschbach[3], D.C. Hezel[1,2], A.B. Woodland[1,2], L.J. Millonig[1,2], J.B. Walters[1,2], A. Schmidt[1,2]

[1]Institut für Geowissenschaften, Goethe Universität, Altenhöferallee 1, 60438 Frankfurt am Main, Germany
[2]Frankfurt Isotope and Element Research Center (FIERCE), Goethe Universität, 60438 Frankfurt am Main
[3]Institut für Angewandte Geowissenschaften, Technische Universität Berlin, Ernst-Reuter-Platz 1, 10587 Berlin, Germany
e-mail: cl.ackermann@gmx.de

Minerals of the garnet supergroup are widespread in, e.g., medium- to high-pressure metamorphic rocks, where they form an integral part of many well-established geobarometers and -thermometers. Since a few years, garnet U-Pb dating by (in-situ) LA-ICPMS is being developed. This method offers rapid analysis of a large set of samples with high spatial resolution and an age precision comparable to other geochronometers. However, the success rate of the method is hampered by our limited ability to predict the suitability of a particular sample for U-Pb dating. This limitation is due to current ambiguities regarding the incorporation of uranium (and Pb) in garnet.

In this study we investigate the incorporation of Uranium in (Ti-bearing) andraditic garnet, from alkaline igneous rocks and skarns. Previous studies on the incorporation of U into the garnet structure were restricted to elbrusite that contains U as a major component (up to 27 wt.%) in conjunction with Zr (Galuskina et al., 2010). Most natural andradite, however, contains only trace levels of U (typically 1–50 µg/g) and the substitution and incorporation mechanisms at this concentration level are unknown. Furthermore, previous studies even have claimed that U is not incorporated in garnet at all, and that the analysed U content is due to U-bearing inclusions (e.g., Lima et al., 2014). On our suite of five andradites, two of which originated from alkaline igneous rocks and three from skarn deposits, we completed a full chemical characterization. This included major and trace-element analyses and mapping by EPMA and LA-ICPMS, determination of the oxidation state of Fe by the EPMA flank method and by Mössbauer spectroscopy, and U-Pb dating by LA-ICPMS. Our results demonstrate that uranium concentrations strictly follow the oscillatory growth zoning of garnet, and one sample even exhibited sector zoning of U in garnet (Fig. 1). In general, U shows a positive correlation with Th and with Ce, and no correlation between U and Zr, showing that the elbrusite substitution vector does not (necessarily) operate at the trace-element level in andradite. Instead, U is likely incorporated in the dodecahedral site and charge compensated by octahedral divalent ions and/or tetrahedral Fe^{3+}.

Our results show that U, together with Th and the LREE, is indeed incorporated into the structure of garnet, as opposed to U being present only in submicroscopic inclusions. Also, the LREE abundance can be used as a proxy for U-enriched zones. Garnet U–Pb geochronology by LA-ICPMS on andraditic garnet will, thus, be able to reveal the age of the garnet crystallization itself, if U-rich inclusions are avoided. This conclusion agrees with mass-balance estimates presented by Millonig et al. (2020) for metamorphic garnet.

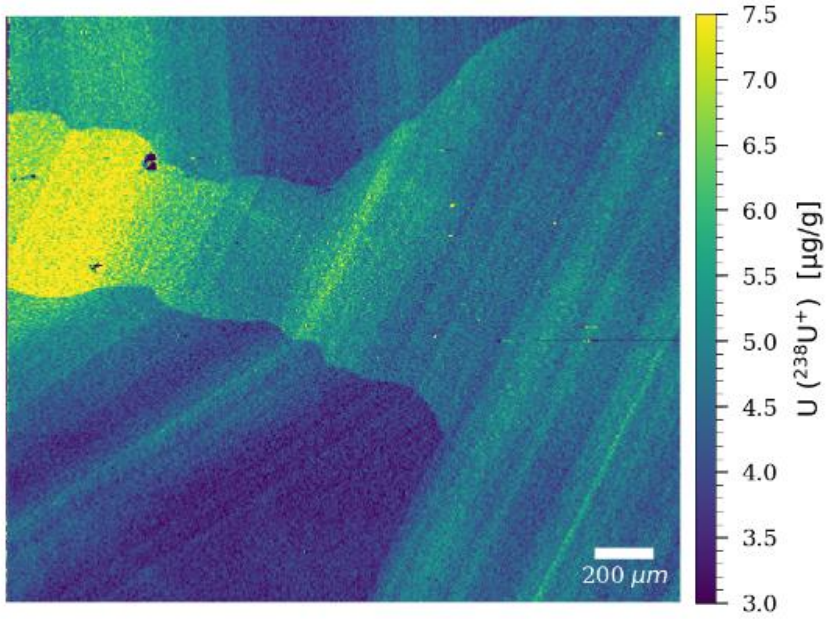

Figure 1. LA-ICP-QQQ-MS mapping of ^{238}U in a Ti-rich andradite from Magnet Cove, Arkansas. Notice the very distinct oscillatory and sector zoning.

Galuskina IO, Galuskin EV, Armbruster T, Lazic B, Kusz J, Dzierżanowski P, Gazeev VM, Pertsev NN, Prusik K, Zadov AE, Winiarski A, Wrzalik R, Gurbanov AG (2010): Elbrusite-(Zr)–A new uranian garnet from the Upper Chegem caldera, Kabardino-Balkaria, Northern Caucasus, Russia. - Amer Mineral 95, 1172-1181

Lima SM, Corfu F, Neiva AMR, Ramos JMF (2012): U-Pb ID-TIMS dating applied to U-rich inclusions in garnet. - Amer Mineral 97, 800-806

Millonig LJ, Albert R, Gerdes A, Avigad D, Dietsch C (2020): Exploring laser ablation U–Pb dating of regional metamorphic garnet The Straits Schist, Connecticut, USA. - EPSL 552, 116589

Plagioclase hosted magnetite micro-inclusions from oceanic gabbro: shape orientation and implication for bulk magnetic properties

O. Ageeva[1], G. Bian[1], G. Habler[1], R. Abart[1]

[1]University of Vienna, Department of Lithospheric Research
e-mail: olga.ageeva@univie.ac.at

In gabbro, fine-grained magnetite (MT) micro-inclusions hosted by rock-forming silicates contribute to bulk-rock magnetism. Specific crystal orientations of micro-inclusions relative to the silicate host may dramatically affect the direction and/or intensity of natural remanent magnetization (NRM) of the rock. Understanding the influence of oriented silicate-hosted magnetite micro-inclusions on rock-magnetism is important for obtaining reliable paleomagnetic data and for revealing rock magnetic fabrics, which may shed light on the mechanisms of rock formation or the tectonic evolution. We studied needle- and lath-shaped magnetite micro-inclusions in plagioclase of oceanic gabbro from the slow-spreading Mid Atlantic Ridge (11-17°N), aiming to reveal the genesis and ferromagnetic contribution of the MT inclusions to the magnetic properties of grains of host plagioclase. To this end, we combined a detailed petrographic study on magnetite-bearing plagioclase with crystal orientation analysis by electron backscatter diffraction (EBSD), measurements of the anisotropy of magnetic remanence (AMR) and alternating field (AF) demagnetization. The results show that:

(i) Needle and lath shaped MT inclusions have systematic shape orientations following eight specific crystallographic directions that coincide with the poles of low-index crystal planes/directions of the plagioclase host.

(ii) Statistically, the MT inclusions show two types of shape orientation distribution (Ageeva et al., 2022): One type is characterized by a predominantly oblate shape orientation distribution, due to a high fraction of needle-shaped inclusions oriented sub-parallel to the (010) plane of plagioclase and forming an about 30º wide "(010)-girdle". These inclusions are considered to be of primary magmatic origin (Bian et al. 2023a). The other type of shape distribution features a high fraction of inclusions oriented parallel to the c-axis of the plagioclase-host. These inclusions are interpreted as secondary (Bian et al. 2023b), replacing primary inclusions in domains where high-temperature hydrothermal alteration of plagioclase was effective.

(iii) Twinning of plagioclase following the Albite, Pericline, Carlsbad and Manebach twin laws increases the dispersion of inclusion orientations within the (010)-girdle, and strengthens the lineation caused by the presence of inclusions oriented parallel to [001] of plagioclase.

(iv) The anisotropic shape orientation distribution of the MT-inclusions causes anisotropy of magnetic remanence (AMR) in the plagioclase grains (Ageeva et al., 2022). A good correspondence between the shape orientation distribution of the MT-inclusions and AMR is established in the majority of the studied plagioclase grains: The direction of minimum magnetic remanence R_{min} is sub-perpendicular to the (010)-girdle. The direction of maximum magnetic remanence R_{max} lies in the (010)-girdle and often is close to parallel to the PL [001] direction, which often corresponds to a maximum in the shape orientation distribution of MT-inclusions in twinned plagioclase.

(v) The vector of natural remanent magnetism (NRM) tends to lay in the (010)-girdle, often parallel to the maximum in the elongation orientation distribution of inclusions or/and parallel to the direction of maximum magnetic remanence.

The results indicate that oriented needle- and lath-shaped MT micro-inclusions in plagioclase endow the grains of host plagioclase with anisotropic ferromagnetism. Consequently, in case of preferred orientation of grains of magnetite-bearing plagioclase, which is typical for many geological settings including mid-ocean ridges and layered intrusions, a magnetic fabric may form. The identified characteristics of the plagioclase magnetic anisotropy are highly relevant for petrological and paleomagnetic studies of oceanic gabbro.

Ageeva O, Habler G, Gilder SA, Schuster R, Pertsev A, Pilipenko O, Bian G, Abart R (2022): Oriented magnetite inclusions in plagioclase: Implications for the anisotropy of magnetic remanence. – Geochem Geophys Geosystems 23, e2021GC010272

Bian G, Ageeva O, Roddatis V, Li C, Pennycook TJ, Habler G, Abart R (2023a): Crystal structure controls on oriented primary magnetite micro-inclusions in plagioclase from oceanic gabbro. - J Petrol 64, egad008

Bian G, Ageeva O, Roddatis V, Habler G, Schreiber A, Abart R (2023b): Oriented secondary magnetite micro-inclusions in plagioclase from oceanic gabbro. - Amer Miner, doi: 10.2138/am-2022-8784

Crystal structure and Li-ion conductivity in $Li_7La_3Zr_{12}O_{24}$ garnets: a review

G. Amthauer[1], D. Rettenwander[2], R. Wagner[1], G.J. Redhammer[1]

[1]*University of Salzburg*
[2]*Norwegian University of Science and Technology Trondheim*
e-mail: Georg.amthauer@plus.ac.at

Recent research has shown that certain Li-oxide garnets with more than 3 Li atoms per formula unit, such as $Li_7La_3Zr_2O_{12}$, have high ionic conductivities, as well as good chemical and physical properties for use in solid-state batteries (Murugan et al. 2007).

"Garnet" is the common name for a large number of natural and synthetic metal-oxide phases. Conventional oxide garnets have the general formula $A_3B_2C_3O_{12}$ and crystallize in the cubic space group $Ia\bar{3}d$. The O^{2-} ions, in the general crystallographic positions 96*h*, form a framework with interstices occupied by the A cations, such as Ca^{2+}, Fe^{2+}, Y^{3+}, La^{3+} in the 8-fold coordinated position 24*c* (point symmetry 222), the B cations, such as Al^{3+}, Fe^{3+}, Zr^{4+}, Sn^{4+}, Sb^{5+}, etc. in the 6-fold coordinated position 16*a* (point symmetry $\bar{3}$), and the C cations, such as Li^+, Al^{3+}, Fe^{3+}, Ga^{3+}, Ti^{4+}, Si^{4+}, etc. in the 4-fold coordinated 24*d* position (point symmetry $\bar{4}$). In addition to these cation sites, there are other interstices within the oxygen framework, which are empty in the conventional garnet structure, e.g. (i) the 6-fold coordinated 16*b* positions with point symmetry 32, (ii) the 6-fold coordinated 48*g* positions with point symmetry 2, and (iii) an additional 4-fold coordinated 96*h* position with point symmetry 1. In **"$Li_7La_3Zr_2O_{12}$"** garnet (LLZO)**,** these interstices are filled by "excess" Li^+ ions giving rise to the excellent ionic conductivity.

There is a low temperature tetragonal modification of pure LLZO (SG: $I4_1/acd$) and a high temperature non quenchable cubic phase of LLZO (SG: $Ia\bar{3}d$). The tetragonal phase has distinctly lower ion conductivity than the cubic phase. Fortunately, the cubic phase can be stabilized at low temperatures by doping with low amounts of Al, Ga, and Fe (Buschmann et al. 2011; Rettenwander et al. 2016). In our contribution the results of single crystal X-ray diffraction studies will be presented. While Al-doped LLZO garnets always crystallize within the space group $Ia\bar{3}d$, Ga and Fe-doped LLZO garnets crystallize within the space group $I\bar{4}3d$ (Wagner et al. 2016). This symmetry change is combined with an increase in ionic conductivity up to 10^{-3} S cm^{-1} which is very high for those kind of solid state electrolytes used in Li-ion batteries. These results will be discussed on the basis of the slightly different topologies of both space groups, respectively. Similar structural changes are observed by the incorporation of Co (Mir et al. 2023).

Buschmann H, Dölle J, Berendts S, Kuhn A, Bottke P, Wilkening M, Heitjans P, Senyshyn A, Ehrenberg H, Lotnyk A (2011): Structure and dynamics of the fast lithium ion conductor "$Li_7La_3Zr_2O_{12}$". - Phys Chem Chem Phys 13, 19378-19392

Murugan R, Thangadurai V, Weppner W. (2007): Fast lithium ion conduction in garnet-type $Li_7La_3Zr_2O_{12}$. - Angew Chem Int Ed 46, 7778-7781

Mir MUD, Ladenstein L, Ring J, Knez D, Smetaczek S, Kubicek M, Sadeqi-Moqadam M, Ganschow S, SalagreE, Enrique G. Michel, Stefanie Lode, Gerald Kothleitner, Iulian Dugulan, Jeffrey G. Smith, Limbeck A, Fleig J, Donald J. DJ, Redhammer GJ, Daniel Rettenwander D (2023): A guideline to mitigate interfacial degradation processes in solid-state batteries caused by cross diffusion. - Adv. Funct Mater 2023, 2303680

Wagner R, Redhammer GJ, Rettenwander D, Senyshyn A, Schmidt W, Wilkening M, Amthauer G (2016): Crystal structure of garnet-related Li-ion conductor $Li_{7-3x}Ga_xLa_3Zr_2O_{12}$: Fast Li-ion conduction caused by a different cubic modification? - Chem Mater 28, 1861-1871

Rettenwander D, Redhammer G, Preishuber-Pflügl F, Cheng L, Miara L, Wagner R, Welzl A, Suard E, Doeff MM, Wilkening M, Fleig J, Amthauer G (2016): Structural and Electrochemical Consequences of Al and Ga cosubstitution in Li7La3Zr2O12 solid electrolytes. - Chem Mater 28, 2384-2392

Decompression of high-grade metamorphic mafic rocks constrained by small-scale compositional layering, Gföhl Unit, Moldanubian Zone

R. Asenbaum[1], M. Racek[2], R. Abart[1]

[1]Department of Lithospheric Research, University of Vienna, Austria
[2]Institute of Petrology and Structural Geology, Faculty of Science, Charles University Prague, Czech Republic
e-mail: rene.asenbaum@univie.ac.at

Mafic–ultramafic lenses embedded in felsic granulites of the Gföhl Unit, Moldanubian Zone, are considered as mantle fragments incorporated into mid-crustal levels of the Variscan orogenic crust. We investigated a several 100 m sized mafic lens mainly formed by eclogites. Several samples were collected from loose boulders. Petrographic features provide evidence for an early HP-HT eclogite-facies peak metamorphism overprinted to variable degrees by HT granulite-facies metamorphism at lower pressures.

The primary eclogite facies mineral assemblage comprises garnet, sodium-rich clinopyroxene (up to $X_{Na\_M2} = 0.29$), kyanite, rutile and quartz. The rocks are characterized by compositional layering on the mm-scale, which is reflected by corresponding systematic variation of the compositions of garnet porphyroblasts. The garnets show homogeneous compositions in their internal domains defining plateaus, the compositional characteristics of which correlate with the compositional layering of the rocks and vary from Alm_{19} Prp_{55} Grs_{27} to $Alm_{15\text{-}18}$ $Prp_{42\text{-}50}$ $Grs_{32\text{-}43}$. The systematic variation of garnet compositions with the bulk rock compositional layering testifies to lack of equilibration on the mm scale during HP-HT eclogite-facies metamorphism.

The HT-granulite-facies overprint is evident from the breakdown of the eclogite facies mineral assemblage. This is evident, for example, from the formation of sapphirine–spinel–an-rich plagioclase symplectites in garnet supposedly replacing garnet-hosted kyanite and clinopyroxene inclusion. Another peculiar feature is represented by the partial resorption of garnet by plagioclase and clinopyroxene in the form of corrosion tubes penetrating the garnet in a worm-like fashion. Finally, garnet is partially or entirely replaced by plagioclase–spinel–orthopyroxene—clinopyroxene symplectite, where Grs-rich garnets are systematically more strongly affected by this replacement than Grs-poor garnets. Quartz is consumed during the decompression reactions and can only be found as rare relic grains. When relic quartz is surrounded by a clinopyroxene matrix, the clinopyroxene becomes successively more Si-rich due to inverse Tschermak substitution towards the relic quartz grain.

Throughout the samples and irrespective of the layer they pertain to, the garnets show similar pronounced secondary compositional zoning in the outermost 200 μm. The zoning is characterized by a strong decrease of the Grs content accompanied by an increase of the Alm and Prp contents towards the rim. The compositional changes in garnet are gradual suggesting diffusion-mediated re-equilibration at decreasing pressures, and the composition of the garnet at the interface to the rock matrix is the same throughout the specimen indicating that the rock equilibrated on the cm scale during the HT overprint.

Pressure and temperature were estimated on the basis of equilibrium phase diagrams. They indicate peak pressures above 1.8 GPa and temperatures of around 1000 °C for the primary mineral assemblages and the different garnet cores. In accordance with peak P-T, the garnet rims indicate pressures of around 1.2 GPa with the same temperature.

Considering the regional metamorphic setting of the Moldanubian Zone, the relatively localized secondary chemical zoning of garnet at its rim indicates that the granulite-facies metamorphism was remarkably short-lived and suggests rapid transport of the mafic-ultramafic lithologies from mantle depths to the mid-crustal level. Very likely incorporation of the relatively hot mafic lens into a supposedly cooler dominantly felsic environment led to immediate cooling of the mafic lens.

The position of vanadium in the crystal structure of zoisite, a variety tanzanite

P. Bačík[1,2], M. Wildner[3], J. Cempírek[4], R. Škoda[4], P. Cibula[1], T. Vaculovič[5]

[1]Comenius University in Bratislava, Faculty of Natural Sciences,
Department of Mineralogy, Petrology and Economic Geology, Ilkovičova 6, 842 15 Bratislava, Slovak Republic
[2]Earth Science Institute of the Slovak Academy of Science,
Dúbravská cesta 9, 84005 Bratislava, Slovak Republic
[3]Institut für Mineralogie und Kristallographie, Geozentrum, Universität Wien,
Josef-Holaubek-Platz 2, 1090 Wien, Austria
[4]Masaryk University, Department of Geological Sciences, Kotlářská 2, 61137 Brno, Czech Republic
[5]Department of Chemistry, Faculty of Science, Masaryk University, Kamenice 5, Brno 62500, Czech Republic
e-mail: peter.bacik@uniba.sk

Tanzanite is the most valued gemmological variety of zoisite in which V is the dominant trace element and chromophore. However, the exact position and state of V in the zoisite structure are quite enigmatic and subject to many hypotheses based mainly on spectroscopic evidence but lacking any definite structural proof. Therefore, we combined a structure refinement with optical absorption spectroscopy and used two separate theoretical approaches to shed some light on this enigma.

Structure refinement of the zoisite–tanzanite structure did not provide sufficient evidence of the V location in the zoisite structure due to the small V content in tanzanite as evidenced by Electron-Probe Micro-Analysis and Laser-Ablation Inductively Coupled Plasma Mass Spectrometry. Structure refinement of the studied sample revealed an average bond length of the less distorted $M1,2O_6$ octahedron lower than 1.90 Å. At the same time, $M3O_6$ has slightly longer bonds with an average of ca. 1.96 Å. The *M*1,2 site has a slightly higher bond valence sum (BVS) of 3.03 vu, whereas BVS of *M*3 is significantly lower (2.78 vu).

Optical absorption spectra of the studied sample with measured bands at 13 160, ~15 500, 16 350, 16 700, 18 800, 26 120, 26 650, and 34 000 (?) cm^{-1} revealed that most V is trivalent with only a small portion likely in a four-valent state. Therefore, a crystal-field superposition-model and bond-valence model calculations were applied here with two necessary basic assumptions: (1) V is at octahedral sites; (2) it can be present in two oxidation states, V^{3+} or V^{4+}. Crystal field superposition model calculations made to interpret the optical spectra indicated that V^{3+} prefers occupying the *M*1,2 site; the preference of V^{4+} was impossible to determine from the present data.

Bond-valence model calculations showed no unambiguous preference for V^{3+}, although based on the simple bond-length calculation, the preference of the *M*3-site could be suggested. In contrast, it is quite straightforward to assume that the *M*1,2 site has a more natural environment for V^{4+}. However, if the calculated octahedral distortions are taken into account, the $M1,2O_6$ octahedron shows a smaller change in distortion if occupied by V^{3+} than the $M3O_6$ octahedron.

Consequently, based on both the crystal field superposition model and bond-valence model calculations, it can be concluded that both V^{3+} and V^{4+} prefer the *M*1,2 site.

"Gold" hydrogen in natural fluid inclusions

R. J. Bakker

Resource Mineralogy, Department Applied Geoscience and Geophysics, Montanuniversity Leoben, Austria
e-mail: bakker@unileoben.ac.at

Fluid inclusions in minerals are natural storage vessels of fluids. The most common fluids that are preserved in inclusions are mixtures of water, carbon-dioxide and salts. In reduced geological environments gases such as methane (and other thermogenic alkanes, also known as "abiotic"), nitrogen, and hydrogen may be included. The present study gives some new results on the occurrence of hydrogen in natural fluid inclusions in specific geological settings.

Hydrogen is a highly volatile gas component that is not assumed to retain within the crust and mantle for a long period, but is continuously outgassed. Several natural seeps of hydrogen-rich fluids are already considered for exploration (so-called "gold" hydrogen). This hydrogen may be captured within fluid inclusions in environments with sufficient concentrations. Both seeps and fluid inclusions are aspects of the existence of a hydrogen-rich fluid that may circulate in rock. The latter may also provide information on hydrogen-rich flows in the geological past, because inclusions may preserve paleo fluid properties.

There are only few studies that mention the existence of hydrogen within fluid inclusions, that provide abundant speculative models of the origin of hydrogen within rock, usually with a lack of sufficient and relevant data. For example, both serpentinization and de-serpentinization were considered as formation processes of hydrogen. Redox conditions in rock are the main factors that define the composition of a fluid phase in deep rock, that only occupy a minor volume fraction of the system. This fluid is buffered by the coexistence of solid phases within the rock. Highly reduced conditions are common within mantle rock. Methane is closely related to the occurrence of hydrogen as both represent these reduced conditions. Similar conditions exist in Si-undersaturation igneous environments (e.g. nepheline syenite). An alternative source of hydrogen is radiolysis, but this is not sufficiently supported by fluid inclusion studies.

Hydrogen-rich fluid inclusions are analysed in three different geological settings: 1. In Upper Cretaceous strongly serpentinized mantle rock (Troodos, Cyprus); 2. In Neogene pegmatites closely related to serpentinite host-rock from metamorphosed ophiolitic-sedimentary tectonic units (Elba, Italy) (Bakker & Schilli, 2016); 3. In Mesoproterozoic metasediments of the Mt Painter Inlier, Arkaroola (Australia) (Bakker & Elburg, 2006)

Inclusions in pyroxene in strongly serpentinized areas in Troodos contain mixtures of CH_4, H_2 and H_2O (Fig. 1). Similar fluids are observed in chromite in mantle rock that is hardly affected by serpentinization (McElduff, 1989).

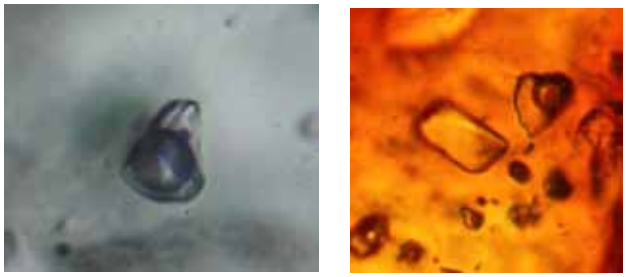

Figure 1. Fluid inclusions (ca. 10 μm) in pyroxene (left) and chromite (right).
The vapour phase is highly enriched in H_2.

Fluid inclusions in pegmatites from Elba represent a complex interaction between magmatic and metamorphic fluids. Multiple pulses of low salinity H_2O-rich magmatic and reduced metamorphic fluid stages are recorded. Magmatic fluids are characterized by the presence of minor amounts of CO_2 and H_3BO_3, whereas the metamorphic fluids contain CH_4 and H_2 (minor N_2, H_2S, and C_2H_6) that may origin from the input of more reduced fluids from serpentinites, that may completely replace the magmatic fluid. H_2-rich fluid inclusions were observed in andalusite, quartz, plagioclase, and tourmaline.

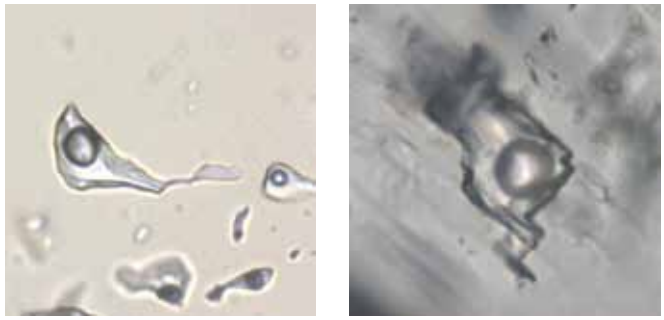

Figure 2. Fluid inclusions (ca. 20 µm) in quartz (left) and plagioclase (right) (Bakker & Schilli, 2016). The vapour phase is a mixture of mainly H_2 and CH_4.

A massive hydrothermal event in Arkaroola is demonstrated by an epithermal hematite-quartz assemblage, bladed calcite, and fluorite (Fig. 3). Fluid inclusions in fluorite contain a mixture of H_2O and H_2. The hydrogen occurs preferentially within the purple fluorite, which also includes some uranium mineralizations (radiation damage centres). These mineralizations are also proposed to be responsible for defining the colour of fluorite from green to purple that grew contemporaneously with the late hydrothermal quartz–hematite mineralization. The origin of hydrogen in fluid inclusions in fluorite is suggested to be radiolysis.

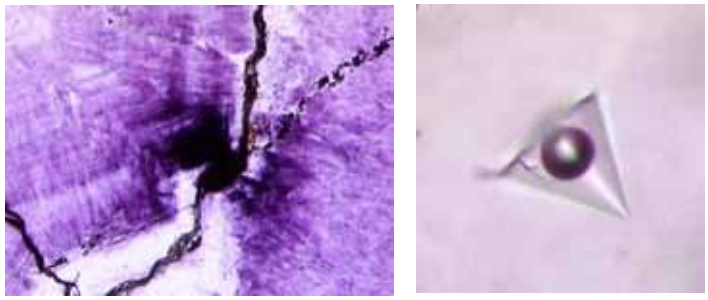

Figure 3. Purple fluorite with radiation damage centres (left), and H_2-rich fluid inclusions, ca. 10 µm (right) (Bakker & Elburg, 2006). Left image has a length of 200 µm.

Diffusion of hydrogen is a common aspect to explain the absence of hydrogen in most rock, even in environments where hydrogen is assumed to be a major fluid component. The examples illustrate that hydrogen may be preserved within fluid inclusions, similar to most fluid components.

Bakker RJ, Elburg MA (2006): A magmatic-hydrothermal transition in Arkaroola (northern Flinders Ranges, South Australia): from diopside-titanite pegmatites to hematite-quartz growth. - Contrib Mineral Petrol 152, 541

Bakker RJ, Schilli SE (2016): Formation conditions of leucogranite dykes and aplite-pegmatite dykes in the eastern Mt. Capanne plutonic complex (Elba, Italy): fluid inclusion studies in quartz, tourmaline, andalusite and plagioclase. - Mineral Petrol 110, 43

McElduff, B (1989): Inclusions in chromite from Troodos (Cyprus) and their petrological significance. - Ph.D. Thesis, Montanuniversität Leoben, Austria

Zircon uses baddeleyite nanoparticles as fundamental building blocks

C. Ballhaus[1], H. Helmy[2], R. Wirth[3], V. Roddatis[3], T. Nagel[4], A. Schreiber[3]

[1]Universität Bonn, Germany
[2]Minia University, Egypt
[3]GFZ Potsdam, Germany
[4]Bergakademie Freiberg, Germany
e-mail: ballhaus@uni-bonn.de

Numerous experiments have been performed in the past to determine the crystallization temperature of zircon from silicate melts (Watson & Harrison 1983; Boehnke et al. 2013; Gervasoni et al. 2016; Borisov & Aranovich 2019; Marxer & Ulmer 2019). In designing those experiments, the implicit assumption was that zircon is a primary magmatic phase that crystallizes directly from the melt. Factors that determine the saturation of zircon are the Zr^{4+} (or ZrO_2) content of the melt, its silica activity ($aSiO_2$), and the cation ratio M = (Na + K + 2Ca) / (AI * Si) (Watson & Harrison 1983). The latter parameter roughly reflects the polymerization degree of a melt.

Our experiments give a somewhat different picture. We performed experiments with a phonolite composition that is modeled on a ne-normative pumice of the Laacher See, Eifel. The composition contains 60.6 SiO_2, 20.1 Al_2O_3, 2.5 FeO and CaO each, MgO 0.5, and total alkalies of 12.5 (all in wt.%). It is just corundum-normative. To prevent the introduction of zircon seeds, a synthetic aliquot of oxides and carbonates (Ca, alkalies) was synthesized. After the sample was sintered at 950 °C and CO_2 was expelled, Zr was added as $ZrCl_2O$ ICP standard solution. The mixture was then equilibrated at 1200 °C and 300 MPa in a piston cylinder press for 2 to 24 hours. After completion of the experiments, the Zr contents of the glasses were 1300 ± 160 ppm (average ± 1σ of 20 EPMA analyses).

Liquidus phases at 1200 °C were silicate melt and corundum (crn). Zircon did not crystallize because the composition is undersaturated with respect to zircon by factor of 10 (Fig. 1). Four Focussed Ion Beam (FIB) sections cut from experimental glasses showed that all charges crystallized at 1200 °C crystalline (and possibly amorphous) ZrO_2 nanophases (baddeleyite) (Fig. 2). The smallest and earliest ZrO_2 nanoparticles are found as inclusions in crn. These nanophases are as small as 3 to 4 nm and comprise perhaps 500 unit cells. They are so small because their growth was arrested after they were trapped by crn.

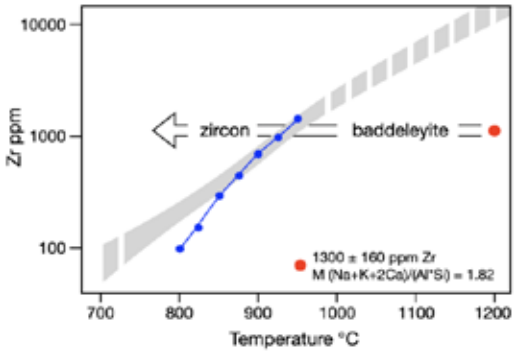

Figure 1. Starting mix with 1300 ± 160 ppm Zr - red circle. Grey - region in Zr-temperature space where magmatic zircon is stabilised (Watson & Harrison 1983; Boehnke et al. 2013; Gervasoni et al. 2016; Borisov & Aranovich, 2019). Blue symbols - zircon satutation experiments by Marxer & Ulmer (2019). For our composition zircon is expected to become stable at ~ 900 °C.

The results imply that zircon uses nanometer-sized ZrO_2 particles as building blocks when it nucleates from silicate melt. Zircon is stabilized by the reaction ZrO_2 (nanoparticle) + SiO_2 (melt) → $ZrSiO_4$ (crystal). We think that in nature this reaction is a solution-precipitation reaction. Direct crystallization of zircon from Zr^{4+} and SiO_2, if it indeed occurs, may be the exception rather than the rule. We assume that the ZrO_2 nanoparticles illustrated in Fig. 2 are stable, that they nucleated in local ΔG minima.

Many igneous rocks undersaturated with zircon may carry baddeleyite (e.g., Heaman & LeCheminant 1993). However, because baddeleyite tends to be extremely small, its presence is easily overlooked.

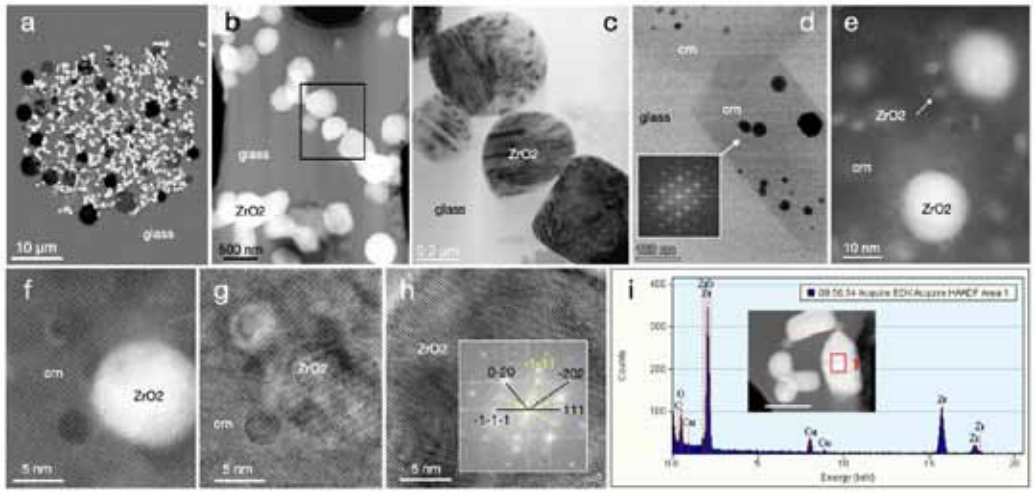

Fig. 2. ZrO_2 nanoparticles. (a) Baddeleyite (bdy) cluster in glass, after 10 hours at 1200 °C, in (b) TEM image at higher magnification; note tendency of bdy to attach and align to clusters and chains. (c) Brightfield (BF) image of twinned bdy in glass. (d) ZrO_2 nanoparticles trapped by liquidus corundum (crn). (e) HAADF image of ZrO_2 nanoparticles < 4 nm, in crn. (f) and (g) HAADF images, ZrO_2 nanoparticles in crn. (h) FFT of HREM, ZrO_2 in crn (crn in yellow). (i) Energy-dispersive spectrum to illustrate composition of bdy.

Boehnke P, Watson EB, Trail D, Harrison TM, Schmitt AK (2013): Zircon saturation re-revisited. - Chem Geol 351, 324–334

Borisov A, Aranovich L (2019): Zircon solubility in silicate melts: New experiments and probability of zircon crystallization in deeply evolved basic melts. - Chem Geol 510, 103-112

Gervasoni F, Klemme S, Rocha-Júnior ERV, Berndt J (2016): Contr Mineral Petrol 171, 21, DOI 10.1007/s00410-016-1227-y

Heaman LM, LeCheminant AN (1993): Paragenesis and U-Pb systematics of baddeleyite (ZrO_2). - Chem Geol 110, 95-126

Marxer F, Ulmer P (2019): Crystallisation and zircon saturation of calc-alkaline tonalite from the Adamello Batholith at upper crustal conditions: an experimental study. - Contr Mineral Petrol, https://doi.org/10.1007/s00410-019-1619-x

Watson EB, Harrison TM (1983): Zircon saturation revisited: temperature and composition effects in a variety of crustal magma types. - Earth Planet Sci Letters 64, 295-304

Unearthing genetic insights through a multi-method geochemical approach of the sediment-hosted Cu-Co Dolostone Ore Formation deposit, Namibia

V. Bertrandsson Erlandsson[1*], R. Ellmies[2], F. Melcher[1]

[1]Montanuniversität Leoben, Leoben, Austria
[2]Gecko Namibia, Swakopmund, Namibia
e-mail: viktor.erlandsson@unileoben.ac.at

The sediment-hosted Cu-Co-Zn Dolostone Ore Formation (DOF) deposit is a recently discovered Cu-Co-Zn mineralization in the Kunene region of northwestern Namibia and is the first recognized Co mineralization in Namibia (Ellmies 2018). Understanding the geological formation processes responsible for Co deposits is vital due to the ever-increasing demand of Co for modern high-tech and green technologies (Alves Dias et al. 2018). As sediment-hosted Cu-Co deposits from the Central African Copperbelt are responsible for ca. 70% of global Co supplies (USGS 2020), the DOF deposit could prove to be a valuable asset for future Co production, especially as the DOF is situated in analogous stratigraphic and tectonic settings to the Co deposits of the Central African Copperbelt (Miller 2013; Bertrandsson Erlandsson et al. 2022). This study applies an array of geochemical methods to constrain genetic aspects of the DOF deposit, with the aim of better the understanding of sediment-hosted Cu-Co deposits.

Hosted in calcareous siltstones and argillites of the Ombombo Subgroup, which is part of the Neoproterozoic Damara Supergroup, the DOF is expressed as a horizon with a bell curve-like Cu-Co-Zn distribution. The highest metal (in particular Co) enrichment is referred to as the "Main DOF horizon", whilst the extended Cu-Zn enrichment is called the "Wider DOF horizon" (Fig. 1). The sulfide mineralogy is relatively simple, with predominantly pyrite, pyrrhotite, chalcopyrite, sphalerite, linnaeite, and subordinate amounts of cobaltpentlandite and galena. Sulfides occur in six types of mineralization styles: disseminated, nodules, clusters, veins, pressure shadows, and "Events". Events are a term coined by the exploration company Gecko Namibia and refer to vein-like structures that portray both ductile and brittle deformation. (Bertrandsson Erlandsson et al. 2022).

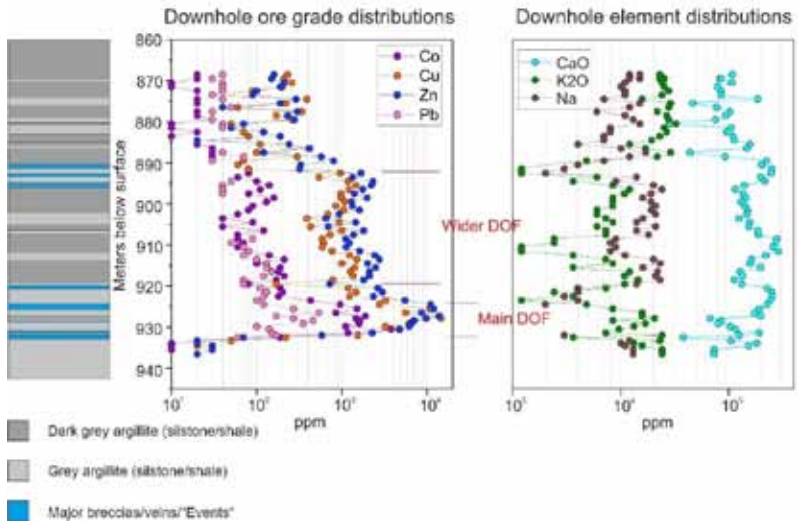

Figure 1. Simple drill core log from one of the studied DOF boreholes, with additional exploration assay data of selected elements, shown besides the drill core log.

Laser ablation inductively coupled mass spectrometry (LA-ICP-MS) analyses of sulfides from the six different mineralization styles reveal two main populations; disseminated, nodule, cluster, and Event sulfides group together (Group 1), whilst Group 2 comprises vein- and pressure shadow-hosted sulfides (Bertrandsson Erlandsson et al. 2022). The Ga-Ge-In-Mn-Fe in sphalerite geothermometer (Frenzel et al. 2016) indicates that the DOF mineralization formed at temperatures >310 °C, which suggests that they formed during regional metamorphism of the Damara Orogeny. Group 2 sulfides seem to have formed at relatively lower temperatures. This together with petrographic observations indicates that Group 2 sulfides (veins and pressure shadows) formed during a late orogenic stage of the Damara Orogeny (Bertrandsson Erlandsson et al. 2022). This interpretation is also supported by ore-associated hydrothermal monazite ages.

Petrographic evidence shows that Group 1 sulfides did not all form at once, but rather through several progressive stages. Cobalt is believed to have been initially hosted in pyrite, which was later remobilized due to changes in oxygen and/or sulfur fugacity to first form cobaltpentlandite and eventually linnaeite. It was after this that Group 1 sphalerite and chalcopyrite precipitated, partially overgrowing the preexisting sulfides. This resulted in extremely Co-rich sphalerite (>1 wt%). Atom probe tomography of this extremely Co-rich sphalerite revealed that the Co^{2+} occurs through direct substitution of Zn^{2+} (Bertrandsson Erlandsson et al. 2023).

Trace element comparison of DOF sulfides to other sediment-hosted Cu(-Co) metallogenic districts (i.e., the Polish Kupferschiefer and the Central African Copperbelt) by Random Forest and Factor analyses indicate that sulfide trace element composition is heavily host basin dependent and that local metal sources dictate the sulfide composition (Bertrandsson Erlandsson et al. *in review*).

Alves Dias P, Blagoeva D, Pavel C, Arvanitidis N (2018): Cobalt: demand-supply balances in the transition to electric mobility. - Publications Office of the EU 10, p. 97710

Bertrandsson Erlandsson V, Foltyn,K, Muchez P, Rantitsch G, Ellmies R, Melcher F (in review). Sulfide geochemistry in sediment-hosted Cu(-Co) metallogenic districts: LA-ICP-MS analyses of chalcopyrite, sphalerite, and pyrite. - Mineral Dep (*in review*)

Bertrandsson Erlandsson V, Gopon P, Waldl H, Misch D, Ellmies R, Melcher F (2023): Sphalerite as a non-traditional critical metal source: Correlative microscopy (EPMA, EBSD, and APT) of cobalt-enriched sulfides from the sediment-hosted copper-cobalt Dolostone Ore Formation deposit, Namibia. - Front Earth Sci, 10.3389/feart.2023.1171859

Bertrandsson Erlandsson V, Wallner D, Ellmies R, Raith JG, Melcher F (2022): Trace element composition of base metal sulfides from the sediment-hosted Dolostone Ore Formation (DOF) Cu-Co deposit in northwestern Namibia: Implications for ore genesis. - Jour Geoch Expl 243, 107105

Ellmies R (2018): Extensive stratiform Cu-Co-mineralisation at Okondaurie, Kunene Region. - Internal Report, Kunene Resources (Pty) Ltd. (unpublished)

Frenzel M, Hirsch T, Gutzmer J (2016): Gallium, germanium, indium, and other trace and minor elements in sphalerite as a function of deposit type—A meta-analysis. - Ore Geo Revs 76, 52–78

Miller R (2013): Comparative Stratigraphic and Geochronological Evolution of the Northern Damara Supergroup in Namibia and the Katanga Supergroup in the Lufilian Arc of Central Africa. - Geosci Canad 40, Article 2, 118–140

USGS (2020): Mineral commodity summaries 2020, DOI: 10.3133/mcs2020

$CaCO_3$ precipitation in drainage systems of subsurface infrastructure – Monitoring approaches and crystal growth control

R. Boch[1], M. Pettauer[1], S. Eichinger[2], A. Leis[3], H. Wagner[2], M. Dietzel[1]

[1]Graz University of Technology, Institute of Applied Geosciences
[2]ÖBB Infrastruktur AG, SAE, FB Bautechnik-Tunnelbau
[3]JR-AquaConSol GmbH
e-mail: ronny.boch@tugraz.at

Methodological approaches and enhanced process understanding interconnecting fundamental research with (geo)technical settings and problems benefit from each other regarding the calcium carbonate chemical system (cf. Boch 2020). The effective draining of subsurface infrastructure is frequently faced with unwanted mineral precipitation (Fig. 1A) based on elevated mineral and gas contents of the discharging groundwater being of high relevance for cleaning downtimes and maintenance of the infrastructure (Eichinger et al. 2020). Owing to regional geology in Austria (limestones, calcareous contents) and construction materials used in subsurface infrastructure (concrete, mortar), carbonate deposits consisting of various $CaCO_3$ polymorphs and accessory constituents are most abundant in the drainage systems (Fig. 1B) next to iron precipitates and interacting biomass (bacterial biofilms).

In the context of existing subsurface infrastructure (e.g. Semmering highway tunnels) and new excavations (e.g. Koralmtunnel) the recent years strongly increased the understanding of critical processes based on in-situ monitoring campaigns as well as related laboratory analyses and computer modelling. The drainage system and maintenance strategies were adapted based on the implementation of an underground "sinter test track" (Fig. 1C) and local test fields with typical construction materials but different constructive designs (Wedenig et al. 2022). The on-site and online application of sensors/data loggers and mobile instrumentation in combination with sample analyses provided new insights to water-gas-mineral-biology-substrate interaction and to the major controls of calcium carbonate precipitation.

An approach to systematically influence the nucleation and crystal growth of the unwanted deposits consists in the application of specific chemical additives ("green inhibitors") to the ground-/drainage waters. In laboratory and field tests various substances (e.g. polyaspartic acid) and concentrations were investigated and a new test procedure was developed (Wedenig et al. 2021). This resulted in new insights concerning relevant parameters such as $CaCO_3$ supersaturation, pCO_2, Mg/Ca and water flow conditions in relation to mineralogy (polymorphism; Fig. 1D), crystal shapes/sizes, substrate effects (e.g. different plastic types) and further regarding proactive controls on fabrics and material consistency (hardness) of the deposits.

Figure 1. Diverse mineral precipitates (A) in the course of continuous groundwater discharge underground can block a tunnel drainage system (B) and were investigated by in-situ field tests (C) targeting an increased process understanding of the precipitation conditions (e.g. D: $CaCO_3$ polymorphism) as well as efficient countermeasures (e.g. optimized drainage design, addition of inhibitors).

Boch R (2020): Carbonates in natural and geotechnical settings – Chemical sediments as environmental archives. – Jb Geol.-BA 159, 67-130

Eichinger S, Boch R, Leis A, Koraimann G, Grengg C, Domberger G, Nachtnebel M, Schwab C, Dietzel M (2020): Scale deposits in tunnel drainage systems – A study on fabrics and formation mechanisms. – Science of the Total Environment 718, 137140

Wedenig M, Boch R, Leis A, Wagner H, Dietzel M (2021): Green inhibitor performance against $CaCO_3$ scaling: Rate-modeling aided test procedure. – Crystal Growth and Design 21, 4, 1959-1971

Wedenig M, Eichinger S, Boch R, Leis A, Wagner H, Dietzel M (2022): Understanding of tunnel drainage scale formation by in-situ monitoring. – Tunnelling and Underground Space Technology, 131(A43), 104853

Monazite stability as a tool used for identification of granite stacking (a case study from the Western Carpathians)

Igor Broska[1], Igor Petrík[1]

[1]Earth Science Institute Slovak Academy of Sciences, 840 05 Bratislava
e-mail: Igor.Broska@savba.sk

The presence of monazite or allanite in granites is not only an important aspect of assessing their parental rocks to the I- or S-type, but their mutual relationship can also help to estimate PTX conditions in a given magmatic system. In the Western Carpathians, allanite and monazite became an effective tool for discrimination Variscan granites in terms of their I- or S-types affinity, in addition to the bulk-rock granite composition (Petrík & Broska 1994). For the S-type granites, typical is a reduction paragenesis of accessory ilmenite, monazite and apatite with higher content of Mn (Mn in reduced bivalent form easily replaces Ca). On the other hand, the I-type granites were identified by the presence of allanite, higher content of apatite with a low Mn and Fe, titanomagnetite, phlogopite (Mg-biotite), titanite, late pure magnetite, and locally also amphibole indicating a higher oxidation stage in this magmatic system compared to the S-type. It probably reflects initially a higher water content manifested also by late or post-magmatic oxidation of titanomagnetite, biotite and allanite.

Primary magmatic monazite and allanite: In arc orogenic granites, such as the Western Carpathian granites the presence of monazite is determined by PTX conditions, where parameter X represents the content of CaO and the REE`s. At a higher ratio of CaO/REE in granite the allanite is stable (Gieré & Sorensen 2004; Janots et al. 2008; Spear 2010). The S-type granites, where the whole-rock CaO content greater than 2.5 wt % stabilises allanite can also produce a monazite due to local decrease of CaO activity, e.g. after massive crystallization of plagioclase which was at the beginning suppressed by higher water contents (Johannes and Holtz 1996). A relict allanite in such case, as a precursor of monazite, was documented in accessory paragenesis of granites from the Tribeč and the Malé Karpaty Mts. Alternatively, some Western Carpathian S-type granites, rich in the REEs, may also have changed early allanite for monazite due to a pressure drop whereby their PT path crosses the Aln/Mnz boundary and the parent granites were emplaced into upper part of the crust. Monazite in this sense represents a mineral whose dating can records the cooling time of the parental granite system.

Monazite breakdown to allanite and REE epidote: In the granites of the Alpine Tatric Unit, monazite is typically stable or only weakly altered, on the other hand (Fig. 1A), the granites from the higher Alpine nappes as the Fatric and Veporic units, show monazite breakdown forming coronas of the apatite and allanite (Fig. 1B). The monazite breakdown into apatite-allanite coronas is facilitated by the higher content of CaO, Al_2O_3, and LREE, and alkali-rich fluids (Budzyń et al. 2011). The monazite breakdown in metamorphic granites is illustrated by stability diagrams of monazite – allanite (Spear, 2010). In the case of the Western Carpathians in the Tribeč crystalline basement, the monazite breakdown in high CaO granites is predicted for the estimated pressure of ca 4 kbar at the temperature of about 450 °C due to crossing the monazite/allanite stability boundary by cooling along a near-isobaric PT trajectory (Broska et al. in prep.). Since an Alpine monazite has not been detected in these granites, the

breakdown of monazite has occurred due to prolonged residence in deeper parts of the Earth's crust achieving the isobaric trajectory. On the other hand, the non-altered monazite presented in the underlying Tatric granites in this Tribeč granite nappe system was preserved by the rapid ascent of granite into the upper crust, where the PT trajectory is close to isothermal. The rapid cooling here in the Tribeč field documents the shallow intrusion of the granites into phyllites.

Granite duplex: The undeformed S-type granites with unaltered monazite in the Tribeč Mts are found at deep part of the crystalline basement, i.e. these underlying granites are attributed to the Tatric Unit where unaltered monazite typically occursed. On the other hand, the granites from the higher, crest part of the mountain range, are metamorphosed and hydrothermally affected (altered) and contain monazite with breakdown coronas (Fig. 1B). Since both granite blocks, the upper metamorphic and the lower non-metamorphic, are similar in the age, the different monazite behaviour indicates existence of two different granite blocks. They had been originally at the time of generation during Variscan orogen at different crustal positions because otherwise they would not have shown different monazite responses. Moreover, the overlying granites with altered monazite are Alpine metamorphosed in PT conditions close to those known in the Veporic or Fatric unit but not high enough to produce a new Alpine monazite. Thus, in the present position of the Tribeč basement, there are two granite blocks one above the other, metamorphic block thrust on the non-metamorphic one. The stacking of the metamorphosed over non-metamorphosed block was flat and inclined to the northwest at an angle of about 20°, and in the present position represents an Alpine granite duplex. With altered granites Lower Triassic quartzites of the Lúžna formation were probably also moved, from which Uher et al. (2009) described a hydrothermal vein mineralization associated with fluids from the underlying granites forming in quartzites spectacular lazulite. The age of granite stacking is indicated by Ar/Ar age from muscovite of the overlying granites and it gives the age of 78 Ma. It postdates the stacking, since the dated muscovites have not been deformed. The identification of Tribeč granite alpine duplex can be considered as an example of the use of monazite stability for solving of geodynamic events.

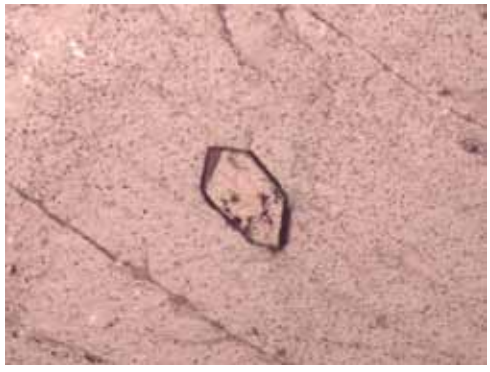

Fig 1A Stable monazite from low a CaO S-type granite; Nízke Tatry Mts, Tatric Unit. (Photo: I. Petrík, polarised light, lengths of monazite crystal is ca 300 μm).

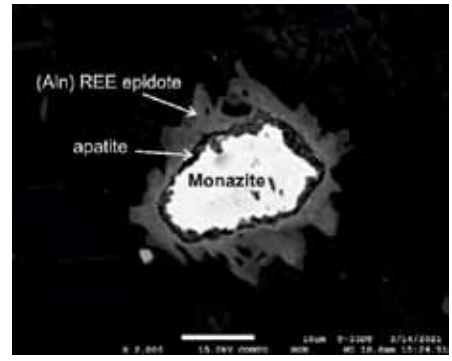

Fig. 1B Monazite breakdown into coronas of apatite and allanite in the S-type granite (Tribeč Mts. Fatric Unit). BSE image.

Acknowledgement: Authors thank to project VEGA 75/20 for financial support.

Budzyn B, Harlov D, Williams ML, Jercinivic MJ (2011): Experimental determination of stability relations between monazite, fluorapatite, allanite, and REE-epidote as a function of pressure, temperature, and fluid composition. - Amer Miner 96, 1547–1567

Giieré R, Sorensen SS (2004): Allanite and other REE-rich epidote-group minerals. In: Liebscher A, Franz G (eds): Epidotes. - Rev Miner Geochem 56, 431-493, http://dx.doi.org/10.2138/gsrmg.56.1.431

Janots E, Engi M, Berger A, Allanz J, Schwarz J-O, Spandler C. (2008): Prograde metamorphic sequence of REE-minerals in pelitic rocks of the Central Alps: implications for allanite-monazite-xenotime phase relations from 250 to 610 °C. - J Metamorphic Geol 26, 509-526

Petrík I, Broska I (1994): Petrology of two granite types from the Tribeč Mts., Western Carpathians: an example of allanite-magnetite vs. monazite-ilmenite dichotomy. - Geol J 29, 59-78, https://doi.org/10.1002/gj.3350290106.

Uher P, Mikuš T, Milovský R, Biroň A, Spišiak J, Lipka J, Jahn J (2009): Lazulite and Ba, Sr, Ca, K-rich phosphates-sulphates in quartz veins from metaquartzites of Tribeč Mountaions, Western Carpathians, Slovakia: Compositional variations and evolution. - Lithos 112, 447-460

Spear FS (2010): Monazite-allanite phase relations in metapelites. - Chem Geol 279, 55-62

Do chromium isotope compositions record signs of oxygenation in the Campbellrand-Malmani Platform (2.56 to 2.52 Ga, South Africa)?

S. Bruggmann[1], C. Thomazo[2], J. Marin Carbonne[1], S. Jaccard[1]

[1]University of Lausanne
[2]University of Burgundy
e-mail: sylvie.bruggmann@unil.ch

The oxygenation history of Earth's surface remains a highly investigated topic, with an increasing number of studies indicating a dynamic change from anoxic to oxic conditions in the Precambrian. The Campbellrand-Malmani platform (Transvaal Supergroup, South Africa) was deposited in a shallow marine environment between 2.56 and 2.52 Ga (Sumner and Grotzinger 2004), just before the Great Oxidation Event. The sedimentary rocks hold a large variety of stromatolites, which can produce oxygen through photosynthetic cyanobacteria. While some studies find indications of oxygen production (e.g., Czaja et al. 2012), post-depositional alteration can challenge interpretations of data from non-traditional isotope systems.

We present Cr isotope compositions ($\delta^{53}Cr$) and concentration data (trace metals) in sedimentary rocks from the Campbellrand-Malmani platform to better constrain the robustness of the Cr isotope system to post-depositional changes. Preliminary results show that even though the detrital contribution is low, most dolostone and chert samples show $\delta^{53}Cr$ values of around -0.12 ± 0.10 ‰ (2SD, n = 14) and are thus similar to the detrital $\delta^{53}Cr$ value. Only two samples fall off the detrital value, with one dolostones sample showing a positive $\delta^{53}Cr$ value of 0.26 ± 0.05 ‰ (2SE).

Our preliminary results indicate that many of the $\delta^{53}Cr$ values in the studied dolostones and cherts were overprinted by post-depositional processes. With the aid of additional isotope (S, N isotope compositions) and auxiliary data (trace metals), we seek to characterise the drivers of the observed $\delta^{53}Cr$ values.

Czaja A, Johnson M, Roden E, Beard B, Voegelin A, Nägler T, Beukes N, Wille M (2012): Evidence from free oxygen in the Neoarchean ocean based on coupled iron-molybdenum isotope fractionation. – Geochim Cosmochim Acta 86, 118-137

Sumner D, Grotzinger J (2004): Implications for Neoarchean ocean chemistry from primary carbonate mineralogy of the Campbellrand-Malmani Platform, South Africa. – Sedimentology 51, 1273-1299

Mineralogical control of synergetic thallium and antimony weathering

T. Đorđević[1,2], M. Stöger-Pollach[1]

[1]University Service Centre for TEM, Technische Universität Wien, Wiedner Hauptstraße 8-10, Wien, Austria
[2]Institut für Mineralogie und Kristallographie, Universität Wien, Josef-Holaubek-Platz 2, Wien, Austria
e-mail: tamara.dordevic@tuwien.ac.at

As metals and metalloids have a strong impact on the environment, methods for their detection and speciation have received a particular attention in the last few years. Thallium (Tl), antimony (Sb) and arsenic (As) are important examples of such toxic elements. Their speciation is of the particular interest owing to their toxicity, bioavailability and reactivity. One of the world most famous deposit hosting all these three elements is Sb-As-Tl-Au Allchar deposit in North Macedonia, which mining waste dumps and technosoils served us as an ideal natural laboratory for the investigations of the oxidative processes on the primary sulfide and sulfosalt minerals. Of the particular interest were the weathering processes in the Sb-rich (Sb: 1000–16500 ppm) central part of the deposit, where Tl-concentrations have been measured in the range between 120-840 ppm (Đorđević et al. 2021).

In the scope of our previous study (Đorđević et al. 2021) we have identified primary and secondary mineralogy of the technosoils in the central part of Allchar deposit. As the main primary Tl-sources we have identified sulfosalts fangite, lorándite and pierrotite. Tl dissolved during weathering under circumneutral conditions is reprecipitated as avicennite and as tiny, fibrous Tl-bearing Mn oxides (up to 8.5 at.% of Tl). Furthermore, tiny spherulitic aggregates (up to 3 μm) of a Tl-Sb-oxide (unknown mineral species) have been found intergrown with quartz, muscovite and minor dolomite. Due to their small aggregate size, we have not been able to closer identify these oxides. Therefore, we have decided to take a closer look at these phases using transmission electron microscopy (TEM). The TEM-lamellae were prepared by means of focused ion beam (FIB) and were investigated under cryogenic condition (–184 °C) using high-resolution scanning transmission microscopy (HR-STEM) coupled with electron dispersive spectroscopy (EDS) and electron backscatter diffraction (EBSD). Just after a short electron exposure, Tl_2O_3 crystals in the size up to 100 nm formed on the surfaces of the Tl-Sb-oxides. EBSD on Tl-Sb-oxide particles confirmed that the Tl-Sb-oxide is crystalline and the EDS-line and area scans confirmed Tl:Sb ratio of 2.5, meaning that Tl enters the crystal structure of the new Tl-Sb oxides and is not hosted as the nanophase.

Both nano- and microcrystalline Tl-minerals are important products of oxidative weathering of Tl-bearing metal-sulphides. Our future study focused on the formation and dissolution of these phases will provide a much deeper insight into the mechanisms of formation of specific mineral association and will help to interpret common features in the alteration paths in general.

This work was supported by the Austrian Science Fund (FWF) [grant number P 36828-N to T. Đorđević]

Đorđević T, Kolitsch U, Drahota P, Majzlan J, Peřestá M, Serafimovski T, Tasev G, Boev I, Boev B (2021): Tl sequestration in the middle part of the Allchar Sb–As–Tl–Au deposit, North Macedonia. - Goldschmidt Virtual Conference, Abstracts, Lyon, France, 4–9 July 2021

Josef Zemann (25. Mai 1923 – 16. Oktober 2022)

H.S. Effenberger[1], R. Miletich[1]

[1]Institut für Mineralogie und Kristallographie, Universität Wien
herta.silvia.effenberger@univie.ac.at

The MinWien2023 meeting is dedicated to Josef Zemann. He was teacher, mentor, colleague, and friend to many colleagues in Vienna but also all over the world. Josef Zemann was born in Vienna on 25 May, 1923, a time of economic uncertainties and social instabilities. His scientific career started with the doctoral thesis entitled "*Über die Struktur des Pharmakosiderits*", for which he received the academic degree *doctor philosophiae* on 17 July, 1946.

Inspired by crystallography, Josef Zemann stayed for one year at the Massachusetts Institute of Technology in Boston with Martin J. Bürger, one of the pioneers of X-ray crystallography. Quite shortly after his return to Vienna, he became associate professor and some years later full professor at the "Mineralogisch-Kristallographisches Institut" at the Georg-August-Universität in Göttingen. During this time Josef Zemann focussed primarily on topics in crystal chemistry, such as the stereochemistry of Li, Cu and Te atoms, electrostatic lattice energies, as well as crystal absorption spectra in the infrared range. His years in Göttingen constituted a fulfilled time, thanks to the great working conditions and an academically inspiring atmosphere. In 1967 he responded to the call to move to the University of Vienna and succeeded his former teacher Prof. Dr. Karl Ludwig Felix Machatschki. As the head the Institut für Mineralogie und Kristallographie at the Alma Mater Rudolfina - Universität Wien for 22 years until his retirement in 1989 he was scientifically active and an internationally recocknised expert in the field of mineralogical crystallography.

Josef Zemann's early work in Vienna, Bosten, and Göttingen was dedicated to the determination of crystal structures by X-ray diffraction. His interest was the recognition of the stereochemistry of cations, especially of Cu^{2+} and Te^{4+} ions that were basically unexplored at that time. In recognition of his research on the stereochemistry of Te^{4+} ions, a novel tellurite mineral was named after him, i.e. zemannite, $[Zn^{2+}Fe^{3+}(TeO_3)_3]_2[Mg(H_2O)_6{\cdot}nH_2O]$, $n \leq 3$. (Fig. 1).

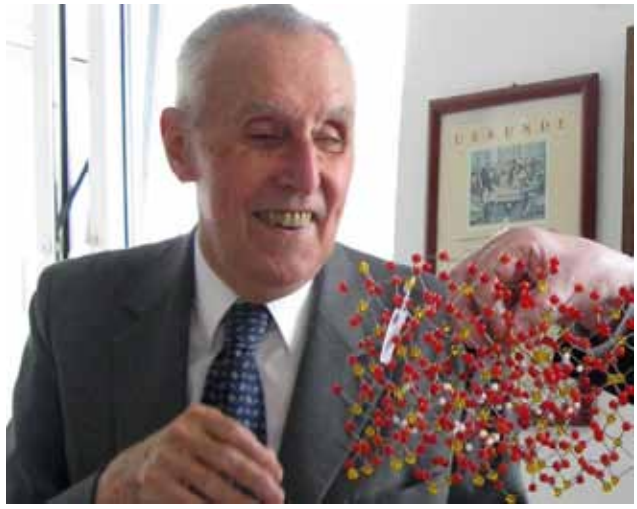

Figure 1. On the occasion of his 85th birthday in 2008 Josef Zemann receives a ball-and-stick model of the crystal structure of his mineral zemannite.
Foto: Kurt Mereiter

Among the milestones of his scientific work were infrared spectroscopic studies, were he tread new conceptual and methodological ground. At one hand he used polarized IR radiation and crystallographically oriented crystal platelets to localize hydrogen bonds associated with OH^- groups or H_2O molecules. At that time, it was practically impossible to localize H atom positions by means of X-ray diffraction techniques. Achievements in applying IR spectroscopy were groundbreaking as he recognized for the first time small amounts of hydroxyl groups to be detectable even in nominally anhydrous rock-forming silicates such as in olivine, andalusite, the three TiO_2 modifications, or in enstatite. Even here he was able to localise the orientation of the OH^- dipols in relation to the crystallographic orientation of the mineral samples and consequently to the atomic arrangement. In addition, it was also possible to discriminate between liquid inclusions and structurally oriented hydroxyl groups incorporated in the crystal lattice. The strong interaction between the IR radiation and the OH^--dipoles allow to detect concentrations in the tenth weight-percent range. In the 1960s it was doubtless assumed that the Earth's mantle does not contain any OH^- or H_2O contents. Today, it is estimated that due to the solubility in the above-mentioned minerals large quantities of OH^- and H_2O are stored in the upper 660 km of the Earth's mantle corresponding to the volume to the Earth's oceans.

Josef Zemann's broad scientific œuvre is supplemented by a series of papers dealing with the crystal chemistry of carbonates, focussing on both the structure types, their topological relations, as well as on the aplanarity of carbonate groups. The calculation of electrostatic lattice energies was a first step towards a modern atomistic modelling and the stability of structure types.

The significance of Josef Zemann's academic work and his reputation within the scientific community was honoured by a large number of honours and awards. He became honorary member of six National Mineralogical Societies (America, Austria, Soviet Union, Poland, Germany, and Romania). The ÖMG appointed him to their Honorary President. He received also numerous awards and medals: the Gustav-von-Tschermak-Seysenegg and the Erwin-Schrödinger medals (both from the Austrian Academy of Science), silver medals (the Abraham-Gottlob-Werner-Medal from the DMG and from the Masaryk University Bruno), a gold medal (Comenius University Bratislava), the Emanuel Bořicky Medal (Karlsuniversität Praha), and he became correspondent of the Geologische Bundesanstalt Wien.

Furthermore, his remarkable contribution to crystal chemistry and his input to the knowledge in mineralogical and crystallographic sciences was honoured by various scientific academic memberships. On leave from Göttingen and as a welcome to Vienna he became Corresponding Member of the Akademie der Wissenschaften zu Göttingen in 1967 and the Österreichische Akademie der Wissenschaften (the latter elected him 1972 as a Full Member). A further membership was awarded by the Academia Mediterranea delle Scienze (Catania, Italy) and a Honorary Membership by the Hungarian Academy of Sciences. He was elected as a Corresponding Member by the Kroatische Akademie der Wissenschaften und Künste and the Polish as well as the Croatian Academies of Sciences. He was particularly pleased, in fact he was proud to become a Member and Senator of the Deutsche Akademie der Naturforscher Leopoldina, which had already founded in 1652.

On the evening of 16 October 2022 Josef Zemann passed away gently and peacefully only a few months ahead of his 100th birthday. His person, his tireless commitment and enthusiasm, his keen sense of observation, but also his kindness and humour remain unforgettable. We will remember Josef Zemann as our teacher, mentor, and an outstanding scientist.

The incorporation of Li in the tourmaline structure

A. Ertl[1,2]

[1]*Mineralogisch-Petrographische Abt., Naturhistorisches Museum, Austria,*
[2]*Institut für Mineralogie und Kristallographie, Universität Wien, Austria.*
e-mail: andreas.ertl@a1.net

Using natural and synthetic samples, it was investigated which Li-containing short-range orders can occur in Li-bearing Al-rich tourmalines. The investigated samples have lattice parameters from a = 15.72, c = 7.07 Å to a = 15.84, c = 7.10 Å. The general tourmaline formula is $XY_3Z_6(BO_3)_3[T_6O_{18}]V_3W$, where the X site is usually occupied by Na, Ca or is vacant. The Y site is in such tourmalines usually occupied by Al and Li, and the Z site is only occupied by Al. The T site can be occupied by Si and by minor amounts of B and Al. The V site is usually occupied by OH and the W site by OH, O or F.

It is still not clear how Li enters the Y site in Li-rich tourmalines. Until now, syntheses have not been successful in producing Li-rich tourmalines (>0.5 apfu ^{Y}Li). It therefore makes sense to take a closer look at which short-range orders Li can be built into. Synthetic Al-rich and Li-bearing tourmalines with no F, but with $^{[4]}$B and $^{[4]}$Al are of special interest, because they contain no Ca, only Na and vacancies (□) at the X site and mainly Al and Li at the Y site (Ertl et al., 2012). Since these tourmalines (synthesized by David London) do not have such a complex composition, relationships are easier to recognize. In Tab. 1 all short-range orders are listed which can contribute to these synthetic samples (Z site is always occupied by Al).

Table 1. Short-range orders in synthetic tourmaline

Number	X site	Y site	T site	W site
1.1	Na	Al_2Li	Si_5B	OH
1.2	Na	Al_2Li	Si_5Al	OH
1.3	Na	Al_3	Si_4B_2	O
2.1	□	Al_2Li	Si_6	OH
2.2	□	Al_3	Si_5B	O
2.3	□	Al_3	Si_5Al	O

Short-range order 2.1 is related to the rossmanite end-member. Short-range order 2.3 is related to the alumino-oxy-rossmanite end-member (Ertl et al., 2022), while 2.2 is related to the B-analogue of this tourmaline. It seems confirmed that the short-range order 1.3 is an essential component. Without it, it is not possible to explain the crystal chemical formulae of these synthetic tourmaline samples. The combination of these different short-range orders makes it clear that the Li content in such a tourmaline containing only Na and vacancies at the X site will be in the range of 0–1 apfu Li. When correlating the component of the different short-range orders in the examined tourmalines, which were synthesized at different temperatures, it can be recognized that with decreasing temperature the component of 2.1 increases, while it decreases with increasing temperature. This explains why the content of the tetrahedrally coordinated B towards lower temperatures significantly increases. There is no evidence that in these synthetic tourmalines a short-range order occurs, where the X and Y sites are occupied as in 1.1, but exclusively Si occupies the T site and only O occupies the W site. Such a short-range order may not be favourable at such pressure/temperature conditions or perhaps even unstable.

A natural Al-rich and Li-bearing tourmaline sample with a vacancy-dominant *X* site (rossmanite; Selway et al., 1998) with the updated crystal chemical formula $^{X}(\square_{0.6}Na_{0.4})$ $^{Y}(Al_{2.2}Li_{0.7}\square_{0.1})$ $^{Z}Al_6$ $(BO_3)_3$ $[Si_{5.6}B_{0.4}O_{18}]$ $^{V}(OH)_3$ $^{W}[(OH)_{0.6}O_{0.3}F_{0.1}]$ seems to consist of the same short-range orders. A minor component may occur additionally: a short-range order with ^{X}Na, $^{Y}(Al_2\square)$, ^{T}Si and ^{W}(OH) (see also Ertl, 2023). However, the dominant component is short-range order 2.2 (Tab. 1), which is not surprising.

There occur natural Al- and Li-rich tourmalines with Li >1.0 apfu. Such tourmalines contain additionally some Ca and significant amounts of F (*e.g.*, Ertl et al., 2006, 2010). The short-range orders occurring in such samples are already listed in Tab. 1, but additional short-range orders might also occur, which are listed in Tab. 2.

Table 2. Additional theoretical short-range orders in natural Al- and Li-rich samples

Number	*X* site	*Y* site	*T* site	*W* site
1.4	Na	Al_2Li	Si_5B	F
1.5	Na	Al_2Li	Si_5Al	F
2.4	□	Al_2Li	Si_6	F
3.1	Ca	Li_2Al	Si_6	F
3.2	Ca	Li_2Al	Si_6	OH
3.3	Ca	$Al_2\square$	Si_5Al	OH
3.4	Ca	$Al_2\square$	Si_5B	OH

Short-range orders 3.1 and 3.2 have (Li_2Al) at the *Y* site. The combination of these components together with short-range orders 1.1, 1.2, 1.4, 1.5, 2.1 and 2.4 produces Li contents in the range 1-2 apfu Li. However, the 2.4 short-range order does not appear to occur, as a summary of approximately 9000 tourmaline analyses from different lithological environments show that for tourmaline with an average *X*-site charge of <+0.5, the maximum F amounts are <0.2 apfu (Henry & Dutrow, 2011). These chemical data of natural tourmalines indicate crystallographic influences. Natural tourmaline with relatively high Li contents always contains relatively high F contents. It seems that the contents of Li and the F are positively correlated (Ertl, 2021). It is therefore possible that short-range orders with Li and F (1.4, 1.5, 3.1; Table 2) are crystal-chemically more favourable than orders with Li and OH (1.1, 1.2, 2.1; Tab. 1; 3.2; Tab. 2). However, further investigations seem to be necessary.

This research was funded by the Austrian Science Fund (FWF) project P 35585.

Ertl A (2021): Why was it not possible to synthesize Li-rich tourmaline? - NATURA 111, 31–32

Ertl A (2023): Are the [6]−coordinated sites in tourmaline in certain cases partially vacant? Mineral Petrol 117, DOI: 10.1007/s00710-023-00815-4

Ertl A, Hughes JM, Prowatke S, Ludwig T, Prasad PSR, Brandstätter F, Körner W, Schuster R, Pertlik F, Marschall H (2006): Tetrahedrally coordinated boron in tourmalines from the liddicoatite-elbaite series from Madagascar: Structure, chemistry, and infrared spectroscopic studies. - Amer Mineral 91, 1847–1856

Ertl A, Rossman G, Hughes JM, London D, Wang Y, O'Leary JA, Darby MD, Prowatke S, Ludwig T, Tillmanns E (2010): Tourmaline of the elbaite-schorl series from the Himalaya Mine, Mesa Grande, California: A detailed investigation. - Amer Mineral 95, 24–40

Ertl A, Giester G, Ludwig T, Meyer H-P, Rossman GR (2012): Synthetic B-rich olenite: Correlations of single-crystal structural data. - Amer Mineral 97, 1591–1597

Ertl A, Hughes JM, Prowatke S, Ludwig T, Lengauer CL, Meyer H-P, Giester G, Kolitsch U, Prayer A (2022): Alumino-oxy-rossmanite from pegmatites in Variscan metamorphic rocks from Eibenstein an der Thaya, Lower Austria, Austria. - Amer Mineral 107, 157–166

Henry DJ, Dutrow BL (2011): The incorporation of fluorine in tourmaline: internal crystallographic controls or external environmental influences? - Canad Mineral 49, 41–56

Selway JB, Novák M, Hawthorne FC, Černý P, Ottolini L, Kyser TK (1998): Rossmanite, $\square(LiAl_2)Al_6Si_6O_{18}(BO_3)_3(OH)_4$, a new alkali-deficient tourmaline: description and crystal structure. - Amer Mineral 83, 896–900

Computational studies of zeolites as adsorbents for the removal of pharmaceuticals and personal care products

M. Fischer[1,2], J. Brauer[1,2]

[1]*Crystallography & Geomaterials Research, Faculty of Geosciences, University of Bremen, Germany*
[2]*Bremen Center for Computational Materials Science and MAPEX Center for Materials and Processes, University of Bremen, Germany*
e-mail: michael.fischer@uni-bremen.de

Pharmaceuticals and personal care products (PPCPs) have received considerable attention as emerging organic contaminants, with some members of this diverse group of compounds possessing a significant environmental hazard potential (Patel et al. 2019). Conventional wastewater treatment plants are not designed for the removal of these species, and a number of PPCPs show recalcitrant behaviour, entering water bodies and other environmental compartments. Adsorption-based processes constitute one possible technology that can improve the PPCP removal efficiency of wastewater treatment facilities. While carbon-based adsorbents are the most widely studied option, hydrophobic high-silica zeolites could be attractive alternatives due to their good regenerability and reduced co-adsorption of natural organic matter (Jiang et al. 2018). In this contribution, it will be discussed how atomistic modelling methods at different levels of theory can be employed to predict and understand the PPCP adsorption behaviour of these materials.

Given the diversity of zeolite frameworks that are available in highly siliceous form and the even larger number of PPCPs of possible environmental relevance, it is evident that an experimental investigation of all zeolite-PPCP combinations of potential interest would be extremely laborious. In previous work, it could be shown that relatively simple force field simulations deliver host-guest interaction energies that are well correlated with experimental removal efficiencies, providing a pathway to determine zeolite-PPCP combinations of potential interest prior to an experimental characterisation (Fischer 2020). Expanding upon this work, the implementation of a multi-step screening procedure allowed the exploration of a large number of combinations (>10 zeolites, >50 PPCPs) at relatively modest computational cost. Additionally, the capabilities of more sophisticated molecular dynamics simulations to calculate free energies of adsorption were explored. Such simulations allow direct predictions whether a given contaminant will be adsorbed in the zeolite or remain in solution.

Whereas the force field simulations are primarily employed for predictive purposes, dispersion-corrected density functional theory (DFT) calculations enable a more detailed understanding of the interactions that govern PPCP adsorption. Two recent studies dealt with the adsorption of carbamazepine (CBZ, Fig. 1a), an anticonvulsant medication, and triclosan (TCS, Fig. 1a), a disinfectant and preservative agent that is widely used in various products, in different zeolites (Fischer 2023a, Fischer 2023b). It was observed that the topology of the zeolite framework has a significant impact on the CBZ adsorption energy, whereas the interaction with TCS is largely determined by the pore size. This qualitative difference can be explained with the higher flexibility of TCS, which can adjust more readily to different pore shapes than the fairly rigid CBZ molecule. In addition to analysing factors that determine the strength of host-guest interactions, guest-guest interactions between co-adsorbed CBZ molecules were investigated. The study of TCS adsorption also addressed the competitive adsorption of the organic contaminant and water in zeolites having different framework compositions (all-silica zeolites and highly siliceous aluminosilicates, see Fig. 1b), permitting insights into the role of adsorbent hydrophobicity.

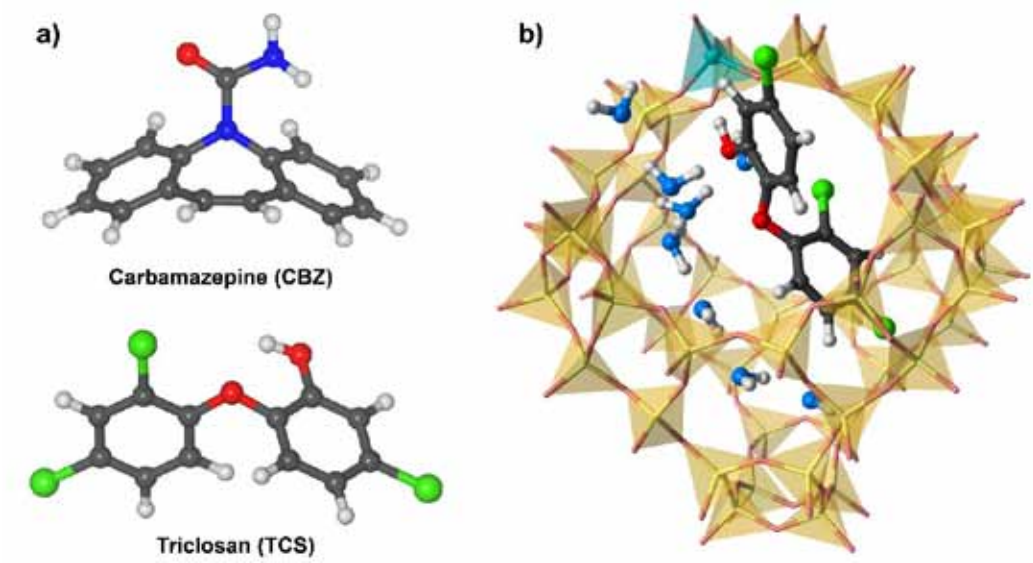

Figure 1. a) Molecular structures of carbamazepine and triclosan. b) Representative snapshot from a DFT-based molecular dynamics simulation addressing the co-adsorption of TCS and H_2O in protonated FAU-type zeolite.

Funding by the German Research Foundation (Deutsche Forschungsgemeinschaft) is gratefully acknowledged (projects 455871835 and 492604837).

Fischer M (2020): Simulation-based evaluation of zeolite adsorbents for the removal of emerging contaminants. – Mater Adv 1, 86

Fischer M (2023a): Adsorption of carbamazepine in all-silica zeolites studied with density functional theory calculations. – Chem Phys Chem 24, e202300022

Fischer M (2023b): Density functional theory study of hydrophobic zeolites for the removal of triclosan from aqueous solution. – Environ Sci Adv – accepted manuscript, DOI: 10.1039/D3VA00078H

Jiang N, Shang R, Heijman S G J, Rietveld, L C (2018): High-silica zeolites for adsorption of organic micro-pollutants in water treatment: A review. – Water Res 144, 145

Patel M, Kumar R, Kishor K, Mlsna T, Pittman C U, Mohan D (2019): Pharmaceuticals of Emerging Concern in Aquatic Systems: Chemistry, Occurrence, Effects, and Removal Methods. – Chem Rev 119, 3510

Metamorphic reaction kinetics at anhydrous to water-saturated conditions

M. Franke[1], B.C. Schmidt[2], R. Stalder[1], B. Joachim-Mrosko[1]

[1]University of Innsbruck, Institute of Mineralogy and Petrography, Innrain 52, 6020 Innsbruck
[2]Department of Mineralogy and Petrology, Geoscience centre, Georg-August-University Göttingen, Goldschmidtstraße 1, 37077 Göttingen
e-mail: bastian.joachim@uibk.ac.at

Metamorphic coronas and reaction rim structures are examples of a net-transfer reaction, where pre-existing mineral phases react to new phases. Growth of these metamorphic structures indicates a change in physical parameters such as pressure or temperature. One of the most important parameters that controls reaction rim growth is the presence of volatiles, which can affect rim thicknesses, phase stabilities or rim microstructures (e.g., Gardés et al. 2012). This implies that reaction rims have the potential to decipher the P-T-t-X history of a sample of interest.

In this study, reaction rim growth experiments were performed between periclase and quartz at nominally anhydrous to water-saturated conditions between 3 to 4 kbar and 1100 to 1300 °C for 66-168 h. Controlled minute amounts of water were added through OH-doped periclase, which allowed to perform experiments at controlled water-undersaturated conditions. For water-saturated experiments that contain wt% amounts of H_2O, controlled amounts of water were added in the form of brucite powder to the samples.

At anhydrous conditions, no reaction rim formed implying that water acts as a catalyst, and a minimum fluid threshold is needed to initiate metamorphic re-equilibration. In all experiments that used either water-doped periclase or brucite as source of water, the rim sequence Per | Fo | En | Qz developed. At water-undersaturated conditions, addition of minute amounts of water results in an increase in the overall reaction rim growth rate by more than 2 orders of magnitude while the relative forsterite/enstatite ratio increases from 0.6 to 2.4. At water-saturated conditions, growth rates reach a plateau valeau between 10^{-15} and 10^{-14} m^2/s while forsterite/enstatite thickness ratios vary between 3 and 12.

This implies that reaction rim growth rates have the potential to monitor variations in water activity at those grain boundaries that serve as fast pathways for component transport at water-undersaturated conditions during metamorphic and metasomatic reactions in natural systems, allowing them to be used as sensitive “geohygrometers”. Additionally, the effect of water on relative layer thicknesses may provide an application for reaction rim microstructures to be used as new physico-chemical gauges that will allow us to discriminate between water-undersaturated and water-saturated conditions during metamorphic events.

Gardés E, Wunder B, Marquardt K, Heinrich W (2012): The effect of water on intergranular mass transport: New insights from diffusion-controlled reaction rims in the MgO-SiO_2 system. - Contr Mineral Petrol 164, 1–16

Bi-Te-S biomineralization in Precambrian Volyn biota (Ukraine)

G. Franz[1], R. Wirth[2], A. Schreiber[2], V. Khomenko[1,3]

[1]Institut für Angewandte Geowissenschaften, Technische Universität Berlin
[2]Deutsches GeoForschungsZentrum Potsdam
[3]Institute of Geochemistry, Mineralogy and Ore Formation, Academy of Sciences, Kyiv
e-mail: gefra548@gmail.com; gerhard.franz@tu-berlin.de

The Volyn biota represent an ancient subsurface lithautotrophic microecosystem with a minimum age of ca. 1.5 Ga (Franz et al. 2023). The fossils are exceptionally well preserved in 3D due to their occurrence in cavities of pegmatites of the 1.8 to 1.7 Ga old Korosten Pluton in NW Ukraine, which experienced no diagenesis, metamorphism or deformation, which is very often the case in sediments. The fossilization occurred during influx of hot, HF-bearing fluids from the granitic source into the large miarolitic cavities, producing a µm-wide rim of Al-silicate minerals (Franz et al., 2022). Some of the fossils were interpreted as biofilms (extracellular protein substance), others show similarities to filamentous fungi-like organisms, supported by the presence of chitosan, others are interpreted as methanogenic organisms.

In some of these filamentous and bulbous fossils we identified mineral inclusions with a size of approximately 50 to 100 nm. These nano-inclusions occur in the central part of the fossils, excluding their origin as post-mortem inclusions. Their composition is variable in the samples, but all are characterized by Bi-Te-S. In one sample they are randomly oriented in a distance of several micrometer. The composition is close to the minerals ingodite Bi(S,Te) or joseite $Bi_4(S,Te)_3$.

In another sample, they occur in a central channel of the organisms, characteristic for some of the filamentous fossils. These nanoparticles are up to approximately 200 nm large, concentrated in aggregates, and their composition is dominantly Bi-Cu-S with Te and Pb as additional components. Electron diffraction patterns of these mosaic crystals indicate an orthorhombic phase with a = 7.70 Å, b = 10.4 Å, c = 6.75 Å, consistent with the phase Cu_3BiS_3. Crystals away from the channel show the same composition Bi-Te-Pb-Cu.

In a bulbous fossil object, the nano-sized biominerals are arranged in groups of several crystals. Their composition is dominantly Bi-Te-S. These crystals are connected by a filament of amorphous material, a few nanometers wide, and similar filamentous extensions from the nanocrystals were observed (Fig. 1).

In modern fungi, Liang et al. (2019) observed the formation of Te- (and Se-) nanoparticles during growth experiments with different fungal species, and microbial reduction of Te (and Se) species shows the immobilization of these elements in intracelular and extracelular nanoparticles (Liang et al., 2020), supporting the interpretation of the fossils as fungi-like organisms.

Franz G, Lyckberg P, Khomenko V, Chournousenko V, Schulz H.-M, Mahlstedt N, Wirth R, Glodny J, Gernert U, Nissen J (2022): Fossilization of Precambrian organic matter (kerite) from the Volyn pegmatite, Ukraine. - BioGeosciences 19, 1795

Franz G, Khomenko V, Lyckberg P, Chernousenko V, Struck U, Wirth R, Gernert U, Nissen J (2023): The Volyn biota (Ukraine) – indications for 1.5 Gyr old eucaryotes in 3D-preservation, a spotlight on the 'boring billion'. - BioGeosciences 20, 1901

Liang X, Perez MAM-J, Zhang S, Song W, Armstrong JG, Bullock LA, Feldman J, Parnell J, Csetenyi L, Gadd GM (2019): Fungal formation of selenium and tellurium nanoparticles. - Appl Microbiol Biotech 103, 7241

Liang X, Perez MAM-J, Zhang S, Song W, Armstrong JG, Bullock LA, Feldman J, Parnell J, Csetenyi L, Gadd GM (2020): Fungal transformation of selenium and tellurium located in a volcanogenic sulfide deposit. Env Microbiol 22, 2346

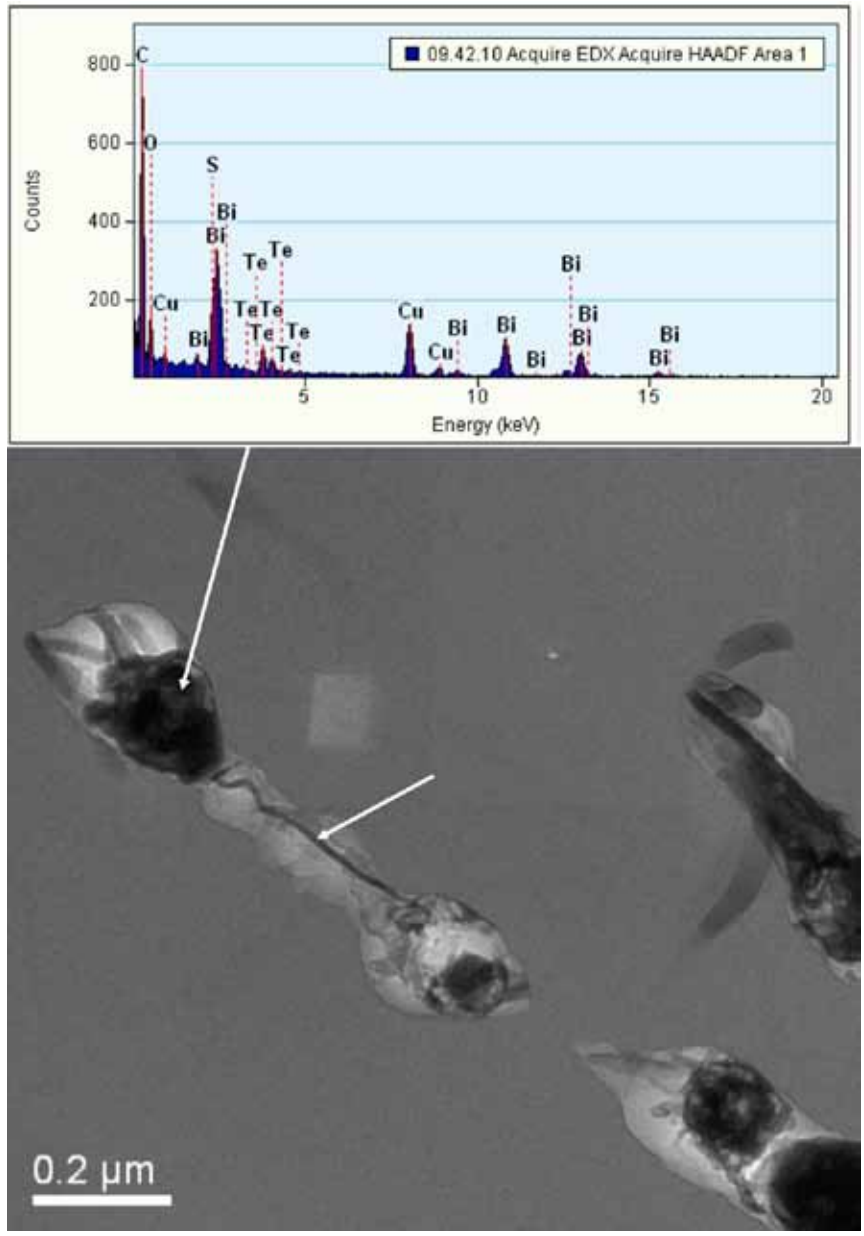

Fig. 1: TEM image and EDS analysis of biominerals in the Volyn biota. Arrows point to the location of the analysis and the thin connection of the nanoparticles.

Enzymatically induced apatite formation as a key mechanism in fish fossilization – an experimental study

F. Gäb[1], S. Karačič[2], R. Wirth[3], G. Bierbaum[2], C. Bultmann[4]

[1]Institut für Geowissenschaften, University of Bonn,
[2]Institut für medizinische Mikrobiologie, University Hospital
[3]GFZ Potsdam
[4]Radiomed Gemeinschaftspraxis für Radiologie und Nuklearmedizin, Wiesbaden
e-mail: fgaeb@uni-bonn.de

Exceptionally preserved fish fossils are known from various locations and throughout most of Earth's history. They play an important role in understanding the history of life and process of evolution, yet the process that leads to their formation remains mostly unclear. Phosphorous is a scarce resource in the whole modern ocean and there is no evidence for this being different over the Phanerozoic. Nevertheless there are numerous examples for fish fossils preserved in apatite e.g. Solnhofen Plattenkalk (Jurassic of S' Germany), Gogo Fm. (Devonian of N' Australia) or Santana Fm. (Cretaceous of E' Brazil). Hence there is a need for a mechanism that provides exceptionally high amounts of P to facilitate the precipitation of large quantities of apatite.

In this study we investigate the role of microbially produced alkaline phosphatase (AP) as a source for the needed phosphate. AP is an ubiquitous enzyme throughout the world of bacteria and liberates phosphate from organic (macro)-molecules. It is known to provide phosphate for the formation of apatite *in vitro* (Cosmidis et al. 2015).

We conducted experiments, where AP was used to liberate phosphate from organic matter and, through oversaturation of the surrounding fluid, ultimately precipitated inorganically as apatite on fish scales. This might be the first step towards permineralization of the organic matter that is needed for fossilization. To strengthen the hypothesis the resulting apatite crystals were compared using TEM analysis with existing fossils. The result of these investigations showed a striking mineralogical similarity between the laboratory made and natural apatite crystals. This suggests that inorganic precipitation of apatite from an oversaturated solution indeed is a possible pathway for permineralization of a carcass which would ultimately lead to an exceptionally preserved fossil. Additionally this could mean that the fossil itself could be used as a geochemical and petrological indicator for the surrounding conditions, both of the sediment and the seawater, during its formation.

Cosmidis J, Benzerara K, Guyot F, Skouri-Panet F, Duprat E, Férard C, Guigner J-M, Babonneau F, Coelho C (2015): Calcium-phosphate biomineralization induced by alkaline phosphatase activity in Escherichia coli: localization, kinetics, and potential signatures in the fossil record. – Frontiers in Earth Science 3, 84

Zircon preservation in hybrid magmas from Mt. Hasan stratovolcano, Central Anatolia, and implications for magma mixing dynamics

G. Gencoglu Korkmaz[1,2], K.A. Cionoiu[2], A.K. Schmitt[2,3]

[1]Konya Technical University, Department of Geological Engineering, Konya, Turkey
[2] Heidelberg University, Institute of Earth Sciences, Heidelberg, Germany
[3]Curtin University, John de Laeter Centre, Perth, Australia
e-mail: Gulin.Gencoglu@geow.uni-heidelberg.de

Mt. Hasan, or Hasan Dağ, is a prominent stratovolcano within the Cappadocian Volcanic Province of central Anatolia. It experienced recurrent eruptions of mostly andesitic-dacitic lava flows from its main edifice on average every 5,000 to 15,000 years over the past 100 ka (Friedrichs et al. 2020). The northeastern flank of Mt. Hasan is dissected by a strand of the Tuz Gölü fault zone (TGFZ) with significant vertical and dextral offsets that in part have displaced lava coulees erupted from the eastern vent region of Mt. Hasan (little Mt. Hasan, or Küçük Hasan Dağ) from their respective source vents (Krystopowicz 2015). The volcano is underlain by a long-lived evolved magma reservoir that has remained viable for producing explosive and effusive eruptions since at least 550 ka (Friedrichs et al. 2020). Mafic magma recharge as evident by the presence of abundant rounded enclaves in Mt. Hasan lavas and geochemical mixing trends (Aydar & Gourgaud 1998) plays an important role in maintaining the magma system viable for such protracted durations. Here, we report mineral and whole-rock geochemical results for a suite of five lava flows from the eastern part of Mt. Hasan which were sampled on both sides of the TGFZ to provide piercing points for fault reconstruction. All lava flows yielded zircon, despite whole-rock compositions and mineral temperatures being clearly outside zircon saturation conditions. The implications of this observation on the timescales and processes of magma mixing are discussed here; geochronological analysis of zircon using U-Th and (U-Th)/He methods to determine crystallization and eruptions ages, respectively, is ongoing.

The investigated lavas compositionally span from basaltic andesite to dacite. They show hypocrystalline porphyritic textures with varying amounts of glass. Basaltic andesites primarily consist of plagioclase, olivine, pyroxene, Fe-Ti oxides, and additionally quartz, which based on embayments and ocellar textures is considered xenocrystic. In the andesites, plagioclase, pyroxene, and Fe-Ti oxide minerals are commonly present, along with amphibole (often with breakdown textures), and rare olivine. Dacites, on the other hand, contain plagioclase, amphibole, pyroxene, Fe-Ti oxides, and scarce quartz microphenocrysts. Apatite and zircon are present as accessory minerals in all lavas. Plagioclase pheno-microphenocrysts in almost all investigated rocks generally show inverse and oscillatory zoning with An-contents between 33 and 70 mol% and total FeO between 0.19 and 0.75 wt%. They typically display various types of sieve textures. Amphibole is ubiquitous in the lavas, and is mostly classified as Mg-rich hornblende. However, the degree of preservation in the basaltic andesite-andesite lavas is low as indicated by intense opacification and thick breakdown rims (4–8 μm). In the dacite lavas, amphibole represents the primary mafic phase and is mostly intact. Except in the most mafic lava flow, minor amounts of biotite are present in the groundmass, typically surrounded by breakdown reaction rims. Olivine with Fo = 89–86 mol% in basaltic andesite-andesite lavas is compositionally in disequilibrium with their host. In comparison, the andesitic lavas contain olivine with lower Fo contents ranging from 79 to 84 mol%. Diopsidic augite and enstatitic orthopyroxenes are commonly present, and they are variably zoned.

Mineralogical and petrographic features of Mt. Hasan lavas indicate a hybrid nature, where evolved magmas were reheated by mafic recharge. The evolved magma resided at comparatively low temperatures in an upper crustal magma reservoir (T = 800–835 °C, P = 110–150 MPa, based on amphibole geothermobarometry using the calibration of Ridolfi (2021), whereas eruption temperatures based on Fe-Ti-oxide pairs are up to 910°C. Taking new and published data for Mt. Hasan (e.g., Aydar & Gourgaud 1998) into account, kinked trends in major element oxides variation diagrams indicate a combination of magma mixing and fractional crystallization. Magma mixing between basaltic and dacitic endmembers can explain the hybrid basaltic andesites, whereby the basaltic endmember is more primitive than the erupted compositions of Mt. Hasan as indicated by the preservation of high-Fo (Fig. 1) and high-Ni olivine in the hybrid lavas. A compositional equivalent to the mafic endmembers in these mixing scenarios are basaltic scoria cones erupted in the vicinity of Mt. Hasan (Gencoglu Korkmaz et al. 2022; Reid et al. 2017). Zircon is preserved in even the most mafic hybrid lavas, where strong undersaturation and high Zr diffusivity in the melt would nominally dissolve zircon at rates of ~10^{-11} m/s (900 °C), so that a zircon sphere 50 µm diameter would become completely resorbed by the melt within ca. 7 weeks. This implies that zircon was either shielded as inclusions in phenocrysts, or that mixing and hybridization occurred only briefly before eruption.

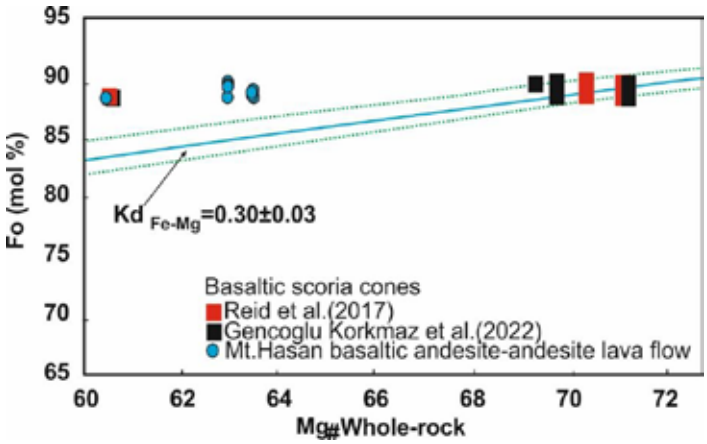

Figure 1. Whole-rock Mg≠ versus Fo (mol%) for olivine from northeastern Mt. Hasan basaltic andesite and andesite lava flows. Whole-rock and olivine compositions from scoria cones from the southwestern part of the Cappadocian Volcanic Province (Reid et al. 2017; Gencoglu Korkmaz et al. 2022) are shown for comparison.

Aydar E, Gourgaud A (1998): The Geology of Mount Hasan Stratovolcano, Central Anatolia, Turkey. - J Volcanol Geotherm Res 85, 129-152

Friedrichs B, Atıcı G, Danisik M.A, Çobankaya M, Harvey JC, Yurteri E. Schmitt AK (2020): Late Pleistocene eruptive recurrence in the post-collisional Mt. Hasan stratovolcanic complex (Central Anatolia) revealed by zircon double-dating. - J Volcanol Geotherm Res 404, 107007

Gencoglu Korkmaz G, Kurt H, Asan K, Petrelli M, Leybourne M (2022): The role of peridotite and pyroxenite melts in the origin of the Karapınar basalts, Cappadocia Volcanic Province, Central Anatolia. - J Geosci 67, 311-329

Krystopowicz NJ (2015):Constraining deformation, uplift, and activity along the Tuz Gölü fault zone, Central Anatolia, Turkey. - Master Thesis, Applied Science: University of Toronto

Reid MR, Schleiffarth WK, Cosca MA, Delph JR, Blichert-Toft J, Cooper KM (2017): Shallow melting of MORB-like mantle under hot continental lithosphere, Central Anatolia. - Geochem Geophys Geosyst 18, 1866-1888

Ridolfi F (2021): Amp-TB2: An updated model for calcic amphibole thermobarometry.- Minerals 11, 324

Eveslogite – Decoding the complexity of eveslogite through three-dimensional electron diffraction

E. Götz[1], M. Klementová[2], W. Depmeier[3], S. V. Krivovichev[4,5], M. Czank[3], M. Schowalter[6], L. Palatinus[2], U. Kolb[1,7]

[1]Institute of Applied Geosciences, Geomaterial Science, Technical University of Darmstadt, Germany
[2]Department of Structure Analysis, Institute of Physics of the Czech Academy of Sciences, Prague, Czech Republic
[3]Institute of Geosciences, Kiel University, Germany
[4]Kola Science Centre, Russian Academy of Sciences, Apatity, Russia
[5]Department of Crystallography, St. Petersburg State University, St. Petersburg, Russia
[6]Institute of Solid State Physics, University of Bremen, Germany
[7]Centre for High-Resolution Electron Microscopy, Johannes Gutenberg University, Mainz, Germany
e-mail: Emilia.goetz@tu-darmstadt.de

Eveslogite is an exceptionally complex mineral, found exclusively at Mt. Eveslogchorr, located in the Khibiny alkaline massif, Kola peninsula, Russia. It occurs as a late-hydrothermal formation in veins breaching a poikilitic nepheline syenite, called rischorrite. Despite its discovery in 2003, the structure of eveslogite remained elusive due to its intricacies and the limitations of available methods and instruments at that time (Men'shikov et al. 2003). It was originally thought that the structure resembled that of a heterophyllosilicate (Ferraris & Gula, 2005), but doubts regarding the applicability of the modular approach arose after the crystal structure of a similar mineral, yuksporite, was determined (Krivovichev et al., 2004). To overcome these challenges, advanced techniques such as three-dimensional electron diffraction (3DED; Gemmi et al., 2019) was used to determine the structure and high-angle annular dark-field scanning transmission electron microscopy (HAADF-STEM) was employed to verify it. These methods allowed the investigation of the eveslogite structure at the nanoscale, as the small crystal size and complex twinning prevented the use of traditional X-ray diffraction techniques. Additionally, energy dispersive X-ray spectroscopy (EDS) provided valuable insights into the elemental composition of the mineral. Contradictory previous findings (Men'shikov et al., 2003) new cell parameters were proposed (a = 14.2359 Å, b = 44.8242 Å, c = 15.9058 Å, α = 90°, β = 109.658°, γ = 90°, with a cell volume of 9558.08 Å^3) and the space group $P2_1$ was unambiguously assigned. This revised cell facilitated the structure determination of eveslogite, which comprises 345 symmetrically independent atom positions [see Figure 1(A)]. Based on the average elemental composition the sum formula of eveslogite is $K_{17.5}(Ba,Sr)_8(Na,Ca)_{40}[(Ti,Nb,Fe,Mn)_{11}Si_{62}O_{179}(OH,F)_{12}(O,OH)_{13}](H_2O)$. The essential building blocks that make up the eveslogite structure are heterosilicate tubular chains (see Figure 1(B) and (C)) as well as double-tubes (see Figure 1(D) and (E)), extending along the a-axis. Zig-zag rows of the tubular building units are interconnected by ribbons of $(Ca,Na)O_x$ polyhedra likewise extending along [100]. The heterosilicate tubular building units of eveslogite show a certain degree of similarity with silicate-only modules occurring in charoite and denisovite (Rozhdestvenskaya et al., 2010; Rozhdestvenskaya et al., 2017). Additional diortho-silicate groups are always connected with the heteroatoms. The double-tubes consist of unbranched dreier double silicate chains connected via (Ti,Nb,Fe,Mn)-heterocations (M) to diortho-silicate groups, resembling the structure of yuksporite. Notably, the M positions form MO_6 octahedra or MO_5 square pyramids within the double-tubes. The findings of this research shed light on the complex structure of eveslogite, emphasizing the importance of avoiding twinning and acquiring data from single nm-sized crystals using 3DED. This study not only contributes to a deeper understanding of this remarkable mineral but also showcases the power of advanced electron microscopy techniques in unravelling the intricate structures of minerals.

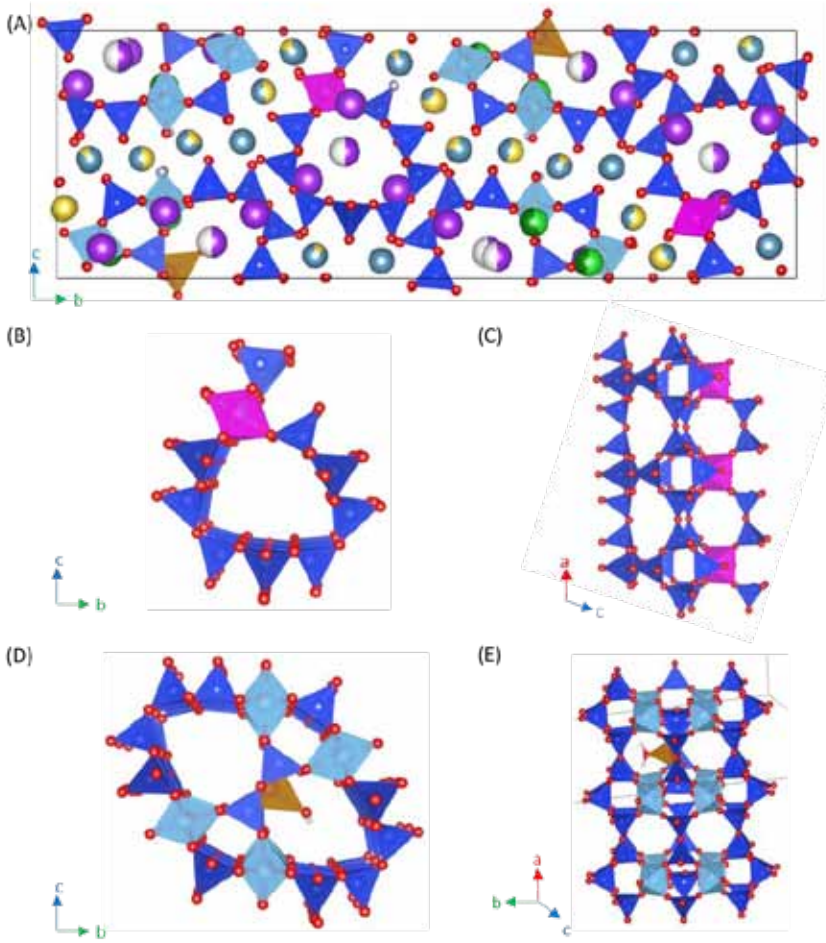

Figure 1: (A) Structure of eveslogite along [100]. The unit cell is marked by a black box. The heterosilicate tubular chains are shown along [100] in (B) and along the [010] in (C). (D) and (E) show the double-tube along [100] and along [329], respectively. Si is displayed in dark blue, M in light blue, (Ti,Nb) in pink, (Fe,Mn) in orange, Ba in light green, Sr in dark green, K in purple, Ca in blue-grey, Na in yellow, O in red, F in grey and H in white

Ferraris G, Gula A (2005): Polysomatic aspects of microporous minerals – heterophyllosilicates, palysepioles and rhodesite-related structures. – Rev Min Geochem 57, 69-104

Gemmi M, Mugnaioli E, Gorelik TE, Kolb U, Palatinus L, Boullay P, Hovmoller S, Abrahams JP (2019): 3D electron diffraction: The nanocrystallography revolution. – ACS Central Science 5, 1315-1329

Krivovichev SV, Yakovenchuk VN, Armbruster T, Döbelin N, Pattinson P, Weber H-P, Depmeier W (2004): Porous titanosilicate nanorods in the structure of yuksporite, $(Sr,Ba)_2K_4(Ca,Na)_{14}(Mn,Fe)\{(Ti,Nb)_4(O,OH)_4[Si_6O_{17}]_2[Si_2O_7]_3\}(H_2O,OH)_n$, resolved using synchrotron radiation. – Amer Min 89, 1561-1565

Men'shikov Y, Khomyakov A, Ferraris G, Belluso E, Gula A, Kulchitskaya E (2003): Eveslogite, $(Ca,K,Na,Sr,Ba)_{24}[(Ti,Nb,Fe,Mn)_6(OH)_6Si_{24}O_{72}](F,OH,Cl)_7$, a new mineral from the Khibina alkaline massif, Kola Peninsula, Russia. – Zap Vseross Mineral Obshch 132, 59-67

Rozhdestvenskaya IV, Mugnaioli E, Czank M, Depmeier W, Kolb U, Reinholdt A, Weirich T (2010): The structure of charoite, $(K,Sr,Ba,Mn)_{15-16}(Ca,Na)_{32}[Si_{70}(O,OH)_{180}](OH,F)_4.nH_2O$, solved by conventional and automated electron diffraction. - Min Mag 74, 1, 159-177

Rozhdestvenskaya IV, Mugnaioli E, Schowalter M, Schmidt MU, Czank M, Depmeier W, Rosenauer A (2017): The structure of denisovite, a fibrous nanocrystalline polytypic disordered 'very complex' silicate, studied by a synergistic multi-disciplinary approach employing methods of electron crystallography and X-ray powder diffraction. - IUCrJ 4, 3, 223-242

A machine learning force field for albite and the diffusion mechanisms of its defects

A. Gorfer[1,2], R. Abart[2], C. Dellago[1]

[1]*Faculty of Physics, University of Vienna, Boltzmanngasse 5, 1090, Vienna, Austria*
[2]*Department of Lithospheric Research, University of Vienna, Josef-Holaubuek-Platz 2, 1090, Vienna, Austria*
e-mail: alexander.gorfer@univie.ac.at

Feldspar is the most abundant mineral in the Earth's crust and the nature of its diffusive phase transformations are essential for reconstructing the thermal histories of magmatic and metamorphic rocks. Due to the large timescales over which these transformations proceed, the mechanism responsible for sodium diffusion and its possible anisotropy has remained a topic of debate. To elucidate the process, we have developed a machine learning force field (MLFF) (reviewed in Unke et al. 2022) trained on first-principle calculations of Albite (Na-feldspar) and its charged defects.

The MLFF has been trained to accurately predict a range of experimental macroscopic properties as well as defect formation energies, incorporating electrostatic corrections of the underlying first-principle calculation. Notably, we have discovered a new type of dumbbell interstitial defect, which is found to be the most favorable interstitial, and its formation free energy at finite temperature has been computed using thermodynamic integration.

Using the force field to drive molecular dynamics (MD) simulations allowed us to gain unprecedented insight into the diffusion mechanisms, as depicted in Figure 1. Through the analysis of jump rates, diffusion coefficients and tracer correlation factors we have determined that correlation plays a significant role, particularly in the ⊥(010) direction due to a distinct dumbbell/interstitialcy mechanism. Moreover, we have observed a high degree of anisotropy in diffusion, with variations up to 27-fold at 1000K, as illustrated in Figure 2. The strong agreement between our results and experimental diffusion coefficients leads us to conclude that MLFFs represent a mature and powerful methodology for investigating the dynamical properties of feldspar and other silicates.

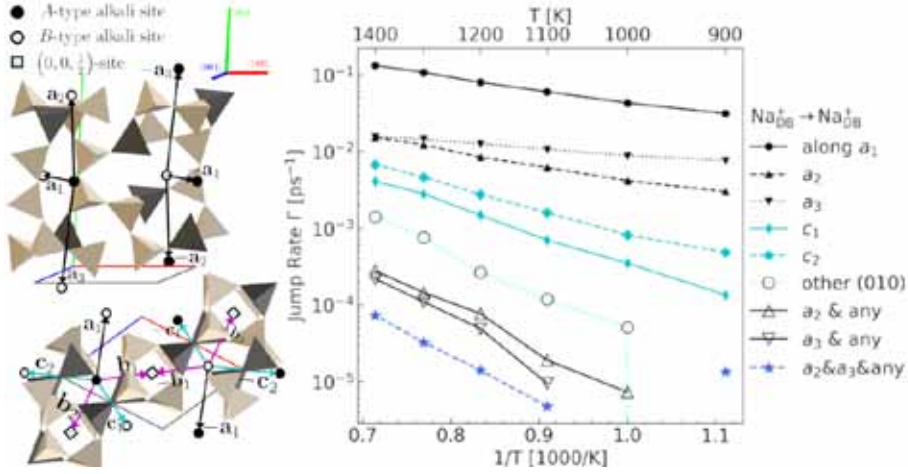

Figure 1. Left: diffusion pathways connecting the different sites. Right: jump rates for paths between alkali sites measured during an MD simulation using the MLFF. The dominance of diffusion along $\mathbf{a}_{1,2,3}$ leads to the high anisotropy.

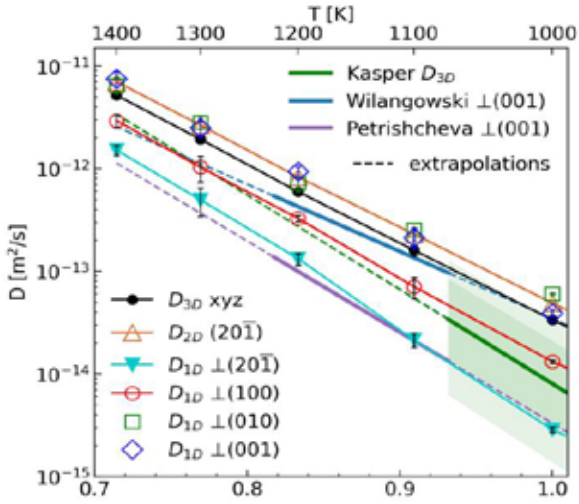

Figure 2. Diffusion coefficients for an interstitial defect measured over all dimensions D_{3D} and projected onto two D_{2D} or one dimension D_{1D} including experimental data of Kasper (1975), Wilangowski et al. (2015), and Petrishcheva et al. (2020)

Unke O, Chmiela S, Sauceda E, Gastegger M, Poltavsky I, Schütt K, Tkatchenko A, Müller KR (2021): Machine Learning Force Fields. - Chem Rev 121 (16), 10142-10186

Kasper RB (1975): Cation and Oxygen Diffusion in Albite - Ph.D. Thesis, Brown University.

Wilangowski F, Divinski S, Abart R, Stolwijk NA (2015) (1962): Radiotracer experiments and Monte Carlo simulation of sodium diffusion in alkali feldspar: evidence against the vacancy mechanism. - Defects Diffus Forum 363, 79–84

Petrishcheva E, Tiede L, Heuser D, Hutter H, Giester G, Abart R (2020): Multicomponent diffusion in ionic crystals: theoretical model and application to combined tracer- and interdiffusion in alkali feldspar. - Phys Chem Minerals 47, 35

Redox processes and metal sources recorded by Se and S isotopes of black smoker sulfides and host rocks

A. Grosche [1], M. Keith[1], R. Klemd[1], H. Strauss[2], S. König[3]

[1]GeoZentrum Nordbayern, Friedrich-Alexander-Universität Erlangen-Nürnberg, Schlossgarten 5, 91054 Erlangen, Germany
[2]Institut für Geologie und Paläontologie, Westfälische Wilhelms-Universität Münster, 48149 Münster, Germany
[3]Instituto Andaluz de Ciencias de la Tierra (IACT), Consejo Superior de Investigaciones Científicas (CSIC) and Universidad de Granada (UGR), Avenida las Palmeras 4, Armilla, 18100 Granada, Spain
e-mail: anna.grosche@fau.de

Black smoker chimneys are products of submarine hydrothermal venting and have a complex internal zoning that is the result of mineral precipitation and maturation at evolving fluid conditions. The composition of the hydrothermal sulfides is thereby controlled by the fluid composition (e.g., temperature, pH, salinity), processes like fluid boiling, and the potential input of magmatic fluids. Advances in analytical techniques allow the quantitative analysis of stable isotope ratios of heavy elements, such as Se, which can provide new insights into the cycling of chalcophile elements in magmatic-hydrothermal systems (König et al. 2019; Rosca et al. 2022).

We sampled different zones of black smoker chimneys from the Nifonea vent field (New Hebrides Arc, W Pacific) from the inner chalcopyrite lining towards the outer rim. Homogeneous sulfide powders were analyzed for high-precision Se isotopes using a double spike and hydride generation sample introduction system attached to a ThermoFisher Scientific® *NeptuneXT*™ MC-ICP-MS at the IACT, Granada. Fractions of the same powders were also analyzed for S isotopes and the resulting data was combined with in-situ trace element data of genetically related sulfides.

The $\delta^{82/76}$Se values (relative to NIST-3149) of chimney sulfides range from -3.7 ‰ to 0.6 ‰ ± 0.2 ‰ (2SD) (Fig. 1), in accordance with previously reported values of seafloor hydrothermal sulfides (Rouxel et al. 2004). The δ^{34}S values (relative to VCDT) range between 2.1 ‰ and 4.0 ‰ reflecting typical mixing of H_2S derived from the host rocks and from thermochemical seawater sulfate reduction lacking any evidence for magmatic fluid input. The highest $\delta^{82/76}$Se values occur in chalcopyrite that precipitated from high temperature fluids (370 °C) and overlap with $\delta^{82/76}$Se values of fresh basaltic glass from the surrounding Nifonea caldera (Fig. 1). This suggests that metals were leached from the host rocks and that no significant isotope fractionation occurred during high temperature precipitation of chalcopyrite.

Decreasing Se/Tl and Co/Tl ratios of pyrite from the inner to the outer chimney wall record a temperature decrease. A coupled decrease of $\delta^{82/76}$Se and δ^{34}S values towards the outer and low temperature zones (Fig. 1) can be related to local temperature-dependent isotope fractionation during redox reactions induced by mixing of the hydrothermal fluid with seawater. Understanding Se isotope fractionation during hydrothermal sulfide precipitation is crucial to subsequently identify the metal sources and the effect of fractionation processes in the upflow zone of submarine hydrothermal systems.

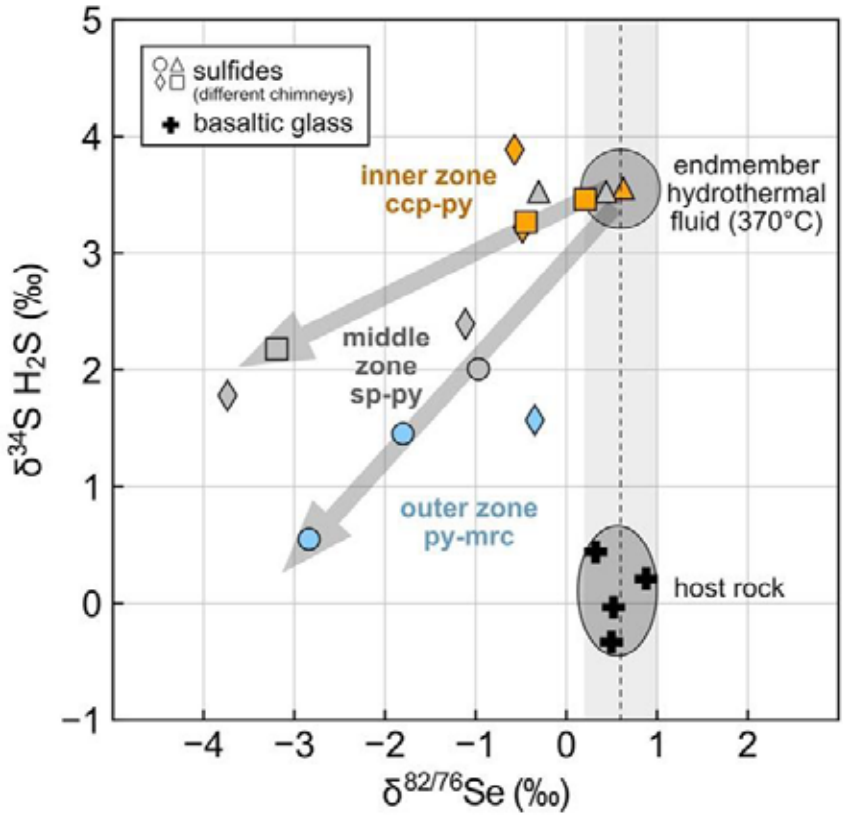

Figure 1. $\delta^{82/76}Se$ (relative to NIST-3149) versus $\delta^{34}S$ (relative to VCTD) values of black smoker sulfides and volcanic glass from Nifonea. The colors indicate whether the sulfide powder was derived from the inner, middle, or outer chimney zone. The symbols mark different vent sites. The $\delta^{34}S$ values of H_2S were calculated from the $\delta^{34}S$ value of the sulfide powder using the equilibrium isotopic fractionation factors by Ohmoto & Rye (1979) for the dominant sulfide phase at estimated fluid temperatures of 370°C (inner zone), 270 °C (middle zone), and 200 °C (outer zone). ccp = chalcopyrite, py = pyrite, sp = sphalerite, mrc = marcasite.

König S, Eickmann B, Zack T, Yierpan A, Wille M, Taubald H, Schoenberg R (2019): Redox induced sulfur-selenium isotope decoupling recorded in pyrite. - Geochim Cosmochim Acta 244, 24–39

Ohmoto H, Rye RO (1979): Isotopes of sulfur and carbon. - In: Barnes HL (ed) Geochemistry of Hydrothermal Ore Deposits. J Wiley and Sons, 509-567

Rouxel O, Fouquet Y, Ludden JN (2004): Subsurface processes at the Lucky Strike hydrothermal field, Mid-Atlantic Ridge: Evidence from sulfur, selenium, and iron isotopes. - Geochim Cosmochim Acta, 68, 2295–2311

Rosca C, Vlastélic I, Varas-Reus MI, König S (2022): Isotopic constraints on selenium degassing from basaltic magma and near-surface capture by fumarolic deposits: Implications for Se redistribution onto the Earth's surface. - Chem Geol 596, 120796

Origin of ultramafic rocks associated with carbonatites and their bearing on the formation of HFSE-deposits

D. Gudelius[1, 2, 3] *, M. W. Marks[3], G. Markl[3], T. F. D. Nielsen[4], J. Kolb[1, 2], B. Walter[1, 2]

[1]Karlsruhe Institute of Technology, Chair of Geochemistry and Economic Geology, Institute for Applied Geosciences, Adenauerring 20b, 76131 Karlsruhe, Germany
[2]Laboratory for Environmental and Raw Materials Analysis (LERA), Adenauerring 20b, 76131 Karlsruhe, Germany
[3] Eberhard Karls University, Institute of Geosciences, Schnarrenbergstrasse 94-96, 72076 Tübingen, Germany
[4] Geological Survey of Denmark and Greenland, Department of Petrology and Economic, 16 Geology, Øster Voldgade 10, Copenhagen, Denmark
e-mail: b.walter@kit.edu

Many carbonatites occur together with large amounts of ultramafic rocks, melilitolites, foidolites and (foid)syenites. There is an ongoing debate if and how these contrasting lithologies were formed by differentiation of a common, mantle-derived silicate magma or rather by metasomatic processes between carbonatite and country rocks (Vasyukova & Williams-Jones, 2022). In order to find petrological evidence for one or the other, two key examples, the Gardiner (E Greenland) and Kovdor (Russia) complexes are compared in this study (Fig. 1). Despite their similar tectonic setting and succession of rock types, they show significant differences in the texture and mineral composition of ultramafic rocks.

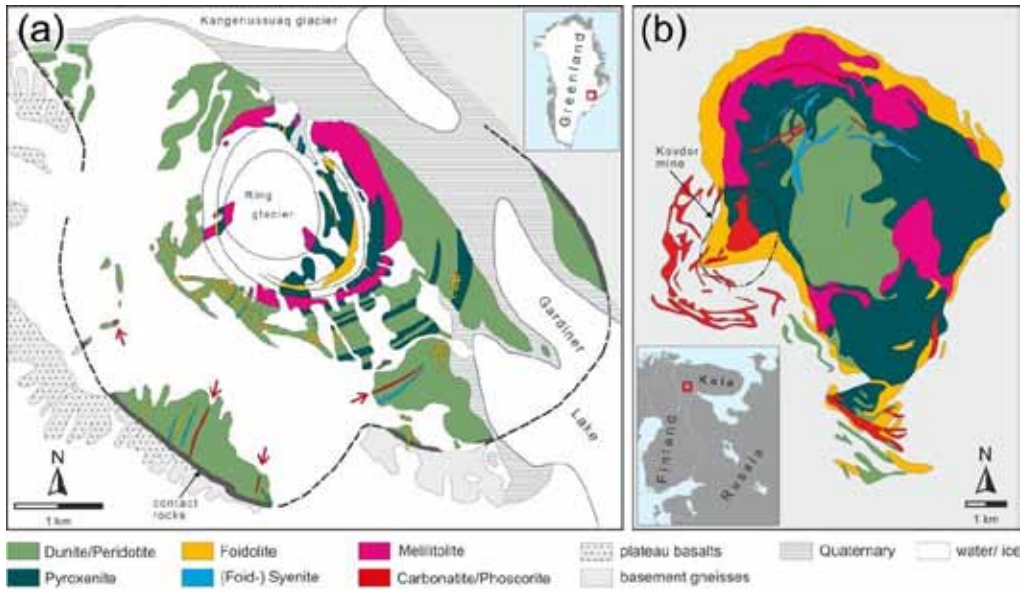

Figure 1: Geological maps of (a) Gardiner (E Greenland) and Kovdor (Russia), taken from Gudelius et al. (2023).

Ultramafic rocks from Kovdor include calcite- and biotite-rich dunites and pyroxenites without typical cumulate textures. They partly consist of Ni-poor forsterite (Fig. 2), Cr-poor diopside and Ni-Cr-poor spinel and are therefore interpreted as metasomatic reaction products between mantle-derived carbonatite melts and silicic host rocks. Similar ultramafic rocks are associated with carbonatites (e. g. at Palabora - South Africa, Afrikanda - Russia, and Salitre - Brazil). In contrast, the ultramafic rocks from Gardiner show well-preserved cumulate textures and consist

of Ni-rich forsterite, Cr-rich diopside as well as Cr-Ni-Ti-rich spinel and also contain F-Cl-rich apatite.

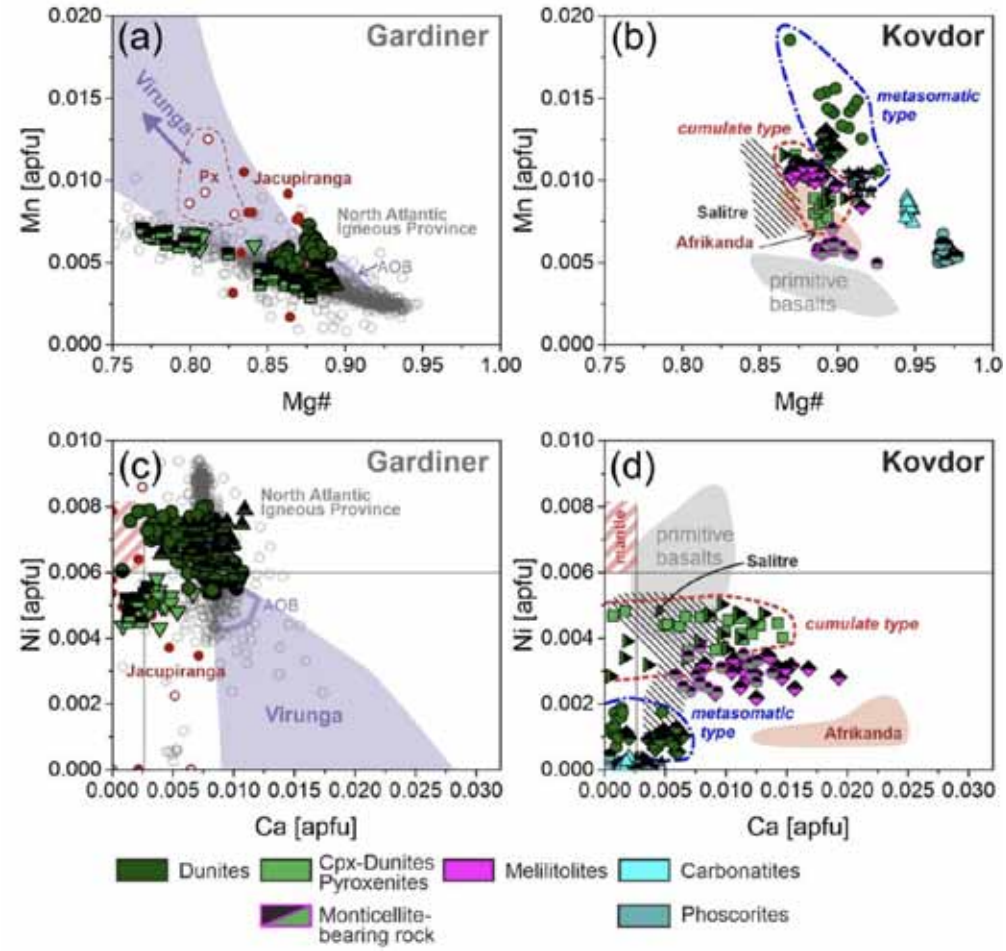

Figure 2: Comparison of olivine compositions from Gardiner (left column) and Kovdor (right column) with literature data (taken from Gudelius et al. 2023)

This indicates that these rocks represent cumulates of an evolving, mafic melt derived from Ti-rich mantle source, similar to other rocks of the North Atlantic igneous province (Fig. 2). In contrast to systems dominated by carbonatite metasomatism like Kovdor, Ti-rich parental silicate magmas can abundantly crystallize Ti phases, as recorded by massive perovskite cumulates in Gardiner melilitolites. This can effectively scavenge HFSE from the magmatic system early in its evolution and likely explains HFSE-barren carbonatites at Gardiner, while those from Kovdor are highly HFSE-enriched. In summary, ultramafic rocks in alkaline complexes can be of both cumulate and metasomatic origin; the specific type has an important bearing on their HFSE enrichment and on the types of ores present in such complexes.

Gudelius, D., Marks, M. W., Markl, G., Nielsen, T. F., Kolb, J., Walter, B. (2023): The origin of ultramafic complexes with melilitolites and carbonatites: a petrological comparison of the Gardiner (E Greenland) and Kovdor (Russia) intrusions. - J Petrol, egad036

Vasyukova, O.V. & Williams-Jones, A.E. (2022): Carbonatite metasomatism, the key to unlocking the carbonatite–phoscorite–ultramafic rock paradox. - Chem Geol 602, 120888

Geochemical patterns in karst bauxite of the Unterlaussa mining district (Upper Austria)

F.J. Hampl[1], F. Melcher[1], I. Dunkl[2], B. Schmidt[3], V. Bertrandsson Erlandsson[1]

[1]Chair of Geology and Economic Geology, Montanuniversität Leoben, Peter-Tunner-Straße 5, 8700 Leoben, Austria
[2]Department of Sedimentology & Environmental Geology, Geoscience Center, Georg-August-Universität Göttingen, Goldschmidtstraße 3, 37077 Göttingen, Germany
[3]Department of Mineralogy, Geoscience Center, Georg-August-Universität Göttingen, Goldschmidtstraße 1, 37077 Göttingen, Germany
e-mail: ferdinand.j.hampl@gmx.at

Numerous studies demonstrated the great potential of karst bauxites as sources of critical metals. The European karst bauxites may thus help to gain more independence from questionable non-European metal suppliers. Yet several European karst bauxites are untouched by modern scientific methods and the processes that are responsible for their element enrichment and depletion patterns are not fully understood. However, understanding the geochemical patterns in karst bauxites is not only fundamental for a prudent economic usage but can also facilitate reconstructions of paleo-environments and redox processes during weathering and diagenesis. To better understand the geochemical patterns, we investigated three profiles of Upper Cretaceous karst bauxite in the Unterlaussa mining district (Upper Austria) and used geochemical and mineralogical methods such as (micro-) X-ray fluorescence, (laser ablation-) inductively coupled plasma mass spectrometry, scanning electron microscopy, electron microprobe mapping and X-ray diffraction.

According to our results, the boehmitic karst bauxite was formed by intense weathering of a polygenetic sediment (parent material) that was deposited on karstified dolostone (Hampl & Melcher, 2023). The presence of detrital chromite in the karst bauxite suggests that sediments formed by weathering of ophiolitic material in the hinterland of the depositional site were also part of the parent material. (Sub)tropical weathering of the composite parent material caused the dissolution of aluminosilicates and the enrichment of weathering-resistant minerals. These weathering processes not only led to chemical depletion and enrichment patterns that are typical for karst bauxites (e.g., pronounced Al_2O_3, Fe_2O_3 and TiO_2 enrichment, and SiO_2, alkali and alkaline earth metal depletion) but also resulted in substantial enrichment of several critical metals compared to the upper continental crust: e.g., rare earth elements (REEs; La-Lu + Sc, Y) up to 2277 ppm, Li up to 900 ppm, or V up to 916 ppm. Most of the REEs and Li are enriched in the lowermost part of the bauxite and clay minerals are the most likely hosts. Moreover, the element distribution patterns also indicate reducing conditions in the lower part and redeposition in the upper part of the bauxite. Even though Cr- and U-mobility normally only plays a subordinate role in karst bauxites, we found a macroscopic, authigenic chromium oxyhydroxide mineralization and discrete U-minerals in reduction spheroids. Aside from U, some of these reduction spheroids are extremely rich in redox-sensitive elements such as V, Cr, or Mn. We discuss possible formation models for this unique U-mineralization.

Our results highlight the economic potential and the ample information content of karst bauxites and call for more European initiative to investigate them.

Hampl FJ, Melcher F (2023): The formation of the Unterlaussa karst bauxite (Austria) – A re-evaluation of the established model. - J Geochem Explor 245, 107141. https://doi.org/10.1016/j.gexplo.2022.107141

The inner beauty of Roman Egyptian blue: micro-CT and mineralogy

J. Heinemann[1], P. Tropper[1], G. Degenhart[2], B. Zerobin[3], G. Goldenberg[3], A. Rodler[4,5]

[1]University of Innsbruck, Institute of Mineralogy and Petrography, 6020 Innsbruck, Austria
[2]Medical University of Innsbruck, Institute of Radiology, 6020 Innsbruck, Austria
[3]University of Innsbruck, Institute of Archaeologies, 6020 Innsbruck, Austria
[4]Austrian Archaeological Institute of the Austrian Academy of Sciences, Franz-Klein Gasse 1, 1190 Vienna
[5]Department of Lithospheric Research, University of Vienna, Josef-Holaubek-Platz 2, 1090 Vienna
e-mail: peter.tropper@uibk.ac.at

Egyptian blue was the first synthetic pigment made by humankind. It mostly consists of the mineral cuprorivaite, which is a calcium-copper-silicate ($CaCuSi_4O_{10}$). This study reports the results of a mineralogical and computer tomographic study of Egyptian blue finds from the Roman sites of Aguntum in East Tyrol, as well as from Retznei and Wagna (formerly Flavia Solva) in southern Styria, Austria. The aim is to expand our understanding of the material processing and production technology of the artificial pigment Egyptian blue. Samples of Egyptian blue pellets were investigated with respect to their elemental composition and spatial distribution of the calcium-copper-silicate cuprorivaite $CaCuSi_4O_{10}$.

A thin section (with three cut layers) of an Egyptian blue pellet from Aguntum was examined using optical microscopy (OP), micro-X-ray fluorescence analysis (μ-XRF) and scanning electron microscopy coupled with energy dispersive X-ray spectroscopy (SEM-EDX). The pigment's initial composition as well as the manufacturing process seem to be the decisive factors for the quality of the final product. A relationship between the presence of trace iron (Fe), titanium (Ti), and sulfur (S) with the quartz and copper source of the initial raw material mixture is discussed.

In addition, micro-computed tomography (μ-CT) of three Egyptian blue finds (Aguntum, Retznei, Wagna-Flavia Solva) was performed, revealing several concise differences between the samples. The pellets from Aguntum and Retznei contained a significantly higher content of cuprorivaite and smaller crystals than the sample from Wagna-Flavia Solva. The spatial distribution of individual mineral phases was analysed with μ-CT-3D images. Here, the connective density, average particle size as well as spacing between individual particles of specific phases can be visualised. This confirms the semi-quantitative measurement of a phase's proportion to the total volume of a sample.

Concerning clues about the initial raw material mixture of the pellets, the results show that chalcosine and possibly quartz from beach sand were used as source for the Egyptian blue pellet from Aguntum. In addition, μ-CT data indicate that the pellet from Retznei contains the highest amount of cuprorivaite, followed by the sample from Aguntum, while that from Wagna-Flavia Solva contains the least amount of cuprorivaite.

Glass transition temperatures and crystallization kinetics of a synthetic, anhydrous, amorphous calcium-magnesium carbonate

K.-U. Hess[1], J. Schawe[2], M. Wilding[3], K.E. Goetschl[4], S. Sturm[5], K. Müller-Caspary[5], E. Sturm[1], W. Schmahl[1], E. Griesshaber[1], T. Bissbort[1], D. Weidendorfer[1], M. Dietzel[4], D.B. Dingwell[1]

[1] Earth and Environmental Sciences, Ludwig-Maximilians-Universität München, Theresienstraße 41/III, 80333 Munich, Germany
[2] Mettler-Toledo GmbH, Analytical, Heuwinkelstrasse 3, 8603, Nänikon, Switzerland
[3] School of Earth Sciences, Wills Memorial Building, Queens Road, Bristol, BS8 1RJ, United Kingdom
[4] Institute of Applied Geosciences, Graz University of Technology, Rechbauerstraße 12, 8010 Graz, Austria
[5] Fakultät für Chemie und Pharmazie, Physikalische Chemie, Ludwig-Maximilians-Universität München, Butenandtstraße 5-13, 81377, Munich, Germany
e-mail: hess@lmu.de

We report the first calorimetric observations of glass transition temperatures and crystallization rates of anhydrous, amorphous calcium-magnesium carbonate using fast scanning differential scanning calorimetry (FDSC). The hydrous amorphous $Ca_{0.95}Mg_{0.05}CO_3 \cdot 0.5H_2O$ (ACMC05) solid was precipitated from a $MgCl_2$–$NaHCO_3$ buffered solution, separated from the supernatant, and freeze-dried. Part of the freeze-dried samples were additionally dried at 250 °C for up to 6 hours in a furnace in a high purity nitrogen atmosphere to produce anhydrous ACMC. The limiting fictive temperature of the anhydrous $Ca_{0.95}Mg_{0.05}CO_3$ was determined (by applying different heating rates (2000-6000 K/s, see Fig. 1) and correcting for thermal lag) to be 376 °C and the intensity of the glass transition or relaxational heat capacity is $\Delta Cp = 0.16$ J/(g K). Additionally, the heating rate dependence of the peak temperature of the corrected crystallization peaks is used to determine the activation energy of crystallization to be 275 kJ/mol. A high-resolution transmission electron microscopy study has been performed on the hydrous and anhydrous samples to provide further characterization of their compositional and structural states.

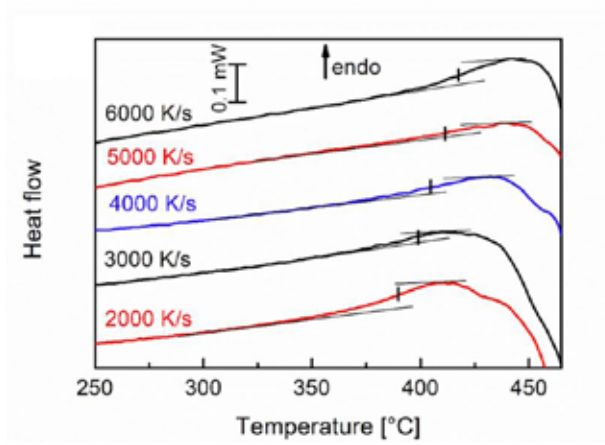

Figure 1. Heat flow curves of ACMC05.

The compositions of coherent exsolution lamellae in alkali feldspar measured with atom probe tomography

D. Heuser[1], R. Dubosq[2], G. Bian[1], G. Habler[1], E. Petrishcheva[1], B. Gault[2], C. Lengauer[3], C. Rentenberger[4], R. Abart[1]

[1]Department of Lithospheric Research, University of Vienna
[2]Department Microstructure Physics and Alloy Design, Max Plank Institut für Eisenforschung GmbH, Düsseldorf
[3]Department of Mineralogy and Crystallography, University of Vienna
[4]Physics of Nanostructured Materials, University of Vienna
e-mail: david.heuser@univie.ac.at

In the past, the compositions of experimentally produced coherent exsolution lamellae in alkali feldspars had to be determined indirectly from the "distorted" lattice parameters, because their small size prevented direct in-situ composition measurements. This indirect approach is based on strain models hinging on elastic constants, which are, however, subject to considerable uncertainties, especially for alkali feldspars with intermediate compositions (Robin 1974; Sipling & Yund 1976). In this study, we directly measured the compositions of experimentally produced exsolution lamellae using atom probe tomography (APT), a technique with near-atomic resolution which became available for non-conductive materials in the last decade.

At first, two K-rich gem quality alkali feldspars (Madagascar orthoclase and Volkesfeld sanidine) were shifted to intermediate Na-K-compositions by cation exchange with NaCl-KCl salt melt at 900 °C and subsequently annealed at ambient pressure and temperatures between 440 and 560 °C. Annealing conditions were within the miscibility gap of disordered alkali feldspar solid-solution and the initial compositionally homogeneous feldspars exsolved into a coherent lamellar intergrowth. Transmission electron microscopy (TEM) investigation of the exsolved feldspars revealed fully coherent exsolution lamellae subparallel to (-801) with lamellar widths of 5-30 nm. As the cell parameters of alkali feldspar exhibit considerable compositional dependence, the lattices of the more Na-rich and the more K-rich lamellae must be distorted in order to maintain coherency across the lamellar interfaces. In electron diffraction patterns this lattice distortion is evident from a splitting of the reflections corresponding to lattice planes sub-parallel to the lamellar interfaces.

APT revealed compositionally distinct domains corresponding to the expected Na-rich und K-rich lamellae. Time series experiments with different annealing durations were done at a given temperature to check when the lamellar compositions become stable, i.e. when thermodynamic equilibrium between the Na-rich and the K-rich lamella is reached. Even at the lowest applied temperatures equilibrium was reached within a few days, and lamellar compositions may be regarded as binodal points. The binodal points obtained at different temperatures delineate the coherent binodal curves. The results were compared to previously determined coherent solvi from the literature. Interestingly, Volkesfeld sanidine and Madagascar orthoclase show similar Na-K element partitioning and thus similar thermodynamic non-ideality of the alkali feldspar solid-solution in feldspar-salt melt cation exchange experiments at ambient pressure and temperatures between 800 and 1000 °C, but the coherent solvus of Volkesfeld sanidine lies well below the one of Madagascar orthoclase.

This apparent discrepancy may either be due to different degrees of thermodynamic non-ideality of the alkali feldspar solid-solution at the comparatively low temperatures of exsolution. Alternatively, this may be explained by different elastic properties of Volkesfeld sanidine and Madagascar orthoclase, which feed into the Gibbs energy of the soldi-solution via the elastic energy associated with coherent lamellar intergrowth.

Robin PYF (1974): Stress and strain in cryptoperthite lamellae and coherent solvus of alkali feldspars. - Amer Mineral 59, 1299-1318

Sipling PJ, Yund RA (1976). Experimental determination of the coherent solvus for sanidine-high albite. - Amer Mineral 61, 897-906

On the existence of a new $MgWO_4$ polymorph

E. Hildebrandt[1], V. Kahlenberg[1], H. Krüger[1], S.Wagner[1]

[1]*University of Innsbruck, Institute of Mineralogy and Petrography, Innrain 52, 6020 Innsbruck, Austria*
e-mail: volker.kahlenberg@uibk.ac.at

Single-crystals of a quenchable high-temperature polymorph of magnesium tungstate ($MgWO_4$-II) have been grown using the flux method. Polycrystalline material of the same compound could be obtained from solid-state reactions performed at 1200 °C. Basic crystallographic data of the previously unknown modification are as follows: triclinic symmetry, space group $P\overline{1}$, $a = 6.5525(6)$ Å, $b = 7.5883(7)$ Å, $c = 7.6976(6)$ Å, $\alpha = 119.064(9)°$, $\beta = 95.545(7)°$, $\gamma = 107.645(8)°$, $V = 304.84(5)$ Å^3 and $Z = 4$. The crystal structure was solved from single-crystal diffraction data using direct methods and subsequently refined including fractional atomic coordinates and anisotropic displacement factors for all atoms to a residual value of $R1 = 2.16$ % for 1517 independent observed reflections ($I > 2\sigma(I)$) and 110 parameters.

Both the divalent and hexavalent cations exhibit an octahedral oxygen coordination environment. The coordination spheres of the two symmetrically independent tungsten cations involve one very long W–O distance each and, therefore, one could also denote them as (5+1) coordinated. By sharing common edges and corners, the octahedra form a three-dimensional network, which can be built up from infinite rod-like elements running along [010] having a 2 × 2 octahedra wide cross section. Actually, a single rod can be imagined to be cut from the ReO_3-structure type and contains a total of four corner-sharing single-chains of octahedra. Within each single chain, strictly alternating cation sequences corresponding to …Mg–W–Mg–W… can be observed. The [WO_6]-groups show a pronounced distortion due to second-order Jahn-Teller effects.

$MgWO_4$-II is topologically equivalent to the monoclinic so-called VO_2(HT) structure-type. A detailed analysis of the relationships with other ABO_4-compounds is presented based on concepts of group theory. Solid-state characterization has been supplemented by micro-Raman spectroscopy. Finally, the thermal expansion tensor of $MgWO_4$-II between ambient temperature and about 700 °C has been determined. The calculations indicate that the thermal expansion in $MgWO_4$-II is highly anisotropic and quasi two-dimensional with a very low value α_2 along the direction of the above-mentioned octahedral chains of the network.

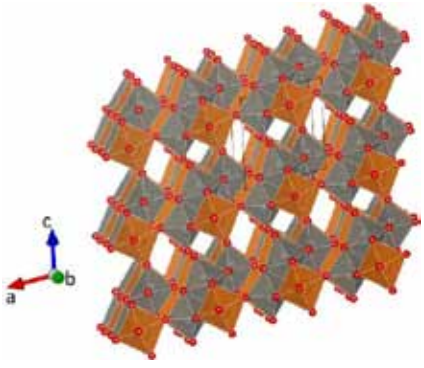

Figure 1. Side view of the crystal structure of $MgWO_4$-II. The MgO_6- and WO_6-octahahedra are colored orange and grey, respectively. Small red spheres represent oxygen atoms. The outline of a single unit-cell is shown as well.

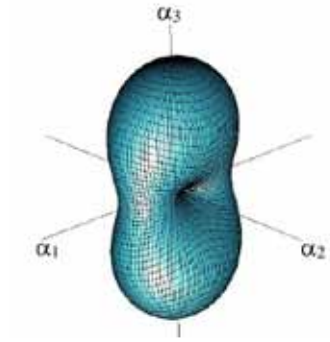

Figure 2. Three-dimensional representation surface of the thermal expansion tensor α_{ij} of $MgWO_4$-II at 500 °C.

Deformation induced dissolution-precipitation of zircon in greenschist facies metasediments

M. S. Hollinetz[1], B. Grasemann[1], C. McFarlane[2], B. Huet[3], D. Schneider[4]

[1)] Department of Geology, University of Vienna
[2)] Department of Earth Sciences, University of New Brunswick
[3)] Department of Hard Rock Geology, GeoSphere Austria
[4)] Department of Earth and Environmental Sciences, University of Ottawa
e-mail: marianne.sophie.hollinetz@univie.ac.at

Dissolution-precipitation coupled to mass transfer via an intergranular fluid is an essential mechanism to allow growth of metamorphic minerals and continuous equilibration during prograde metamorphism at greenschist facies conditions where the temperature is too low for allowing significant solid-state diffusion. As the prevailing stress field may control sites of preferred dissolution and precipitation, and mass transfer in the fluid may be highly anisotropic depending on the orientation and abundance of grain boundaries, all processes involved are inevitably linked with deformation. Although dissolution-precipitation and fluid-mediated mass transfer is well established for major components and growth metamorphic index minerals, little is known about the effects of these processes on accessory minerals that are considered nonreactive during metamorphism, consisting of elements that are considered as chemically immobile (e.g. Zr, Ti, Th). In this contribution, we present two case studies from the Staufen-Höllengebirge Nappe (Austroalpine Unit, Eastern Alps) which allow us to investigate the behaviour of Zr during greenschist facies prograde metamorphism in metasediments. At each locality we characterized detrital and metamorphic zircon populations with high-resolution SEM imaging and use a novel laser-ablation based strategy termed 'bulk inclusion dating' (Hollinetz et al. 2022) as a proxy for quantifying the extent of metamorphic zircon formation.

The first case study focuses on a chloritoid-bearing schist sampled at the base of the Staufen-Höllengebirge Nappe. Thermodynamic modelling predicts chloritoid growth in a P-T field between 450–490 °C and 0.5–0.7 GPa, indicating upper greenschist facies conditions. A conspicuous feature of this rock are numerous minute (0.1–3 μm), euhedral zircon crystals found both in chloritoid porphyroblasts and as matrix phases. From the zircon morphology, crystal size distribution, orientation and spatial distribution of different micro-zircon populations in the chloritoid core, its rim and the matrix, we interpret syntectonic zircon precipitation and progressive coarsening from a Zr-bearing fluid migrating along grain boundaries. Since no detrital zircon grains are observed in this sample, the Zr source is most likely a detrital Ti-phase that broke down during prograde metamorphism (e.g., titanite). Bulk inclusion dating of the chloritoid rim and its zircon inclusions yields a U-Pb age of 116.7 ± 9.1 Ma (MSWD: 1.5, n: 79), consistent with the Early Cretaceous timing of nappe stacking (Ortner et al. 2008). Systematic imaging of the targeted chloritoid domain combined with trace element data clarifies the abundance and size of different U-Pb bearing inclusions and unambiguously link the U-Pb age to micro-zircon inclusions. Our data therefore implies total mobilization of Zr during late prograde metamorphism.

The second case study focuses on metaconglomerates and -sandstones sampled in the Permian cover of the Staufen-Höllengebirge Nappe. In these lower greenschist facies samples, sedimentary features are preserved, but overgrown by a metamorphic mineral assemblage

consisting of chloritoid + pyrophyllite + muscovite + hematite + rutile + quartz that is consistent with P-T conditions of c. 350 °C and 0.2-0.6 GPa. Although all samples contain the same metamorphic mineral assemblage, they preserve significant differences regarding their primary sedimentological features (i.e., size of detrital clasts, layering) as well as secondary structural features (i.e. pressure solution cleavages). We investigated low-strain samples that exhibit a weakly developed fabric and high-strain samples with a pronounced spaced cleavage. Large, rounded detrital zircon grains that are occasionally fractured and/or porous are abundant in all samples. However, only in high-strain samples we find tiny zircon outgrowths on detrital grains and sparse submicron zircon (0.1–1 μm) in chloritoid. U-Pb ages of detrital zircon dominantly are between 700–400 Ma with the youngest concordant ages at c. 290 Ma. Bulk inclusion micro-zircon data in low-strain samples yield pre-Cretaceous dates younger than the detrital population, which indicates limited metamorphic zircon growth. In the "high-strain" samples, the bulk inclusion dates suggest significant micro-zircon crystallization in the Early Cretaceous. Combining microstructural observations and bulk-inclusion zircon data strongly suggests that Zr mobility and metamorphic zircon growth may be linked to intensity of deformation assisted by dissolution-precipitation.

We document deformation assisted Zr mobility in greenschist-facies metasediments and show that dissolution-precipitation coupled to mass transfer via an intergranular fluid is a process that is also relevant for elements reputed as immobile. As ongoing technological advances continuously shrink the limits imposed by instrumentation, the bulk-inclusion strategy can fill the gap in our understanding of the geological process leading to the precipitation of micro-zircon. This approach allows integration between metamorphic conditions, deformation and age constraints and opens up new applications in the investigation of low-grade metamorphic rocks, potentially including dating of deformation.

Hollinetz MS, Schneider DA, McFarlane CRM, Huet B, Rantitsch G, Grasemann B (2022): Bulk inclusion micro-zircon U–Pb geochronology: A new tool to date low-grade metamorphism. - J Metamorphic Geol 40, 207-227

Ortner H, Ustaszewski M, Rittner M (2008): Late Jurassic tectonics and sedimentation: breccias in the Unken syncline, central Northern Calcareous Alps. - Swiss J Geosci 101, 55-71

Fluid “self-purification” – Insight from the particle attachment processes during the growth of three-dimensional mineral dendrites

Z. Hou[1], D. Woś[2], A. Rogowitz[1,3], C. Tschegg[4], A.H.N. Rice[1], L. Nasdala[1], F. Fusseis[5], P. Szymczak[2], B. Grasemann[1]

[1]University of Vienna
[2]University of Warsaw
[3]University of Graz
[4]Glock Health, Science and Research GmbH, Deutsch-Wagram, Austria
[5]The University of Edinburgh
e-mail: zhaoliang.hou@univie.ac.at

Manganese (Mn) dendrites are a common type of mineral dendrites which can typically be found as two-dimensional branch-like patterns on rock surfaces, such as bedding planes and joints suggesting a fluid-rock interaction. Their three-dimensional (3D) counterpart has so far been massively overlooked, and thus little is known about 3D mineral dendrite growth processes and potential implications for fluid-rock interaction. Here, we combined high-resolution X-ray, electron-based micro-analyses with numerical modelling to show that the formation of natural 3D dendrites is an aggregation process of Mn-oxide nanoparticles in an aqueous environment. The dendrites form a < 15 mm high "forest" (Figure 1) in clinoptilolite-tuffs (zeolites), with trunks and branches, both having a core-rim structure and in the upper part of the forest, an alternating concentric core-rim layering. Secondary electron microscope (SEM) observations indicate dendrite growth reduced the rock´s original porosity from ~17% in the matrix to ~1% - 4% in the internal rims and 0% in the cores. High-resolution SEM shows dendrite-forming Mn oxides are built by sub-angular to rounded, several-nanometer- to 1-µm-sized particles that have been aggregated forming larger clusters. Using the lattice Boltzmann method we modelled the formation and evolutionary processes of the 3D Mn dendrites. This allowed us to track the diffusing population of Mn ions and oxygen molecules as well as the reaction between them that led to the formation of Mn-oxide nanoparticles. The mobility and aggregation of nanoparticle populations were then tracked.

Our numerical models suggest sensitive feedback between dendrite morphology and the volume of infiltrating fluids, as well as the concentrations of Mn ions. Our work provides three important findings. First, 3D mineral dendrites can offer a simple system to investigate the affecting physical parameters of particle attachment processes in nature, such as the interplay of diffusion and surface energy effects between particles on dendrite growth dynamics. Second, the growth of the 3D dendrites, aggregating the particles in the surrounding fluids, can be seen as a fluid "self-purification" process. Third, the formation of the banding structures of the 3D dendrites, as well as the sensitive growth of dendrites in relation to the volume of infiltrating fluid and concentrations of Mn ion, strongly suggest the dendrites encode the hydrogeochemical history of the hosting rocks.

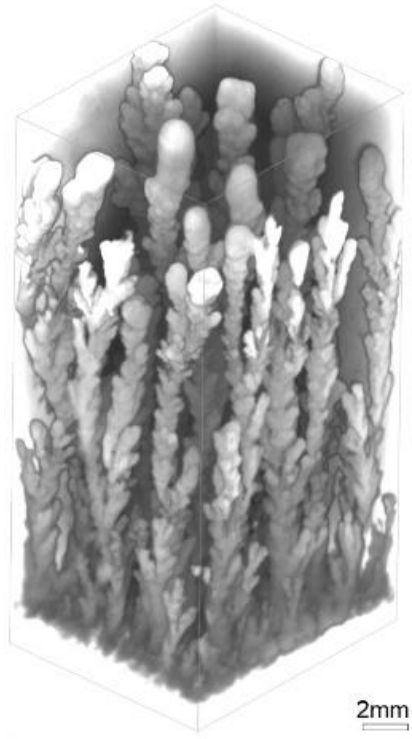

Figure 1. X-ray microtomography data show a 3D mineral dendrite forest.

Creep, fail, and creep again at eclogite facies: interactions between metamorphism and deformation at the Hohl eclogite body (Koralpe, Eastern Alps, Austria)

B. Huet[1], A. Rogowitz[2], S. Schorn[2]

[1]GeoSphere Austria
[2]*Institute of Earth Sciences, University of Graz*
e-mail: benjamin.huet@geosphere.at

We present (micro)structural, petrographical, and chemical data from a series of low Mg – high Ti eclogite samples collected at the Hohl eclogite body (Koralpe, Eastern Alps, Austria). The eclogite mass is characterized by a pronounced foliation defined by the shape preferred orientation of the major minerals (average: 030/40) and mineral lineation defined by the shape preferred orientation of prismatic minerals (average: 324/18). In addition to omphacite, garnet, amphibole, epidote and rutile, minor euhedral quartz grains are present. Overall, grains show rather straight grain boundaries and uniform extinction. Thermodynamic forward modelling indicates that eclogitization occurred under fluid saturated conditions at about 1.8 GPa and 640 °C, which is slightly below the peak conditions.

The eclogite fabric is crosscut by a complex network of mineral veins characterized by coarse elongated crystals. These veins have a thickness comprised between a few millimeters and a few centimeters and contain the same assemblage as the host eclogite. In comparison to the host, they are enriched in quartz and epidote and depleted in garnet. Minerals composition is similar to the composition of the host eclogite indicating that veining occurred at eclogite facies conditions. One vein set is subperpendicular to the main foliation (average: 234/27) and the other is subparallel to it (average: 055/51). In both sets, the long axis of crystals is subparallel to the vein boundary and strikes NW-SE, which is compatible with crystal growth in the same tectonic regime as the eclogite fabric. Wing cracks indicate that the veins formed as shear fractures. Deflection of the eclogite fabric adjacent to the veins implies ductile reactivation of the veins as flanking structures and strain localization under top-to-the-W shearing. In consequence, the reactivated veins are characterized by undulatory extinction, twinning and subgrain formation in quartz, all being indicative of dislocation creep.

Our investigations document strong interactions between chemical (i.e., metamorphism) and mechanical (i.e., deformation) processes operating at eclogite facies and illustrate how metamorphic reactions dictate the deformation style of an eclogite. The microstructures of the eclogite host are interpreted as evidence of fluid-triggered syn-tectonic prograde eclogitization accommodated by diffusion and dissolution-precipitation processes. Ongoing prograde metamorphism resulted in progressive dehydration and minor melting of the already equilibrated eclogite. Subsequent increase in the pore-fluid pressure induced brittle failure and allowed precipitation of an eclogite facies assemblage in the vein. Finally, the quartz enriched veins localized ductile strain and deformed by dislocation creep. Hence, within the same tectonic event and without remarkable change of boundary conditions, eclogite can creep, fail and creep again.

Thermodynamic forward modelling of main and REE-bearing phases linking in situ U-Th-Pb REE-epidote ages and pressure-temperature conditions

B. Huet[1], D.A. Schneider[2], G. Rantitsch[3]

[1]GeoSphere Austria, Vienna
[2]Department of Earth and Environmental Sciences, University of Ottawa
[3]Department of Applied Geosciences and Geophysics, Montanuniversität Leoben
e-mail: benjamin.huet@geosphere.at

REE-epidote is a solid solution of epidote-group minerals with rare earth elements plus yttrium that is a common phase of greenschist facies metapelites and a popular target for geochronology. Linking the time information to metamorphic conditions is however complicated by the diversity of reactions leading to the formation of REE-epidote as these involve REE- and/or Ca-bearing phases (e.g., monazite, apatite, calcite and plagioclase). We compiled a thermodynamic dataset for the system NaKCaFeMgAlSiTiHCOCeYPF from several sources (Berman, 1988; Connolly, 1995; Franzolin et al., 2011; Gaboreau et al., 2005; Hoschek, 2016; Pourteau et al., 2014; Spear, 2010; Spear & Pyle, 2010) in order to model equilibrium assemblages and phase chemistry for both main and REE-bearing phases in metapelites, especially in the greenschist facies.

We tested the dataset on a graphitic micaschist of the Schwarzkopf Formation collected at the foot of the Hochgamsburg (Fusch valley, Tauern Window). The sample shows relatively simple phase relationships and exhibits evidence for only one metamorphic event. The metamorphic assemblage consists of porphyroblasts of chloritoid, kyanite, REE-epidote and apatite in a matrix of muscovite, paragonite, margarite and quartz. Small rutile, graphite, xenotime and zircon are present as inclusions or in matrix. REE-epidote occurs as euhedral to subhedral, 250-1000 µm long grains and displays a microstructural and chemical core-mantle-rim zonation. The core has a patchy or oscillatory BSE pattern and is rich in inclusions of amoeboid quartz and minute graphite, as well as subordinate muscovite, chloritoid, rutile, xenotime and thorite. The mantle is discontinuous (< 60 µm thick), inclusion-free and shows a bright smoother BSE pattern. The rim corresponds to dark and thin discontinuous overgrowths (< 20 µm thick). Core, mantle and rim contain decreasing contents of REE+Th+U in the range 0.5–0.6, 0.4–0.6 and 0.1–0.3 a.p.f.u., respectively. The core and mantle are LREE-rich whereas the rim is HREE+Y-rich. LA-ICPMS analyses of REE-epidote mantle were carried out using a 20 µm laser spot diameter. All thirty-one analyses define a 27.5 ± 1.3 Ma U-Th-Pb isochron date (MSWD: 0.69) that is consistent with the conventional Tera-Wasserburg U-Pb date of 27.0 ± 2.3 Ma (MSWD: 0.36).

Thermodynamic forward modelling indicates that the observed assemblage chloritoid+kyanite+REE-epidote+muscovite+paragonite+margarite+apatite+rutile+xenotime+quartz is stable together with a graphite buffered COH-fluid in a narrow field centred at 12 kbar – 500 °C, in agreement with results of Raman spectroscopy on carbonaceous material (511 ± 26 °C). This field corresponds to the innermost part of the REE-epidote stability domain, in which the Ce-concentration progressively decreases from the margin to the centre. Modelling helps with interpreting the zonation of REE-epidote. The core grew from U-Th-rich monazite and most likely lawsonite once REE-epidote became stable. Xenotime inclusions represent products of this reaction. The mantle formed during continued growth further inside the REE-

epidote stability domain under increasing temperature. The HREE+Y-rich rim finally grew in an environment depleted in LREE, where xenotime was the main REE-source. Additionally the modelled compositions of chloritoid, white micas and apatite is compatible with the measured ones. Tests on the effect of unknown inputs (e.g., the bulk rock concertation of F) or poorly constrained thermodynamic data (e.g., the standard enthalpy of endmember allanite) indicate that these parameters have little impact on the results.

We could therefore acquire estimates for pressure and temperature and timing as well as coupling them tightly through thermodynamic modelling. The U-Th-Pb isochron date 27.5 ± 1.3 Ma represents the timing of the REE-epidote mantle growth and therefore corresponds to conditions close to peak metamorphism at 12 kbar – 500 °C. These P-T-t constraints are entirely consistent with the Barrovian metamorphic event that is widespread in the Tauern Window ("Tauernkristallisation").

Berman RG (1988): Internally-consistent thermodynamic data for minerals in the system Na_2O-K_2O-CaO-MgO-FeO-Fe_2O_3-Al_2O_3-SiO_2-TiO_2-H_2O-CO_2. - J Petrol 29, 445-522

Connolly JAD (1995): Phase diagram methods for graphitic rocks and application to the system C-O-H-FeO-TiO_2-SiO_2. - Contr Miner Petrol 119, 94-116

Franzolin E, Schmidt MW, Poli S (2011): Ternary Ca-Fe-Mg carbonates: subsolidus phase relations at 3.5 GPa and a thermodynamic solid solution model including order/disorder. - Contr Miner Petrol 161, 213-227

Gaboreau S, Beaufort D, Vieillard P, Patrier P, Bruneton P (2005): Aluminum phosphate-sulfate minerals associated with Proterozoic unconformity-type uranium deposits in the East Alligator River Uranium Field, Northern Territories, Australia. - Canad Miner 43, 813-827

Hoschek G (2016): Phase relations of the REE minerals florencite, allanite and monazite in quartzitic garnet-kyanite schist of the Eclogite Zone, Tauern Window, Austria. – Eur J Miner 28, 735-750

Pourteau A, Bousquet R, Vidal O, Plunder A, Duesterhoeft E, Candan O, Oberhänsli R (2014): Multistage growth of Fe-Mg-carpholite and Fe-Mg-chloritoid, from field evidence to thermodynamic modelling. - Contr Miner Petrol 168, 25 pp

Spear FS (2010): Monazite–allanite phase relations in metapelites. - Chem Geol 279, 55-62

Spear FS, Pyle JM (2010): Theoretical modeling of monazite growth in a low-Ca metapelite. - Chem Geol 273, 111-119

Structure and vibrational properties of hydrous and anhydrous amorphous SiO_2 at high pressures

S. Jahn[1], M. Herrmann[1], M. Schulze[1], J. Dreschmann[1], W. Morgenroth[2], G. Garbarino[3], M. Mezouar[3], M. Wilke[2]

[1] Institut für Geologie und Mineralogie, Universität zu Köln, Zülpicher Straße 49b, 50674 Köln, Germany
[2] Institut für Geowissenschaften, Universität Potsdam, Karl-Liebknecht-Str. 24, 14476 Potsdam, Germany
[3] ESRF, CS 40220, 38043 Grenoble Cedex 9, France
e-mail: s.jahn@uni-koeln.de

Volatiles such as H_2O are important components in natural silicate glasses and melts. Their solubility and structural incorporation mechanisms depend on many parameters, and they change continuously with pressure and temperature. For a systematic understanding of those changes, in situ measurements are required. Here, we study the pressure-induced structural evolution of hydrous amorphous SiO_2 in diamond and moissanite anvil cells up to 40 GPa by Raman spectroscopy and X-ray diffraction, and compare the results to those from the respective anhydrous samples. The hydrous sample contains 10 wt% H_2O. Both hydrous and anhydrous samples show the characteristic features of the 4-fold to 6-fold Si coordination transition, which is essentially completed at the highest pressures of this study. Raman spectra indicate the predominance of molecular H_2O species over hydroxyl groups in the whole pressure range. However, the spectra change significantly at wavenumbers in the range of the O-H stretching vibrations. By analogy to spectra of pure liquid and crystalline H_2O, a transition from water-like to ice-VI-like behavior is observed, before the spectra become very broad at the highest pressures. The interpretation of the experimental data is supported by *ab initio* molecular dynamics simulations.

This work was supported by BMBF project 05K19PK2. Simulations were performed on the JUWELS supercomputer at Jülich Supercomputing Centre (JSC).

$Ca_2(Mn,Ti)O_4$, a potentially new mineral with the Ruddlesden-Popper structure

R. Juroszek[1], B. Krüger [2], G. Cametti[3]

[1] Institute of Earth Sciences, University of Silesia, Katowice, Poland
[2] Institute of Mineralogy and Petrography, University of Innsbruck, Innsbruck, Austria
[3] Institute of Geological Science, University of Bern, Bern, Switzerland
e-mail: rafal.juroszek@us.edu.pl

A potentially new mineral $Ca_2(Mn,Ti)O_4$, was found within the xenolith sample from the Bellerberg volcano in Germany. It is an accessory phase in partially altered xenolith composed mainly of cuspidine, fluorapatite, and gehlenite. It forms flat plate dark-brown crystals up to 100 μm in size. The empirical formula, established by electron microprobe analyses, is $(Ca_{1.98}Ce_{0.06})_{\sum 2.04}(Mn^{4+}_{0.36}Ti_{0.35}Fe^{3+}_{0.19}Al_{0.09})_{\sum 0.99}O_4$.

This mineral exhibits a Ruddlesden-Popper type structure characteristic for perovskite-like layered oxides of general formula $A_{n+1}M_nO_{3n+1}$, where A is typically an alkaline or rare earth ion, and M is a transition or post-transition metal ion (Ruddlesden and Popper, 1957). The diffraction pattern of the analysed crystal reveals a tetragonal lattice with unit cell parameters a = 3.7666(2) Å, c = 11.9861(8) Å, and volume V = 170.050(17) Å^3. The A site was refined with Ca^{2+} and Ce^{3+} scattering factors, whereas for the M site, a mixed scattering curve was used (0.55 Mn/Fe + 0.36 Ti + 0.09 Al) according to the chemical analyses. The final structure refinement converged to R = 2.74%. The crystal structure of $Ca_2(Mn,Ti)O_4$ exhibits a modular nature and consists of $Ca(Mn,Ti)O_3$ perovskite layers, which are packed between CaO rock-salt layers arranged along the c-axis (Fig. 1).

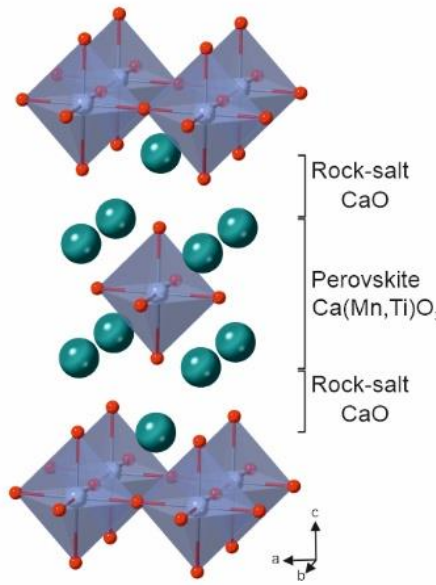

Figure 1. The $Ca_2(Mn,Ti)O_4$ phase with Ruddlesden-Popper structure, comprising rock-salt (CaO) and perovskite layers $Ca(Mn,Ti)O_3$ build by Ca-green spheres and $(Mn,Ti)O_6$ octahedra.

Previous reports indicate that Ruddlesden-Popper calcium manganates exhibit functional electronic properties and are interesting for various electronic phenomena, such as insulator-to-metal transitions, charge-ordering, and colossal magnetoresistance effect (Fawcett et al. 1998; Autret et al. 2004).

The investigation was partially supported by the National Science Center of Poland Grant (grant number 2021/41/B/ST10/00130).

Autret C, Martin C, Hervieu M, Retoux R, Raveau B, André G, Bourée F (2004): Structural investigation of Ca_2MnO_4 by neutron powder diffraction and electron microscopy. – J Solid State Chem 177, 2044-2052

Fawcett I.D, Sunstrom J.E, Greenblatt M, Croft M, Ramanujachary K.V (1998): Structure, magnetism, and properties of Ruddlesden-Popper calcium manganates prepared from citrate gels. – Chem Mater 10, 3643-3651

Ruddlesden S, Popper P (1957): New compounds of the K_2NiF_4 type. – Acta Crystallogr 10, 538-539

Structural news from the quaternary system Na_2O-K_2O-CaO-SiO_2

V. Kahlenberg[1], H. Krüger[1], S. Garber[1], J. Aschauer[1]

[1]University of Innsbruck, Institute of Mineralogy and Petrography, Innrain 52, 6020 Innsbruck, Austria
e-mail: volker.kahlenberg@uibk.ac.at

The crystalline compounds and sub-solidus equilibria in the ternary subsystems Na_2O-CaO-SiO_2 and K_2O-CaO-SiO_2 have been studied frequently in the past. On the contrary, the quaternary system containing both alkali oxides is rather uncharted territory and no thermodynamic or detailed phase-analytical data are available. So far, only a few potassium-sodium-calcium silicates such as $K_{1.08}Na_{0.92}Ca_6Si_4O_{15}$ (Kahlenberg et al. 2018a) or $Na_{1.5}K_{0.5}Ca_6Si_4O_{15}$ (Kahlenberg et al. 2018b) or $NaKCa_4[Si_9O_{23}]$ (Kasatkin et al. 2019) have been structurally characterized. While the first two members are mixed-anion silicates and isostructural with ternary phases, the latter compound corresponding to the mineral patynite represents a previously unknown structure type and belongs to the group of tubular inosilicates.

Our own recent synthesis experiments in the quaternary system K_2O-Na_2O-CaO-SiO_2 proved that there exists a complete solid-solution series between $Na_4CaSi_3O_9$ and its K-counterpart: $Na_{4-x}K_xSi_3O_9$. Lattice parameters of the cubic materials (space group $Pa\bar{3}$) obtained in polycrystalline form from solid-state reactions vary between 15.0998 (x = 0) and 15.9472 (x=4) Å. The silicate anions form strongly corrugated 12-membered tetrahedral rings.

Furthermore, we were able to prepare a previously unknown compound with composition $K_{0.72}Na_{1.71}Ca_{5.79}Si_6O_{19}$. Single-crystals of sufficient size and quality could be retrieved from a starting mixture with a K_2O:Na_2O:CaO:SiO_2 ratio of 1.5:0.5:2:3. The crystal structure was determined by direct methods at 25 °C from single crystal X-ray diffraction data (tetragonal symmetry, space group $P4_122$, a = 7.3659(2) Å, c = 32.2318(18) Å, V = 1748.78(12) Å^3, Z = 4, R_1 = 0.026, wR_2 = 0.063, for 1690 observed reflections with I > 2σ(I)). The silicate anion consists of highly puckered unbranched six-membered oligogroups of composition $[Si_6O_{19}]$ having point-group symmetry 2 (C_2). Even though several thousands of natural and synthetic oxidosilicates have been structurally characterized, the present compound is the first representative for this type of catena-hexasilicate anion - at least to the best of our knowledge.

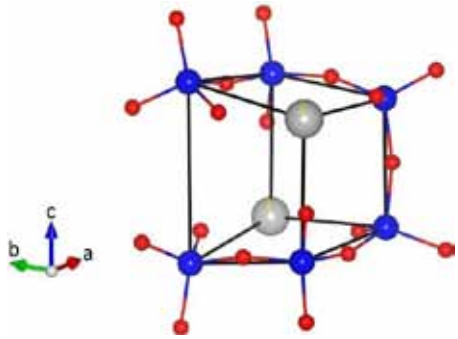

Figure 1. Conformation of a single $[Si_6O_{19}]$ group in $K_{0.72}Na_{1.71}Ca_{5.79}Si_6O_{19}$. The six Si atoms (blue) can be thought of as being located at the corners of an imaginary distorted cube with edge lengths between 3.22 and 4.60 Å. The remaining two corners are occupied by Na/Ca cations (grey/yellow). Oxygen atoms are shown in red.

Kahlenberg V, Mayerl MJP, Schmidmair D, Krüger, H (2018a): First investigations on the quaternary system Na_2O-K_2O-CaO-SiO_2: synthesis and crystal structure of $K_{1.08}Na_{0.92}Ca_6Si_4O_{15}$. - Miner Petrol 112, 219-228

Kahlenberg V, Mayerl, MJP, Schmidmair D, Krüger H, Tribus M (2018b): Preparation and characterization of $Na_{1.5}K_{0.5}Ca_6Si_4O_{15}$ and $Na_{1.41}K_{0.19}Ca_{2.20}Si_2O_7$: two new phases in the system Na_2O–K_2O–CaO–SiO_2. - Eur J Mineral 30, 957-966

Kasatkin AV, Cámara F, Chukanov NV, R. Škoda, F. Nestola, AA Agakhanov, DI Belakovskiy, V.S Lednyov (2019): Patynite; $NaKCa_4[Si_9O_{23}]$, a new mineral from the Patynsky massif. - Minerals 6, 611, 18 pp

Children's and teenagers' geoscience projects at the Mineralogical State Collection Munich (MSM)

M. Kaliwoda[1,2], M. Junge[1,2], F. Hentschel[1], F. Joseph[1], W.W.Schamahl[1,2]

[1]Mineralogical State Collection Munich, SNSB
[2] Department of Earth and Environmental Sciences, LMU, Ludwig Maximilians University, Munich
e-mail: kaliwoda@snsb.de

The Museum Mineralogia München is the publicly accessible part of the Mineralogical State Collection Munich (MSM), which belongs to the Bavarian State Natural Science Collections (SNSB). The aim of the State Collection is to impart knowledge in the STEM subjects, i.e. especially in the field of geosciences. The MSM has been trying to fulfil this task for more than 16 years and has thus gained a great amount of experience in the teaching-learning field.

Since the geosciences are unfortunately not a school subject, but geoscientific topics are becoming more and more relevant for socio-political concerns, it is important to sensitize and inspire children and young people for the geosciences at an early age.
The Museum Mineralogia therefore offers a variety of activities on topics such as (1) volcanism, (2) the cycle of rocks, (3) meteorites, (4) the construction of a smartphone and critical raw materials. In addition, there are special exhibits each year on a variety of earth science topics that are incorporated into the student projects and tours. All projects offered can also be booked as school and kindergarten projects, if there is capacity. In addition, there is a network with other science laboratories for schoolchildren both in Munich (Muc-Labs) and throughout Germany (LeLa). Participation (e.g., in Girls'Day, Science Days (Forscha), or the Children's Culture Summer) as well as many different projects in Munich and the surrounding area with other museums and research institutes also strengthen the reach. In addition to national projects, international projects (e.g. with Austria, Italy, Norway) are carried out.

As a further concept, internships are also offered for school students from the age of 14. In addition, the Mineralogische Staatssammlung Munich has successfully participated in two funded programs on ease-Corona (BMBF - catching up after Corona). Here, especially children and teenagers who show Corona and Lock-down induced learning deficits should be supported.

Raman spectroscopy as an important tool for the petrological study of different meteorite samples

M. Kaliwoda[1,2], I. Drozdovsky[3], F. Joseph[1], F. Dellefant[2], W.W. Schmahl[1,2]

[1]Mineralogical State Collection Munich, SNSB, Munich, Germany
[2]Departnemt of Earth and Environmental Sciences, LMU, Ludwig Maximilians University, Munich, Germany
[3]European Astronaut Centre (EAC) - European Space Agency, Cologne, Germany
e-mail: kaliwoda@snsb.de

Spectroscopic methods with their capability to gain information on different rocks and minerals as well as on fluids and other types of inclusions are becoming more and more relevant in earth sciences in order to open up new fields of research and providing solutions to problems in various scientific disciplines.

Raman spectroscopy represents a fast and at the same time precise method to characterize materials in different types of environments. Furthermore, Raman spectroscopy can be an important tool to investigate extraterrestrial bodies, because the measurements are more or less independent of the surrounding environmental effects including the temperatures. Therefore, it will be an important goal to gain as much experience as possible by Raman measurements of meteorites in order to be able to apply this experience to extraterrestrial bodies.

At the mineralogical state collection Munich (MSM) Raman spectroscopy is used to characterize different meteorites, with main focus to mars, moon and vesta, in order to find out the composition of the various minerals, the high pressure phases, the possible glass components and the inclusions. All the measured phases are collected in an in-house Raman database (Kaliwoda et al. 2013, 2021; Drozdovsky et al. 2020).

Raman spectroscopy make it possible to gain more information about the mineral composition and the original pressure and temperature conditions on these extraterrestrial bodies. In addition, it is possible to draw parallels to the composition and to the formation history of the early earth. In another Raman study we aim at getting more detailed information about the earth mantle and investigate therefore mantle-xenoliths and ophiolitic mantle sections.

One examples of our research targets is NWA11266 meteorite, discovered in 2017, that has already been classified as lunar feldspar breccia (Gattacceca et al., 2019). In the MSM we did further investigations with Raman spectroscopy. The main minerals are mafic olivines and pyroxenes, beside anorthitic feldspar minor graphite and tiny little glass patches. Furthermore, metallic components and accessory phases like apatite and zircon could be identified. In addition, we like to compare brecciated meteorites with other terrestrial Breccias, like those from the Nördlinger Ries.

Drozdovskiy I, Ligeza G, Jahoda P, Franke M, Lennert P, Vodnik P, Payler SJ, Kaliwoda M, Pozzobon R, Massironi M, Turchi L, Bessone L, Sauro F (2020): The PANGAEA Mineralogical Database. - Data in Brief 31, S2352-3409(20), 30879-9, https://doi.org/10.1016/j.dib.2020.105985

Gattacceca J, Bouvier A, Grossman J, Metzler K, Uehara M (2019): The meteoritical bulletin, no. 106. -Meteorit Planet Sci 54, 469–471

Kaliwoda, M, Giordano, D, Krüger ME, Uysal I, Akmaz MR, Hoffman, V, Hochleitner R, Schmahl WW (2021): Raman spectroscopy as a tool for the quantitative estimate of chromium aluminium oxide content in chromite. - Spectroscopy 36, 17-23

Kaliwoda M, Hochleitner R, Hoffmann VH, Mikouchi T, Gigler AM, Schmahl WW (2013): New Raman spectroscopic data of the Almahata Sitta Meteorite. - Spectroscopy letters 46, 141-146

Antimony isotope evolution during hydrothermal precipitation and during oxidative weathering of diverse antimony mineralization in the Western Carpathians (Slovakia)

A. Kaufmann[1,2], M. Lazarov[1*], S. Weyer[1], J. Majzlan[2]

[1] Institute of Mineralogy, Leibniz University Hannover, Germany
[2] Institute of Geosciences, Friedrich Schiller University Jena, Germany
**e-mail: m.lazarov@mineralogie.uni-hannover.de*

Numerous hydrothermal Sb or Sb-Au mineralization and ore deposits are seated in a Variscan basement of the Western Carpathians (Slovakia). Stibnite is the most common mineral in all of them. However, each deposit has its specific mineralization association and Sb is found in a variety of sulfides, sulfosalts, or oxides, in combination with Cu, Pb, Fe, or Ag. All these minerals, on macro- or microscale, carry information about the ore-forming processes. In this study, a variety of Sb minerals from four ore deposits: Dve Vody, Magurka, Dúbrava and Pezinok, are investigated for their Sb isotope composition. Measurements were conducted *in-situ* by deep UV-fs laser ablation system coupled with MC-ICP-MS following the procedure of Kaufmann et al. (2021).

The δ^{123}Sb values of all investigated primary hydrothermal minerals show a range of -0.8 to +1.0 ‰. Variations of δ^{123}Sb for each deposit do not exceed 0.8 ‰. Combining information from textural relationships and Sb isotope compositions, in some cases also mineral trace-element contents, implies that mineral δ^{123}Sb can be correlated with the mineral precipitation sequence. This relationship can be observed on hand-specimen as well as on ore body and ore deposit scale. The systematic increase of δ^{123}Sb values during progressive precipitation of primary Sb minerals can be rationalized by a Rayleigh crystallization model, applying a uniform isotope fractionation factor for all minerals that was determined for stibnite by Zhai et al. (2021).

Each ore deposit has its own distinct mean of δ^{123}Sb. Dúbrava displays the lowest values of around -0.11 ±0.56 ‰, followed by Magurka and Pezinok with a mean of 0.08±0.59 ‰ and 0.24±0.48 ‰, respectively. The overall heaviest isotopic compositions are observed for Dve Vody ~ 0.53±0.88 ‰. These differences may indicate that either different sources or differently developed fluids, or both were responsible for each deposit formation.

A similar spread of δ^{123}Sb (-0.50 to +0.8 ‰) was observed for secondary Sb minerals formed near surface as the result of weathering. Depending on the amount of leached, primary mineral, and redox changes during transport and formation of secondary minerals, Sb isotope fractionation of more than 0.3 ‰ was observed. While the Sb oxides tend to become isotopically heavier, Sb hydroxides, Fe,Sb oxides or silicates prefer the ^{121}Sb isotope and display lower δ^{123}Sb signatures, compared to the coexisting primary minerals.

Thus, considering all studied deposits, mineral δ^{123}Sb may help to constrain the precipitation sequences in primary ore deposits, to decipher hydrothermal remobilization or near-surface weathering of primary ores and to constrain the potential source(s) of the metalloid.

Kaufmann AB, Lazarov M, Kiefer S, Majzlan J, Weyer S. (2021): In-situ determination of antimony isotope ratios in Sb minerals by femtosecond LA-MC-ICP-MS. - JAAS 36, 1554-1567

Zhai D, Mathur R, Liu SA, Liu J, Godfrey L, Wang K, Vervoort J. (2021): Antimony isotope fractionation in hydrothermal systems. - Geochim Cosmochim Acta 306, 84-97

Isotope fractionation of antimony during oxidative weathering of stibnite (Sb_2S_3)

A.B. Kaufmann[1,2], M. Lazarov[2], J. Majzlan[1], S. Weyer[2]

[1]Friedrich-Schiller University Jena
[2]Leibniz University Hannover
e-mail: a.kaufmann@mineralogie.uni-hannover.de

Antimony (Sb) has two stable isotopes with almost equal abundances (^{121}Sb = 57.213 %, ^{123}Sb = 42.787 %). Similar to Mo, V, Fe and U, Sb is redox-sensitive, however, with a higher redox potential (Eh value) than the aforementioned elements. It can occur in four formal (-I, 0, +III, +V) oxidation states with commonly +III and +V encountered in nature. Therefore, stable Sb isotope signatures could have great potential as a redox proxy in low-temperature surface studies to reconstruct the weathering conditions of recent and Early-Earth environments. The transport of Sb in the environment (including soils, water and sediment) was reviewed by Herath et al. (2017), however, only scarce experimental data exist, regarding the environmental release of Sb (e.g., Biver et al. 2012) under different Eh conditions. In this study, we experimentally explored the leaching behaviour of stibnite (Sb_2S_3), the most common Sb mineral in nature, and associated isotope fractionation. For this, we performed leaching experiments with an isotopically homogeneous stibnite powder (0.14 g) and three different acids (0.05 M HCl, 0.5 M HNO_3 and 0.1 M oxalic acid) with a volume of 200 ml each. Antimony concentration, isotope composition, pH, and Eh values were determined at selected time steps in a time interval from 30 minutes to 13 days. During the leaching experiments, the pH value of oxalic acid and HCl solutions remained constant at 1.4 and 1.5, respectively, whereas that of HNO_3 rapidly increased from 0.7 to 1.2 and stabilized at 1. The Eh of the HCl solution was adjusted at 570 mV during the first 20 hours, whereas the Eh of HNO_3 and oxalic acid decreased to <630 mV till the end of the experiment. During the first 6 hours, with high Eh (>730 mV) for HNO_3 and oxalic acid, stibnite released almost 1% of Sb (>900 µg), resulting in ~0.1 ‰ heavier and ~0.3 ‰ lighter δ^{123}Sb for oxalic acid and HNO_3, respectively. In comparison, HCl, without large Eh changes, preferentially mobilized the lighter Sb isotope, resulting in δ^{123}Sb ~ -0.4 ‰ compared to the precursor material (δ^{123}Sb = -0.21 ‰). In the HCl experiment, equilibrium was achieved after 20h with constant Sb concentration and δ^{123}Sb. Conversely, progressive leaching with HNO_3 and oxalic acid, accompanied with a Eh drop, resulted in an increase of the Sb content (>2 %) with preferential mobilisation of the heavy Sb isotope. The leachate for the first 20 hours of leaching is marked by <0 saturation indexes relative to Sb oxides, resulting into progressive dissolution of Sb. After a further slight decrease of Eh values (e.g. from 630 mV to down to 565 mV for oxalic acid) at >20 hours, the leachate became alternately over- and undersaturated relative to Sb oxides, resulting in the precipitation of Sb oxides along with additional Sb leaching. In comparison, natural secondary minerals show an isotopic variation of -0.5 to +0.3 ‰ with also preferentially enrichment of light Sb isotope compared to primary minerals (isotopic range: -0.4 to +0.8) that are consistent with our leaching results with weak acids of HNO_3 and HCl, which generates heavy isotopic Sb enriched residues. With this in mind, our first results indicate the potential of Sb isotopes as a new proxy to interpret modern and past weathering and hydrothermal alteration environments.

Biver M, Shotyk W (2012): Stibnite (Sb_2S_3) oxidative dissolution kinetics from pH 1 to 11. – Geochim Cosmochim Acta 79, 127-139

Herath I, Vithanage M, Bundschuh J (2017): Antimony as a global dilemma: Geochemistry, mobility, fate and transport. – Environmental Pollution 223, 545-559

Reconstruction of a 3.5-billion-year-old marine environment: Evidence from trace element data of iron formation from the Daitari Greenstone Belt, Singhbhum Craton, India

S. Kienle[1], S. Viehmann[2], J. Jodder[3,4], A. Hofmann[4], T. Schulz[1], C. Koeberl[1]

[1]Department of Lithospheric Research, University of Vienna, Austria
[2]Institute of Mineralogy, Leibniz University Hanover, Germany
[3]Evolutionary Studies Institute, University of the Witwatersrand, South Africa
[4]Department of Geology, University of Johannesburg, South Africa
e-mail: a01616435@unet.univie.ac.at

Banded Iron Formations (BIF) are marine chemical sedimentary rocks common in Precambrian volcano-sedimentary sequences. BIFs serve as geochemical archive of the composition of Precambrian seawater, and their trace element composition aids to investigate the geochemical evolution of the early Earth.

The Daitari Greenstone Belt (DGB) in the Singhbhum Craton of India hosts a ca. 3.5–3.3 Ga old volcano-sedimentary sequence with BIFs preserved within the Tomka Formation (Jodder et al. 2023). The DGB has only experienced greenschist-facies metamorphic conditions (Hofmann et al. 2022) providing a unique record for marine chemical sediments from the early Archean. Here we studied the Tomka BIF, which might serve as an excellent geochemical archive to reconstruct physico-chemical conditions of the 3.5-billion-year-old marine environment in the Daitari area. It may provide unique insights into the state of Earth's oceans, continents, and atmosphere within this critical time window.

Trace element compositions of high pressure-high temperature digestions of individual chert-, Fe- and mixed Fe- and chert-microbands were determined via quadrupole ICP-MS following the protocol described in Viehmann et al. (2016). Trace element compositions of chemical sediments can be used to reconstruct the depositional environment and physico-chemical conditions of the ambient atmosphere and hydrosphere. The Tomka BIF samples have very low concentrations of incompatible elements such as Al, Hf, Th, and Zr. In addition, the concentrations of rare earth elements and yttrium (REY) show no correlations with fluid-mobile elements such as Sr. The chemical compositions thus highlight their usefulness as a geochemical archive of Paleoarchean seawater. Pure chert, Fe- and mixed layers of the Tomka BIF display typical REY distribution patterns of Archean seawater (e.g., Alexander et al., 2008) and shale-normalized (subscript SN) REY_{SN} patterns similar to modern seawater, i.e., enrichment of heavy to light REY_{SN} (Yb_{SN}/Pr_{SN}: 2.67-20.4), positive La_{SN} (La_{SN}/La_{SN}*: 1.43-3.43) and Gd_{SN} (Gd_{SN}/Gd_{SN}*: 1.12-1.64) anomalies and super-chondritic Y/Ho ratios (41.2-66.7). The presence of positive Eu_{SN} (Eu_{SN}/Eu^*_{SN}: 1.37-3.17) anomalies indicate REY contributions from high-temperature hydrothermal fluids in seawater of the Tomka depositional environment. The lack of negative Ce_{SN} (Ce_{SN}/Ce^*_{SN}: 0.67-1.37) anomalies suggests anoxic atmospheric-hydrospheric conditions during BIF deposition.

The presence or absence of Eu anomalies in chondrite-normalized (subscript CN) REY patterns of BIFs can be used to distinguish between Archean and Post-Archean chemical sedimentary rocks. REY data of pure BIFs show that Eu_{CN}/Eu^*_{CN} ratios of Precambrian seawater follow a general global evolution curve with BIFs displaying strong positive Eu_{CN} anomalies in the Eoarchean, followed by decreasing Eu_{CN}/Eu^*_{CN} ratios until the Neoarchean (Viehmann et al. 2015). Eu data from BIFs in the time frame around 3.5 Ga, however, are lacking to date. Eu_{CN}/Eu^*_{CN} ratios of the Tomka BIF that fall into this time window do not follow the global seawater Eu curve but show significantly lower Eu_{CN}/Eu^*_{CN} values than expected. These values may indicate a less pronounced flux of high-temperature hydrothermal REY to the Archean ocean 3.5 Ga ago.

Alexander BW, Bau M, Andersson P, Dulski P (2008): Continentally-derived solutes in shallow Archean seawater: Rare earth element and Nd isotope evidence in iron formation from the 2.9 Ga Pongola Supergroup, South Africa. - Geochim Cosmochim Acta 72(2), 378–394

Hofmann A, Jodder J, Xie H, Bolhar R, Whitehouse M, Elburg M (2022): The Archaean geological history of the Singhbhum Craton, India – a proposal for a consistent framework of craton evolution. - Earth-Science Reviews 228, 103994

Jodder J, Hofmann A, Xie H, Elburg MA, Wilson A 2023: Geochronology of the Daitari Greenstone Belt, Singhbhum Craton, India. - Precamb Res 388, 106997

Viehmann S, Bau M, Bühn B, Dantas EL, Andrade FRD, Walde DHG (2016): Geochemical characterisation of Neoproterozoic marine habitats: Evidence from trace elements and Nd isotopes in the Urucum iron and manganese formations, Brazil. - Precamb Res 282, 74–96

Viehmann S, Bau M, Hoffmann JE, Münker C (2015): Geochemistry of the Krivoy Rog Banded Iron Formation, Ukraine, and the impact of peak episodes of increased global magmatic activity on the trace element composition of Precambrian seawater. - Precamb Res 270, 165–180

Special exhibitions are suitable for knowledge transfer

D. Kleinschrot[1]

[1]*University of Wuerzburg*
e-mail:kleinschrot@uni-wuerzburg.de

The most beautiful exhibits are in the showcases of our museum and attract numerous visitors who want to see these original objects from locations all over the world. The permanent exhibition can be visited at any time during opening hours and gives visitors enough time and space to learn more about the objects or to deal with a specific topic. In the temporary exhibitions of the Mineralogical Museum, for example, current topics such as raw materials in smartphones are dealt with. Scientists take the opportunity to present their research results to a broad public and thus emphasize their importance for society. In 2007 we presented 25 years of Antarctic research. Mining in Namibia and the exploration of eclogite and gold were also themes of exhibitions. Collaborations with various artists attract visitors to the museum who previously had little or no interest in geosciences. Together with other institutions, museums, and students, we organized an interdisciplinary exhibition project that showed the different aspects of color. Today we are still showing a showcase from this exhibition. The formats of the respective exhibitions are different. We have the showcase that changes quarterly, showing a mineral's properties, its origin and use as a raw material. Every one to two years we create larger exhibitions lasting 6 to 12 months. The museum team conveys the complex content in easy-to-understand exhibition texts, organizes lectures, guided tours, action Sundays for families and hands-on stations in order to reach a broad target group and, above all, to introduce young people to science. The amount of work is enormous and a temporary exhibition is usually associated with high costs. In order to convince sponsors of our work, we carried out visitor statistics, among other things. We can thus show that the number of visitors is increasing during special exhibitions and that the accompanying program is being used for further training by school classes and individuals of different ages.

GEOROC 2.0: A globally connected geochemical database to facilitate interdisciplinary, data-driven research

M. Klöcking[1], A. Sturm[2], B. Sarbas[1], L. Kallas[1], S. Möller-McNett[1], K. Lehnert[3], K. Elger[4], W. Horstmann[2], D. Kurzawe[2], M. Willbold[1], G. Wörner[1]

[1]Geoscience Centre, Universität Göttingen
[2]Göttingen State and University Library
[3]Columbia University, New York
[4]GFZ Data Services, Potsdam
e-mail: gwoerne@gwdg.de

The GEOROC database is one of the leading, open-access sources of geochemical and isotopic datasets that provides access to curated compilations of igneous and metamorphic rock and mineral compositions from >20,600 publications. It is an international data resource that supports hundreds of new research publications each year across multiple geoscientific and related disciplines (Chamberlain et al., 2021; Klöcking et al., 2023).
In this context, the Digital Geochemical Data Infrastructure (DIGIS) initiative is currently developing a new IT and data infrastructure for GEOROC 2.0 to facilitate modern solutions to data submission, discovery and access (Fig. 1). GEOROC data compilations are made accessible via a web search interface and trough a dedicated API. DIGIS also maintains a direct data pipeline of GEOROC compilation data to the EarthChem Portal (Fig. 2), which enables combined searches across six distinct geochemical databases. The DIGIS infrastructure further includes a domain repository for direct submission of geochemical datasets by the community (Fig. 2). This repository is hosted and curated in partnership with the GFZ Data Services of the GFZ (German Research Centre for Geosciences) in Potsdam. In addition, this repository can also be used for archiving citeable database versions.

Fig. 1: Setup and IT-environment of the GEOROC database

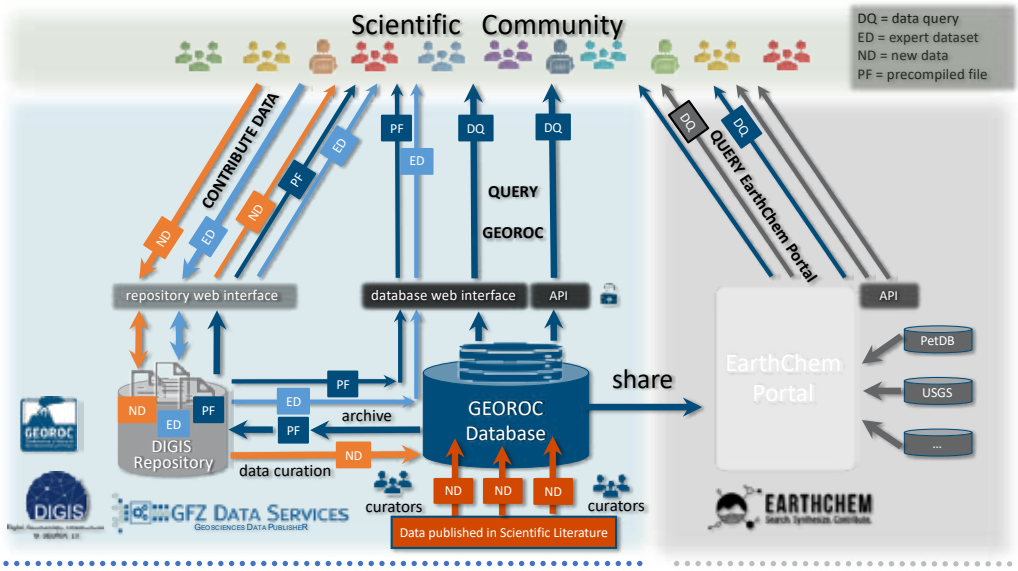

Fig. 2: The GEOROC data base and links to geochemical data services

In an effort to standardise geochemical data reporting, DIGIS collaborates with EarthChem, Astromat, and MetBase to develop common vocabularies that will enhance international interoperability of geo- and cosmochemical data systems. Part of this cooperation is the development of a joint, browser-based data entry tool for the GEOROC, PetDB and Astromat synthesis databases, which will avoid duplication of data and ensure consistent data and metadata quality through common curation policies. With these efforts, and as a participant of the "OneGeochemistry" initiative, DIGIS is working towards the goal of globally harmonised and FAIR geochemical data and support interdisciplinary, data-driven research.

Klöcking M, Wyborn L, Lehnert K, Ware B, Prent A, Profeta L, Kohlmann F et al. (2023): Community recommendations for geochemical data, services and analytical capabilities in the 21st century. - Geochimica et Cosmochimica Acta 351, 192-205, DOI: https://doi.org/10.1016/j.gca.2023.04.024

Chamberlain KJ, Lehnert KA, McIntosh IM, Morgan DJ, Wörner G (2021): Time to change the data culture in geochemistry. - Nat Rev Earth Environ (2021), https://doi.org/10.1038/s43017-021-00237-w

Petrogenetic information stored in needle-shaped rutile inclusions in pegmatoid garnet

V. Kohn[1], T. Griffiths[1], E. Libowitzky[1], O. Ageeva[1], R. Abart[1], G. Habler[1]

[1]University of Vienna, Josef-Holaubek-Platz 2, 1090 Wien, Austria
e-mail: victoria.kohn@univie.ac.at

We investigate the petrogenetic information stored in needle-shaped rutile inclusions hosted by garnet. For this purpose, microstructural and compositional zoning of almandine-spessartine garnet (Grt) in a pegmatoid from the Gföhl Unit (Bohemian massif, AT) is correlated with host-inclusion crystallographic and shape orientation relationships along the transition between microstructurally distinct garnet growth zones. The transition from the Grt core to the garnet rim (R1) is defined by a gradual increase in the aspect ratio of rutile (Rt) inclusions accompanied by a reduction in Grt colour intensity. The coloured outer core of Grt hosts equant rutile inclusions, whereas the uncoloured Grt zone R1 contains rutile needles of c. 100 – 150 µm length (Figure 1).

More than 11 different crystallographic orientation relationships (CORs) between Grt host and Rt inclusions are known (Hwang et al. 2016; Griffiths et al. 2016). The new dataset documents a systematic correlation of the shape preferred orientations (SPOs) of rutile inclusions in garnet, and the CORs between the two phases. This allows grouping specific CORs according to the particular crystallographic axes that coincide with the needle elongation directions: Group A Rt⟨103⟩‖Grt⟨111⟩*, Group B Rt⟨001⟩‖Grt⟨111⟩** and Group C Rt⟨001⟩‖⟨100⟩***. The two microstructural domains show remarkable differences in the frequencies of these COR groups. In the outer core of garnet Group A CORs are predominant (> 70%), while Grt zone R1 shows a predominance of Group B CORs, as well as a significantly higher abundance of CORs assigned to Group C, which are almost absent in the outer core.

As the major element profile of garnet along this microstructural transition is continuous, and the trace element distribution in Grt allows us to exclude significant re-equilibration by diffusion, we conclude that other factors than changes in the PT-conditions are responsible for the differences in the garnet microstructure and COR frequencies.

Growth zone R1 is characterized by the exclusive presence of Qtz inclusions and elevated Na_2O and OH^- content compared to the Grt core, implying an increase in the water activity during R1 growth. Hydrogen content in Alm-Sps garnet has been confirmed to increase from wall to core zones of pegmatites and to serve as tracer for their evolution (Arredondo et al. 2001). Consistently, we also observe an increase in anorthite content in matrix plagioclase (Pl). In analogy to basaltic systems, Pl crystallising from a melt at constant or decreasing temperature can be referred to an increase in water activity (Lange et al. 2009, Housh and Luhr, 1991). Therefore, change in Pl-composition caused by increasing water activity could represent the source of Si and Na during R1 garnet growth. In summary, the observed compositional zoning trends of garnet and plagioclase are consistent with an increase in H_2O concentration of the melt, without need for significant changes in PT-conditions during garnet core and R1 growth.

The comparison of the studied sample with a pegmatite garnet from the Koralpe (Eastern Alps, AT) shows remarkable similarities (Griffiths et al. 2014; 2016). There, the coloured garnet core comprises mostly equant rutile inclusions and corundum, while colourless garnet rim domains contain needle-shaped rutile inclusions and aluminosilicates, and are intergrown with Qtz. Most interestingly, the Koralpe pegmatite garnet rim also has a higher abundance of Group B CORs, compared to the garnet core domains of the same sample. We

conclude that the observed microstructural transition is possibly connected with an increase of Si and/or H_2O-concentration in the melt.

As the formation of dispersed needle-shaped rutile inclusions in garnet is often referred to exsolution from the host garnet (Griffin et al. 1971; Gou et al. 2014), the frequencies of shape preferred orientations (SPOs) of rutile in garnet zone R1 were studied on the basis of > 2500 rutile needles. We observe SPOs of rutile along particular garnet crystal directions, where rutile needle elongation parallel to <111>Grt by far exceeds Rt needle elongation direction parallel to <100>Grt. Based on the assumption that the exsolution of rutile inclusions from garnet would lead to equal abundance of SPOs in symmetrically equivalent directions, each individual needle orientation was counted in R1 zones of two {112}Grt growth sectors corresponding to different crystallographically equivalent garnet facets. We find that those rutile needles parallel to <111>Grt with the lowest angle to the garnet growth direction have a higher abundance, whereas rutile needles with their elongation direction parallel to the particular Grt growth facet plane are absent in both studied growth sectors. Due to this growth-related effect on the SPO frequencies we conclude that the rutile needles originate from co-growth with their host crystal (Griffiths et al. 2020).

* Group A contains the specific CORs with a common axial relationship: COR-1, 2, 2', 3, R3a and an undescribed COR defined by Rt ⟨100⟩‖Grt{112} and Rt ⟨320⟩‖Grt{120},
** Group B contains COR-4 and 4b,
*** Group C contains COR-5 and 5a (Hwang et al 2016; Griffiths et al. 2016).

Figure 1. Optical micrograph (plane polarized light) of the microstructural transition from the outer garnet core to the garnet growth zone R1 in a {112}Grt growth sector. Note the increasing aspect ratio of rutile (Rt) inclusions and the decrease in garnet (Grt) colour intensity from the outer core to R1.

Arredondo E, Rossman G, Lumpkin G (2001): Hydrogen in spessartine-almandine garnets as a tracer of granitic pegmatite evolution. - Amer Mineral 86, 485-490

Gou L, Zhang C, Zhang L, Wang Q (2014): Precipitation of rutile needles in garnet from sillimanite-bearing pelitic granulite from the Khondalite Belt, North China Craton. - Chin Sci Bull 59, 4359-4366

Griffin WL, Jensen BB, Misra SN (1971): Anomalously elongated rutile in eclogite-facies pyroxene and garnet. – Norsk Geologisk Tidsskrift 51, 177-185

Griffiths TA, Habler G, Rhede D, Wirth R, Ram F, Abart R (2014): Localization of submicron inclusion re-equilibration at healed fractures in host garnet. - Contrib Mineral Petrol 168, 1-21

Griffiths TA, Habler G, Abart R (2016): Crystallographic orientation relationships in host–inclusion systems: New insights from large EBSD data sets. - Amer Mineral 101, 690-705

Griffiths TA, Habler G, Abart R (2020): Determining the origin of inclusions in garnet: challenges and new diagnostic criteria. - Amer J Sci 320, 753-789

Housh TB, Luhr JF (1991): Plagioclase-melt equilibria in hydrous systems. – Amer Mineral 76, 477-492

Hwang SL, Shen P, Chu HT, Yui TF (2016): On the forbidden and the optimum crystallographic variant of rutile in garnet. - J Appl Cryst 49, 1922-1940

Lange RA, Frey HM, Hector J (2009): A thermodynamic model for the plagioclase-liquid hygrometer/ thermometer. - Amer Mineral 94, 494-506

Litharge from El Centenillo and Fuente Espi: A geochemical and mineralogical investigation of Spanish silver processing in the Sierra Morena

P. Krause[1,2], S. Klein[2,3], C. Domergue[4], C. Berthold[5,6], N. Jöns[1]

[1]Institut für Geologie, Mineralogie und Geophysik, Ruhr-Universität Bochum, Universitätsstrasse 150, 44801 Bochum, Germany
[2]Forschungsbereich Archäometallurgie, Deutsches Bergbau-Museum Bochum, Am Bergbaumuseum 31, 44791 Bochum, Germany
[3]Institut für Archäologische Wissenschaften, Ruhr-Universität Bochum, Am Bergbaumuseum 31, 44791 Bochum, Germany
[4]Laboratoire TRACES (UMR 5608 CNRS), Université Toulouse-Jean Jaurès, Allées Antonio Machado, 31058 Toulouse Cédex 9, France
[5]Competence Center Archaeometry, Baden-Wuerttemberg (CCA-BW), Eberhard Karls-Universität Tübingen, Wilhelmstraße 56, 72074 Tübingen, Germany
e-mail: Paul.Krause@ruhr-uni-bochum.de

Galena is treated as the most important silver ore in antiquity and especially in Roman mining history, but many other silver mineralisation and phases occur in the Earth's crust that also contain valuable amounts of silver for exploitation. This study addresses the silver-containing sulfosalts and how to decide between the alternative ores when only metallurgical remains are preserved and the mining context is not evident. Numerous samples of ore minerals, slags, lead metal and stones were collected by one of us (C. Domergue) over several years in the Spanish Sierra Morena, including two Roman foundry sites: Cerro del Plomo and Fuente Espi, both in the mining district of Linares-La Carolina. Cerro del Plomo is closely associated with lead-bearing ore veins near the foundry, while the mines that supplied Fuente Espi with lead ore have not yet been archaeologically explored. The metallurgical remains from the two foundries were analysed for their microstructure, mineralogy and phase composition using microscopy, electron microprobe analysis, and X-ray diffraction. It was hoped that the litharge in particular would provide information about the ores used. Metal inclusions of copper and lead were identified, both still containing some silver. The cooling history and stratigraphy of the litharge cakes were developed and parallels drawn with earlier cupellation models. The litharge cakes from Cerro del Plomo and Fuente Espi are comparable in terms of microstructure and phase composition. Chemical and isotope analysis will follow and be the subject of a separate publication.

The "Societät für die gesammte Mineralogie zu Jena" – Members and minerals from Austria, Slovakia, and Hungary

B. Kreher-Hartmann[1]

[1]*Friedrich-Schiller-University Jena, Mineralogical Collection*
e-mail: Birgit.kreher@uni-jena.de

The "Societät für die gesammte Mineralogie zu Jena" is the first purely geoscientific society in the world. It was founded in 1797 by Johann Georg Lenz (Fig. 1) at the University of Jena, Germany, and its members were scattered all over the globe. Of the more than 2,500 known members, particularly many members came from the then Hungarian region (i.e. today's Slovakia, Hungary, and Romania). These members sent minerals and rocks from their home countries from localities that are often no longer accessible today. The members established networks and in Hungary a Hungarian Mineralogical Society was founded following the Jena model. Famous contemporaries such as Johann Rudolf von Gersdorff, Daniel Mihalyik, or Christian Andreas Zipser can be found among the members. Not all members were mineralogists, many teachers, also theologians, and pharmacists were among them. But the occupation with the formations, parageneses, and formation conditions of the minerals united them.

Figure 1. Johann Georg Lenz (1745-1832).

Domokos Teleki de Szék was elected the first president of the Society. He died unexpectedly already in his first year in office. A gift collection of opals from Červenica, Slovakia, among others, which he had initiated, reached Jena only after his death.

When they arrived at the Mineralogical Collection in Jena, the gift collections received were arranged chronologically, according to their arrival. So were for example K-Feldspars from Karlovy Vary area with pyromorphites from different European areas and granites from Silesia side by side on display. Over the many years and after several moves, these gift suites were torn apart and systematically sorted into the collection that has now existed for more than 240 years. With the help of the catalogs and member letters, more than 6,500 specimen could be reassigned to the original suites in recent years.

Kreher-Hartmann B (2014): Die Mineralogische Societät zu Jena – Beiträge aus den Sammlungen der Universität Jena, Bd. 3

Lenz G Schwabe (1823): Neue Schriften der Großherzoglich-S. - Societät für die Gesammte Mineralogie in Jena 1, Neustadt, O

Mechanical-thermochemical process combination for the recycling of fine fractions from waste treatment plants – A journey into waste mineralogy

T. Kremlicka[1], T. Sattler[1], S. Steiner[2], S. A. Viczek[3], K. P. Sedlazeck[1]

[1]Chair of Waste Processing Technology and Waste Management, Montanuniversitaet Leoben, Leoben, Austria
[2]Institute of Technology and Testing of Construction Materials, Graz University of Technology, Graz, Austria
[3]Holcim (Österreich) GmbH, Trabrennstraße 2A, 1020 Vienna, Austria
e-mail: thomas.kremlicka@unileoben.ac.at

Austria produces approximately 1.5 million tons of municipal solid waste annually. Additionally, about 500,000 tons of slags and ashes from thermal waste treatment plants are generated. There are an estimated 1.9 million tons of fine fractions, which includes one million tons of rubble from construction waste, per year, most of which are landfilled (BMK, 2021).

These fine fractions often contain high amounts of metal and mineral contents, however, they may also include pollutants (Viczek et al. 2021b, Vollprecht et al. 2020). This poses a challenge for recycling, as it is essential to avoid keeping mobile pollutants in the material cycle. Recycling fine fractions can immobilize contaminants, like heavy metals, in stable phases (Sarmiento et al. 2019).

The "MeteoR" project aims to close material cycles by reintegrating these fine fractions as resources and therefore to further develop the circular economy, reduce CO_2 emissions and increase the recycling quota in Austria. The following objectives are pursued:

1. Mineralogical and chemical characterization of fine fractions and mechanical processing.
2. Testing of different thermochemical treatment methods.
3. Investigation of the mineralogy and leachability of the slags resulting from the thermochemical treatment.
4. Removal/immobilization of contaminants in the fine fractions.
5. Life cycle assessment (LCA) of recycling routes and systemic evaluation of waste management.

An interdisciplinary consortium of universities and industrial partners (see Fig. 2) is dedicated to achieving the project's goals.

The first steps will be sampling selected waste streams, chemical and mineralogical analysis. The mineralogical analysis will consist of, but is not limited to, powder X-ray diffraction, X-ray fluorescence and electron probe microanalysis. Mechanical processing is then used to produce concentrates that are analyzed similarly to the sampled waste. These concentrates are then tested by the project partners for suitability for the various recycling routes. The project plan and the resulting dependencies are shown in Fig. 1

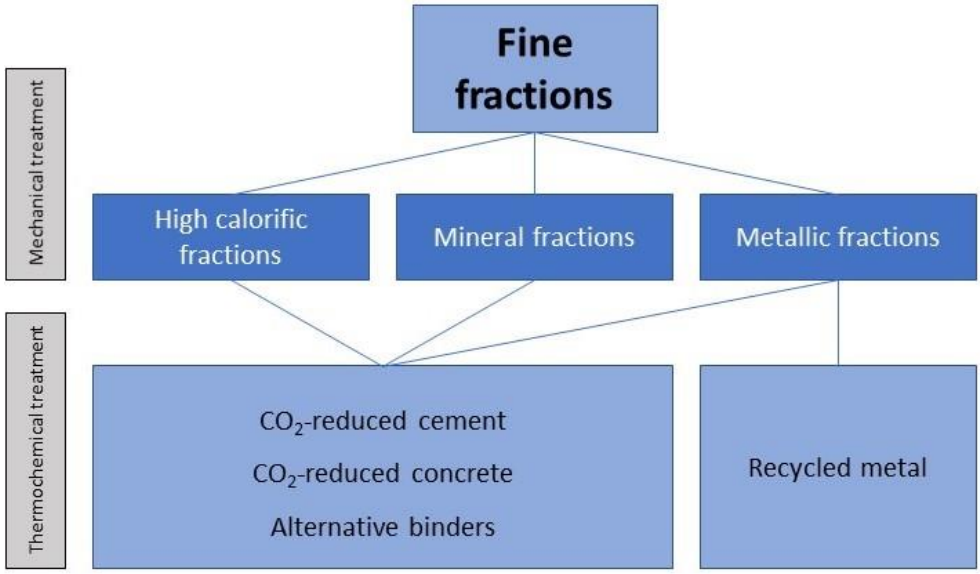

Figure 1. Scheme of the MeteoR project

By achieving the project goals, unused waste fractions containing raw materials can be utilized. Applying waste mineralogy methods, the mineral fractions can be characterized and optimized for reuse. The project enables more efficient use of resources and reintegrating waste into production chains and recycling cycles. This project is funded by the Austrian Research Promotion Agency (FFG, www.ffg.at), grant number 889863.

Figure 2. Logos of the consortium partners, funding agency and ministry of climate action, environment, energy, mobility innovation and technology in random order

Bundesministerium für Klimaschutz, Umwelt, Energie, Mobilität, Innovation und Technologie (BMK) (2021): Die Bestandsaufnahme der Abfallwirtschaft in Österreich – Statusbericht (Referenzjahr 2019)

Sarmiento LM, Clavier KA, Paris JM, Ferraro CC, Townsend TG (2019): Critical examination of recycled municipal solid waste incineration ash as a ineral source for Portland cement manufacture – a case study. - Resour Conserv Recycl 148, 1-10

Viczek SA, Khodier K, Kandlbauer L, Aldrian A, Redhammer G, Tippelt G, Sarc R (2021): The particle size-dependent distribution of chemical elements in mixed commercial waste and implications for enhancing SRF quality. - Sci Total Environ 776, 154343

Vollprecht D, Hernández Parrodi JC, Lucas HI, Pomberger R (2020): Case study on enhanced landfill mining at Mont-Saint-Guibert landfill in Belgium: mechanical processing, physico-chemical and mineralogical characterization of fine fractions <4.5mm. - Detritus 10, 26-43

Oriented triphylite rods in apatite (Stankuvatske Li deposit, Ukraine): result of pegmatite–wall rock interaction

S. Kurylo[1], I. Broska[1], R. Gieré[2], N. Lyzhachenko[3]

[1]Earth Science Institute, Slovak Academy of Sciences,840 05 Bratislava
[2]Department of Earth and Environmental Science, University of Pennsylvania, Philadelphia, USA
[3]SI, "Institute of Environmental Geochemistry of the National Academy of Sciences of the Ukraine", UK Kyiv
e-mail: kurylo.sergiy@savbb.sk

Introduction. Exomorphic haloes found around pegmatites in the Stankuvatske Li deposit (SLD) (Ukraine) are enriched in Rb, Cs, Li, Be, Nb and Ta, and such types of haloes around evolved magmatic systems are important for the concentration of critical mineral sources. Metasomatic processes in the SLD can be an example for the formation of apatite as a geochemical barrier with metallogenetic implications, which takes place at the contact between a rare-metal pegmatite and amphibolite. The aim of current report is to describe the unique occurrence at the SLD of oriented triphylite rods in green apatite, resulting from the interaction between pegmatite- and amphibolite-derived fluids. A genetic interpretation of a two-way directed element mobility in an evolved pegmatite are presented here for the first time.

Geological background. The petalite- and spodumene-pegmatite dykes of the SLD are located in the NW part of the Lypniazhka Dome Structure in the western part of the Inhul Domain in the Ukrainian Shield. Pegmatite dykes intruded amphibolite and ultrabasic rocks and were subsequently overprinted by tectonic activity forming metapegmatites. According to the classification of Černý &Ercit (2005), the studied pegmatite dykes show affinity to the rare-element class, and the petalite or spodumene subtype of the LCT family. The general characteristics of the pegmatites have already been reported (Syomka et al. 2022; Kurylo et al. 2022).

Results and discussion. The contact zone was investigated by the drill core materials (No 61-89) on a complete cross section from the host amphibolite to the adjacent metapegmatite dyke. A parallel mineral layering in the metapegmatite endocontact with host amphibolite was formed in the contact zone.

The exocontact *biotite zone* (BT) in the host amphibolite was formed as a result of metasomatic alteration of rock-forming amphibolite by the intruded pegmatite; newly formed biotite (with up to 2.5 wt.% of Rb_2O) and holmquistite are characteristic minerals in this zone. The pegmatite endocontact has a width of ca 8 cm and consists of four thin zones: (1) *aplitic* (APL), (2) *fluorapatite* (AP), which contains apatite with tiny, needle-shaped and oriented parallel c-axis inclusions of triphylite (Figure 1), (3) *triphylite (TR)*, and (4) *transitional zone* (TRN). Within of the endocontact, Nb-Ta-Sn oxides, ilmenite, gahnite, native bismuth, chrysoberyl, and relics of zircon rimmed by brabantite or thorite have been identified. The adjacent metapegmatite (PGM) represents petalite and spodumene bearing metapegmatite. A detailed description of all zones is currently in preparation.

Two stages of metasomatic alteration can be distinguished in the studied metapegmatite – wall-rock amphibolite system: (i) K-Rb-F metasomatism at low P activity, and (ii) the metasomatic Li-P precipitation. The analysis of the studied metasomatic contact zone provides evidence for a two-way directed interaction between host-amphibolite and pegmatite, whereby a fluid derived from the amphibolite infiltrated the adjacent pegmatite while a fluid derived from the pegmatite dykes migrated into the amphibolite.

The presence of TR, AP, and APL zones in the endocontact of the pegmatite offers an understanding of the mobility of Ca, P, and Li in a pegmatite-amphibolite geochemical system. The main source for Ca represents the host amphibolite, which released Ca by alteration of hornblende to biotite. The Ca-enriched fluid was driven towards the pegmatite, which was primarily enriched in P and Li as an evolved system. The interaction of these two fluid systems, one enriched in Ca, the second in P and Li led to the formation of apatite, which represent a geochemical barrier and preserved Li from further migration outside of pegmatite. In such terms, apatite became the main geochemical barrier for the Li flow from the pegmatite towards the host-rock amphibolite, which also indicates the formation of triphylite clusters at the contact with the apatite layer.

Figure 1. Apatite with needles of oriented triphylite (under plane-polarized light).

Acknowledgement: The authors are grateful for the financial support provided by grant PEGMAT within the ERA MIN2 framework.

Černý P, Ercit S (2005): The classification of granitic pegmatites revisited. - Canad Miner 43, 2005–2026

Kato S, Ikeda S, Saito K, Ogasawara M. (2018): Fe incorporation into hydroxyapatite channels by Fe loading and post-annealing. - J Solid State Chem, 265, 411–416

Kurylo S, Uher P, Broska I, Lyzhachenko N, Bondarenko S, Gieré R. (2022): Fine-grained petalite and spodumene dykes in the Stankuvatske Li-deposit, Ukrainian Shield: products of tectono–metamorphic recrystallisation. - Mineral Mag 86, 863–882

Syomka V, Ponomarenko O, Stepanyuk L, Bondarenko S, Sukach, V, Kurylo S, Donskyi M (2022): Lithium ores of Stankuvatka and Polokhivka ore fields (Ukrainian Shield). - Mineral J 44, 102–124

Characterization of NaOH gas attack on silica bricks by experimental alkali vapour tests and thermochemical modelling by FactSage™

N. Lechner[1]

[1]RHI Magnesita, Technology Center Leoben, Global R&D – Mineralogy,
Magnesitstraße 2, 8700, Leoben, Austria
e-mail: nikolaus.lechner@rhimagnesita.com

Silica bricks are used as refractory lining in the crown area of glass melting furnaces. During glass production the bricks are subjected to highly corrosive NaOH vapour evaporating from the subjacent glass bath. The interaction between NaOH gas and the refractory leads to a lowering of the melting point and the formation of alkali bearing SiO_2-rich melts within the product. A high volumetric amount and loss of the liquid phase appearing in the refractory could decrease the static stability and the lifetime of the glass furnace crown significantly. Thus, a detailed understanding about the atmospheric conditions favouring NaOH gas formation from the glass bath and its consequent interaction with the silica brick crown lining is of crucial importance to avoid lifetime shortening of the refractory. For that purpose, a mineralogical study by using a combination of experimental alkali vapour tests with thermochemical phase equilibrium modelling by FactSage™ and XRD-Rietveld analyses has been executed to evaluate the corrosive behaviour of a NaOH bearing glass furnace atmosphere on silica bricks. It is shown that a varying concentration of gaseous N_2, CO_2 and H_2O in the furnace atmosphere influences (1) the efficiency of Na_2O evaporation into NaOH gas and (2) the NaOH partial pressure that play a major role for the corrosive interaction with the silica bricks. Furthermore, the condensation behaviour of NaOH gas within the refractory and subsequent corrosion by liquid phase formation strongly depends on a temperature gradient developing in the product during operation.

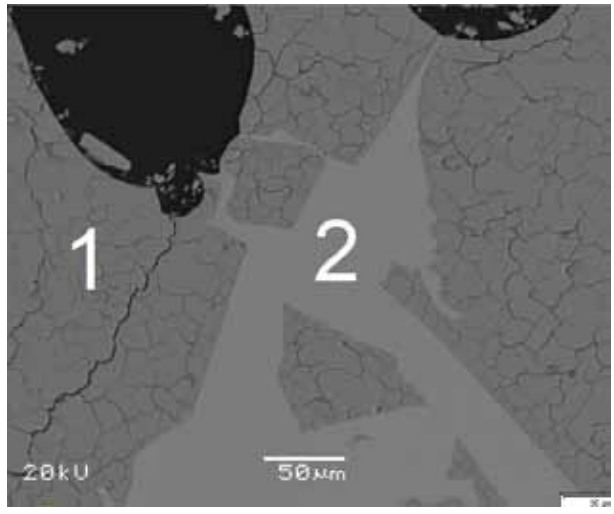

Figure 1. Micrograph of a typical silica brick after use in a glass melting furnace crown lining. Cristobalite (1). Glass phase (2).

Stable Ba isotopes of Apline mantle peridotites

C. Li[1,2,3]

[1]Research Centre for Planetary Science, Chengdu University of Technology, Chengdu, China
[2]School of Earth and Space Science, University of Science and Technology of China, Hefei, China
[3]Insitut for Geologie und Mineralogie, Universität Köln, Germany
email: lichunhui@cdut.edu.cn

Barium is a highly incompatible and fluid-mobile lithophile element. Previous studies on basalts and metamorphic rocks from subduction zones have shown that Ba isotopes can revealed more details of recycle of surface materials into the mantle. However, to our knowledge Ba isotopic data of mantle peridotites have not been investigated in detail. In this session,we report our new measurement of Ba isotope compositions of Alpine mantle peridotites. These samples include lherzolite, harburgite and pyroxeneite which were not thought to have contain crustal and surface materials. The Ba isotopes compositions of the investigated samples show large variations which we interpret as results of modifications by subduction and contamination of continental crust during the up-welling of the mantle materials. Our data suggest mantle peridotites, even the most clean and pristine ones, may have recorded mantle-crust interaction.

H_2O degassing experiments of the lower Laacher See Phonolite – on the way to eruption

P. Marks[1], M. Nowak[1]

[1]Eberhard Karls University Tübingen, Germany
e-mail: patricia.marks@uni-tuebingen.de

The Laacher See volcano is one of the youngest volcanoes in Germany with its last eruption 13,006 ± 9 years BP (Reinig et al. 2021). About 6.3 km³ of phonolitic magma was explosively erupted by phreatomagmatic and plinian eruptions in less than 10 days (Wörner and Schmincke 1984). The eruption behavior of such volcanic systems is determined by the phase separation mechanism of H_2O fluid from the supersaturated hydrous silicate melt, caused by the pressure decrease of the magma. The number of fluid vesicles per unit volume of silicate melt (*VND*) is a standard parameter used to quantify the efficiency of fluid-melt separation and thus the acceleration of magma ascent. Two important homogeneous vesicle formation mechanisms are established in the investigation and evaluation of the degassing behavior of silicate melt systems. According to the classical nucleation theory, the *VND* increases strongly with decompression rate (Toramaru 2006) and is therefore a proper parameter for quantifying ascent rate. Recently and specifically for phonolitic melts, the process of spinodal decomposition has been demonstrated, which manifests in the independence of *VND* from the decompression rate (Allabar and Nowak 2018).

To characterize the degassing behavior of the lower Laacher See composition, systematic decompression experiments were conducted in the internally heated pressure vessel. The melts were hydrated with 5.7 or 5.0 wt% H_2O at 200 MPa and 1523 K for 96 h and then continuously decompressed at 1323 K with 0.064 – 1.7 MPa/s to final pressures between 110 MPa and 30 MPa. By reaching the final pressure, the samples were rapidly quenched to room temperature to preserve the vesicle textures and the residual H_2O contents in the melts and to minimize vesicle shrinkage until the glass transition temperature was reached. The *VND*s and the spatial distribution of the vesicles, as well as the H_2O contents in the decompressed melts were analyzed with quantitative image analysis, transmission light microscopy, and FTIR-spectroscopy.

Upon reaching sufficient supersaturation pressure of >100 MPa, all samples exhibit homogeneously dispersed vesicles in the sample center (Fig. 1). Vesicle sizes range from 2 to 13 µm in diameter. Preliminary results indicate that *VND* is independent of decompression rate at all decompression rates. Irrespective of the decompression rate, high log*VND*s of 4.1 to 5.6 mm^{-3} are observed. Further decompression of the degassed melts leads to the formation of coalescence, resulting in a significantly reduced *VND* of the melts.

These observations are consistent with that of Allabar and Nowak (2018), who determined a log*VND* of ~5.2 mm^{-3} for hydrous phonolitic melt of the AD79 Vesuvius white pumice composition. From this, a trend emerges that at least for hydrated phonolitic melt, spinodal decomposition plays a crucial role in the degassing behavior of the melt and thus in the explosive eruption behavior of the volcanic systems.

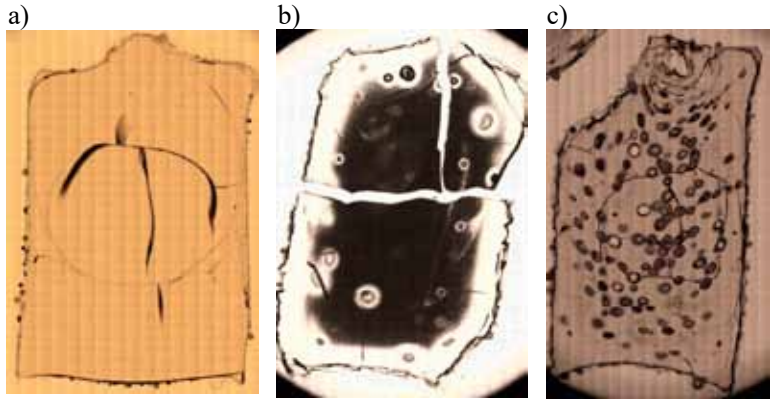

Figure 1. The three degassing steps of an ascending melt. a) No vesicle formation was initiated yet. b) Spontaneous phase separation was triggered by the extreme supersaturation of the melt. c) Further decompression leads to coalescence of the growing vesicles.

Allabar A, Nowak M (2018): Message in a bottle: Spontaneous phase separation of hydrous Vesuvius melt even at low decompression rates. - EPSL, 501, 192-201

Reinig F, Wacker L, Jöris O, Oppenheimer C, Guidobaldi G, Nlevergelt D, Adolphi F, Cherubini P, Engels S, Esper J, Land A, Lane C, Pfanz H, Remmele S, Sigl M, Sookdeo A, Büntgen U (2021): Precise date for the Laacher See eruption synchronizes the Younger Dryas. – Nature, 595, 66-69

Toramaru A (2006): BND (bubble number density) decompression rate meter for explosive volcanic eruptions. - J. Volcanol. Geotherm. Res.154, 303-316

Wörner G, Schmincke H-U (1984): Petrogenesis of the Zoned Laacher See Tephra. - J. Petrol., 25, 805-835

Structural changes in *Ln*-monazites under swift heavy ion irradiation

J. Marquardt[1], T. Lender[2], L. Bayarjargal[1], E. Haussühl[1], C. Trautmann[3], L. Peters[2], B. Winkler[1]

[1]Institute of Geoscience, Johann Wolfgang Goethe-University Frankfurt am Main
[2]Institute of Crystallography, RWTH Aachen
[3]GSI Helmholtz Centre for Heavy Ion Research, Darmstadt
e-mail: marquardt@kristall.uni-frankfurt.de

The safe disposal of nuclear waste is one of the intergenerational issues which needs to be solved. A potential route to effectively immobilize radionuclides could be realized by their incorporation into crystalline solid phases in future radioactive waste repositories. In particular, the immobilization of specific waste streams containing minor actinides (Np, Am, Cm) or plutonium in crystalline solid phases may be advantageous compared to glass matrices, which may be less resistant to leaching and disintegration (Donald et al. 1997; Ewing 1999; Lumpkin et al. 2006). Due to their radiation stability and chemical and structural flexibility, monazite-type compounds are considered suitable matrix materials (Schlenz et al., 2013).

To better understand structural changes due to radiation damage, synthetic monazite single crystals with different chemical compositions (La, Nd, Pm, Sm)PO_4 were irradiated at the UNILAC beamline of GSI Helmholtz Centre Darmstadt using 1.7 GeV Au ions and fluences of up to 1e13 ions/cm^2. The irradiated single crystals were characterized by Raman spectroscopy, secondary electron microscopy and single crystal X-ray diffraction.

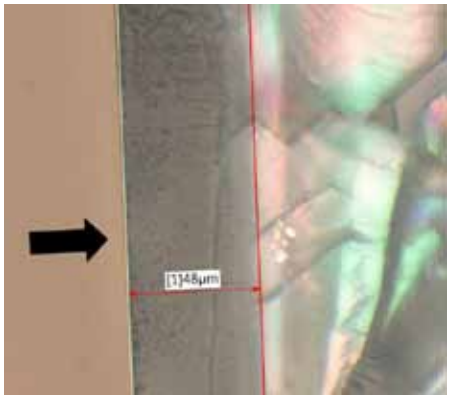

Figure 1. Cross section of a (Pr,Nd)PO_4 monazite crystal, prepared parallel to the direction of the irradiation indicated by the black arrow

The irradiation of monazite with 1.7 GeV Au ions results in an embrittlement of the crystals and the formation of a glassy surface layer of about ~48 µm thickness (Fig. 1), which correlates well with the projected range of ~44 µm according to SRIM-2013 calculations (Ziegler et al. 2010). The irradiation results in a significant broadening of all Raman modes up to the complete disappearance of the symmetric stretching mode ν_1 and further changes in the lattice dynamics. X-ray diffraction experiments revealed the amorphization of the surface layer.

Donald IW, Metcalfe BL, Taylor RNJ (1997): The immobilization of high level radioactive wastes using ceramics and glasses. - J Mater Sci 32, 5851-5887

Ewing RC (1999): Nuclear waste forms for actinides. - PNAS 96, 3432-3439

Lumpkin GR (2006): Ceramic waste forms for actinides. - Elements 2, 365-372

Schlenz H, Heuser J, Neumann A, Schmitz S, Bosbach D. (2013): Monazite as a suitable actinide waste form. - Z Kristallogr – Cryst Mater 228, 113-123

Ziegler JF, Ziegler MD, Biersack JP (2010): SRIM - The stopping and range of ions in matter. - Nucl Instrum Methods Phys Res B 268, 1818-1823

J.M & B.W. acknowledge the German Federal Ministry of Education and Research (BMBF) for financial support in the project No. 02NUK060E. T.L. & L.P. acknowledge support by BMBF under project number 02NUK060B.

High-pressure gneiss with pseudomorphs after jadeite from the Variscan Erzgebirge in Saxony

H.-J. Massonne[1]

[1]*School of Earth Sciences, China University of Geosciences, Wuhan, P.R. China*
e-mail: h-j.massonne@mineralogie.uni-stuttgart.de

The Erzgebirge in Saxony is known for occurrences of various ultrahigh-pressure (UHP) rocks (Massonne, 2001, 2003), but gneiss, the major rock type there, was rarely addressed in scientific studies (e.g., Willner et al. 1997). A paragneiss (sample E98-36), rich in quartz and white mica, was sampled very close to an eclogite body of the Gneiss-Eclogite Unit (GEU) c. 5 km north of the Saidenbach reservoir where UHP rocks were found.

Millimetre-sized garnet grains in this gneiss can be zoned with a relatively Ca-poor core (XCa = Ca/(Ca+Fe^{2+}+Mg+Mg) around 0.04, XMg = 0.16, XMn = 0.005) surrounded by a mantle with XCa = 0.07-0.09, XMg = 0.13-0.18, and XMn = 0.01. The contact between these two garnet generations is sharp. Large oriented white mica flakes are phengite with Si contents around 3.42 per formula unit (pfu) in the core and slightly decreasing Si contents towards the rim. A new generation of potassic white mica with lower Si contents formed at the rim of these flakes. A peculiar feature of the studied paragneiss is the occurrence of mm-sized clusters of small albite grains with thin potassic white mica flakes in between. The Si contents of these flakes is between 3.23 and 3.31 pfu and, thus, similar to those of the rim generation of large flakes. The observed elongated clusters, being oriented in the same direction as the large mica flakes, are interpreted as former jadeite grains, which decomposed during exhumation of the rock under infiltration of K-bearing hydrous fluids.

Thermodynamic modelling with PERPLE_X (Connolly, 2005: version 6.6.6) was applied to decipher the metamorphic evolution of the paragneiss. According to the calculated pressure-temperature (P-T) pseudosection contoured with various isopleths for garnet and potassic white mica, an early metamorphic stage (Ca-poor garnet core) occurred at P-T conditions of 0.9±0.1 GPa and 635±25 °C (Fig. 1). The conditions of the high-pressure (HP) stage (garnet mantle) were difficult to determine precisely because compositions of the early garnet mantle and phengite can coexist over a wider P-T range. Thus, a temperature increase from 580-600 °C to 660 °C can be accompanied by a slight pressure decrease from 1.8 to 1.7 GPa, but also by a clear one from ca. 2.4 to 1.7 GPa. This not well determinable portion of the P-T path is compatible with the presence of jadeite and absence of primary biotite. Further decompression without deformation resulted in the formation of pseudomorphs after jadeite. The obtained conditions of 660 °C at 1.7 GPa are similar to those of 715 °C at 1.8 GPa determined for the adjacent eclogite (Massonne 2011).

In-situ U-Th-Pb dating of monazite with the electron microprobe (e.g., Rahimi & Massonne, 2018) yielded an average age of 338.4 ± 2.3 (2σ) Ma (40 of 44 monazite analyses). This age was assigned to the HP event according to previous studies of rocks from the GEU (e.g., Hallas et al. 2021). A small monazite grain enclosed in garnet yielded an age of 386.4 ± 10.5 (2σ) Ma, which was related to the garnet core-forming event (Fig. 1).

Based on the here presented data and those gathered from the literature, the following conclusions are drawn: (1) An Early Carboniferous continent-continent collisional scenario was responsible for the HP event in the GEU. Evidence for metamorphism at UHP is lacking in metasediments and metagranitoids. Diamondiferous rocks in the Erzgebirge in Saxony are crystallization products of melts, which ascended from great Earth's depths and intruded the

Early Carboniferous HP rocks. (2) These HP rocks of the GEU, including eclogites, originally experienced Late Devonian medium-pressure, medium-temperature metamorphism and were constituents of a medium to lower portion of the downgoing plate in the Early Carboniferous collisional scenario. (3) Jadeite should characterize medium-temperature metasediments and metagranitoids that had experienced lithostatic pressure in excess of 1.6 GPa. This study demonstrates that jadeite can be recognized in corresponding HP rocks even after complete decomposition. This means that previously suggested UHP terranes worldwide, lacking relics and pseudomorphs of jadeite and coesite, have never experienced UHP.

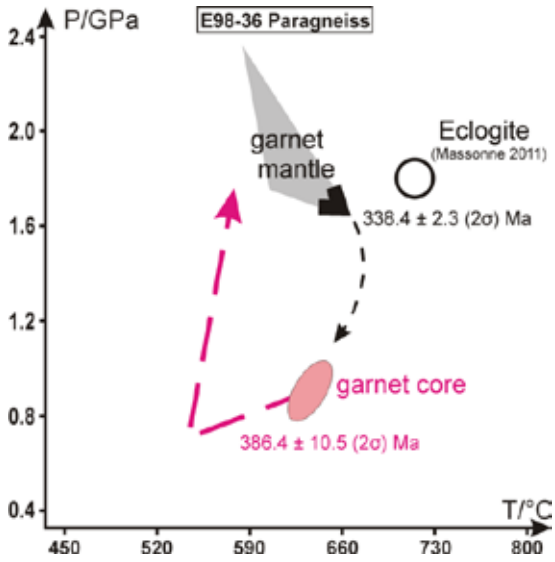

Figure 1. P-T evolution of paragneiss E98-36 developed by thermodynamic modelling. The broken paths were estimated. The given ages resulted from monazite dating using the electron microprobe. The open circle refers to P-T conditions derived by Massonne (2011) for eclogite adjacent to E98-36.

Connolly JAD (2005): Computation of phase equilibria by linear programming: a tool for geodynamic modeling and its application to subduction zone decarbonation. - Earth Planet Sci Lett 236, 524-541

Hallas P, Pfänder J A, Kroner U, Sperner B (2021): Microtectonic control of $^{40}Ar/^{39}Ar$ white mica age distributions in metamorphic rocks (Erzgebirge, N-Bohemian Massif): Constraints from combined step heating and multiple single grain total fusion experiments. - Geochim Cosmochim Acta 314, 178-208

Massonne H-J (2001): First find of coesite in the ultrahigh-pressure metamorphic region of the Central Erzgebirge, Germany. - Eur J Mineral 13, 565-570

Massonne H-J (2003): A comparison of the evolution of diamondiferous quartz-rich rocks from the Saxonian Erzgebirge and the Kokchetav Massif: are so-called diamondiferous gneisses magmatic rocks? - Earth Planet Sci Lett 216, 347-364

Massonne H-J (2011): Pre-conference field trip: Erzgebirge (Ore Mountains), Germany and Czech Republic; German part of the Saxonian Erzgebirge. - Geolines 23, 29-59

Massonne H-J (2023): A new type of saidenbachite with pseudomorphs after coesite phenocrysts from the north-western Bohemian Massif, Germany. - Terra Nova in press, https://doi.org/10.1111/ter.12659

Rahimi G, Massonne H-J (2018): Pressure-temperature-time evolution of a Variscan garnet-bearing micaschist from the northern Fichtelgebirge, NW Bohemian Massif in central Europe. - Lithos 316-317, 366-384

Willner A P, Rötzler K, Maresch WV (1997): Pressure-temperature and fluid evolution of quartzo-feldspathic metamorphic rocks with a relic high-pressure, granulite-facies history from the Central Erzgebirge (Saxony, Germany). - J Petrol 38, 307-336

The effects of anion and cation substitution on the crystal structure of Cu-based quaternary chalcogenides

D. Matzdorff[1,2], M. Avdeev[3], D. Sheptiakov[4], G. Gurieva[1], S. Schorr[1,2]

[1]Helmholtz-Zentrum Berlin für Materialien und Energie, Hahn-Meitner-Platz 1, 14109 Berlin, Germany
[2]Institut für Geologische Wissenschaften, FU Berlin, Malteserstraße 74-100, 12249 Berlin, Germany
[3]Australia's Nuclear Science and Technology Organisation, Sydney, Australia
[4]Paul Scherrer Institute, Villigen PSI, Switzerland
e-mail: david.matzdorff@helmholtz-berlin.de

The research of quaternary Cu-based chalcogenide semiconductors has caught a large interest for photovoltaic applications, as these materials consist of non-toxic and earth abundant elements. While being environmentally friendly and low cost and stable under environmental conditions, materials like Cu_2MnSnS_4 or Cu_2MnGeS_4 are very promising candidates for use as top cell absorbers in tandem solar cells, because they can cover a wide bandgap range of 1.52-1.72 eV (Beraich et al. 2020; Ramasamy et al. 2018). Compounds like $Cu_2MnSnSe_4$ could even be considered for the application in single junction solar cell with a band gap energy of 1.21 eV (Gurieva et al. 2022). This study presents new insight into the structural transformation mechanisms within the $Cu_2Mn(Ge,Sn)(S,Se)_4$ solid solution series via neutron powder diffraction.

Since Cu^+ and Ge^{4+} are isoelectronic cations and Mn^{2+} is electronic similar to Cu^+ and Ge^{4+}, they cannot be differentiated in a structural analysis based on X-ray powder diffraction data alone. However, their neutron scattering lengths are considerably different, that is why we apply neutron diffraction to analyze the crystal structure of $Cu_2Mn(Ge,Sn)(S,Se)_4$ mixed crystals. Moreover, the basis of our investigations is a careful determination of the chemical composition of the mixed crystals by WDX spectroscopy.

The endmembers of the $Cu_2Mn(Ge,Sn)(S,Se)_4$ solid solution series crystallize in different structure types: Cu_2MnSnS_4 and $Cu_2MnSnSe_4$ crystallize in the tetragonal stannite-type structure (space group $I\bar{4}2m$), whereas Cu_2MnGeS_4 and $Cu_2MnGeSe_4$ adopt the orthorhombic wurtz-stannite structure (space group $Pmn2_1$). Thus, within the solid solution series with mixed cations a structural transition from the tetragonal to the orthorhombic crystal structure can be expected.

For the presented study the compounds were synthesized by solid state reaction of pure elements in evacuated silica tubes at temperatures of 730 °C (Se-only compounds), 740-780 °C (mixed anion compounds) and 800 °C (S-only compounds). The chemical composition and homogeneity of the synthesized polycrystalline powder materials were investigated by WDX spectroscopy using an electron microprobe system. It was revealed that the synthesized powders contained the desired phase as a chemically single, homogeneous quaternary phase with slight shifts in the stoichiometric composition as well known in this type of materials (Schorr et al. 2020). LeBail refinement of the powder X-ray diffraction data was used to determine the lattice parameters of the mixed crystals. The cation distribution in the unit cell was defined by applying the average neutron scattering length analysis method (Schorr 2011) which is based on the site occupancy factors determined by Rietveld refinement of the neutron diffraction data. The derived cation distribution model is the basis to conclude on the crystal structure and structural disorder as well as to elucidate the mechanism of structural phase transition.

It will be shown that Sn-rich mixed crystals adopt the stannite type structure, whereas Ge-rich mixed crystals of the mixed cation solid solution series adopt the wurtz-stannite type structure. Within the intermediate range, two chemically identical but structurally different quaternary phases coexist, adopting the tetragonal and the orthorhombic structure respectively. It will also be shown that the respective anions influence the concentration of intrinsic point defects differently and independent to the off-stoichiometric composition.

The results of the chemical composition study in combination with structural characterization and optical bandgap evaluation from diffuse reflectance of $Cu_2Mn(Ge,Sn)(S,Se)_4$ mixed crystals will be presented. These investigations enabled us not only to determine the type and concentration of intrinsic point defects, but to show as well the structure type transformation from the stannite- to the wurtz-stannite-type structure.

Beraich et al. (2020): Facile synthesis of the wurtz stannite (orthorhombic) Cu2MnGeS4 thin film via spray ultrasonic method: Structural, Raman, optical and electronic study. - J All Comp 845, 156216

Gurieva G, Niedenzu S, Siminel N, Franz A, Schorr S (2022): The kesterite–stannite structural transition as a way to avoid Cu/Zn disorder in kesterites: the exemplary case of the Cu2(Zn,Mn)SnSe4. - Faraday Discussions 239, 51-69

Ramasamy et al. (2018): Nanocrystals of CuMSnS4 (M = In or Ga) for solar energy conversion applications. - Chemical Communications 54, 11757

Schorr (2011): The crystal structure of kesterite type compounds: A neutron and X-ray diffraction study. - Sol. Energy Mat Solar Cells 95, 1482-1488

Schorr et al. (2020): Point defects, compositional fluctuations, and secondary phases in non-stoichiometric kesterites. - J Phys Energy 2, 012002

The authors gratefully acknowledge the Australia's Nuclear Science and Technology Organisation (ANSTO) for providing us beamtime (proposal number 13403) at the ECHIDNA end station and the Paul Scherrer Institute and the Swiss Spallation Neutron Source (SINQ) for providing us beamtime (proposal number 20202094) at the HRPT diffractometer.

Trace element geochemistry and isotopic data of sulphides in Alpine-type Pb-Zn deposits in the Eastern and Southern Alps

F. Melcher[1], V. Bertrandsson Erlandsson[1], V. Gartner[1], E. Henjes-Kunst[1], P. Onuk[1], J. Raith[1], G. Rantitsch[1], F. Henjes-Kunst[2], B. Potočnik Krajnc[3], A. Šoster[3]

[1]Department of Applied Geosciences and Geophysics, Montanuniversität Leoben, Austria
[2]Federal Institute of Geosciences and Natural Resources (BGR), Hannover, Germany
[3]Faculty of Natural Sciences and Engineering, University of Ljubljana, Slovenia
e-mail: F.Melcher@unileoben.ac.at

More than 500 occurrences of Pb-Zn ores are documented in Mesozoic carbonate sequences of the Eastern and Southern Alps. They are invariably hosted by shallow lagoonal and reef carbonates of Middle and Upper Triassic (Anisian and Carnian) age and are collectively termed "Alpine-type" (APT) deposits. The district has a long mining history starting in Roman times and terminating in the early 1990ies when the last operations closed at Bleiberg (Austria), Cave del Predil/Raibl (Italy), and Mežica/Mies (Slovenia) (Schroll 2008). The Bleiberg deposit was closed in 1993 after more than 700 years of mining. It is regarded as a world-class deposit (Leach et al. 2005) and represents the type locality of APT Pb-Zn deposits. The historical total metal production from APT deposits exceeded 6 x 10^6 tons (Mt) Zn and Pb from a resource exceeding 110 Mt (Cerny 1989; Cerny & Schroll 1995; Leach et al. 2003; Spangenberg & Herlec, 2006). Renewed interest in base metals, and especially in their by-products such as Ge, Ga, In and Cd, has initiated modern exploration activities in some of the mining districts. Germanium and Cd have been recovered from ores in the past; about 200 tons Ge, mostly from Bleiberg and Raibl, were produced from APT deposits.

Although the deposits occur in a wide region, they share common features such as a simple mineralogical composition, complex ore textures, light sulphur isotopic compositions, Late Palaeozoic Pb model ages, and trace element compositions in sphalerite, galena and pyrite. Ore textures are complex and often equivocal. They include rare examples indicating syngenetic to early diagenetic origin, besides abundant epigenetic textures such as crosscutting veins and breccia ores. However, biogenic textures and relict bacteria colonies are present (Kucha et al. 2010). Therefore, some mineralization must have precipitated at shallow level at low temperature.

Sphalerite is low in Fe (commonly 0.01-0.5 %), Mn, Co, Ga and In, but commonly contains elevated Cd, Ge, As, Tl and Pb concentrations. Median concentrations of Ge determined by LA-ICP-MS are 846 ppm in the Fladung deposit, 229 ppm at Bleiberg and 222 sppm at Raibl where the highest contents of As and Tl have been determined. Sphalerite chemistry indicates that temperatures of formation range from 60 to 140 °C. This is lower than suggested by previous fluid inclusion data, but in line with results of thermal modelling. Metamorphosed sphalerite (>450 °C) in the Brenner and Stangalm Mesozoic reveals metal exchange to higher Fe and Mn, and lower Ga, Ge, As and Tl concentrations. Galena is Ag-poor, although Ag concentrations both in sphalerite and galena increase towards the north of the Austroalpine nappe system. Pyrite- and marcasite-rich ores display an As-Tl-(Hg) association, and are low in Co and Ni. Pyrite is stable to higher temperatures, keeping its original low-temperature trace element compositions.

The sulphur isotope composition of sulphides in APT deposits varies over a wide range and is often bimodally distributed, attaining a maximum at highly negative values ($\delta^{34}S \leq$-20 ‰) explained by bacteriogenic sulphate reduction, and a second maximum at $\delta^{34}S$ = -10 to 0 ‰ explained by thermogenic sulphate reduction from a second source (Schroll & Rantitsch 2005). APT ores in general show lead isotopic compositions above the crustal lead growth curves. The variable enrichment in ^{207}Pb and ^{208}Pb originated from an isotopically enriched continental source (Köppel 1997). Local differences in the bedrock geology and/or its variable common Pb composition are responsible for the Pb isotopic variability of the individual APT deposits. A metal source from the Paleozoic basement and Triassic sedimentary rocks is most likely.

Rb-Sr isochrons of sphalerite from the Bleiberg deposit indicate two phases of ore deposition: a first one at about 229 Ma and a second at about 207-201 Ma. Initial $^{87}Sr/^{86}Sr$ of the early (229 Ma) sphalerite agrees with Carnian seawater composition. The Carnian Rb-Sr isochron age corresponds to U-Pb ages of calcite associated to ore minerals of the (Southalpine) Gorno deposit (Giorno et al. 2022). The younger (≈205 Ma) age reflects fluid flow within the carbonate sequence, probably due to fracturing of the platform during initial rifting of the Penninic Ocean. This process is probably related to ongoing tectonic instability following sedimentation of the Upper Hauptdolomit with formation of deep basins, where hydrocarbon source rocks were deposited. In a wider context of central and southern Europe, mineralizing processes during the Mesozoic have been explained as a response to the Pangaea breakup (Burisch et al. 2022). The oldest hydrothermal processes in the circum-Mediterranean are related to the initial rift axes. Mineralization spans a range from 230 to 160 Ma with a maximum at 230-200 Ma.

Burisch M, Markl G, Gutzmer J (2022): Breakup with benefits - hydrothermal mineral systems related to the disintegration of a supercontinent. - Earth Planet Sci Let 580, 117373

Cerny I (1989): Die karbonatgebundenen Blei-Zink-Lagerstätten des alpinen und außeralpinen Mesozoikums. Die Bedeutung ihrer Geologie, Stratigraphie und Faziesgebundenheit für Prospektion und Bewertung. - Arch Lagerstforsch Geol Bundesanst 11, 5-125

Cerny I, Schroll E (1995): Heimische Vorräte an Spezialmetallen (Ga, In, Tl, Ge, Se, Te und Cd) in Blei-Zink- und anderen Erzen. - Arch Lagerstforsch Geol Bundesanst 18, 5-33

Giorno M, Barale L, Bertok C, Frenzel M, Looser N, Guillong M, Bernasconi SM, Martire L (2022): Sulphide-associated hydrothermal dolomite and calcite reveal a shallow burial depth for Alpine-type Zn-(Pb) deposits. – Geology 50, 853-858

Köppel V (1997): 3.5. Bleiisotope. – Arch Lagerstforsch Geol Bundesanst 19, 485-495

Kucha H, Schroll E, Raith JG, Halas S (2010): Microbial sphalerite formation in carbonate-hosted Zn-Pb ores, Bleiberg, Austria: Micro- to nanotextural and sulphur isotope evidence. – Econ Geol 105, 1005-1023

Leach DL, Bechstädt TH, Boni M, Zeeh S (2003): Triassic-hosted MVT Pb-Zn ores of Poland, Slovakia and Italy. - In: Kelly JG et al. (eds.): Europe´s major base metal deposits. Irish Ass Econ Geol, 169-213

Leach DL, Sangster DF, Kelley KD, Large RR, Garven G, Allen CR, Gutzmer J, Walters S (2005): Sediment-hosted Pb-Zn deposits: A global perspective. - Econ Geol 100th Anniv Vol, 561-607

Schroll E (2008): Die Blei-Zink-Lagerstätte Bleiberg. Die Geschichte ihrer Erforschung. - Carinthia II 62, 287 pp

Schroll E, Rantitsch G (2005): Sulphur isotope patterns from the Bleiberg deposit (Eastern Alps) and their implications for genetically affiliated lead-zinc deposits. - Mineral Petrol 84, 1-18

Spangenberg JE, Herlec U (2006): Hydrocarbon biomarkers in the Topla-Mežica zinc-lead deposits, Northern Karavanke/Drau Range, Slovenia: paleoenvironment at the site of ore formation. - Econ Geol 101, 997-1021

Atomistic processes in actinolite and tremolite at elevated temperatures

B. Mihailova[1], C. Rösche[1], N. Petrova[2], T. Malcherek[1], J. Schlüter[3]

[1]FB Erdsystemwissenschaften, Universität Hamburg, Grindelallee 48, 20146 Hamburg, Germany
[2]Institute of Mineralogy and Crystallography "Acad. Ivan Kostov", Bulgarian Academy of Sciences, Acad. Georgi Bonchev Str. 107, 1113 Sofia, Bulgaria
3Mineralogisches Museum, Leibniz-Institut zur Analyse des Biodiversitätswandels, Grindelallee 48, 20146 Hamburg, Germany
e-mail: boriana.mihailova@uni-hamburg.de

Elucidating the atomistic mechanism of high-temperature transformations of iron-containing amphiboles ($AB_2C_5T_8O_{22}W_2$, with C_5 = $M(1)_2M(2)_2M(3)$) may have important implications in several fields, including metamorphic petrology, geophysics, and environmental sciences. Here the effect of octahedrally coordinated Fe^{2+} on the temperature-driven dehydrogenation/dehydroxylation in Mg-rich amphiboles is analysed by a comparative study of tremolite and actinolite via *in situ* high-temperature Raman spectroscopy, thermogravimetric/mass-spectrometry analyses, and X-ray diffraction (Rösche et al. 2022).

We show that similar to Fe-rich amphiboles (Mihailova et al. 2021, 2022, Bernardini et al. 2023) thermally activated delocalized e^- and H^+ are also formed in Fe-bearing magnesian amphiboles, but at much higher temperatures than in ferrous (e.g. grunerite) and mixed-valence iron-rich amphiboles (e.g. riebeckite). The delocalized electrons in actinolite couple with polar FeO_6 phonons to form polarons. However, the polaronic dipoles in actinolite are not mutually aligned as in the case of Fe-rich amphiboles, because iron cations are present in the actinolite structure as isolated octahedra or dimers of octahedra, while the majority of MO_6 octahedra in the strips are occupied by Mg. The final product of the thermally-induced decomposition of both actinolite and tremolite is a single phase of monoclinic pyroxene with an intermediate chemical composition between diopside and clinoenstatite, having vacancies at the octahedral sites and, for actinolite, also Fe^{3+}. Cristobalite occurs only as a minor phase in amounts less than 1% and ~5% for tremolite and actinolite, respectively. The dehydroxylation of tremolite causes immediate collapse of the silicate double chain into SiO_4 single chains, which is followed up by a rearrangement of the amphibole B-type and C-type cations into pyroxene octahedral sheets. The actinolite-to-pyroxene breakdown is preceded by a state of "oxo-actinolite" in which all Fe^{2+} are exchanged to Fe^{3+}, all $^{W}(OH)^-$ groups next to Fe-containing $M(1)M(1)M(3)$ configurations are exchanged to $^{W}O^{2-}$, and all H^+, including those from *W*-site anions next to MgMgMg triads, are delocalized, but still in the bulk of the crystal grain.

Bernardini S, Della Ventura G, Schlüter J, Mihailova B (2023): Thermally activated electron hopping in Fe-rich amphiboles: implications for the high-conductivity anomalies in subduction zones. - Geochem 83, 125942

Mihailova B, Della Ventura G, Waeselmann N, Xu W, Schlüter J, Galdenzi F, Marcelli A, Redhammer GJ, Boiocchi M, Oberti R (2021): Atomistic insight into lithospheric conductivity revealed by phonon-electron excitations in hydrous iron-bearing silicates. - Commun Mater 2, 57

Mihailova B, Della Ventura G, Waeselmann N, Bernardini S, Xu Wei, Marcelli A (2022): Polarons in rock-forming minerals: physical implications. - Condens Matter 7, 68

Rösche C, Waeselmann N, Petrova N, Malcherek T, Schlüter J, Mihailova B (2022): Oxidation processes and thermal stability of actinolite. - Phys Chem Mineral 49, 47

Mineralogical characteristics of agates and their host rocks in Chihuahua, Mexico

M. Mrozik[1,2], J. Götze[2]

[1] Geowissenschaftliche Sammlungen, TU Bergakademie Freiberg, Brennhausgasse 14, 09599 Freiberg
[2]Institute of Mineralogy, TU Bergakademie Freiberg, Brennhausgasse 14, 09599 Freiberg
e-mail: Maximilian.mrozik@geosamm.tu-freiberg.de

Agates from the state of Chihuahua in Mexico are known worldwide among collectors and jewelry dealers because of their color variety and high quality. The single deposits are limited to different areas which are distributed in the whole federal state of Chihuahua. The agates of the different localities partly differ in their basic coloring as well as in their general appearance and the abundance of pseudomorphs. Despite the wide distribution and individual locality-typical characteristics, most of the best-known deposits can be assigned to the same volcanic unit, the so-called Rancho el Agate Andesite. This is an approximately 300 m thick unit of intermediate lava flows, which all have a strongly vesicular texture (Keller et al. 1982). The host rocks for most of the presently mined agate deposits in the main production area of the Sierra del Gallego can be classified almost exclusively as quartz-free latite (Mrozik et al. 2023). The intermediate chemism of the rocks can be explained by a mixing of magmas with different SiO_2 contents.

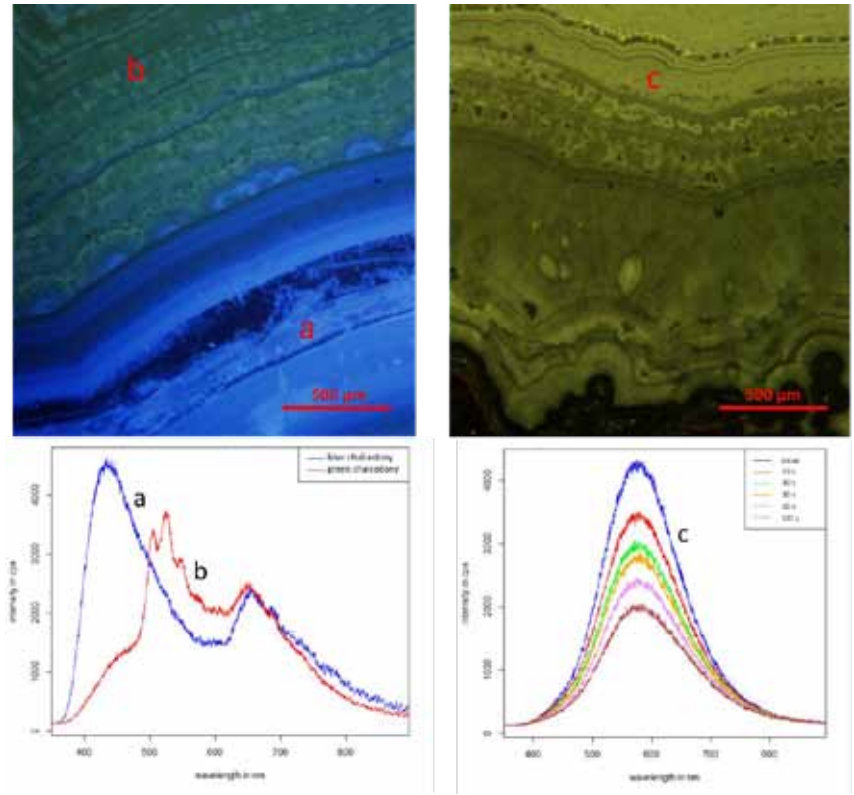

Figure 1. CL-micrographs with the associated CL-spectra. The CL-colors and spectra reveal different structural defects as well as the incorporation of trace elements and compounds like for example the uranyl-ion within the green luminescent parts of the chalcedony. (Figure from Mrozik et al. 2023)

Different reasons for the coloration of the agates could be determined by various spectroscopic methods as well as with trace element analyses and microscopic studies. While different structural defects can be detected in many areas of the mineralization (Fig. 1) the coloration of most of the bands in the agates is caused by inclusions, for example hematite and goethite. The different colors are not exclusively caused by the mineral phase but also by the particle size as well as the distribution of the coloring components within the matrix of the chalcedony. Some of these inclusions were incorporated within the agates during the initial crystallization of the chalcedony, others were later fixed within the matrix by secondary infiltration (Fig. 2) (Mrozik et al. 2023).

A mixture of near-surface weathering solutions with deep hydrothermal fluids from the Tertiary volcanism has led to the formation of the agates. The enrichment of differently mobile elements which were fixed during the formation of the agates in the structure of the chalcedony itself as well as in the paragenetic inclusions indicate the involvement of hydrothermal fluids. Due to the very different contents of under weathering conditions rather immobile elements like zirconium and chromium as well as almost exclusively hydrothermally accumulated elements like antimony and zinc a variable influence of deep hydrothermal fluids in the different agate occurrences can be assumed. Thus, the local differences in the agate formation are not caused by a basically different formation process but by a various influence of the respective fluids as well as slightly different local geochemical conditions. In the current studies different generations of chalcedony could be determined within the mineral formations (Fig. 2) which indicates that many of the agates were not formed by a single geochemical process but underwent a multiphase formation with partly different fluids under slightly differentiated conditions. (Mrozik et al. 2023)

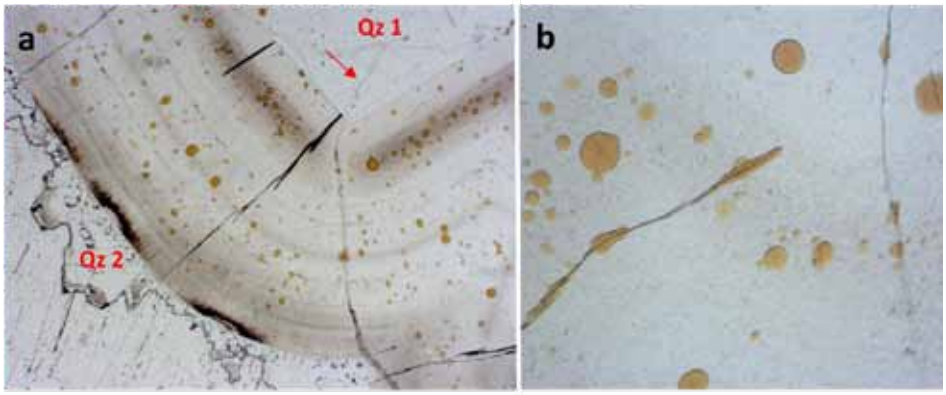

Figure 2. (a) The micrograph shows different generations of the SiO_2-mineralization with at least two generations of macrocrystalline quartz (Qz 1, Qz 2). The red arrow marks a secondary crack which can be followed within the first generation but ends at the second generation of quartz. (b) The micrograph shows a detailed view of the same agate which shows the distribution of different inclusions within the chalcedony matrix. Note that some of the inclusions are arranged along secondary cracks, which assigns a later formation of some of the coloring particles by infiltration. (Figure from Mrozik et al. 2023)

Mrozik M, Götze J, Pan Y, Möckel R (2023): Mineralogy, Geochemistry and Genesis of Agates from Chi-huahua, Northern Mexico. - Minerals 13, 687, https://doi.org/10.3390/min13050687

Keller PC, Bockoven NT, McDowell FW (1982): Tertiary volcanic history of the Sierra del Gallego area, Chihuahua, Mexico. - Geol Soc Amer Bull 93, 303-314

Special exhibition
Wonder world agate - fascination between legend and science

M. Mrozik[1], J. Götze[2], A. Massanek[1], M. Gäbelein[1]

[1] Geowissenschaftliche Sammlungen, TU Bergakademie Freiberg, Brennhausgasse 14, 09599 Freiberg
[2]Institute of Mineralogy, TU Bergakademie Freiberg, Brennhausgasse 14, 09599 Freiberg
e-mail: Maximilian.mrozik@geosamm.tu-freiberg.de

Due to their variety of colours and shapes, agates belong to the most fascinating mineral formations of nature and have played an important role as jewellery and gemstones since ancient times. The name "agate" appears in literature as early as 350 B.C. (Theophrast) and was probably derived from deposits on the river Achates (now Drillo) in Sicily.

Agate deposits and agate processing are recorded worldwide in both historical and currently mined regions. Of particular interest are the almost inexhaustible deposits of agate in the province of Rio Grande do Sul in Brazil, which have been supplying the world markets with raw agates for centuries. In China there is a centuries-old tradition of agate processing as a stone-carving art (Fig. 1). In the city of Fuxin in the province of Liaoning, also known as the "world city of agate", 60,000 people currently work in the agate industry. In Saxony, the systematic search for agate and "precious stones" was promoted early on by Elector August (1553 - 1586) and later especially by the Saxonian King "August the Strong". Therefore, systematic collections and descriptions already exist from this time. The region around Idar-Oberstein is also famous in history as a supplier and processing centre for high-quality agates.

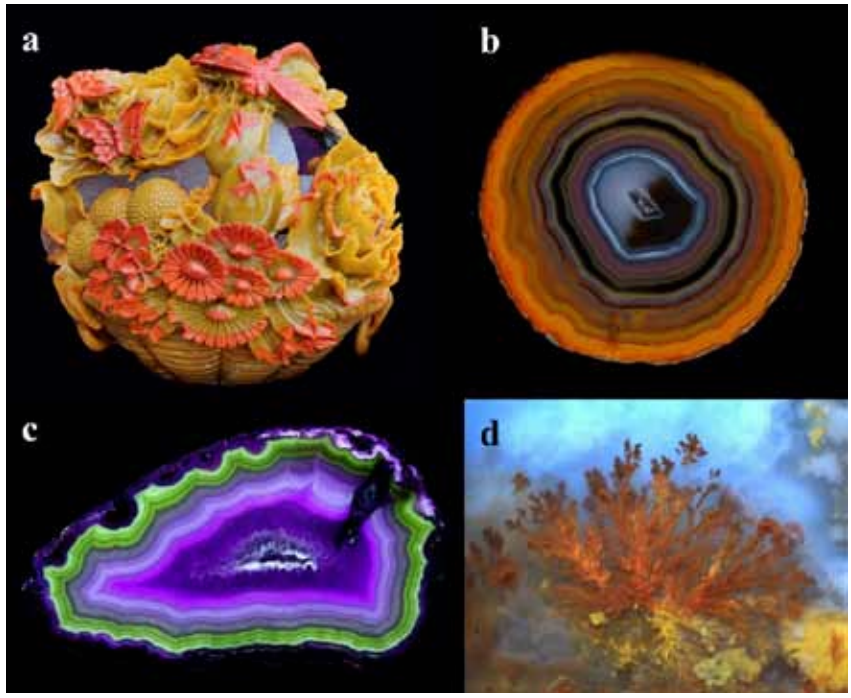

Figure 1. Different photographs and micrographs of agate samples. (a) stone carving art made from an agate from Xuanhua, China; (b) polished agate sample from Xuanhua, China; (c) luminescence colours under UV-light (254 nm) of an agate from Rancho Coyamito, Chihuahua, Mexico; (c) micrograph of an “Orpheus”-agate from Kardzhali, Bulgaria.

Besides their impressive aesthetics, agates also provide many clues for scientific research. This is mainly due to the fact that the formation of agate cannot be observed directly and also that until today no successful agate syntheses exist on a laboratory scale. One of the most discussed questions of the agate problem is probably the "secret" of agate formation, which has led to many speculations in the past and present. But the micro-world of agates also provides exciting insights into the complex processes of nature.

The exhibition gives an insight into the fascinating world of agates. With Wonder World Agate for the first time a combined special exhibition is housed in the three different collections in the city of Freiberg, which together form the largest mineralogical collection complex worldwide. The main part of the exhibition (Fig. 2), which presents impressive specimens from the most important agate deposits of the world, is displayed in the terra mineralia. You can find the different showcases arranged according to the different continents and most important agate deposits. Additionally, there are some thematic display cases (e.g. different types of agates, special agates or pictures in agates) as well as interactive elements explaining for example luminescence effects in agates or different microstructures. The whole exhibition is accompanied by numerous knowledge boards and art-like pictures of microstructures in agates to explain some exciting questions regarding the formation and properties of agates.

The Mineralogical Collection of Germany hosts agate samples from whole Germany. This part of the special exhibition shows the great variety and importance of German agate deposits.

The third part is housed in the Wernerbau framed by the historic mineralogical collection of the TU Bergakademie Freiberg. This exhibition part displays agates from some special localities in Saxony and shows the relation between primary and secondary agate deposits in one of the mineral richest states of Germany.

Figure 2. Some impressions of the actual special exhibition Wonder World Agate.

Minerals in a greenhouse environment: a cross-disciplinary exhibition

S.P. Mueller[1]

[1]*Mineralogical Museum, University of Marburg, Germany*
e-mail: s.mueller@geo.uni-marburg.de

During the winter months of 2023, the Mineralogical Museum Marburg was 'on tour' in the greenhouses of the Botanical Garden of the University of Marburg. In a collaborative, cross-disciplinary effort, we highlighted links between mineralogy and botany in a variety of display cases, in reference to the respective topical focus of the houses: e.g., which ore minerals are needed to build a smartphone, and how does their mining affect tropical rainforests? How do ferns turn into coal (and ultimately into diamonds)? Which minerals are typical for the Australian outback? How (and where) is amber formed?

The exhibition was open on a total of 9 Sundays during the winter months (a peroid the greenhouses are normally closed to the public) and attracted a large number of visitors to the botanical garden during this time. In particular, the interdisciplinary linking of what at first glance appear to be very different disciplines within natural sciences was positively highlighted in many of the visitors' feedbacks.

Rates, mechanisms and microstructures of transport-controlled reaction front propagation

T. Müller[1], S. Piazolo[2]

[1]*Geoscience Centre Göttingen, Georg-August-University, Germany*
[2]*School of Earth and Environment, The University of Leeds, United Kingdom*
e-mail: thomas.mueller@geo.uni-geottingen.de

Fluid-mediated mineral reactions are governing the redistribution of elements and isotopes in the geosphere. Incomplete elemental redistribution is preserved in the rock record in the form of geochemical reaction fronts. Key features of such systems are reaction induced creation/destruction of porosity increasing/decreasing permeability and further focussing of fluid into/away from the zone of reaction; hence this results in a positive or negative feedback between reaction, fluid ingress and further reaction. To the same end, sluggish element mobility can lead to variations in fluid chemistry within the propagating reaction front controlling the stable mineral assemblage and its chemical/isotopic composition. Recent studies provided conclusive evidence for the presence of transport-controlled reaction fronts in mineral reactions such as the replacement of calcite single crystals by Mg-carbonates (Jonas et al. 2015; 2017). Here, we present a follow-up investigation providing detailed chemical and microstructural data as well as a model for the kinetically controlled evolution of the reaction rim.

The replacement reactions of single calcite cubes (2 mm) were carried out experimentally in batch reactor vessel at 200 °C using a 1 M $MgCl_2$ fluid and a water-to-rock-ratio of 10 for run durations of 2-30 days. Solid reaction products have been characterized using an FEG-SEM including EBSD and chemical variations have been measured using an electron microprobe.

Experimental results reveal the time-dependent formation of a layered, multiphase reaction rim by dissolution-precipitation forming Mg-carbonate phases of different composition and variable porosity. The initial reaction rim is formed of small, rhombic almost pure magnesite crystals which become more Ca-rich as the reaction progresses. Subsequently, a sharp interface marks the change to the precipitation of high magnesium calcite (HMC) instead of magnesite, albeit the HMC precipitates with a constant X_{Mg} of 0.4. With increasing run durations, the reaction does not progress but grains in the existing reaction rim exhibit grain coarsening and elimination of (interconnected) porosity. This grain growth is accompanied by a chemical adjustment starting from the former magnesite-HMC interface initiating two new reaction fronts adjusting the magnesite composition, i.e., replacing Ca by Mg and the recrystallization of HMC by a VHMC phase with X_{Mg} of 0.5 representing a dolomite stoichiometry. EBSD analysis reveal that the recrystallization of the inner part of the reaction rim is accompanied by the formation of subgrain boundaries and rotation of c-axis during grain coarsening.

This study highlights the importance to quantitatively understand the link between reaction progress, fluid composition, fluid transport and the evolution of fluid pathways to describe and model reaction front propagation in reactive transport models.

Jonas L, Müller T, Dohmen R, Baumgartner L, Putlitz B (2015): Transport-controlled hydrothermal replacement of calcite by Mg-carbonates. - Geol 43, 779-782, doi: https://doi.org/10.1130/G36934.1

Jonas L, Müller T, Dohmen R, Immenhauser A, Putlitz B (2017): Hydrothermal replacement of biogenic and abiogenic aragonite by Mg-carbonates: Relation between textural control on effective element fluxes and resulting carbonate phase. - Geochim Cosmochim Acta 196, 289-306, doi: https://doi.org/10.1016/j.gca.2016.09.034

Thermoelastic properties of radiation-damaged zircon

M. Münchhalfen[1], J. Schreuer[1]

[1]Ruhr-Universität Bochum, Institut für Geologie, Mineralogie und Geophysik,
Universitätsstraße 150, Bochum, 44801, Germany
e-mail: marie.muenchhalfen@rub.de

Radioactive decay of unstable isotopes causes damage to zircon, which significantly reduces its elastic stiffnesses (e.g., Özkan, 1976). These damages can be partially healed by temperature treatment of the zircon crystal. In order to study in situ the recrystallization of radiation-damaged zircon, thermoelastic properties, and thermal expansion data were collected between 100 K and 1600 K utilizing resonant ultrasound spectroscopy, dilatometry, and high-temperature powder x-ray diffraction. The investigated samples of natural gem-quality zircon belong to the damage stage I introduced by Holland & Gottfried (1955), i.e., the damage in the crystal structure is mainly dominated by the accumulation of isolated point defects.

While non-metamict zircon samples display a linear decrease in elastic stiffnesses, the partial radiation-damaged zircon samples undergo strong irreversible effects detected in all utilized methods. The increase of elastic stiffnesses starts at about 700 K, while the thermal expansion decreases (Fig. 1). The severity of this effect becomes more pronounced with an increasing initial state of damage and thus can be related to the healing of defects induced by radioactive decay. A second effect sets in at about 1100 K, likely related to a transition from static to dynamic behavior. This supports the idea that reducing radiation damage is a multi-stage process, including point defect healing and recrystallization of an amorphous fraction.

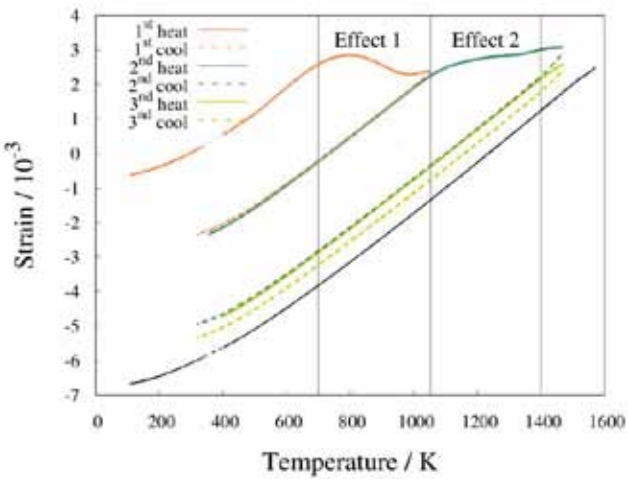

Figure 1. Different effects observed in thermal strain of radiation damaged zircon compared to non-metamict zircon (black line).

Özkan H (1976): Effect of nuclear radiation on the elastic moduli of zircon. - J Appl Phys 47, 4772-4779
Holland H, Gottfried D (1955): The effect of nuclear radiation on the structure of zircon. - Acta Cryst 8, 291-300

Gem spinel in the Imperial Crown of the Holy Roman Empire: Evidence for very early gemstone heating?

L. Nasdala[1], T. Lamers[2], H.A. Gilg[3], C. Chanmuang N.[1], M. Griesser[2], F. Kirchweger[2], A. Erlacher[1], M. Böhmler[4], G. Giester[1]

[1]Institut für Mineralogie und Kristallographie, Universität Wien, 1090 Vienna, Austria
[2]Kunsthistorisches Museum Wien, 1010 Vienna, Austria
[3]School of Engineering and Design, Technische Universität München, 80333 Munich, Germany
[4]WITec Wissenschaftliche Instrumente und Technologie GmbH, 89081 Ulm, Germany
e-mail: chutimun.chanmuang@univie.ac.at

The Imperial Crown of the Holy Roman Empire, part of the Imperial Regalia, is the key exhibit in Vienna's Imperial Treasury. It is currently investigated within the three-year interdisciplinary project 'Crown' (www.projekt-reichskrone.at) led by Kunsthistorisches Museum Vienna. The research aims, among others, at issues regarding the Imperial Crown's materials, manufacturing technology and time, as well as its state of preservation. During the first measurement campaign in Spring 2022, we had the task to determine conclusively – and, if possible, to characterise further – all 172 (inorganic) gemstones in the crown, whereas studies of the pearls were planned for the second measurement campaign (2023).

Figure 1. The front plate of the Imperial Crown of the Holy Roman Empire (size 11.2 cm × 14.9 cm) contains two spinels, a pink stone (#A3) in the upper row, left side, and a large red stone (#A25) in the centre of the third row. Photo © KHM-Museumsverband (Christian Mendez); reproduced with permission.

Non-destructive spectroscopic analyses were done on site, using a fibre-coupled WITec confocal Raman probe system equipped with an alpha300 controller. Photoluminescence (PL) and Raman spectra were excited with a 457 nm diode laser (0.05–8.5 mW measured behind the objective). An Olympus 20× objective (free working distance 25 mm) was used.

Besides 71 blue sapphires, 50 garnets, 20 emeralds, 13 amethysts, four chalcedonies and 11 glass imitates, there are three spinels in the Imperial Crown, two in the front plate (Fig. 1) and one in the central cross (Nasdala et al. 2023). The analytical identification of spinel in the

Imperial Crown is of art-historical interest. So far the first appearance of gem spinel in European jewellery was known for the thirteenth century (e.g., Ogden 2021) whereas the central, large spinel in the front plate (#A25) seems to be original; that is, set into the Imperial Crown about 1000 years ago already. This stone hence represents one of the very earliest uses of spinel in jewellery. Furthermore, the stone has two drill holes that indicate an even older use.

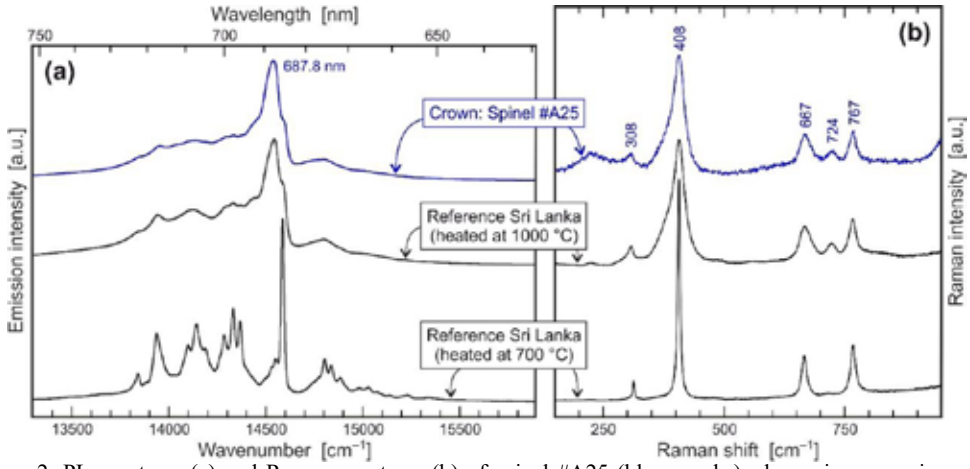

Figure 2. PL spectrum (a) and Raman spectrum (b) of spinel #A25 (blue graphs), shown in comparison with reference spectra (black graphs) obtained from a gem-quality spinel from Sri Lanka that was heat-treated in air.

The central spinel in the front plate (stone #A25) turned out to be of particular scientific interest, as it did not yield PL and Raman spectra that are typical of $MgAl_2O_4$ with (close to) normal occupation of cation sites. Instead, the PL spectrum (Fig. 2a) is characterised by loss of fine structure. Such spectra are obtained from natural Mg-Al spinel only after being heat-treated (Widmer et al. 2015; Liu et al. 2022). Similarly, heat-treatment results in significant broadening and asymmetry of Raman bands (Fig. 2b). These spectroscopic phenomena are assigned to heating-induced cation disorder; that is, increase of partial inversion of the cation occupation, according to $^{[4]}Mg\ ^{[6]}Al_2\ O_4 \rightarrow\ ^{[4]}(Mg_{1-x}Al_x)\ ^{[6]}(Al_{2-x}Mg_x)\ O_4$ (with $x > 0.2$) (Widmer et al., 2015; Ma et al., 2022). The spectra obtained from spinel #A25 hence give strong indication that this stone was heated to close to 1000 °C. This is supported also by the presence of a multitude of healed fractures, 'lily pad' inclusions, and melted sulphides at the surface.

Heating of red 'yāqūt' to enhance colour and transparency is known back to the ninth century (e.g., Troupeau 1998). 'Yāqūt' (an Arabian term) has generally be assumed to refer to gem corundum, but the possibility cannot be eliminated that it – and hence also the early heating – may have included spinel as well. Our spectroscopic results indicate that, as early as about 1000 years ago, spinel #A25 may have been subjected to heat-treatment.

Liu Y, Qi L, Schwarz D, Zhou Z (2022): Color mechanism and spectroscopic thermal variation of pink spinel reportedly from Kuh-i-Lal, Tajikistan. - Gems Gemol 58, 338-353

Ma Y, Bao X, Sui Z, Zhao X, Liu X (2022): Quantifying Mg–Al cation distribution in $MgAl_2O_4$-spinel using Raman spectroscopy: An experimental calibration. - Solid Earth Sci 7, 60-71

Nasdala L, Lamers T, Gilg HA, Chanmuang N C, Griesser M, Kirchweger F, Erlacher A, Böhmler M, Giester G (2023): The Imperial Crown of the Holy Roman Empire, part I: Photoluminescence and Raman spectroscopic study of the gemstones. - J Gemmol 38(5), 448

Ogden JM (2021): Gem knowledge in the thirteenth century: The St Albans jewels. - J Gemmol 37(8), 816

Troupeau G (1998): Le premier traité arabe de minéralogie: Le livre de Yūḥannā Ibn Māsawayh sur les pierres précieuses. - Ann Islamologiques 32(6), 219

Widmer R, Malsy A-K, Armbruster T (2015): Effects of heat treatment on red gemstone spinel: Single-crystal X-ray, Raman, and photoluminescence study. - Phys Chem Miner 42(4), 251

Mirdita ophiolites, Albania: Refertilization of spinel-plagioclase-peridotites in the shallow Mantle Lithosphere

T. Ntaflos[1], P. Koutsovitis[2], K. Onuzi[3], C. Hauzenberger[4]

[1]Department of Lithospheric Research, University of Vienna, Josef-Holaubek-Platz 2, 1090 Vienna, Austria
[2]Department of Geology, University of Patras, Greece
[3]Instituti i Gjeoshkencave,Rr. "Don Bosko", Nr.60, Tirane, Albania
[4]Department of Earth Sciences – NAWI Graz Geocenter, University Graz Universitaetsplatz 2, Austria
e-mail: theodoros.ntaflos@unive.ac.at

The Albanian ophiolites are located between the Dinarides (N. Macedonia and Serbia) in the east and the Hellenides in the west. The Mirdita Ophiolites in Albania are divided into two units namely the western ophiolitic unit with MORB geochemical affinity and the eastern ophiolitic unit with SSZ affinity. The western unit consists of the Krabbi, Puka, Comsique and Skenderbeu massifs where intrusives and dykes are present as well. All massifs represent upper mantle, variably serpentinized spinel and plagioclase peridotites.

The Krabbi massif with a diameter of 30 km is a piece of upper mantle ultramafic body consisting of spinel-plagioclase lherzolites and harzburgites with bulk-rock Mg# ranging from 89.5 to 91.8 and Ca/Al ratio varying from 1.13, that is slightly higher than the Primitive Mantle ratio of 1.1, to 1.26 indicating an excess of Ca in the studied samples. Minor and trace elements trends such as Ni, V and Yb versus Mg# are very similar to those of the orogenic peridotites. The chondrite normalized REE abundances have convex upward patterns where the majority of the samples show that the Yb_N is slightly higher compared to La_N suggesting moderate metasomatic events affecting the LREE.

Besides the rock forming mineral olivine, orthopyroxene, clinopyroxene and spinel there are also disseminated plagioclases and kaersutites. Strongly tectonized samples show secondary protogranular and porphyroclastic textures. Rounded spinel occurs mainly as inclusion in olivine and orthopyroxene whereas holly-leaf shaped spinel is interstitial.

The plagioclase neither coexists nor surrounds spinel, which precludes any subsolidus transition from spinel- to plagioclase-peridotite stability field. However, the clinopyroxene, as can be inferred from their negative Eu-anomaly in the chondrite normalized REE patterns, appears to be in equilibrium with coexisting plagioclase. Apparently, the plagioclase-rich residual melt affected the peridotites in the spinel-peridotite field but crystallized and equilibrated with clinopyroxene at shallow depths.

A striking textural feature is the frequent replacement of olivine grains by orthopyroxene with simultaneous formation of Ti-rich diopside and Al-rich spinel, suggesting metasomatic infiltration of a melt with tholeiitic composition. This feature has been observed in the samples with Mg# = 89.5, Al_2O_3 = 4.3 wt% and CaO = 3.77 wt% similar to the composition of the Primitive Mantle.

The existence of fertile peridotites with similar to the Primitive Mantle composition suggests that the otherwise strongly depleted oceanic lithospheric mantle has been refertilized after metasomatic introduction of melts with tholeiitic composition.

Fahlore analyses from a prehistoric work and settlement site in Kundl, Tyrol

L. Oettel[1], P. Tropper[1], L.M. Eß[2]

[1]University of Innsbruck, Institute of Mineralogy and Petrography
[2]University of Innsbruck, Institute of Archaeology
e-mail: lena.oettel@uibk.ac.at

Between 2018 and 2019, the largest prehistoric area excavation in North Tyrol to date took place in Kundl (district of Kufstein). On an area of about 11,600 m^2 in the Wimpissinger gravel pit, horizons from the 1st millennium BC were uncovered.

The excavated work area offers a unique large-scale insight into the work stages between mining and metal production. The phases of use of this work area extend from the Early Bronze Age to the late Iron Age.

During the excavations, in addition to hundreds of slag remains from the Early and Late Bronze Age, three storage vessels were excavated, which can also be assigned to the Late Bronze Age (Eß, unpublished). Around one of the storage vessels fahlore ore lumps were draped and examined in the context of an origin determination of the smelted ores.

Figure 1. Storage vessel with fahlore wreath (picture: Talpa GnbR 2019)

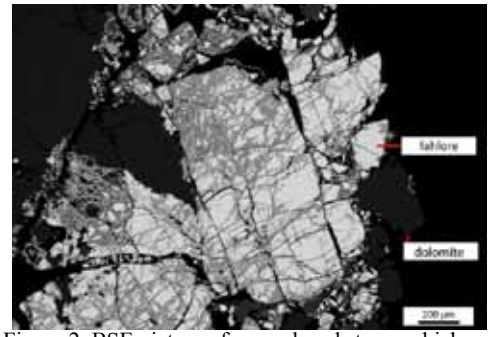

Figure 2. BSE picture of an analysed stone, which was drapped around the storage vessel (picture: L. Oettel 2020)

Electron probe microanalysis of these fahlore minerals were undertaken for putting possible provenance constraints on the ores. Since this examination did not yield a satisfying match within the HiMAT mineral chemical database, the source of the smelted fahlores could yet not be determined. For this reason, additional 37 samples of fahlores were taken from a wide variety of localities/tectonic units (e.g. Northern Limestone Alps, Engadin Window) and examined by electron beam microprobe to increase the chemical database considerably.

Phosphorus in the deep Earth: An experimental investigation of Ca-phosphates at upper- to lower-mantle P-T conditions

T. Pausch[1], B. Joachim-Mrosko[1], A.C. Withers[2], T. Ludwig[3], J. Vazhakuttiyakam[1], J. Konzett[1]

[1]Institute for Mineralogy and Petrography, University of Innsbruck
[2]Bayerisches Geoinstitut, Universität Bayreuth
[3]Institute of Earth Sciences, Heidelberg University
e-mail: tristan.pausch@uibk.ac.at

During subduction and dehydration of oceanic crust, P can be transported into the mantle wedge by fluids or melts, and either enters silicate phases, in particular garnet and olivine, or, if bulk P concentrations are sufficiently high, forms apatite. This P-enriched peridotite will then be dragged down with the subducted slab into the deep mantle. When apatite reaches its upper pressure stability limit, the anhydrous Ca-phosphate tuite will form. While the role of Ca-phosphates in the global P-cycle is well understood for the crust and shallow upper mantle, this is not the case for the deep silicate Earth near and below 660 km depth.

In this study we investigated the *P-T* stability, phase relations, and compositional evolution of tuite in a peridotitic bulk composition at *P-T* conditions of the upper- to lower-mantle transition. For this purpose, multianvil experiments were performed at 15 to 25 GPa and 1600 to 1800 °C. A synthetic peridotite, based on the composition of a moderately fertile spinel lherzolite, was used as starting material. This peridotite was doped with 3% synthetic β-$Ca_3(PO_4)_2$, 1% of a trace element mix containing a range of HFSE, LILE and REEs, and approx. 2200 µg/g of Br and Cl each.

The coexisting phases stable within the studied *P-T* range include tuite, majoritic garnet, ringwoodite, forsterite, clinoenstatite, bridgmanite, davemaoite, ferropericlase, and melt. Tuite breaks down between 1700 and 1750 °C at 20 to 25 GPa and between 1750 and 1800 °C at 15 GPa, which yields a negative slope for the tuite-out reaction.

Beyond the *P*-stability of apatite, tuite and/or garnet are the main P carriers in a typical peridotite dependent upon the bulk P content. With increasing depth, the modal amount of Ca-phosphates decreases due to a progressive phosphate-to-silicate P transfer, leading to P contents of up to 4.8 wt% P_2O_5 in majoritic garnet at 1600 °C and 20 GPa. However, as soon as garnet reaches its stability limit, tuite is very likely the most important P-carrying phase at subsolidus conditions while bridgmanite and davemaoite contain small to negligible P (< 60 µg/g and <380 µg/g respectively) even when buffered by tuite.

Discerning different nucleation mechanisms in synthetic trachybasalts: example from three Titanomagnetite populations in single experiments

S. Peres[1], T.A. Griffiths[1], F. Colle[2], S. Iannini Lelarge[3], M. Masotta[3,4], A. Pontesilli[5], L. Mancini[6]

[1]Department of Lithospheric Research, University of Vienna, Josef-Holaubek-Platz 2,1090 Wien, Austria
[2]Dipartimento di Scienze Chimiche, della Vita e della Sostenibilità Ambientale, Università di Parma, Campus Universitario, Parco Area delle Scienze157A, 43124, Parma, Italy
[3]Dipartimento di Scienze della Terra, University of Pisa, Via Santa Maria 53, 56126 Pisa, Italy
[4]CISUP, Centro per l'Integrazione della Strumentazione Universita' di Pisa, Lungarno Pacinotti 43, 56125 Pisa, Italy
[5]Instituto Nazionale di Geofisica e Vulcanologia, Via di Vigna Murata 605, 00143 Roma, Italy
[6]ZAG - Slovenian National Building and Civil Engineering Institute, Dimičeva ulica 12, 1000 Ljubljana , Slovenia
e-mail: stefano.peres@univie.ac.at

Heterogeneous nucleation, i.e. nucleation on a pre-existing surface, is energetically more favourable than homogeneous nucleation because it requires overcoming a lower energetic barrier in order to form a critical nucleus. In most natural and experimental crystallizing magmas, heterogeneous nucleation is suggested to be the main nucleation mechanism, but robust criteria to prove the heterogenous nucleation origin of a given crystal or phase in natural rocks and ex-situ samples are lacking.

Here we apply multiple analytical methods in order to assess the nucleation mechanism of titanomagnetite (Tmt) crystals that crystallized in the proximity of clinopyroxene (Cpx) crystals in a synthetic trachybasaltic melt (with 2 wt.% added H_2O) in crystallisation experiments carried out in a piston-cylinder apparatus at a constant pressure of 4 kbar. After 30 minutes of superheating at 1300 °C, the samples were cooled at a rate of 80°C / min to the final resting temperatures of 1150 °C and 1100 °C. These temperatures correspond to a respective undercooling (ΔT expressed as T liquidus – T experiment) of 30° and 80°. The dwell times at these temperatures were 30 minutes and 8 hours, respectively.

3D image processing and 3D image analysis of high-resolution synchrotron X-ray computed microtomography (SR μCT) data resulted in a precise phase segmentation of Cpx, Tmt, glass and bubbles. Moreover, it was possible to discriminate three main Tmt populations spatially distributed alongside Cpx crystals but morphologically different to each other: a) Tmt grains > 100 μm in size, skeletal in shape, and mostly isolated in the melt (population 1); b) Tmt grains between up to 100 μm in size, anhedral to partially skeletal in shape, and always decorating Cpx grains edges and tips (population 2); c) needle-to-flattened Tmt grains almost completely enclosed within Cpx grains (population 3).

The pair correlation function g(r), i.e. a measure of the frequency of an interpoint distance (of r), has been evaluated for the 3D point pattern composed by the centroids of each Tmt population, extracted from several VOIs inside 3D scans of the samples. Tmt grains of population 1 have an unclear 3D point pattern characterized by g(r) near 1, a possible sign of a randomly distributed point pattern. Populations 2 and 3 show clear clustered 3D point patterns, characterized by g(r) > 1 and interpoint distances r up to 200 μm.

Electron backscatter diffraction (EBSD) analysis enables us to clarify the crystallographic orientation relationships (CORs) between Cpx and Tmt crystals which share boundaries. Less than 60 % of the total shared Cpx-Tmt boundary length of population 1 Tmt crystals is characterized by the presence of CORs. Individual crystals of this population show no CORs between the two crystal phases at all, or boundary misorientations dispersed around known specific CORs. In contrast, more than 85% of the total shared Cpx-Tmt boundary length in Tmt populations 2 and 3 follows a COR. Locally, clusters of multiple Tmt decorating single Cpx crystals show more than 95% of the cumulative shared length characterized by the presence of CORs.

Considering the skeletal-to-euhedral shape, the unclear 3D point pattern distribution and the lack of CORs in some Cpx-Tmt pairs classified as Population 1, we suggest that the isolated single grains from this class are most likely formed by homogeneous nucleation. Individual large grains of this same population showing CORs may represent unusually large heterogeneously nucleated Tmt grains, Cpx grains heterogeneously grown on a pre-existing Tmt crystal, or potentially Tmt-Cpx interaction after nucleation apart.

Considering the anhedral or acicular shape, the highly clustered point pattern, and the ubiquitous presence of CORs, we interpret Population 2 and 3 Tmt grains to have formed by heterogeneous nucleation on top of pre-existing Cpx crystals.

In conclusion, multiple Tmt morphologies and distributions coupled with different COR systematics imply different nucleation mechanisms and growth histories for the three populations. Notably, the different Tmt nucleation mechanisms occurred during or right after a single cooling event. Multiple microstructural populations of crystals in natural magmas should be carefully assessed before inferring the existence of complex thermal (or other) histories. A multi-methodological approach which combines 3D SR μCT data with 2D crystallographic one is indispensable to confidently discern between homogeneous and heterogenous nucleation mechanisms.

Funded by the Austrian Science Fund (FWF): P 33227-N

Mineral reactions in thermally treated calcareous clays for brick production

P.R. Pesek[1], C.L. Lengauer[1], R. Abart[2], A. Kurka[3], G. Früh[4], W. Gaggl[4]

[1]University of Vienna, Department of Mineralogy and Crystallography, Josef-Holaubek-Platz 2, 1090 Vienna, Austria
[2]University of Vienna, Department of Lithospheric Research, Josef-Holaubek-Platz 2, 1090 Vienna, Austria
[3]Wienerberger AG, Wienerbergerplatz 1, 1100 Vienna, Austria
[4]Wienerberger AG, Hauptstraße 4, 2332 Hennersdorf, Austria
e-mail: patrick.pesek@univie.ac.at

The commercial production of bricks usually requires firing temperatures in the range of 800-1000 °C. Some raw materials for brick production may contain up to several wt% carbonates. These carbonates thermally decompose in the range of 600-900 °C and subsequently induce the formation of new mineral phases and microporosity. This allows the production of high thermal insulating clay blocks which contribute for an energy efficient building stock, however, the additional release of CO_2 is an unfavorable side effect regarding the overall carbon footprint. Strongly supporting the European Green Deal, Wienerberger AG is striving to find solutions for a reduction of these raw material related process emissions. Therefore, an approach was targeted to find and evaluate additives, which allow lower firing temperatures in the range of decomposition temperatures of carbonates concurrently keeping the physico-technical parameters of the fired products comparable to available products. In this context, it is particularly important that the pure clay-type raw material and its thermal behavior is foremost characterized so that comparisons with clay-additive mixtures can later be made.

Test specimens were extruded, dried, and fired at 620 °C, 700 °C, 760 °C and 880 °C. The mineral phases, chemical composition and thermal behavior of the green body and the fired sherds were determined using PXRD, XRF and TA, respectively. SEM-EDX and EPMA were used for high-resolution images of microstructures and phase identification as well as for identifying mineral reactions.

The results revealed a multitude of processes occurring during the firing process of the investigated calcareous clay. A selection of relevant mineral reactions is listed below:

(i) Individual clay minerals were dehydroxylated at 620 °C, while the matrix was visibly molten at a firing temperature of 880 °C (Fig. 1A). Within the reduction core, a higher level of melting was present than at the rim, possibly due to FeO that rather acts as a fluxing agent than Fe_2O_3 (Fischer 1987).

(ii) The beginning of decomposition of carbonates was observed at 620 °C. Decomposing carbonates can react with clay minerals, which leads to a densification of sherds at 600 °C (Fischer 1987). Small dolomite grains displayed an advanced level of decomposition at 700 °C with grains exhibiting a dolomite-type core surrounded by MgO and a Ca-rich shell. This degree of decomposition was also visible within larger dolomite grains at 760 °C. Calcite was also partially decomposed and consisted of a calcite-type core surrounded by a Ca-rich shell. At 880 °C almost all of the carbonate grains had vanished. Remaining MgO or pores with or without carbonate residues were surrounded by a rim of Ca-Mg-Al-silicates due to significant diffusion of Ca and Mg into the matrix (Fig. 1B). PXRD exhibited newly formed gehlenite and akermanite at this temperature.

(iii) Pyrite thermally decomposed between 300-600 °C, gaseous SO_2-SO_3 was formed (c.f. Schmidt, 1968) and confirmed by evolved gas analysis. The SO_2-SO_3 gas, however, stayed at most in the sherds and reacted with MgO and CaO of the decomposing carbonates thus forming sulfates (Schmidt 1968). Low concentrations of S were detected in carbonates at 700 °C. The amount of detected S increased with increasing firing temperature. Domains with elevated S contents were formed along the rims of the remaining carbonate grains at 760 °C. At a firing temperature of 880 °C, S could be found in the residues of former carbonates and in the Ca-Mg-Al-silicate reaction rims (Fig. 1B).

(iv) Some Na-rich feldspars exhibited a K-enriched rim at 880 °C (Fig. 1C) due to an exchange of Na^+ for K^+ (Riccardi et al. 1999). Collapsed clay minerals (Riccardi et. al. 1999) and partially collapsed muscovite (Ionescu & Hoeck 2011) can be considered as sources of K^+.

(v) Some quartz grains were characterized by a rim enriched in Al, Na, K and Fe at 880 °C (Fig. 1C). The interaction of these foreign elements indicates a softening or partially melting of quartz grains (Ionescu & Hoeck 2011).

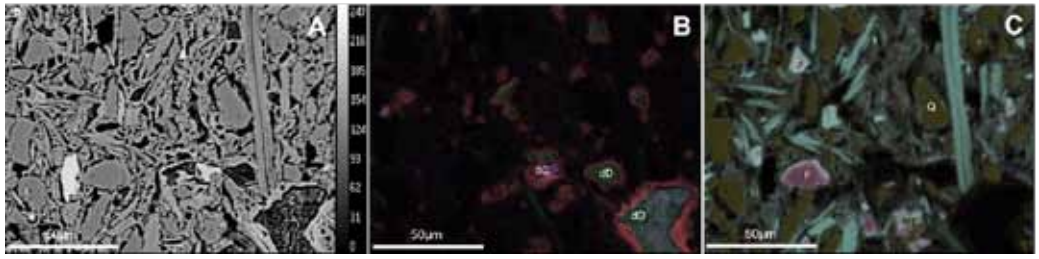

Figure 1. (A) BSE-image of a calcareous clay fired at 880 °C; (B) Stacked element maps of Mg (green), Ca (red) and S (purple); (C) Stacked element maps of Si (yellow), Na (magenta) and K (cyan).
Abbreviations: dC decomposed calcite, dD decomposed dolomite, F feldspar, Q quartz.

The outlined observations made are an important basis for firing experiments of clay-additive mixtures. Various mineral reactions were identified, and observations reported in literature were confirmed. The two most significant processes observed in detail are the gradual decomposition of carbonates starting from 620 °C and the melting of the matrix between 760-880 °C. Especially, the role of sulfur during the decomposition of carbonates provides important information for brick producing processes, since the formation of water-soluble sulfates causes severe efflorescence (Schmidt 1961).

Fischer P (1987): Die Bildung des grobkeramischen Scherbens beim Brennen, Teil II. – ZI-Jahrbuch 88, 96
Ionescu C, Hoeck V (2011): Firing-induced transformations in Copper Age ceramics from NE Romania – Eur J Miner 23, 937-958
Ricciardi MP, Messiga B, Duminuco P (1999): An approach to the dynamics of clay firing – Appl Clay Sci 15, 393-409
Schmidt E (1961): Ausblühungen. – Die Ziegelindustrie 5, 132
Schmidt E (1968): Die physikalischen und chemischen Veränderungen beim Ziegelbrand – ZI-Jahrbuch 68, 208

STOE Diffractometers empowering Mineralogical Crystallography

T. Pippinger[1]

[1]*STOE & Cie GmbH, Darmstadt, Germany*
e-mail: pippinger@stoe.com

STOE, established in 1887, manufacturing equipment for the optical examination of crystals, has been at the forefront of powder and single crystal X-ray diffraction since the 1960s. STOE invented and patented the transmission geometry technique for Powder XRD and additionally, they developed the first pixel detector XRD system with an open Eulerian cradle for single crystals.

Headquartered in Darmstadt, Germany, STOE maintains complete in-house capabilities for research and development, software programming, electrical and mechanical engineering, and production. This integrated approach enables STOE to offer both standard and customized solutions to its customers. Whenever it comes to quality, STOE accepts no compromises.

STOE´s latest instruments facilitate precise profile and Rietveld analyses, as well as ultrafast single crystal diffraction experiments on even the tiniest crystals. Furthermore, high-temperature and high-pressure accessories are available, which can be seamlessly integrated in the hardware and software, allowing for the convenient simulation of non - ambient inner earth conditions.

These solutions tailored to Mineralogical Crystallography and more will be discussed in the presentation.

Clays from the Westerwald area as a source for high reactive main cement constituent

C. J. Piribauer[1], R. Diedel[1], H. Knapp[1], W. Heuser[1], M. Schellhorn[1]

[1]Steaphan Schmidt Group,
e-mail: christoph.piribauer@stephan-schmidt.group

The cement and concrete industry are currently in a state of transition due to high CO_2 emissions. According to a study of the vdz (Deutscher Verband der Zementindustrie), there are three main levers to lower the emissions: alternative fuels, CCS / CCU and clinker reduced cements. As most of the emissions are so called process emissions and the potential for CCS / CCU is limited in a close range to the cement producers, there is a strong focus on the development and usage of clinker reduced cements. Calcined clays play an important role here as a substitute for the cement clinker made from limestone. To meet the decarbonisation targets of the German cement industry, 6.8 to 7.5 million tonnes/a of clay will be needed by 2030 (Basten, 2022). In order to cover this very high demands for clays, waste clays from treatment processes, such as filter cakes and clays from sludge ponds, are considered in addition to conventionally mined clays. As these secondary raw materials occur only in relatively small quantities with strongly varying compositions, they are likely to play only a minor role in the future due to the strong influence of the mineralogical-chemical composition on the calcination conditions and therefore on the resulting reactivities and technological properties.

Figure 1. Mine Wimpsfeld 3, white kaolinitic-illitic clays with an overburden of bentonites and basalt. – Picture: Stephan Schmidt Group

Stephan Schmidt KG operates 20 open-cast clay mining operations in Germany, 16 in the Westerwald area. From these deposits, more than 100 clays were selected for a screening process not only focussing on their basic suitability for calcination, but also with regards to a long-time availability for a constant material supply of a calciner. In a first screening step, the carbonate content (< 5 mass-%), the sulphide concentration (< 1.5 mass-%) and the clay mineral/quartz ratio (> 50 %) were assessed. Clays that met these requirements were calcined at 750 °C and subjected to a test for pozzolanic properties. The Surana method (Surana and Joshi, 1990) was chosen to determine the pozzolanicity. By chemically treating the calcinates after Surana, the available reactive Si and Al ions could be determined via ICP-OES. At a concentration >80,000 ppm (Al+Si), suitability as a clinker substitute is ensured, comparable to the performance of blast furnace slag and fly ash (Schulze and Rickert, 2019). Next to this information, also the influence of the calcined clays on the early strength can be estimated, as a higher Al content leads to the formation of CA phases. The final step in the evaluation of calcined clays involves the testing of CEM I cements (activity index/EN 450-1; water demand/EN 196-3; compressive strength/EN 196-1), in which 25 % of the cement clinker phase is replaced by calcined clays.

Based on this knowledge, 2 main supply areas have been identified. While the raw material mixture from Arbon/Wimpsfeld 3 (Fig. 1) has a high smectite content, the Sedan mixture is kaolinitic-illitic dominated. Each site allows the delivery of 250,000 t clay/a, which corresponds to the production of 200,000 t/a of calcinate.

Basten M (2022): Die Nachfrage nach Primär- und Sekundärrohstoffen der Steine-und-Erden-Industrie bis 2040 in Deutschland. - Bundesverband Baustoffe Steine und Erden e.V. Berlin

Surana M, Joshi S (1990): Estimating reactivity of pozzolanic materials by a spectrophotometric method. - Advances in Cement Research 3, 81-83

Schulze S, Rickert J (2019): Suitability of natural calcined clays as supplementary cementitious material. - Cement and Concrete Composites 1, 92-97

An uncommon terrestrial rock that was believed to be a meteorite

L. Pittarello[1,2], S. Chernonozhkin[3], H. Downes[4], O. Marchhart[2], S. Merchel[2], A. Wieser[2], F. Vanhacke[5], J. Villeneuve[6], S. Goderis[7]

[1]Naturhistorisches Museum, Vienna, Austria
[2]University of Vienna, Austria
[3]Montanuniversität Leoben, Austria
[4]Birkbeck University of London, United Kingdom
[5]Ghent University, Belgium
[6]CRPG, Université de Lorraine, Vandœuvre les Nancy, France
[7]AMGC, Vrije Universiteit Brussel, Belgium
e-mail: lidia.pittarello@nhm.at

Ureilites are achondrite meteorites, which can be associated to mantle restites, but containing up to 8 wt% carbon and which have experienced melting, smelting, and shock (e.g., Goodrich 1992; Goodrich et al. 2007). In the framework of a research project on isotopic zoning across olivine grains from selected ureilites (Chernonozhkin et al. subm.), a chip from Dyalpur was loaned from the Natural History Museum London (sample BM.51185). Petrographic and geochemical analysis of this sample revealed some features, which are not consistent with the previous characterization of Dyalpur and ureilites in general. However, as clasts with peculiar characteristics are not uncommon among ureilites (e.g., clast ALM-A with a trachyandesitic composition; Bischoff et al. 2014), we decided for further investigations. Oxygen isotopic ratios are close to the terrestrial fraction line, but this can also indicate mixing of different components by impact on the parent body (e.g., for angrites, Rider-Stokes et al. 2023). However, cosmogenic radionuclide measurements by accelerator mass spectrometry (Lachner et al. 2021) finally confirm a terrestrial origin of the sample. The (yet preliminary) upper limit of $^{26}Al/^{27}Al$ $4.4x10^{-12}$ corresponding to 0.3 dpm/kg (^{26}Al) measured is >60 times lower than the one of true Dyalpur sample, and also far lower than literature values for ureilites including Dyalpur (e.g., Aylmer et al. 1990).

The typically terrestrial features, including the occurrence of pargasite-hornblende amphibole and hazlewoodite (a Ni-sulfide), both never described before in ureilites, are associated with other features, which are quite uncommon for terrestrial rocks, such as the presence of carbon-rich veins inducing chemical reduction along their margin, and a Fo_{91} groundmass, embedding sub-rounded amphibole clasts. Geothermobarometric estimates (e.g., Hammarstrom & Zen 1986; Ridolfi & Renzulli 2012; etc.) on amphibole resulted in pressure estimate of 6-7 kbar and temperature estimate of 790-840 °C.

Terrestrial rocks presenting similar features are rare, mostly consisting of metasomatized peridotite-xenoliths in basalts recording breakdown of amphibole due to heating and decompression during transport (e.g., Ban et al. 2005; Kaeser et al. 2007). Further studies are planned to identify the nature of the sample and to reconstruct the case leading to its classification as Dyalpur ureilite in the collection of the NHM London.

Aylmer D, Vogt D, Herzog GF, Klein J, Fink D, Middleton R. (1990): Low ^{10}Be and ^{26}Al contents of ureilites: Production at meteoroid surfaces. - Cosmochim Acta 54, 1775-1784

Ban M, Witt-Eickschen G, Klein M, Seck HA. (2005): The origin of glasses in hydrous mantle xenoliths from the West Eifel, Germany: incongruent break down of amphibole. - Contrib Mineral Petrol 148, 511-523

Bischoff A, Horstmann M, Alix Barrat J-A, Chaussidon M, Pack A, Herwartz D, Ward D, Vollmer C, Decker S (2014): Trachyandesitic volcanism in the early Solar System. - P Natl Acad Sci USA 111, 12689 -12692

Chernonozhkin SM et al. (subm.): Early differentiation and core formation on the ureilite parent body recorded in the stable isotopic signatures of Fe, Zn and Mg.

Goodrich CA (1992): Ureilites. A critical review. - Meteoritics 27, 327-352

Goodrich CA, Orman vanJA, Wilson L (2007): Fractional melting and smelting on the ureilite parent body. – Geochim Cosmochim Acta 71, 2876

Hammarstrom JM, Zen E (1986): Aluminum in hornblende: An empirical igneous geobarometer. - Amer Mineral 71, 2876-2895

Kaeser B, Kalt A, Pettke T (2007): Crystallization and breakdown of metasomatic phases in graphite-bearing peridotite xenoliths from Marsabit (Kenya). - J Petrol 48, 1725-1760

Lachner J, Martschini M, Kalb A, Kern M, Marchhart O, Plasser F, Priller A, Steier P, Wieser A, Golser R (2021): Highly sensitive ^{26}Al measurements by Ion-Laser-InterAction Mass Spectrometry. - Int J Mass Spectrom 465, 116576

Rider-Stokes BG, Greenwood RC, Anand M, White LF, Franchi IA, Debaille V, Goderis S, Pittarello L, Yamaguchi A, Mikouchi Z, Claeys P (2023): Impact mixing among rocky planetesimals in the early Solar System from angrite oxygen isotopes. - Nat Astron (2023). https://doi.org/10.1038/s41550-023-01968-0

Ridolfi F, Ranzulli A (2012): Calcic amphiboles in calc-alkaline and alkaline magmas: thermobarometricand chemometric empirical equations valid up to 1,130°C and 2.2 GPa. - Contrib Mineral Petrol 163, 877-895

U-Pb garnet, zircon, and rutile petrochronology of eclogite xenoliths from the Navajo Volcanic Field (USA)

J.E. Pohlner[1], R. Albert[1], S. Aulbach[1], S. Hao[1], A. Gerdes[1], J.B. Walters[1], D.J. Schulze[2], H. Helmstaedt[3]

[1]Institut für Geowissenschaften and Frankfurt Isotope and Element Research Center (FIERCE), Goethe-Universität Frankfurt
[2]Department of Earth Sciences and Department of Chemical and Physical Sciences, University of Toronto, Mississauga, Canada
[3]Department of Geological Sciences and Geological Engineering, Queen´s University, Kingston, Canada
e-mail: pohlner@em.uni-frankfurt.de

Complementary insights from multiple mineral geochronometers are often indispensable to disentangle the complex multi-stage history of subduction-related rocks. Previous geochronological work on eclogite xenoliths of the Navajo Volcanic Field (NVF) sparked controversies about their origin, especially whether they are derived from oceanic crust of the Farallon plate, or from older continental lithosphere, based on occasional Proterozoic zircon U-Pb ages. We present new LA-ICP-MS U-Pb data from garnet, zircon, and rutile alongside geochemical and geothermobarometric data to test models for the origin and evolution of the NVF xenoliths.

The NVF comprises intrusions of serpentinized ultramafic microbreccia (SUM) which intruded the Colorado Plateau at ~30 Ma. Eclogite xenoliths from this SUM are mineralogically unusual, strongly resembling orogenic rather than typically bimineralic kimberlite-borne equivalents. Besides ubiquitous rutile, many contain zoisite pseudomorphs after lawsonite (with rare lawsonite relics), matrix monazite, and/or abundant pyrite along with rare coesite. Previous studies obtained peak P-T conditions around 4 GPa and 600°C. Chemically, some of the eclogites resemble mid-ocean ridge basalts, whereas most experienced varying degrees of multi-stage metasomatism. Zoned omphacite with Na-rich rims accompanied by an increase of whole-rock Na_2O contents (up to 11 wt%) and omphacite modes (sometimes >90%) reflects interaction with a siliceous fluid. Mg-rich garnet rims with mantle-like $\delta^{18}O$ are interpreted to reflect a massive hydration event just prior to entrainment in the SUM. The latter is also thought to have caused the crystallization of monazite with published ~30 Ma ages.

The various xenoliths yield variable garnet U-Pb dates, indicating garnet growth at different stages, but exclusively from the Cretaceous to shortly before SUM formation. The non-uniform garnet data may suggest that the NVF eclogite xenolith suite was assembled from rocks that entered the eclogite facies diachronously over tens of Myr. Metamorphic zircon ages cover a range similar to the garnet ages. Various stages of potential interaction with internally-derived (from lawsonite dehydration) and externally-derived (metasomatic) fluids may have induced (re)crystallization and/or partial re-setting of geochronometer minerals over a considerable time span.

There is currently no evidence for pre-Mesozoic metamorphism in the eclogites. By contrast, the hypothesis of a Proterozoic protolith origin is still under consideration, and can only be tested by dating rare igneous zircon cores. A zircon and rutile U-Pb dating campaign planned for the near future will reveal how the resultant ages relate to those obtained from garnet.

Electron Diffraction – Structure Elucidation of Nano-Crystalline Materials

A. Portieri[1], P. Simoncic[1]

[1]Eldico Scientific, Badenerstraße 790, 8048 Zurich-Altstetten, Switzerland
e-mail: simoncic@eldico.ch

Electron diffraction (known also as ED, 3D ED or microED) performing nano-crystallography on crystals smaller than 1 μm is increasingly gaining momentum in science and industry. Complementary to neutron-, powder-, and single-crystal X-ray diffraction, the disruptive technology of electron diffraction opens up fascinating new perspectives for a wide variety of compounds in the fields of chemical, pharmaceutical, and advanced materials research. The recent introduction of dedicated instrumentation to perform ED experiments is a key aspect of the continued growth and success of this technology. ELDICO Scientific presents the electron diffractometer ED-1, a smart combination of a 5-axis nanometer-precise goniometer, a large sample chamber, radically simplified electron optics, and an ultra-high-speed hybrid-pixel Dectris Quadro® camera for diffraction data acquisition. Several examples of data collected on ELDICO ED-1 are showcased to demonstrate the potential and advantages of a dedicated electron diffractometer, covering selected applications and challenges of electron diffraction: 1) polymorphism, 2) crystal mapping and extrapolation to powder XRD, and 3) structure elucidation of energy storage materials as well as zeolites and minerals.

Thracian marbles from Archaic to Roman Times – Imports or local production?

W. Prochaska, S. Ladstätter, V. Anevlavi

Austrian Archaeological Institute, Austrian Academy of Sciences, Franz Klein-Gasse 1, 1190 Vienna, Austria
e-mail walter.prochaska@oeaw.ac.at

Marble use and trade in the region of Thracia took place extensively already before it became Roman province in 46 AD. Within this territory some of the most prominent and renowned marble sources of antiquity are located (e.g., Prokonnesos or Thasos). The coastal regions at the Aegean, Marmara, and Black Sea, as well as the islands, were shaped by Greek culture and these marbles were widely exported throughout the empire. Accordingly, the marble trade in these coastal or island regions was always connected to the international commerce. Recent extensive studies in the course of the project "Fingerprinting White Marbles - Quarries and Cities of Roman Thrace, 1st-3rd century AD" (Austrian Science Fund) revealed that these marbles also were extensively used not only in the coastal areas but also in the larger inland cities of Thrace. In contrast to these renowned international marbles, the numerous marble deposits in the interior, in particular in today's Bulgaria, have received far less attention, however, as will be shown in this paper, they were of considerable economic importance.

Figure 1. Geologic/geomorphological zonation of Bulgaria (Zagorchev 2009) with the marble producing areas.

The integration of the territory into the Roman Empire was followed by urbanisation and the extension of the infrastructure. Evidence of Roman marble production in the inland territory of Thrace is known in different areas: The most important geologic unit for economic marble production are the Rhodope Mountains with high-grade marble deposits. In the eastern parts of the Sredna Gora region further marble deposits occur with different metamorphic grades. Furthermore, in greenschist facies series of the NW Balkan Mountains near the town of Berkovitsa fine-grained marbles occur. Initial analyses indicate that these marbles were not only employed in the province itself, but were also exported. On the other hand, architecture and sculpture in the province of Thrace reveal striking connections to Asia Minor. By means of a sampling of the Thracian quarries on one hand and of Roman artefacts throughout the province on the other hand, the question regarding marble trade as well as the cultural and technological transfer will be discussed in the presentation. One example of far distant trade of the marble of that region is the "boarhunt" found during excavations in 2010 in Felix Romuliana in today's Serbia sculptured from Berkovitsa marble.

.

Figure. 2: The sculpture "boarhunt" made of marble from Berkovitsa SW of the town of Montana in today's Bulgaria. The sculpture or its marble was transported along a distance of more than 100 km in beeline.

More than 1400 samples from ancient quarries in Thrace and samples from artefacts in the museums all over the region were analysed in order to assign the marble of a given artefact to a corresponding quarry or quarry area. To achieve reliable results a multi method approach was applied using stable isotope analysis (O- and C-isotopes), trace element analysis by ICP-MS and petrographic investigations. Naturally, this large number of variables analysed has to be evaluated by statistical means. We used the programme packages STATISTICA and SPSS. On this basis the different marbles of Thracia can be told apart, and a very precise correlation of the artefacts to the corresponding sources can be achieved.

Zagorchev I (2009): Geomorphological zonation of Bulgaria. Principles and state of the art.- Proceedings of the Bulgarian Academy of Sciences 628(8), 981-992.

Prochaska W Zivic M (2018): The marbles of the sculptures of Felix Romuliana in Serbia. in Proceedings of the XI ASMOSIA Conference (Split May 2015) pp 301-311

Modern non-ambient X-ray diffraction for the investigation of minerals, metals and industrial materials of any type

B. Puhr[1], A.O.F. Jones[1], B. Schrode[1], M. Kremer[1], P. Vir[1], A. Paiva[1]

[1]Anton Paar GmbH, Graz, Austria
e-mail: barbara.puhr@anton-paar.com

Modern powder X-ray diffraction (XRD) systems must nowadays be able to meet the challenges faced by multi-user and multi-application facilities. Instruments must be capable not only of routine XRD measurements, but also have to offer advanced capabilities such as measurements under non-ambient conditions (varying temperature, pressure, gas atmosphere, humidity, …) which can drastically change material properties.

The recently launched XRDynamic 500 automated multipurpose powder X-ray diffractometer from Anton Paar (Fig. 1) has set new standards in terms of data quality, automation and efficiency for laboratory powder diffractometers. The core of XRDynamic 500 is the TruBeam™ concept that comprises a large goniometer radius and evacuated optics units, automatic change of the beam geometry and all optics components, and automated instrument and sample alignment routines. All of these features combine to deliver outstanding data quality that can be measured with high efficiency in a straight-forward manner. The high level of automation means that you can perform measurements on one or many samples with different geometries and instrument configurations in one batch with no user intervention needed.

XRDynamic 500 can also be equipped with different non-ambient attachments to perform measurements under non-ambient conditions. These attachments are perfectly integrated into the hard- and software (plug-and play mode, integrated control unit, built-in connections) and guarantee best-in-class convenience for your non-ambient XRD studies.

To highlight the potential of XRDynamic 500, we will present key instrument features and benefits in addition to recent application data on non-ambient diffraction. Examples include in-situ structural changes of bentonite samples and materials used for technical applications (Fig. 2), how salt mineral compositions change under the influence of gas and humidity, and the study of the tempering temperature on the properties of steel.

Figure 1. The XRDynamic 500 automated multipurpose powder X-ray diffractometer from Anton Paar.

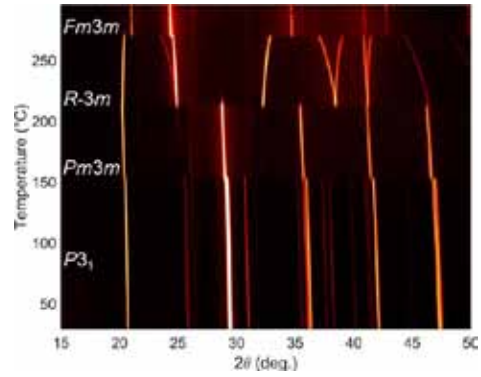

Figure 2. Temperature-induced phase transitions of $RbNO_3$ (Weidenthaler & Ternieden, 2022).

Weidenthaler C, Ternieden J (2022): Data measured by C. Weidenthaler and J. Ternieden (Max-Planck-Institut für Kohlenforschung, Mülheim an der Ruhr, Germany

Machine learning-assisted pyrite indicator mineral approach in mineral exploration

S. Raič[1], F. Molnár[2], N. Cook[3], P. Nikkola[4], K. Szentpéteri[4], H. O'Brien[4], A. Taivalkoski[5], J.-P. Ranta[5]

[1]Institue of Applied Geosciences, University of Technology, Graz, Austria
[2]Department of Mineralogy, Institute of Geography and Earth Sciences, Eötvös Loránd University, Budapest, Hungary
[3]Sustainable Minerals Institute, University of Queensland, Indooroopilly, Queensland, Australia
[4]Geological Survey of Finland, Espoo, Finland
[5]Oulu Mining School, University of Oulu, Oulu, Finland
e-mail: sara.raic@tugraz.at

Discovering new ore deposits that supply and satisfy the growing industrial demand for green transition metals is becoming more important than ever for transitioning into a non-fossil fuel future. This task however, appears to be unprecedented, when considering the required amount of technology metals. It becomes therefore highly relevant to develop and implement innovative and sustainable, but time- and cost-efficient exploration methods for deeply buried, undiscovered mineral deposits. A way to tackle this challenge is by using known European mineral deposits as testing grounds for new exploration technologies. For this purpose, the domestic mineral resources in northern Finland provide an ideal ecosystem and diversity of profitable green transition metals such as nickel, copper, cobalt and gold. The glaciated terranes in which these mineral systems occur, however, require special exploration methods such as the indicator mineral approach. Indicator minerals (e.g. sulfides, oxides and native gold) are recovered from glacial sedimentary samples and their individual grains are used for trace element analysis by LA-ICP-MS, which ideally could provide key information on the character of their source bedrocks, type of mineralization, as well as the glacial transport direction.

In this study we have tested the indicator mineral approach in the Rompas-Rajapalot Au-Co project areas in the Paleoproterozoic Peräpohja belt in northern Finland, by analyzing and comparing the trace element geochemistry of pyrite grains from bedrock and till samples. A machine learning-based approach was implemented using unsupervised self-organizing maps (SOM) and k-means clustering for mineralization-related pattern recognition. The obtained results show that pyrite grains recovered from till can be discriminated and clustered based on their compositions, and further correlated with pyrite from two hydrothermal deposit types within the study area: (i) the Au-Co mineral system at Rajapalot, and (ii) the vein-style Au system at Rompas. Mapping of recognized patterns, in accordance with ice flow directions, assists in (i) the localization of potential target-areas, (ii) and improves our understanding of similar mineral systems.

Tungsten mineralization in East Tyrol – repeated recycling of W in the crust?

J. G. Raith[1], F. Altenberger[1], F. Hutter[2], J. Weilbold[3], C. Auer[3]

[1]Montanuniversität Leoben, Leoben
[2] GeoSphere Austria, Vienna
3 geo.zt gmbh, Hall in Tirol
e-mail: johann.raith@unileoben.ac.at

Geochemical tungsten anomalies and occurrences were discovered in the Lienz area in the 1980-ies during regional W prospecting campaigns (e.g., Neinavaie & Ronge 1985) and are summarized as "Polymetallic skarn district Drauzug-Gurktal nappe system Lienz-Hochstein" in the IRIS data base. Low- to medium grade metamorphic Austroalpine units were intruded by a pluton west of Lienz in the Oligocene (Edenwald intrusion, ≈30 Ma). A km-sized contact metamorphic aureole with metapelitic hornfelses developed around the composite intrusion especially at its western to southern contacts (Linner et al. 2013).

Three types of scheelite mineralization are distinguished in the region: (1) Strata-bound scheelite in low-grade metamorphic metabasites in the Early Palaeozoic Thurntal Quartzphyllite (disseminations, stringers, deformed quartz veinlets; e.g., Tafinalpe). The association of W-As (arsenopyrite) is specific for this type (Portugaller 2010); (2) Sulfide-scheelite skarn mineralization (disseminations, veins; e.g., Edenwald). Massive sulfides (pyrrhotite, chalcopyrite etc.) are associated with thin intercalations of marble and calc-silicate rocks (Ca amphiboles, calcian plagioclase, grossular, diopside-hedenbergite, vesuvianite, wollastonite) (Hutter 2022). This type is interpreted as a reduced magmatogenic skarn, a mineralization style very rare in the Eastern Alps. (3) Scheelite in quartz veins and clefts within the intrusive rocks. This pure scheelite mineralization is controlled by brittle division surfaces in the intrusive rocks.

The Oligocene plutonic rocks span a wide petrographic composition from metaluminous (gabbro)diorite, tonalite, to more evolved peraluminous granodiorite/granite. They are magnesian showing calc-alkaline magma characteristics. The high W bulk values (up to hundreds of ppm W) to are due to post-magmatic (type 3) hydrothermal processes.

LA-ICP-MS trace element analyses of scheelite allow to discriminate these different mineralization styles. We present combined micro-textural features (obtained from CL imaging) and trace element data of scheelite in their geological/petrographic context, we discuss the possible applications for exploration and propose that tungsten has undergone several stages of crustal recycling.

Hutter F (2022): Wolframvererzungen und Intrusionsgesteine am Lienzer Schlossberg, Osttirol. - Masterarbeit, Montanuniversität Leoben

Linner M, Reitner JM, Pavlik W (2013) Geologische Karte 179, Lienz 1:50.000.- Geologischen Bundesanstalt, Wien

Neinavaie MH, Ronge W (1985): Wolframprospektion 1984 in Teilen Osttirols, Kärntens, Niederösterreichs und der Steiermark sowie petrographische Untersuchungen an neu aufgefundenen Wolframvererzungen im Arbeitsgebiet. - Unveröffentlichter Ber VOEST-ALPINE, Eisenerz

Portugaller T (2010): Scheelitvererzungen im Thurntaler Quarzphyllitkomplex, Osttirol: Petrographische und chemische Untersuchungen an Nebengesteinen und Bachsedimenten. - Masterarbeit, Montanuniversität Leoben

Pressure prediction in a poly-metamorphic terrain based on µ-EDXRF. An example from the Archean Vumba Schist Belt, Botswana

D. Rammlmair[1]

[1]Leibniz University Hannover, Germany
e-mail: d.rammlmair@mineralogie.uni-hannover.de

The Archean Vumba Schist Belt in the NE of Botswana comprises komatiitic successions, bimodal volcanics, sediments, Archean soils, banded iron formation, rodingites, and is intruded by several generations of granitoids, late pyroxenite and dolerite dykes. The belt experienced three metamorphic events, where due to strong uplift and tilting a shift of metamorphic centers from high grade in the NW to medium grade in the center and low grade in the SE can be observed. Shear zone and quartz vein hosted gold deposits are related to the late low grade metamorphic impact.

Several hundred rock slices were mapped by the µEDXRF M4 Tornado, Bruker nano. The measurement was performed in 20µm steps, 2msec acquisition time using a Rh-tube at 50kV and 600 µA, a poly-capillary beam guide, no filters, two silicon drift detectors arranged in 180°, 90° to the tube with 51° take off or incidence angle, respectively.

The mapping provided bulk area chemical information and phase distribution for the very same area. Phase distribution was obtained by supervised endmember-based classification using the spectral angle mapper (SAM) algorithm of the hyperspectral software ENVI for 165 spectral regions of interest. The minimum per channel per pixel was obtained for both detectors to widely omit diffraction signals of individual grains. Both, area chemistry and modality were used to select samples of similar chemistry along strike from NW to SE to compare the metamorphic impact. A series of mafic rocks was selected and investigated in detail putting focus on the amphibole chemistry by masking all other phases and applying a second SAM classification based on amphibole solid solution endmembers only. The amphibole endmembers were derived from EPMA analyses and amphibole classification by Li et al. (2022) following the classification scheme of Hawthorne et al. (2012). This second classification is the key to differentiate the impact of individual metamorphic events within individual mafic rock slices by visualizing amphiboles classified according to chemistry representative for different PT environments. The pressure estimation provided by Li et al. (2022), referring to the method of Hollister et al. (1987), was used for pressure prediction of amphiboles in individual samples across the belt. The dominant pressure is around 8.9 kb, but relics indicate values of >10 kb, and retrograde alteration shows values of > 4 kb.

Automated mineralogy applied to µEDXRF, provided a detailed endmember data base exists, is a fast and easy to apply method, despite obscuring effects such as grain boundaries, grain size, shape as well as orientation-based diffraction. Information on rock and mineral chemistry, modality, and mineral sub-classes can be obtained for large sample numbers for preselection of most adequate samples for polished thin sections and EPMA investigations.

Li X, Zhang C, Behrens H, Holtz F (2020): Calculating amphibole formula from electron microprobe analysis data using a machine learning method based on principal components regression. - Lithos 362-363, 105469, 10.1016/j.lithos.2020.105469.

Hawthorne FC, Oberti R, Harlow GE, Maresch WV, Martin RF, Schumacher JC, Welch MD (2012): Nomenclature of the amphibole supergroup. - Amer Mineral 97, 2031–2048

Hollister LS, Grissom GC, Peters EK, Stowell HH, Sisson VB (1987): Confirmation of the empirical correlation of Al in hornblende with pressure of solidification of calc-alkaline plutons. - Amer Mineral 72, 231–239

Recycling of Mineral Waste Materials by Geopolymerization – First Results

B. Ratz[1], T. Sattler[1], F. Steindl[2], S. Raič[2], I. Zögl[2], S. Radinger[2], O. Rudić[3], F. Mittermayr[3], C. Grengg[2]

[1]Montanuniversitaet Leoben, Chair of Waste Processing Technology and Waste Management, Franz-Josef-Straße 18, 8700 Leoben, Austria
[2]Institute of Applied Geosciences, Graz University of Technology, Rechbauerstraße 12, 8010 Graz, Austria
[3]Institute of Technology and Testing of Construction Materials, Graz University of Technology, Inffeldgasse 24, 8010 Graz, Austria
e-mail: bettina.ratz@unileoben.ac.at

The building and construction industry is responsible for 40 % of the anthropogenic CO_2 emissions and consumes enormous amounts of resources. In recent decades, there has been a significant increase in the production of waste, of which mineral waste is the largest stream in Austria, accounting for 76 % of the total waste. It is currently mostly disposed in landfills. To counteract the negative environmental impact of building and construction and to reduce the amount of landfilled waste, a Christian Doppler Laboratory for waste-based geopolymer construction materials in the CO_2-neutral circular economy ($GECCO_2$) was launched at Graz University of Technology. The goal is to produce environmentally friendly, highly resilient and Portland-cement-free geopolymer construction materials, also known as alkali-activated materials, from currently unexploited mineral waste materials. These geopolymers are then to be used in, for example, the environment of biochemically aggressive waste systems, such as sewer manholes, tanks and basins, or biowaste treatment facilities. Tasks of the Chair of Waste Processing Technology and Waste Management at the Montanuniversitaet Leoben, include the identification and selection of relevant mineral waste streams and the mineralogical, chemical and environmental characterization of selected waste materials, and elaboration of potential pretreatment strategies. With the obtained results, a material portfolio of suitable Austrian waste materials and industrial by-products will be created. First results will be presented regarding the mineralogical and chemical characterization of the selected waste materials.

Preliminary EBSD analysis and interpretation of Spinel-Olivine-Plagioclase pseudomorphs in skarnoid xenoliths from Southern Slovakia

L. Reato[1], M. Huraiová[1], T. Griffiths[2], G. Habler[2], R. Abart[2], V. Hurai[3], P. Konečný[4]

[1]Comenius University, Faculty of Natural Sciences, Department of Mineralogy, Petrology and Economic Geology, Ilkovičova 6, 842 15 Bratislava, Slovakia
[2]University of Vienna, Department of Lithospheric Research, Josef-Holaubek-Platz 2, 1090, Vienna
[3]Slovak Academy of Sciences, Institute of Earth Sciences, Dúbravská Cesta 9, 840 05 Bratislava, Slovakia
[4]State Geological Institute of Dionýz Štúr, Department of Special Laboratories, Mlynská Dolina 1,817 04 Bratislava, Slovakia
e-mail: reato1@uniba.sk

Calc-silicate skarnoid xenoliths, with dimensions of up to 20 cm in diameter, were collected from Pleistocene alkali basalts of Southern Slovakia. Their general mineralogy and petrology have been described in Reato et al. (2022). They are composed of layers of relict augitic diopside, skeletal olivine and interstitial ternary feldspar (An_{57-86}), alternating with layers of anorthite (An_{95-100}) ± high Al, Fe^{3+} clinopyroxenes [$Ca(Al,Fe^{3+})AlSiO_6$] ± melilite inclusions. Such a mineral assemblage is indicative of thermal metamorphism in a high fO_2 environment and can be found in skarn or paralava (Foit et al. 1987; Pascal et al., 2005). Occasional pockets and veins of calcite ± aragonite can be present in both layers. Most of the xenoliths contain pseudomorphs comprising olivine (Ol), spinel (Spl), and ternary feldspar with an integrated average composition resembling tschermakitic amphibole. The pseudomorphs are characterised by very fine grained (1-100 μm^2) skeletal to dendritic olivine and spinel, surrounded by interstitial ternary feldspar. The interstitial ternary feldspar within the pseudomorphs (An_{53-96}) has compositions similar to the one in the diopside + olivine layer (An_{57-86}). A sharp chemical boundary between the pseudomorphs and the anorthite layer is present. The olivine within the pseudomorphs is richer in Mg and has a more restricted composition (Fo_{85-88}) compared to olivine outside the pseudomorphs (Fo_{66-88}), which is characterised by much bigger (>100 μm) crystals, growing perpendicular to the elongation direction of the pseudomorphs.

The sample's lineation and foliation were determined by X-ray micro-computed tomography using an industrial v|tome|x L 240 tomograph from the Institute of Earth Sciences - SAS in Banská Bystrica, and thin sections were cut parallel to the lineation and perpendicular to the foliation. Locations with interesting micro-structural features were selected through transmitted light microscopy. The mineralogy of the selected areas was quantified through EMPA at the State Geological Survey of Slovakia in Bratislava, using a CAMECA SX-100 electron microprobe. EBSD analysis, together with EDS maps, were produced at the Laboratory for Field-Emission Scanning Electron Microscopy and Focused Ion Beam Applications at the University of Vienna, using the FEI QuantaTM 3D FEG instrument. After this, data were re-indexed and processed using EDAX OIM Analysis™ at the University of Vienna, and the Matlab™ toolbox MTEX (Bachmann et al. 2010).

A region containing a pseudomorph at the contact between the anorthite layer and the diopside + olivine layer was selected to determine the microstructural characteristics of the three different domains and their interactions. Both anorthite and ternary feldspar outside the pseudomorph keep the same crystal orientation inside the pseudomorph, despite their change in composition. The grain boundary misorientation angle distribution between olivine and spinel inside the pseudomorph shows a peak at 56°. When only the Spl-Ol boundary segments in the range 55°-57° misorientation angle are considered, a very strong misorientation axis

peak, suggestive of a near-specific crystallographic orientation relationship (COR), was observed. This was confirmed by plotting Spl directions with respect to Ol for the selected boundaries, revealing alignment of one of the {111}Spl planes with the (100)Ol plane and one of the {110}Spl planes with (001)Ol, with minor dispersion (generally <5°) around the perfect relationship.

The observed COR between spinel and olivine implies an interaction between the two lattices, most likely during simultaneous growth. Similar plane relationships have been found in experimental petrology studies and were related to the exsolution of spinel from olivine occurring in the mantle transition zone (Hamaya & Akimoto 1982; Green, 1984). However, the xenoliths' protolith was formed and transformed within the crust (Reato et al. 2022), implying a different simultaneous growth process is responsible for the COR in this case. Concerning the behaviour of plagioclase within the pseudomorph, we can conclude that it has likely grown after olivine and spinel, using the plagioclase crystals from outside the pseudomorphs as a template for its growth within them, analogous to the formation of myrmekites (Phillips and Evans, 1980; Yuguchi & Nishiyama 2008). This feature is typical of rapid cooling systems, which is in accordance with the geological context and history of the xenoliths, which are thought to have undergone high-T thermal metamorphism before being collected by the host alkali basalt (Reato et al. 2022).

Bachmann F, Hielscher R, Schaeben H (2010): Texture Analysis with MTEX – Free and Open-Source Software Toolbox. Sol. St. Phen 160, 63–68

Foit FF, Hooper RL, Rosenberg PE (1987): An unusual pyroxene, melilite, and iron oxide mineral assemblage in a coal-fire buchite from Buffalo, Wyoming. - Amer Mineral 72, 137-147

Hamaya N, Akimoto SI (1982): On the mechanism of the olivine-spinel phase transformation. - Phys Earth Plan In 29, 6-11

Green HW (1984): How and why does olivine transform to spinel? - Geophys Res Lett 11, 817-820

Phillips ER (1980): On polygenetic myrmekite. - Geol Mag 117, 29-36

Pascal M, Katona I, Fonteilles M, Verkaeren J (2005): Relics of high-temperature clinopyroxene on the join Di–CaTs with up to 72 mol.% $Ca(Al,Fe^{3+})AlSiO_6$ in the skarns of Ciclova and Magureaua Vatei, Carpathians, Romania. - Can Mineral 43, 857–881

Reato L, Huraiová M, Konečný P, Marko F, Hurai V (2022): Formation of esseneite and kushiroite in tschermakite-bearing calc-silicate xenoliths ejected in alkali basalt. - Minerals 12, 156

Yuguchi T, Nishiyama T (2008): The mechanism of myrmekite formation deduced from steady-diffusion modeling based on petrography: Case study of the Okueyama granitic body, Kyushu, Japan. - Lithos 106, 237-260

Structural peculiarities in (1-x)$Na_{0.5}Ba_{0.5}TiO_3$-$x$$BaTiO_3$ at the morphotropic phase boundary studied by high-pressure XRD and Raman spectroscopy

C. Rösche[1], T. Boffa-Ballaran[2], T. Malcherek[1], C. Paulmann[1], R. J. Angel[3], B. Mihailova[1]

[1]FB Erdsystemwissenschaften, Universität Hamburg, Germany
[2]Bayerisches Geoinstitut, Universität Bayreuth, Germany
[3]Istituto di Geoscienze e Georisorse, CNR, Padova, Italy
e-mail: constanze.roesche@uni-hamburg.de

Perovskite-type (ABO_3) ferroelectric solid solutions are widely used functional materials, whose properties are utilized, for example, in sensors and actuators. The currently market-leading ferroelectric ceramics $Pb_{1-x}Zr_xTiO_3$ contain lead, which is undesirable from an environmental point of view. The solid solution $Na_{0.5}Bi_{0.5}TiO_3$-$x$$BaTiO_3$ (NBT-xBT) is one of the promising lead-free alternatives, however, its properties still need to be accurately constrained. Compositional variations may change the symmetry of the ferroelectric phase and shape the nanoscale structure, allowing to tune the properties by chemical substitutions. At the morphotropic phase boundary (MPB) with x = 0.05 - 0.06 for NBT-xBT the dielectric permittivity, piezoelectric coefficient, and electromechanical coupling factor are enhanced (Ge at al. 2011) due to an increased structural flexibility (de la Flor et al. 2019), making such compositions a good starting point for improvement by additional chemical doping. For an effective modification of the material, better understanding of the relation between the chemical composition and the nanoscale structural features in NBT-xBT is needed.

In this study, we have analyzed the response of the structure of NBT-0.048BT to external hydrostatic stress by performing high-pressure single-crystal X-ray diffraction (XRD) and Raman spectroscopic experiments up to 9 GPa, using the diamond-anvil-cell technique. It is known that in the case of Pb-based relaxor ferroelectrics pressure suppresses the polar order, while it enhances the antiferrodistortive order. Thus, the complementary high-pressure analyses of Bragg scattering, informative of long-range order, X-ray diffuse scattering (XDS), indicative of intermediate-range order and Raman scattering, sensitive to the intermediate-/short-range order can help to reveal subtle structural features, which are hard to detect at ambient pressure (Mihailova et al. 2011). The combination of different experimental methods allows us to obtain a comprehensive picture of the pressure-induced structural transformations ranging from the local to the long-range scale. At ambient and low pressure the deviations from the average pseudo-cubic perovskite structure produce strong diffuse scattering, which evolves into sharp Bragg peaks with increasing pressure [see Fig. 1 (a) and (c)]. The appearance of additional Bragg peaks indicates a phase transition between 4.4 and 5.5 GPa. The Raman data [Fig. 1 (b) and (d)] resolve the multistep local scale structural changes that lead to the change in symmetry. First a reduction of the Ba-induced local BO_6 anisotropy is taking place at 0.5 - 0.9 GPa, followed by decoupling of adjacent A- and B-site dipoles near 1.2 GPa. This allows for development of antipolar order of A-cation off-center displacements starting above 1.9 GPa, similar as it has been observed by Kreisel et al. (2003) in pure NBT at lower pressures. Furthermore, there is a strong amplification and increase in correlation length of octahedral tilts above 2.7 GPa and a change in the tilt pattern at 4 - 4.5 GPa.

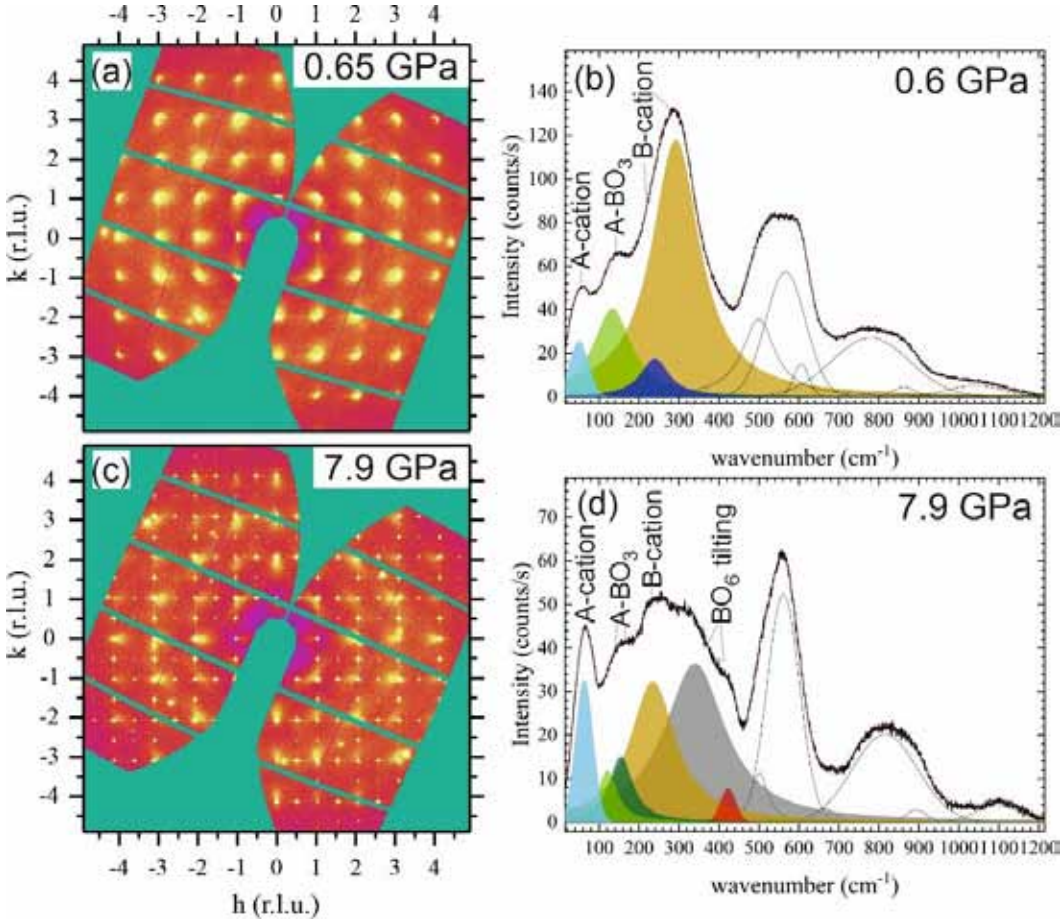

Figure 1. X-ray diffraction pattern in *hk*0 plane (a) and (c) and Raman scattering (b) and (d) of NBT-0.048BT at ~0.6 GPa and 7.9 GPa. The colored peaks in (b) and (d) are associated with A-cation off-centering vibrations (light blue), A-BO_3 translations (light and dark green), B-cation off centering vibrations (dark blue and orange) and BO_6 tilting vibrations (grey and red).

Ge W, Cao H, DeVreugd C, Li J, Viehland D, Zhang Q, Luo H (2011): Influence of $BaTiO_3$ content on the structure and properties of $Na_{0.5}Bi_{0.5}TiO_3$ crystals. - J Amer Ceram Soc 94, 3084-3087

De La Flor G, Gorfman S, Mihailova B (2019): Local-scale structural response of (1-*x*)$Na_{0.5}Bi_{0.5}TiO_3$-*x*$BaTiO_3$ to external electric fields. - Appl Phys Lett 114, 42901

Mihailova B, Angel RJ, Maier BJ, Welsch AM, Zhao J, Gospodinov M, Bismayer U (2011): The structural state of lead-based relaxor ferroelectrics under pressure. - IEEE Trans Ultrason Ferroelectr Freq Control 58, 1905-1913

Kreisel J, Bouvier P, Dkhil B, Thomas PA, Glazer AM, Welberry TR, Chaabane B, Mezouar M (2003): High-pressure x-ray scattering of oxides with a nanoscale local structure: Application to $Na_{1/2}Bi_{1/2}TiO_3$. - Phys Rev B68, 14113

Highly siderophile element and Re-Os isotope compositions of the 3.5 Ga Tomka Iron Formation, Daitari Greenstone Belt, India

A. Salzmann[1], T. Schulz[1], S. Viehmann[2], J. Jodder[3], A. Hofmann[4], C. Koeberl[1]

[1]Department für Lithosphärenforschung, Universität Wien, Österreich
[2]Institut für Mineralogie, Leibniz Universität Hannover, Deutschland
[3]Evolutionary Studies Institute, University of the Witwatersrand, South Africa
[4]Department of Geology, University of Johannesburg, South Africa
e-mail: a01610854@unet.univie.ac.at

Banded iron formations (BIFs) are Precambrian sedimentary rocks that are the product of chemical precipitation from seawater diagenetic, and metamorphic processes. Their abundance reach a maximum at around 2.4 Ga and appear to correlate with the Paleoproterozoic rise of atmospheric oxygen (Great Oxidation Event) with the subsequent change from anoxic to oxic conditions in the shallow parts of the ancient oceans. BIFs may thus represent robust archives, traced by rare earth elements and Yttrium (REY) and the Sm-Nd isotope system (Viehmann et al. 2015b) for the physico-chemical evolution of early Earth's atmosphere and oceans.

Following earlier studies that applied the redox-sensitive highly siderophile element (HSE) abundances and the Re-Os isotopes system to the Neoarchean Temagami BIF (Schulz et al. 2021) and the Neoproterozoic Urucum BIF ((Prost 2023), we investigate the application of these geochemical tools to a BIF of the Paleoarchean Daitari Greenstone Belt, Singhbhum Craton, India. This multiproxy approach has the potential to record the influence of different source contributions to the BIF forming seawater column (i.e., continental vs. hydrothermal vs. possibly meteoritic). Analyses were conducted using the laboratory and thermal ionization mass spectrometry facilities at the GeoIsotope Core Facility of the Department of Lithospheric Research at the University of Vienna and (for isotope dilution concentration measurements of selected HSEs) in cooperation with the mass spectrometry facilities at the Freie Universität Berlin.

The Tomka, as well as any other, BIF can only serve as a geochemical seawater archive if devoid of detrital contamination and pristine (i.e., devoid of diagenetic, metamorphic, and hydrothermal overprints). The Tomka BIF is a promising candidate to preserve primary seawater signatures, because it was only subjected to greenschist-facies metamorphism, whereas other old iron formations (e.g., Isua BIF) almost exclusively underwent higher grade metamorphism (Nutman et al. 2017; Jodder et al. 2023).

A comparison between literature data for immobile elements such as Zr, and fluid mobile elements, such as Sr (Bau & Möller, 1993; Kamber et al. 2004; Viehmann et al. 2015a, 2016), in combination with the $^{187}Os/^{188}Os$ ratios reported in this study for the Daitari BIF layers (chert-, magnetite- and mineralogically mixed layers) might indicate only minor syn- and postdepositional disturbances. Accordingly, most of the analyzed samples have a weak linear correlation in the $^{187}Os/^{188}Os$ vs. $^{187}Re/^{188}Os$ diagram and scatter around a ~3.5 Ga reference isochron. The $^{187}Os/^{188}Os$ ratios range from mantle-like values of ~0.14 to more radiogenic values up to ~0.41 (which is still significantly less radiogenic than the present-day upper continental crust with a value of ~1.4; Peucker-Ehrenbrink & Jahn 2001). Iridium

contents of the analyzed samples are exclusively crust-like at ~0.03 ppb, thus excluding any extraterrestrial component, while Os concentrations (mostly ranging between 0.1 and 0.3 ppb) can be as high as 1 ppb. More data, including Pt, Ru and Pd concentrations, will be presented at the conference.

Bau M, Möller P (1993): Rare earth element systematics of the chemically precipitated component in early precambrian iron formations and the evolution of the terrestrial atmosphere-hydrosphere-lithosphere system. - Geochim Cosmochim Acta 57, 2239–2249, doi:10.1016/0016-7037(93)90566-F

Jodder J, Hofmann A, Xie H, Elburg MA, Wilson A (2023): Geochronology of the Daitari Greenstone Belt, Singhbhum Craton, India. - Precamb Res 388, 106997, doi:10.1016/j.precamres.2023.106997

Kamber BS, Bolhar R, Webb GE (2004): Geochemistry of late Archaean stromatolites from Zimbabwe: evidence for microbial life in restricted epicontinental seas. - Precamb Res 132, 379–399, doi:10.1016/j.precamres.2004.03.006

Nutman AP, Bennett VC, Friend CRL (2017): Seeing through the magnetite: Reassessing Eoarchean atmosphere composition from Isua (Greenland) ≥3.7 Ga banded iron formations. - Geosci Front 8, 1233–1240, doi:10.1016/j.gsf.2017.02.008

Peucker-Ehrenbrink B, Jahn B (2001): Rhenium-osmium isotope systematics and platinum group element concentrations: Loess and the upper continental crust. - Geochem Geophys, Geosystems 2, paper no. 2001GC0001172, 22pp, doi:10.1029/2001GC000172

Prost T (2023): Direct radiometric dating of a Neoproterozoic iron formation – Rhenium-Os and highly siderophile element systematics of the Urucum Iron Formation, Brazil. - Master's thesis, Univ Vienna, 113 pp

Schulz T, Viehmann S, Hezel DC, Koeberl C, Bau M (2021): Highly siderophile elements and coupled Fe-Os isotope signatures in the Temagami Iron Formation, Canada: Possible signatures of Neoarchean seawater chemistry and Earth's oxygenation history. - Astrobiology 21, 924–939, doi:10.1089/ast.2020.2311

Viehmann S, Bau M, Bühn B, Dantas EL, Andrade FRD, Walde DHG (2016): Geochemical characterisation of Neoproterozoic marine habitats: Evidence from trace elements and Nd isotopes in the Urucum iron and manganese formations, Brazi. -Precamb Res 282, 74–96, doi:10.1016/j.precamres.2016.07.006

Viehmann S, Bau M, Hoffmann JE, Münker C (2015a): Geochemistry of the Krivoy Rog Banded Iron Formation, Ukraine, and the impact of peak episodes of increased global magmatic activity on the trace element composition of Precambrian seawater. - Precamb Res 270, 165–180, doi:10.1016/j.precamres.2015.09.015

Viehmann S, Bau M, Smith AJB, Beukes NJ, Dantas EL, Bühn B (2015b): The reliability of ~2.9 Ga old Witwatersrand banded iron formations (South Africa) as archives for Mesoarchean seawater: Evidence from REE and Nd isotope systematics: J African Earth Sci 111, 322–334, doi:10.1016/j.jafrearsci.2015.08.013.

Hydrogen induced changes in the mineralogical phase composition of downhole cements: fundamentals research within the context of Underground Hydrogen Storage

T. Sammer[1], K. Ravi[2], J. G. Raith[1]

[1]Chair of Resource Mineralogy, Montanuniversität Leoben
[2]Chair of Drilling and Completion Engineering, Montanuniversität Leoben
e-mail: thomas.sammer@unileoben.ac.at

Hydrogen is nowadays commonly considered a promising way of storing energy from renewable energy sources, hence increasing the efficiency of renewable energy sources. However, to store large volumes of hydrogen on a seasonal (e.g., winter – summer) time scale fast storage volumes are needed (Reitenbach et. al. 2015). Underground hydrogen storage (UHS, e.g., the idea of using natural geological reservoirs like depleted gas fields) promises exactly that. To make UHS a feasible process, fundamentals research investigating not just the integrity of reservoir and cap rocks, but also the interaction of hydrogen with downhole materials (e.g., cement) used in boreholes is essential. Boreholes provide access to geological reservoirs but are also the bottleneck of any production or storage operation. In general, boreholes are lined with downhole materials, consisting of a steel casing surrounded by cement. The cement acts as a bonding between the steel casing and the wallrock, providing mechanical stability and tightness for the hole. However, the effect that hydrogen might have on the mineralogical phase composition and subsequently on physical and mechanical parameters of downhole cement is still very scarcely known (Reitenbach et. al. 2015). This project, which is part of a PhD programme on H_2 production and storage at Montanuniversität Leoben, Austria aims to contribute to a better understanding of this issue.

The mineralogical phase composition of a cement class G, a standard type portland cement used in the petroleum industry, before and after hydrogen treatment was investigated and the influence was evaluated that potential reactions might have on the physical and mechanical properties.

The mineralogical methods applied were: XRD, FE-SEM, EPMA. Physical parameters such as porosity, pore size distribution and permeability were measured using Hg-porosimetry, N_2 sorption and nitrogen permeation, respectively. The mechanical properties were characterized by determining compressive and tensile strength. Additionally Young´s modulus was determined from the stress-strain curves obtained during compressive strength testing.

Additionally, thermodynamic modelling using Gibbs Energy Minimization Software (GEMS) was carried out. The modelling indicates that certain redox-sensitive phases within hardened cement pastes are susceptible to hydrogen alteration caused by the strong reducing character of hydrogen. Especially ferric iron and sulphate bearing phases like brownmillerite, monosulfoaluminate (AFm) and ettringite (AFt) are altered, resulting in the formation of native iron, magnetite, and iron sulphides.

Reitenbach V, Ganzer L, Albrecht D, Hagemann B (2015): Influence of added hydrogen on underground gas storage: a review of key issues. – Environ Earth Sci 73, 6927

Thermoelastic properties and phase transition of natural pollucite

J. Schreuer[1], M. Münchhalfen[1], E. Hartman[1]

[1]Ruhr-Universität Bochum, Institut für Geologie, Mineralogie und Geophysik, Universitätsstraße 150, Bochum, 44801, Germany
e-mail: schreuer@rub.de

Pollucite (Cs,Na)AlSi2O6· *y*H2O, a cesium-bearing zeolite belonging to the analcim group characterized by ANA topology of its tetrahedral framework, has long been considered to be a suitable material for use in fixation and deposition of radioactive Cs isotopes in high-level nuclear waste. Particularly favorable properties are the stability and low thermal expansion at high temperatures, the capability to host large amounts of Cs, and the low leaching rate of Cs. However, below about 500 K, the three-dimensional framework gradually changes from an "expanded form" to a "collapsed form" which is accompanied by a significant shrinkage of the unit cell volume without a change of symmetry (e.g., Kobayashi et al. 1997). Phase transformations from the cubic phase to a low-temperature tetragonal phase are also known (e.g., Kobayashi et al. 2006). Both processes can negatively affect the mechanical integrity of pollucite crystals and ceramics. The aim of our work is, therefore, to investigate the thermoelastic behavior of pollucite between 100 K and 673 K using dilatometry and resonant ultrasound spectroscopy.

The elastic properties of our pollucite samples at room temperature are in reasonable agreement with values reported by Sanchez-Valle et al. (2010). The temperature coefficients of the three independent elastic stiffnesses are uncharacteristically positive for stable materials. In the course of the framework “collapse”, the longitudinal stiffness c_{11} and the shear resistance c_{44} soften between 673 K and 133 K by nearly 50% and 35%, respectively. At the same time, the deviations from the Cauchy-relations take on negative values, indicating the increasing importance of directional interactions.

Sanchez-Valle C, Chio C-H, Gatta, GD (2010): Single-crystal elastic properties of (Cs,Na)$AlSi_2O_6 \cdot H_2O$ pollucite: A zeolite with potential use for long-term storage of Cs radioistopes. - J Appl Phys 108, 093509

Kobayashi H, Yanase I, Mitamura T (1997): A new model for the pollucite thermal expansion mechanism. - J Am Ceram Soc 80, 2161-2164

Kobayashi H, Sumino S, Tamai S, Yanase I (2006): Phase transition and lattice thermal expansion of Cs-deficient pollucite, Cs1−*x*Al1−*x*Si2+*x*O6 ($x \leq 0.25$). - J Am Ceram Soc 89, 3157-3161

Inorganic crystal structure database

A. Steudel[1], S. Rühl[1], S. Rehme[1]

[1]FIZ Karslruhe – Leibniz-Institute for Information Infrastructure,
Hermann-von-Helmholtz-Platz 1, 76344 Eggenstein-Leopoldshafen, Germany
e-mail: annett.steudel@fiz-karlsruhe.de

ICSD (Inorganic Crystal Structure Database) is the world's largest database for fully determined inorganic crystal structures. It is made available to the scientific community and industry by FIZ Karlsruhe. ICSD contains the crystallographic data of published crystalline inorganic structures, including atom coordinates, dating back to 1913. Organometallic and theoretical structures have been added within the past years. The ICSD data are of excellent quality. Only data that have passed thorough quality checks are included.

The ICSD database now contains more than 280,000 crystal structures. Around 12,000 new structures are added every year. Through our continuous quality assurance, existing content is modified, supplemented or duplicates removed. As a result, and by filling gaps from previous years, even the older content is not static.

Highlights of ICSD:

- All important crystal structure data are available, including unit cell, space group, complete atomic parameters, site occupation factors, Wyckoff sequence, molecular formula and weight, ANX formula, mineral group, etc.
- 80 % of the structures are allocated to about 10,000 structure types. This allows for searches for substance classes.
- Continuous selection and evaluation of theoretical structures. They can serve as a basis for developing new materials through data mining processes.
- Keywords to describe to physical and chemical properties are provided.
- Abstracts for a quick grasp of the article content are available.
- Simulation of Powder Diffraction Data

Last year the revision of the mineral names took place, which included a standardization of the mineral names. The standardization of the mineral names was done following the International Mineralogical Association (IMA) and this enabled us to link mineral entries to the two mineral databases "webmineral.com" and "mindat.org", so that further information about the minerals can be retrieved.

For a large part of the minerals, we have also included the hierarchical classification. This makes it easier to find minerals in the same hierarchical level (or below) and thus can also be used in teaching for improved understanding.

Since the last update of ICSD, topological information is included in the database for about half of the inorganic structures in ICSD. As a first step, this information can be used to search for the coordination of a central atom. This coordination can then also be represented visually. The topological data provide much more information which will be made available in future updates.

Digital Microscopy Solutions: Practical Analysis for different applications

A.R. Szalai[1]

[1]KEYENCE VHX 7000
e-mail: r.szalai@keyence.eu

Due to the high depth of field and depth composition, the system offers fully sharp images within seconds. With tilting and rotating stage, it is possible to inspect the crystals in all angles, giving the user an all-around view of the sample. The 4K resolution provides high quality for a detailed analysis. Keyence VHX lenses can be used with all lightning options such as brightfield, darkfield, transmitted light, diffuser, polarisation, DIC, mix light, and shadow effect mode for the surface analysis. Intuitive software design and a steering console secure comfortable usability for the operator, which makes an experience to microscope.

Next to 2D and 3D measurement, profile- and area measurement are available for perform analysis. Automatic report functions shorten the process of documentation.

Unravelling the true nature of Martian ´lh´-kieserite

D. Talla[1], M. Wildner[1]

[1]Institut für Mineralogie und Kristallographie, Josef-Holaubek-Platz 2, 1090 Wien, Österreich
e-mail: dominik.talla@univie.ac.at

The confirmed presence of hydrous sulfates on celestial bodies in our solar system such as Mars or the icy moons of Jupiter and Saturn has been a hotly debated topic for several decades (recently e.g., Clark et al. 2005; Bishop et al. 2009; Noel et al. 2010). Especially Mg-sulfate hydrates, with the ability to change their hydration state based on local humidity and temperature, are regarded as one of the key components governing the water budget at equatorial latitudes on Mars (Milliken et al. 2007).

Furthermore, these and other sulfate compounds are supposed to play an important role on the icy moons of Jupiter and Saturn, where their presence, possibly along with pressure-induced structural changes (e.g., Meusburger et al. 2020), influences thermodynamic equilibria leading to the presence of subsurface oceans, potentially even supporting life (Solomonidou et al. 2009).

Especially kieserite, $MgSO_4 \cdot H_2O$, given its broad field of stability compared to the other hydrates, is also believed to form on the surface of the icy moons via decomposition of higher Mg-sulfate hydrates by cosmic rays and UV radiation, with the stability of the sulfate monohydrate strongly enhanced by the surrounding vacuum (Zolotov & Shock 2001).

A still unsolved enigma is the structural and spectroscopic character of the so-called ‘lh’-kieserite polytype (where ‘lh’ stands for ‘low-humidity’), which, according to dehydration experiments under simulated Martian conditions performed by Wang et al. (2009), is presumed to be the dominant variant of monoclinic kieserite on the surface of Mars. Until now, however, no thorough investigation of this new ‘polytype’ has been conducted.

Comparing the powder patterns of ‘lh’-kieserite as documented by Wang et al. (2009) to other sulfate species, we observed a striking resemblance between this enigmatic compound and the tetragonal Mg-hydroxide sulfate hydrate (‘MHSH’) mineral caminite. To date, the latter was found on Earth in an entirely different environment compared to that on the surface of Mars – namely in black smokers on oceanic rift zones, reflecting its experimentally confirmed reverse solubility (e.g., Hochella et al. 1983). An entire range of such MHSH compounds is anticipated, where the cell metrics are dictated by variable occupancy of the Mg and H sites.

Taking the reverse solubility of the MHSH mineral group into account, we designed a novel autoclave prototype, allowing venting of the aqueous solvent at maximum temperature, preventing re-dissolution of the high-temperature phase assemblage upon cooling. Indeed, we were already able to synthesize several representatives of the said tetragonal compounds as single crystals with the expected variability in the Mg- and H-site occupancy, proving the existence of an (at least partial) MHSH solid solution series, with tetragonal ‘MHS’ (Mg-hydroxide sulfate, c = 12.885 Å; Fleet & Knipe 1997) and monoclinic kieserite ($2d_{001}$ = 13.499 Å; Bechtold & Wildner 2016) as theoretical endmembers. As the Mg-site occupancy decreases in favour of the H content, the tetragonal c-lattice parameter lengthens, conversely to the a axis.

The comparison of powder patterns of 'lh'-kieserite and MHSH shown in Fig. 1 (using CuKα radiation) is quite conclusive: the prominent reflection doublet at 26.5 and 28° 2θ, along with the characteristic pair at ~55° 2θ present in both phases, strongly indicates that both compounds are indeed one and the same substance.

This leaves the question as to why the MHSH group has not been previously considered as 'lh'-kieserite. Firstly, naturally occurring minerals belonging to this series are scarce, with only the aforementioned caminite found in nature to date. Secondly, both IR and Raman spectra of kieserite and MHSH bear striking resemblance (Fig. 2), making a spectroscopic discrimination rather ambiguous, more so taking into account the limited signal-to-noise ratio of remote measurements from orbiter instruments.

Our contribution aims to corroborate the existence and properties of the MHSH mineral group, which seems, in light of the newest findings, to represent an important constituent of sulfate assemblages present on celestial bodies in our solar system.

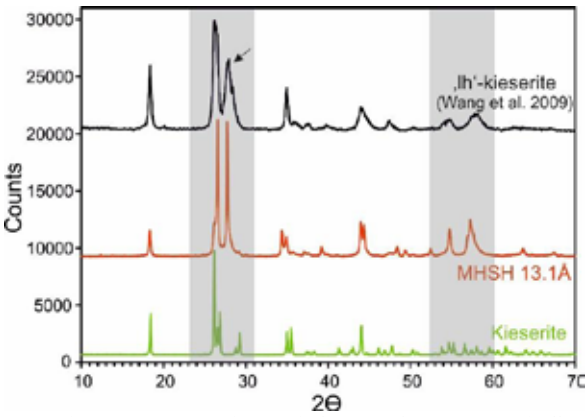

Figure 1. Comparison of the powder pattern of 'lh'-kieserite, MHSH and kieserite. Note the close match between Bragg reflections in 'lh'-kieserite and the MHSH variant with the *c*-cell parameter equal to 13.1 Å (highlighted in grey).

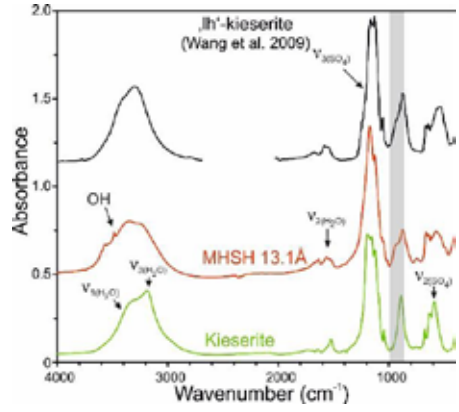

Figure 2. Close resemblance between IR spectra of 'lh'-kieserite, MHSH and kieserite. Apart from a shoulder at ~950 cm^{-1}, diagnostic for MHSH, the spectral envelopes are quite similar.

We gratefully acknowledge financial support of this work by the FWF grant-in-aid P34227-N.

Bechtold A, Wildner M (2016): Crystal chemistry of the kieserite–cobaltkieserite solid solution, $Mg_{1-x}Co_x(SO_4)\cdot H_2O$: well behaved oddities. - Eur J Miner 28, 43-52

Bishop JL, Parente M, Weitz CM, Noe Dobrea EZ, Roach LH, Murchie LS, McGuire PC, McKeown NK, Rossi CM, Brown AJ, Calvin WM, Milliken R, Mustard JF(2009): Mineralogy of Juventae Chasma: Sulfates in the light-toned mounds, mafic minerals in the bedrock, and hydrated silica and hydroxylated ferric sulfate on the plateau. - J Geophys Res 114, E00D09

Clark BC, Morris RV, McLennan SM, Gellert R, Jolliff B, Knoll AH, Squyres SW, Lowenstein TK, Ming DW, Tosca NJ, Yen A, Christensen PR, Gorevan S, Brückner J, Calvin W, Dreibus G, Farrand W, Klingelhoefer G, Waenke H, Zipfel J, Bell III JF, Grotzinger J, McSween, HY, Rieder R (2005): Chemistry and mineralogy of outcrops at Meridiani Planum. - Earth Planet Sci Lett 240, 73-94

Fleet ME, Knipe SW (1997): Structure of magnesium hydroxide sulfate, $[2MgSO_4\cdot Mg(OH)_2]$ and solid solution in magnesium hydroxide sulfate hydrate and caminite. - Acta Cryst B53, 358-363

Hochella MF, Keefer KD, deJong BHWS (1983): The crystal chemistry of a naturally occurring magnesium hydroxide sulfate hydrate, a precipitate of heated seawater. - Geochim Cosmochim Acta 47, 2053-2058

Meusburger JM, Ende M, Matzinger P, Talla D, Miletich R, Wildner M (2020): Polymorphism of monohydrate sulfate kieserite under pressure and its occurrence on giant icy Jovian satellites. - Icarus 336, 113459

Milliken RE, Mustard JF, Poulet F, Jouglet D, Bibring J-P, Gondet B, Langevin Y (2007): Hydration state of the Martian surface as seen by Mars Express OMEGA: 2. H_2O content of the surface. - J Geophys Res 112, E08S07

Noel A, Bishop JL, Al-Samir M, Gross C, Flahaut J, McGuire PC, Weitz CM, Seelos F, Murchie S (2015): Mineralogy, morphology and stratigraphy of the light-toned interior layered deposits at Juventae Chasma. - Icarus 251, 315-331

Solomonidou A, Coustenis A, Bampasidis G, Kyriakopoulos K, Moussas X, Bratsolis E, Hirtzig M (2011): Water oceans of Europa and other moons: implications for life in other solar systems. - J Cosmol 13, 4191-4211

Wang A, Freeman JJ, Jolliff BL (2009): Phase transition pathways of the hydrates of magnesium sulfate in the temperature range 50°C to 5°C: Implication for sulfates on Mars. - J Geophys Res 114, E04010

Zolotov MY, Shock EL (2001): Composition and stability of salts on the surface of Europa and their oceanic origin. - J Geophys Res 106, 32815-32827

Defect adamantines: potential materials for photovoltaic applications

Y. Tomm[1], G. Gurieva[1], D. M. Többens[1], S. Schorr[1,2]

[1]Helmholtz-Zentrum Berlin für Materialien und Energie
[2]Institute of Geological Sciences, Freie Universität Berlin
e-mail: susan.schorr@helmholtz-berlin.de

Compounds of the Adamantine family includes kesterite (Cu_2ZnSnS_4), currently the most promising material for fully inorganic thin film photovoltaic technology that is free of critical raw-materials and thus provides sustainable solutions.

Ternary adamantines like the chalcopyrites can be transferred by chemical substitution to a quaternary adamantine such as $A^I_2B^{II}C^{IV}X^{VI}_4$ (e.g., Cu_2ZnSnS_4) and $A^I\square B^{III}C^{IV}X^{VI}_4$ compounds, the latter are called defect adamantines (Pamplin 1981).

Defect adamantines like $Cu\square GaGeS_4$ and $Cu\square GaSnS_4$ can be seen as a compound within the solid solution between gallite – radvaniceite (Sejkora et al. 2022), $(CuGaS_2)_{1-x}(GeS_2)_x$ and gallite – berndtite $(CuGaS_2)_{1-x}(SnS_2)_x$, at x = 0.5, respectively.

Single crystals of these defect adamantines were grown by chemical vapor transport using iodine as transport agent. Aiming for chemical compositions according to the defect adamantine, chemical analysis of the grown crystals by X-ray fluorescence (XRF) has shown, that crystals in the system $(CuGaS_2)_{1-x}(GeS_2)_x$ show Cu/(Ga+Ge) rations between 0.45 and 0.9 as well as Ge/(Ga+Ge) ratios between 0.15 and 0.6. Thus the single crystals show a quite strong deviation from the stoichiometric composition (Cu/(Ga+Ge) = Ge/(Ga+Ge) = 0.5). We explain this behavior by the flexibility of the crystal structure of the end members and the defect adamantine. Their crystal structures are based on a corner-sharing network of tetrahedra (CuS_4, GaS_4, GeS_4 or $\square S_4$). By multiple energy anomalous synchrotron X-ray diffraction (MEAD) it was shown, that $Cu\square GaGeS_4$ crystallizes in the tetragonal chalcopyrite-type structure. It compares to the crystal structure of gallite, but with a higher fraction of vacancies.

The single crystals grown aiming for $Cu\square GaSnS_4$ adopt the chalcopyrite-type structure and the Cu/(Ga+Sn) values are close to 1. Thus there is only a very limited solubility in the $(CuGaS_2)_{1-x}(SnS_2)_x$ system. Berndtit (SnS_2) crystallizes in a trigonal structure type where the Sn^{4+} cations are coordinated by 8 sulfur anions. The very limited solubility between Gallite and Berndtite may be explained by the different coordination of the four-valent cation.

The band gap energy (determined by UV-Vis spectroscopy) of the mixed crystals in the $(CuGaS_2)_{1-x}(GeS_2)_x$ system cover a range of 2.1 to 2.4 eV, showing a strong bowing behavior in the dependency on the chemical composition parameter x. The crystals obtained in the system $(CuGaS_2)_{1-x}(SnS_2)_x$ have band gap energies within 1.7 and 2.0 eV. Thus, such defect adamantines are interesting materials for photovoltaic applications.

Figure 1. Single crystals of off-stoichiometric $Cu\square GaGeS_4$ (left) and $Cu\square GaSnS_4$ (right).

Pamplin B (1981): The adamantine family of compounds. - Prog Cryst Growth Charact 3, 179

Sejkora J (2022): Radvaniceite, GeS_2, a new germanium sulphide, from the Kateřina Mine, Radvanice near Trutnov, Czech Republic. – Minerals 12, 222

nanoGPS navYX™ – HORIBAs collaborative and inter-instrumental solution for correlative microscopy

M. Trapp[1], C. Lenz[1]

[1]HORIBA Jobin Yvon GmbH, Oberursel, Germany
e-mail: christoph.lenz@horiba.com

A comprehensive characterization of geological or mineralogical samples requires the application of more than one method to combine their complementary strengths. For example, the synergetic combination of µ-XRF (or SEM-EDX) with Raman microscopy provides information on both, the element composition as well as phase and structural properties of a specimen. However, relocation of points of interest (POI) on a µm-scale is one of the most tedious and time-consuming issue if the specimen is transferred between various instruments, especially if the imaging technique strongly differs (e.g., SEM vs. light microscopic image). Here, we present HORIBAs nanoGPS navYX™ technology that provides a unique solution to this problem and is independent from the respective instrument or manufacturer (Acher et al. 2021). Typical requirements to successfully apply this technique include the option for microscopic sample imaging or visualization (min. 2x to 5x magnification) and software-controlled, motorized sample stage positioning. Nearly all types of microscopy techniques, such as SEM, µ-XRF, AFM, Raman or light microscopy, hence, may be correlated using nanoGPS navYX™. To do so, a small relocation tag with a patented reading pattern is attached to the sample. This tag defines a virtual coordination system that is read by the dedicated navYX™ software and saves all points and measurement sites of interest. On every calibrated instrument, the saved POIs may be easily relocated independently of sample positioning or rotation via direct conversion of the virtual nanoGPS coordinates into the instrument's stage coordinates.

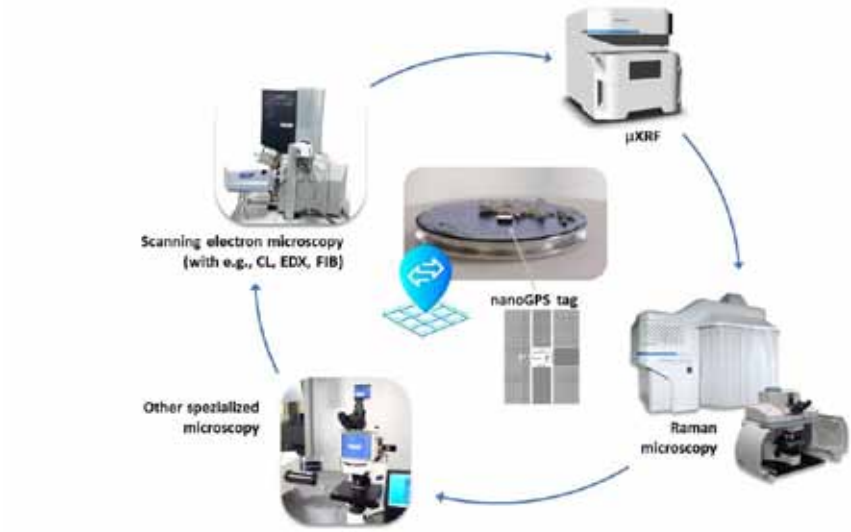

Acher O, Nguyên T L, Podzorov A, Leroy M., Carles P A, Legendre S (2021): An efficient solution for correlative microscopy and co-localized observations based on multiscale multimodal machine-readable nanoGPS tags. - Meas Sci Technol 32(4) 045402

Visible and invisible complexities in rocks: mineralogical and petrological constraints on the Variscan metamorphic gradient in the Southalpine metamorphic basement (Brixen quartzphyllites)

P. Tropper[1], T. Klotz[2], A. Wzietek[1], H. Pomella[2]

[1]*University of Innsbruck, Institute of Mineralogy and Petrography, 6020 Innsbruck, Austria*
[2]*University of Innsbruck, Institute of Geology, 6020 Innsbruck, Austria*
e-mail: peter.tropper@uibk.ac.at

The basement of the Southern Alps is represented by the Brixner Quartzphyllite whose Variscan *P-T* conditions correspond to a greenschist-facies metamorphic overprint. This metamorphic basement shows a metamorphic gradient ranging from the lower greenschist-facies in the S to the amphibolite-facies in the N. This metamorphic gradient reached peak metamorphic conditions in the Brixen area and decreases in a southern direction. Due to the emplacement of Permian intrusions into this basement, locally a Permian contact metamorphic overprint can be observed. The aim of this study was to provide mineralogical and mineral-chemical constraints of major mineral phases as well as accessories such as apatite on this gradient and if possible obtain *P-T* conditions along a profile from north to south.

The quartzphyllite samples were collected along a traverse from Reccoaro (TKP054) in the S to Brixen (TKP022) in the N. Petrographic investigations revealed that the metapelites contain quite a complex polyphase mineral assemblage. The mineral assemblage in the S is represented by chlorite + muscovite + albite + quartz. Towards the center of the traverse, biotite occurs in the mineral assemblage, which has subsequently been replaced by chlorite. Samples in the vicinity of the Permian Cima d'Asta intrusion show petrographic evidence for contact metamorphism since K-feldspar, chloritoid and andalusite occur. In the N the mineral assemblage is chlorite + muscovite + plagioclase + quartz + garnet. Therefore, the metapelitic zones of chlorite, biotite and garnet could be observed along the traverse.

Mineral chemical investigations revealed further complexities. The chemical compositions of muscovite, chlorite and plagioclase vary continuously with increasing *P-T* conditions from S to N. Si in muscovite decreases (from 3.3 to 3.1 apfu) with increasing Al^6 (from 2.4 to 2.7 apfu). Muscovite also shows an increase in the paragonite component from 4% to 13%. Similarly chlorite changes its composition also showing a decrease in Si and an increase in Al^6. Plagioclase changes from pure albite to anorthite contents of 30%. The data also revealed that the southernmost sample (TKP054) shows evidence for a later *T*-accentuated overprint (Permian?) texturally not visible. Also, the second southern sample (TKP056) from the traverse shows two plagioclase generations, which are also likely due to a later overprint.

The chemical composition of apatite also changes continuously from S to N with slightly increasing F contents. F increases from 3.6 wt.% in the S to 3.8 wt.% in the N. A contemporaneous increase in FeO, Y_2O_3, and Cl has also been observed. Geothermobarometry yielded so far *P-T* conditions of 554 ± 11 °C and 6.49 ± 1.3 kbar in the northernmost sample TKP022. Currently it is planned to apply muscovite-chlorite-quartz geothermobarometry to the rest of the samples of the traverse to obtain more quantitative data on the *P-T* gradient from the southern samples. This study clearly shows that quartzphyllites indeed are able to record complex metamorphic histories hidden in petrographic and mineral chemical data.

Geochemical insights into one of the earliest marine habitats on Earth – the reliability of 3.5-billion-year-old jaspillites from the Dresser Fm., Australia

S. Viehmann[1], D. Krämer[2], C. Koeberl[3], S.V. Hohl[4], M.J. van Kranendonk[5]

[1]University of Hannover, Institute of Mineralogy, Hannover, Germany
[2]Federal Institute of Geosciences and Natural Resources (BGR), Hannover, Germany
[3]University of Vienna, Deptartment of Lithospheric Research, Vienna, Austria
[4]State Key Laboratory of Marine Geology, Tongji University, Shanghai, P.R. China
[5]University of New South Wales Sydney, Australian Centre for Astrobiology, Sydney, Australia
e-mail: s.viehmann@mineralogie.uni-hannover.de

The ca. 3.5 billion-year-old Dresser Formation in the Pilbara Craton, Western Australia, is famous for its traces of early life in the form of microfossil assemblages and stromatolites. These unique rock types provide fascinating windows into habitats of microbial life and the state of the ambient atmosphere-hydrosphere system. Among several pioneering studies targeting interdisciplinary fields of geo(micro)biology and geochemistry, trace elements in combination with Fe isotopes of jaspilites from different units within the Dresser Formation have recently been reported to reconstruct ancient paleo-environments (Johnson et al. 2022). This geochemical study targeted jaspillites, i.e., chemical sediments that are proposed to directly reflect ancient fluid chemistry from which the jaspillites formed, from four consecutive horizons of the Dresser Formation. They propose severe and fluctuating paleo-environmental changes during the deposition of these units in combination with changing nutrient availability and limitation during land-sea transitions based on Rare Earth's and yttrium (REY) and Fe isotope systematics. While this study provides a crucial milestone in understanding the earliest microbial habitats on Earth, the source of elements providing nutrients among other elements in the ancient Dresser aqueous environments remains still incompletely understood.

To determine the sources affecting water chemistry in the Dresser Formation, we obtained trace element and radiogenic Nd isotope compositions of high pressure-high temperature digestions of jaspilitic cherts directly overlying the famous "candelabra"-stromatolites from a terrestrial hot spring deposit (Djokic et al. 2017). The trace element data corroborate the endmembers (Johnson et al. 2022): endmember I shows seawater-like shale-normalized (subscript SN) REY_{SN} patterns with positive La_{SN}, Gd_{SN} anomalies, heavy REY_{SN} over light REY_{SN} enrichment, and super-chondritic Y/Ho ratios. In contrast, the endmember II is characterized by the lack of typical seawater-like anomalies, sub-chondritic Y/Ho ratios, and light REY_{SN} over heavy REY_{SN}. Positive Eu_{SN} anomalies representing REY contributions from high-temperature, hydrothermal fluids in the ancient Dresser depositional environment are present in both endmembers. Radiogenic Nd isotope compositions, commonly used to determine the local sources of REY in modern and ancient seawater due to the short residence time of Nd, show a significant impact of post-depositional alteration and a reset of the Sm-Nd isotope system in the Dresser Formation jaspillites. A best-fit isochron calculation yields a Sm-Nd age of 2260 Ga ± 180 Ma that overlaps with thermo-tectonic events in Pilbara Craton between 2430 to 2400 Ma and 2215 to 2145 Ma (Rasmussen et al. 2005), respectively, suggesting that Nd isotope of the Dresser Formation jaspillites are unreliable geochemical proxies to reconstruct sources in Dresser fluids 3.5 Ga ago. We – however- strongly emphasize that overall REY distributions and Fe isotope compositions must not necessarily be affected by these events, although the Nd isotope compositions in the Dresser jaspillites show significant disturbances.

Djokic T, Van Kranendonk1 MJ, Campbell KA, Walter MR, Ward CR (2017): Earliest signs of life on land preserved in ca. 3.5 Ga hot spring deposits. - Nat Comm 8, 15263

Johnson CM, Zheng X-Y, Djokic T, Van Kranendonk MJ, Czaja AD, Roden EE, Beard BL (2022): Early Archean biogeochemical iron cycling and nutrient availability: New insights from a 3.5 Ga land-sea transition. - Earth Sci Rev 103992

Rasmussen B, Fletcher IR, Sheppard S (2005): Isotopic dating of the migration of a low-grade metamorphic front during orogenesis. - Geology, 33, 773-776

Tracking transformation processes in the Mg phosphate mineral system – A mineralogical study for environmental applications

R. Volkmann[1,2], R. Blukis[3], C. Schmidt[1], L. G. Benning[1,2]

[1]German Research Centre for Geosciences Potsdam
[2]Freie Universität Berlin
[3]Leibnitz-Institut für Kristallzüchtung Berlin
e-mail: rebeccav@gfz-potsdam.de

Phosphorous is an essential component of all living beings and is an important component in fertilizers. It is a scarce element on Earth and mining of phosphorous deposits is environmentally harmful (Manning, 2008). Therefore, recent research is focusing on P-recovery from anthropogenic sources, e.g., from wastewaters. The mineral struvite ($MgNH_4PO_4 \cdot 6H_2O$) is recovered from wastewater and reutilized as a slow-release nitrogen and phosphorus fertilizer (Le Corre et al. 2009). However, struvite is unstable under atmospheric conditions, leading to its decomposition and transformation into other phosphate phases (Tansel et al. 2018). This subaerial transformation has not yet been characterized and kinetic parameters for the transformation reactions are unknown.

In this study, the decomposition and transformation of struvite was investigated by altering synthetic µm- and mm-sized crystals at different temperatures (22–60 °C) in open and closed systems for up to 10 months. Phase transformations were monitored by optical microscopy and Raman spectroscopy and transformation kinetic parameters were quantified by powder X-ray diffraction (XRD) and Rietveld analysis.

Struvite transformed to different products following different mechanisms. In open systems, and at 22 °C, struvite transformed to newberyite ($Mg(PO_3OH) \cdot 3H_2O$) by losing its ammonia and three of its water molecules. However, struvite remained fairly stable and at 22 °C this transformation proceeded only by 15 % even after 10 months. In contrary, at 37 and 60 °C, struvite transformed faster and primarily to another phase - dittmarite ($MgNH_4PO_4 \cdot H_2O$) which retained its ammonia but lost five out of six water molecules; newberyite occurred only as a minor product (< 5 wt.-%). In the open system, the phase formation proceeded about 35 % faster at 37 °C and 100 % faster at 60 °C compared to 22 °C. In contrast, in the closed system even after 10 months at 60 °C struvite remained stable and the transformation barely started (< 2 wt.-%). The XRD data showed that after about 8 months at 37 °C and after 2 months at 60 °C in the open system amorphization of struvite occurs through the complete loss of ammonia and water.

Microscopic imaging revealed that both newberyite and dittmarite were characterized by pseudomorphic overgrowth after struvite, while showing similar optical properties. Yet, the kinetic data indicates different formation mechanisms for the two phases. The partial pressure of water and ammonia in the reacting atmosphere, which was documented by the differences in open and closed kinetic rates, as well as differences in the crystal structures were the main drivers for the breakdown of struvite to the two other magnesium phosphate phases.

As struvite is used as a slow-release fertilizer in agriculture, our results document that its transformation to newberyite leads to the loss of ammonia, which has important implications for fertilizer storage. Even at 22 °C, after 10 months 15 % of the ammonia is lost. Although at higher temperatures (≥ 37 °C) the transformation leads to the retaining of ammonia in the

dittmarite structure, such a temperature requires a higher energy demand for storage. Therefore, our study indicates that struvite fertilizer should not be stored at ambient conditions, but at temperatures below 22 °C and in closed containers.

Manning DAC (2008): Phosphate minerals, environmental pollution and sustainable agriculture. – Elements 4, 105-108

Le Corre KS, Valsami-Jones E, Hobbs P, Parsons SA (2009): Phosphorus recovery from wastewater by struvite crystallization: A review. - Crit Rev Environ Sci Technol 39, 433-477

Tansel B, Lunn G, Monje O (2018): Struvite formation and decomposition characteristics for ammonia and phosphorus recovery: A review of magnesium-ammonia-phosphate interactions. – Chemosphere 194, 504-514

Provenance studies on raw garnets from the Zillertal (Tyrol), Ahrntal (South Tyrol), and Radenthein (Carinthia)

S. Wagner[1], B. Zerobin[2], R. Köchl[3], P. Tropper[1], G. Goldenberg[2]

[1]Institute of Mineralogy and Petrography, University of Innsbruck
[2]Department of Archaeologies, University of Innsbruck
[3]Department of History and European Ethnology, University of Innsbruck
e-mail: simon.wagner@uibk.ac.at

There is evidence of the use of the mineral garnet as a gemstone in jewellery since the early Middle Ages. In the Alps, too, garnet is still used today in the form of traditional costume jewellery, especially the garnet variety almandine. From the middle of the 19th century, garnet mining began in the Zillertal, Ahrntal and Radenthein, of which all three remained important sites until the early 20th century. However, due to the export to the gemstone-cutting factories in the Czech Republic at the time, the raw garnets lost their actual origin and were henceforth traded as "Bohemian garnets". Nevertheless, a chemical differentiation and determination of origin is possible even in this state with suitable analytical methods (EPMA, micro-XRF, etc.). On a macroscopic level, it is not possible to distinguish visually between the different garnet deposits. The most significant features are the size and colour of cut garnets, since the true Bohemian garnets often only measure a few millimetres and show a more intense red colour than alpine garnets. A further criterion for distinguishing between the different alpine deposits can be achieved via the individual inclusion pattern, which can be attributed to the different conditions of garnet formation and differing host rock composition. Typical inclusions of Zillertal and Ahrntal garnet are, for example, chlorite, apatite, zircon, quartz, ilmenite, and epidote. In contrast, garnets from Radenthein show oriented growth, which is typically seen with the ilmenite and rutile inclusions. The clearest differences are due to chemical differences in the composition of the garnets, which can also be attributed to different formation conditions (P-T-X). Typically, these chemical differences can be clearly visualized by plotting certain oxides against each other. This method has proven to be very effective in distinguishing garnet deposits on a global scale and therefore forms the basic discrimination method in provenance studies (e.g. Then-Obłuska et al. 2021). On a local scale apparent chemical differences are only visible to a limited extent. However, the use of compositional data analysis allows a clearer distinction between the different alpine garnet deposits. In the case of chemical composition, certain conditions must be met to achieve a successful evaluation of discrimination features. With the help of software like *CoDaPack 2.0* (Comas-Cufí & Henestrosa 2011), these analyses can be carried easier and allow therefore a better differentiation between the different garnet deposits within Austria. Applying PCA on this big dataset, consisting of samples directly from the deposits and the former warehouse in Zell am Ziller, clearly shows that the biggest variance in the data set is produced by the three oxides MgO, MnO and CaO. By plotting these in a ternary diagram five different groups can be identified.

Anhydrite formation in planetary surface environments – The case of the Atacama Desert

N. Wehmann[1], C. Lenting[1], T.M. Stawski[2], L. Agudo Jácome[2], S. Jahn[1]

[1]Institut für Geologie und Mineralogie, Universität zu Köln, Zülpicher Straße 49b, 50674 Köln, Germany
[2]Bundesanstalt für Materialforschung und -prüfung (BAM), Department for Materials Engineering, Unter den Eichen 87, 12205 Berlin, Germany
e-mail: n.wehmann@uni-koeln.de

Gypsum ($CaSO_4 \cdot 2H_2O$), bassanite ($CaSO_4 \cdot 0.5H_2O$), and anhydrite ($CaSO_4$) are essential evaporite minerals for the evolution of hyper-arid surface environments on Earth and Mars (Voigt et al. 2019; Vaniman et al. 2018). The formation mechanism of especially anhydrite has been a matter of scientific debate for more than a century (van't Hoff et al. 1903). To date, there exists no model that can reliably predict anhydrite formation at earth's surface conditions. While thermodynamics favor its formation, it is hardly achieved on laboratory time scales at conditions fitting either the Atacama Desert on Earth, or the surface of Mars (Wehmann et al. 2023, subm.). In light of most recent developments (e.g. Stawski et al. 2016), that advocate for a complex, non-classical nucleation mechanism for all calcium sulphates, we present an analysis of natural samples from the Atacama Desert to identify key features that promote the nucleation and growth of anhydrite under planetary surface conditions. Our analyses reveal at least three distinct anhydrite facies, with differing mineralogy and micro- to nano-structures. The facies are (1) aeolian deposits with sub-µm grain sizes, (2) (sub-)surface nodules that formed from aeolian deposits and (3) selenites with secondary anhydrite rims. Possible mechanisms of their formation will be discussed.

Hoff JVT, Armstrong EF, Hinrichsen W, Weigert F Just G (1903). Gips und Anhydrit. - Z Phys Chem 45(1), 257-306

Stawski TM, Van Driessche AE, Ossorio M, Diego Rodriguez-Blanco J, Besselink R, Benning LG (2016): Formation of calcium sulfate through the aggregation of sub-3 nanometre primary species. - Nature Comm 7, 11177

Vaniman DT, Martínez GM, Rampe EB, Bristow TF, Blake DF, Yen AS, ... Sumner DY (2018): Gypsum, bassanite, and anhydrite at Gale crater, Mars. - Amer Miner 103, 1011-1020

Voigt C, Klipsch S, Herwartz D, Chong G, Staubwasser M (2020): The spatial distribution of soluble salts in the surface soil of the Atacama Desert and their relationship to hyperaridity. - Global and Planetary Change 184, 103077

Wehmann N, Lenting C, Jahn S (2023): Calcium sulfates in planetary surface environments. - Available at SSRN 4479259

Crystallography in energy applications

C. Weidenthaler

[1]*Max-Planck-Institut für Kohlenforschung, Mülheim an der Ruhr, Germany*
e-mail: weidenthaler@mpi-muelheim.mpg.de

The energy transition requires the implementation of sustainable energy carriers. Hydrogen is one of these options, but the storage is still a challenge. Ammonia, NH_3, is intensively investigated as a suitable candidate as an H_2 storage medium and is already used for heavy-duty transportation systems. The efficient splitting of NH_3 into H_2 and N_2 for fuel cell applications requires the development of catalysts where supported transition metals are one amongst others.

To understand the function of a catalyst, it is inevitable to use in situ/operando techniques in addition to ex-situ analytics. This contribution presents a combination of different in situ techniques that were used to investigate structure-property relationships of several types of Co- and Ni-based catalysts supported on different oxides such as La_2O_3, Al_2O_3, and MgO. In addition to in situ X-ray diffraction experiments, X-ray total scattering and X-ray absorption methods reveal structure changes of the catalysts and the supports on different lengths scales from bulk to the atomic scale. In addition to the results obtained from structure studies, the reduction behaviour, surface chemistry, and catalytic activities will be included to the overall discussion.

For Co-based catalysts supported on Al_2O_3, it could be shown that a significant fraction of the Co catalysts reacts with Al_2O_3 and forms catalytically inactive $CoAl_2O_4$ (Weidenthaler et al. 2022). The Co content in the spinel cannot be compensated by higher metal loadings. Alumina is known to prevent sintering and a re-dispersion of metallic Co after the reaction was observed. However, the disadvantage of its tendency to form inactive cobalt aluminates predominates.

The second system, Co on basic La_2O_3 support, forms in situ during NH_3 cracking from a $LaCoO_3$ pre-catalyst. The structural transformation from $LaCoO_3$ to the catalysts via several intermediate phases was monitored by means of operando X-ray diffraction experiments. The catalytically active metallic Co neither reacts with La_2O_3 nor re-disperses after the reaction. The conversion for Co on La_2O_3 is comparable to the most active Co on Al_2O_3 catalyst, despite having multiple higher Co-loading.

The third system involves Ni on MgO, which shows a clear dependence of the catalytic conversion on the activation process and the associated structural changes.

Weidenthaler C, Schmidt W, Leiting S, Ternieden J, Kostis A, Ulucan TH, Budiyanto E (2022): In-situ investigations of Co@Al_2O_3 ammonia decomposition catalysts: The interaction between support and catalyst. - Chem Cat Chem 14, e202200688

Confocal μ-XANES as a tool to analyse Fe oxidation state in heterogeneous samples: The case of melt inclusions in olivine from Hekla volcano

M. Wilke[1], R. Botcharnikov[2], J. Garrevoet[3], M. Portnyagin[4], K. Klimm[5], S. Krasheninnikov[1,6], R. Almeev[6], S. Moune[7], G. Falkenberg[3]

[1]Institut für Geowissenschaften, Universität Potsdam, Germany
[2]Institut für Geowissenschaften, Johannes-Gutenberg Universität Mainz, Germany
[3]Deutsches Elektronen-Synchrotron, DESY, Hamburg, Germany
[4]GEOMAR Helmholtz-Zentrum für Ozeanforschung, Kiel, Germany
[5]Institut für Geowissenschaften, Goethe Universität Frankfurt, Germany
[6]Institut für Mineralogie, Leibniz Universität Hannover, Germany
[7]Observatoire de Physique du Globe de Clermont-Ferrand, Université Clermont Auvergne, France
e-mail: wilkem@uni-potsdam.de

Here we present a confocal Fe K-edge μ-XANES method for the analysis of Fe oxidation state in melt inclusions of one-side polished samples, potentially applicable to any heterogeneous sample. The new technique allows for an analysis of small volumes with high spatial 3D resolution of <100 μm^3. Using a confocal setup, the probed volume is restricted to that just beneath the surface of the exposed object. This protocol avoids contamination of the signal by the host mineral and minimizes self-absorption effects. This technique has been calibrated and tested on a set of experimental glasses with a wide range of $Fe^{3+}/\sum Fe$ ratios. The method was applied to the analysis of natural melt inclusions trapped in forsteritic to fayalitic olivine crystals of the Hekla volcano, Iceland. Our measurements reveal changes in $Fe^{3+}/\sum Fe$ from 0.17 in basaltic up to 0.45 in dacitic melts, whereas magnetite-ilmenite equilibrium testifies redox conditions with $Fe^{3+}/\sum Fe \leq 0.20$ (close to FMQ, Fayalite-Magnetite-Quartz redox equilibrium) along the entire range of Hekla melt compositions. This discrepancy indicates that the oxidized nature of glasses in the melt inclusions could be related to post-entrapment process of diffusive hydrogen loss from inclusions and associated oxidation of Fe in the melt. The $Fe^{3+}/\sum Fe$ ratio in silicic melts is particularly susceptible to this process due to their low FeO content and it should be critically evaluated before petrological interpretation.

Investigating the metal sources of the Early Nordic Bronze Age through a multi-proxy approach

A. Wittke[1], B. Cornelis[1], D. Berger[1]

[1]Curt-Engelhorn-Zentrum Archäometrie, Mannheim, Germany
e-mail: andreas.wittke@ceza.de

The Early Nordic Bronze Age (NBA Period IB, 1600–1500 BC) is characterized by huge amounts of metal products reaching northern Germany and Scandinavia for the first time, demonstrated by the appearance of a refined repertoire of bronze products (Nørgaard et al, 2019). Examples for these products are the blades of swords and daggers of the Sögel and Wohlde district, which suddenly appear as highly sophisticated metal artefacts without local precursors. Both blade types have hilt-plates with four or five rivets, while Sögel blades have a rounded and Wohlde plates have a trapezoidal formed hilt-plate. One of the great desiderates of archaeologists is determining the origin of archaeological bronzes and their metal sources (copper and tin). To reconstruct the provenance of the source materials isotope and elemental compositions of metals have since become important tools. This work pursues a multi-isotope approach combining Pb, Cu and Sn isotopes with trace element composition (Berger et al. 2022) of about 300 blades of the Sögel and Wohlde type from the Early NBA to investigate the origin of the raw material sources and of the blades. Additionally, we search for evidence of source mixing and/or recycling to gain a better insight into the manufacturing practices and to validate the provenance analysis. For this, the blades are isotopically and chemically analysed and compared with ores and typologically related blades from other regions in Central and Southern Europe. This may help to reconstruct relationships between artefacts of different origins and to reveal cultural and trade networks. Moreover, a critical evaluation of the data will be undertaken against the background of potential metal/ore mixing and recycling.

First results of 49 blades from the Early NBA indicate the Alpine Mitterberg as a potential source region for the copper based on Pb and Cu isotope composition, and trace element patterns. The majority of the blades consists of low-impurity copper of chalcopyrite quality typical for the Mitterberg. However, some blades were likely produced from Slovakian copper ores and there could even be indications of mixing both copper sources. Regarding tin, the Erzgebirge would be a very likely supplier, but some regions of Cornwall are also possible because of matching Sn isotope values. Based on the isotopic data of a single blade (Pb, Cu, Sn), we are able to comprehend the manufacturing steps of the object and their meaning for the choice of source materials. In future research, more artefacts from the NBA and Central and Southern Europe, as well as copper ores of the Mitterberg and the Slovakian Ore Mountains will be studied to conduct statistical analysis and to check for mixing practices.

Berger D, Brügmann G, Bunnefeld J-H, Pernicka E (2022): Identifying mixtures of metals by multi-isotope analysis: Disentangling the relationships of the Early Bronze Age swords of the Apa–Hajdúsámson type and associated objects. - Archaeometry 64, 44–74, https://doi.org/10.1111/arcm.12714

Nørgaard HW, Pernicka E, Vandkilde H (2019): On the trial of Scandinavia's early metallurgy: Provenance, transfer and mixing. PLoS ONE 14, 1-32, https://doi.org/10.1371/journal.pone.0219574

Study of natural As_2S_3 glass

T. Witzke[1], G. Nénert[1], M. Gateshki[1]

[1]Malvern Panalytical B. V., Lelyweg 1, 7602 EA, Almelo, The Netherlands,
e-mail: thomas.witzke@malvernpanalytical.com

At the burning mine dump of the Lichtenberg open cast, Ronneburg, Thuringia, Germany (mined for uranium-bearing alum shale) and the burning mine dump of the Katerina coal mine, Radvanice, Czech Republic, orange-red to red glassy crusts and droplets with the composition As_2S_3 were found. The material was solidified from a melt, which was probably a sublimation product from a gas phase. X-ray diffraction showed that the material is amorphous. No peaks, but just a flat, very broad hump around d = 5 Å were observed in the diffraction patterns.

To be able to characterize structurally this amorphous mineral, Pair Distribution Function (PDF) analysis has been carried out. Similarly, to previous studies on the synthetic materials (Georgiev et al. 2003), the PDF data show that this mineral is intrinsically phase separated into small As-rich (As_4S_4) and large S-rich clusters. We show in Fig. 1 the PDF fit of the as-collected data using the previously reported model. This result suggests that this new mineral is closely related to the synthetic As_2S_3 glass.

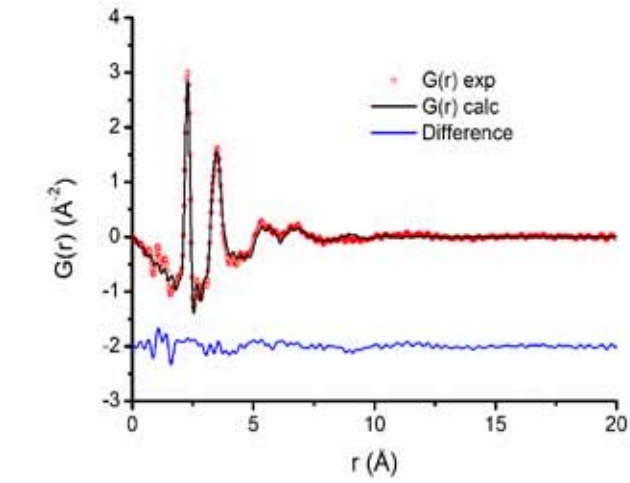

Figure 1: PDF fit of the experimental data using a phase separation model made of As_4S_4 and Sulfur cluster

Georgiev DG, Boolchand P, Jackson KA (2003): Intrinsic nanoscale phase separation of bulk As_2S_3. – Philosophical Mag 83, 2941-2953

Cement analysis by X-ray diffraction and X-ray fluorescence

S. Wollstadt[1], T. Füllmann[1], E. Hartmann[1]

[1]Rigaku Europe SE, Hugenottenallee 167, 63263 Neu-Isenburg, Germany
e-mail: elmar.hartmann@rigaku.com

Cement is one of the most important materials for construction and reacts with water to form hydrates, which gradually condense and harden. This hardening is caused when the formed hydrates coat cement particles and bind them together. A detailed understanding of the hydrate formation process is expected to lead to the elucidation of the mechanism of condensation and hardening. X-ray diffraction (XRD) techniques can identify crystalline hydrates such as ettringite and monocarbonate in cement. We report on the observation of changes in the crystalline phase or ordinary Portland cement over time with a water/cement ratio of 25% using a liquid sample holder which can prevent the sample from drying in an ambient environment by covering the sample surface with a film. Fig. 1 exemplifies changes in the XRD pattern of cement during a hydration reaction.

In addition, X-ray fluorescence (XRF) techniques are used to control the chemical composition of cement products and interim products. Since the fusion method can eliminate sample heterogeneity problems, such as grain size and mineralogical effects, it is possible to obtain high accuracy for cement samples and to establish calibrations using a variety of materials. ASTM C114-18 covers chemical analysis of hydraulic cements. In this standard, mainly procedures of wet chemical analysis are described and XRF spectrometry is mentioned as an example of "Rapid Test Methods". In practice, XRF spectrometry has been used for chemical composition analysis of cement owing to its simple sample preparation and high precision. We will show quantitative analysis for Portland cements by the fusion method according to ASTM C114-18, as displayed in Table 1, using a multi-channel simultaneous wavelength dispersive XRF (WDXRF) spectrometer, which enables the simultaneous measurement of all the elements in the sample under investigation. The counting time of the measurement was 40 seconds for twelve elements in cement.

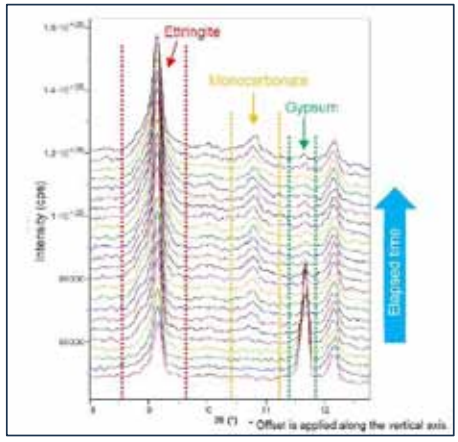

Figure 1. Overlaid X-ray diffraction patterns of hydrated cement.

Analysis component	Analysis range	Difference between duplicates		Qualified
		Limit (ASTM)	Maximum difference	
SiO_2	18.637 – 22.38	0.16	**0.05**	✓
Al_2O_3	3.875 – 7.06	0.20	**0.01**	✓
Fe_2O_3	0.152 – 3.09	0.10	**0.003**	✓
CaO	57.58 – 67.87	0.20	**0.14**	✓
MgO	0.814 – 4.475	0.16	**0.01**	✓
SO_3	2.086 – 4.622	0.10	**0.01**	✓
Na_2O	0.021 – 1.068	0.03	**0.006**	✓
K_2O	0.093 – 1.228	0.03	**0.004**	✓
TiO_2	0.084 – 0.3663	0.02	**0.003**	✓
P_2O_5	0.022 – 0.306	0.03	**0.001**	✓
ZnO	0.0048– 0.107	0.03	**0.0004**	✓
Mn_2O_3	0.0073– 0.2588	0.03	**0.001**	✓

Table 1. Qualification test results (unit: mass%)

Stable tungsten (W) isotope behavior during the early diagenesis in the Gulf of California

R. Yang[1,2], M. Gutjahr[2], F. Scholz[2], F. Kurzweil[1], S. Eroglu[3], C. Münker[1]

[1]Institute of Geology und Mineralogy, University of Cologne, Zülpicher Straße 49b, 50674 Cologne, Germany
[2]GEOMAR Helmholtz Centre for Ocean Research Kiel, Wischhofstraße 1-3, 24148 Kiel, Germany
[3]Institute of Geology and Paleontology, Westfälische Wilhelms Universität,
Correns Straße 24, 48149 Münster, Germany
e-mail: ryang2@uni-koeln.de

The stable W isotope system has recently emerged as a promising redox indicator, but its modern oceanic budget is not yet fully understood. Specifically, the mechanisms of W delivery to the sediments and its behavior during early diagenesis remain unknown.

In this study, three sediment cores in the gulf of California were thoroughly analyzed. Our findings indicate that W in marginal sediments is a combination of authigenic and detrital W components, with varying contributions at different depths. Authigenic W is likely bound to Mn oxides and released into the pore water in the Mn reduction zone. The delivery of W is primarily associated with Mn shuttling. Light W is adsorbed and released upon reductive dissolution of Mn oxides.

The sub-surface conditions in all the three cores are anoxic, leading to limited enrichment of W in sediments. Despite being geochemical twin elements, W and Mo display contrasting behaviors in sulfidic environments. Consequently, the distinctive behavior of W makes it a valuable indicator for identifying the cycling of Mn, an essential element for biological processes, and for tracing the oxidation history of the early Earth's oceans.

How to predict strength and optimum mix-designs of mineral-waste-based geopolymers

I. Zögl[1], O.Rudić[2], C. Grengg[1], F. Steindl[1], D. Etezad[1], M. Dietzel[1], S. Raič[1]

[1]Institue of Applied Geoscience, Graz University of Technology
[2]Institute of Technology and Testing of Construction Material, Graz University of Technology
e-mail: iris.zoegl@tugraz.at

Reducing the carbon footprint of building material production (*ca.* 9 % of anthropogenic CO_2) in the short term is essential to achieve global climate targets. In this regard, mineral wastes and industrial secondary raw materials show large potential as a low-CO_2 alternative to traditional carbonate-based binder systems. In order to promote and establish the use of mineral waste based binders as strong future competitors in the construction industry, optimal combinations of solid and liquid binder components have to be developed in so-called mix designs to meet material requirements. In this context, the desired material properties, such as adequate workability, high strength, improved chemical resistance and minimal shrinkage strongly depend on elemental ratios (*e.g.* Si/Al, Al/K) within the mix design. These are multi-variable challenges that are conventionally solved by changing one variable of the mix design at a time, until the desired results are achieved. In order to ensure a more time-and cost-efficient strategy, and to generate optimum experimental conditions, we are applying the Design of Experiment (DoE) and Response Surface Methodology (RSM) approaches to alkali-activated waste-based binder systems. DoE is a widely used procedure that seeks to predict a desired outcome (*e.g.* compressive strength, elemental ratios), which is then systematically optimized by a set of statistical techniques (RSM). In the current study, we evaluated the most desirable relative contents of the mix design components metakaolin, mineral wastes and aqueous potassium silicates (waterglass as alkaline activator) under the conditions of (i) maximizing the content of mineral wastes and (ii) achieving the desired material properties (e.g,. compressive strength). Preliminary results demonstrate how a minimum number of experimental runs and samples enables a refinement of possible mix-ratio-combinations. Re-iterations of these experimental procedures allow to accurately predict relevant material properties such as mechanical performance of the hardened mineral-waste-based binder material. Additionally, economic and ecological decisions could be already made during early stages of experimental approaches by including manufacturing costs and CO_2 emissions to the existing DoE models.